Extending the uses of lipid-membrane coated electrodes: Next generation of lipid membrane biosensors and smart implantable cell-electrode devices

Amani Alghalayini

A thesis submitted in fulfillment of the requirements for the degree of Doctor of Philosophy

UNIVERSITY OF TECHNOLOGY SYDNEY

School of Life Sciences

Faculty of Science

Feb 2020

Certificate of Original Authorship

I, Amani Alghalayini, declare that this thesis is submitted in fulfillment of the requirements for the award of a Doctor of Philosophy, in the School of Life Science at the University of Technology Sydney.

This thesis is wholly my own work unless otherwise reference or acknowledged. In addition, I certify that all information sources and literature used are indicated in the thesis. This document has not been submitted for qualifications at any other academic institution.

This research is supported by the Australian Government Research Training Program, as well as the Australian Research Council (ARC) Discovery Program (DP) and the ARC Research Hub for Integrated Device for End-user Analysis at Low-levels (IDEAL) (IH150100028).

Signature:

Production Note:
Signature removed prior to publication.

Amani Alghalayini

Date: 24-Jan-2020

Dedication

To the one whom I discovered my life with,

To my soulmate,

To my paradise on earth,

To Tariq

Acknowledgment

During the last three years in my Ph.D. journey, I was surrounded by many great people that provide me with support, help, encouragement and care. I am much thankful for you all; without you, this journey would not have been possible.

First of all, I would like to express my sincere thankfulness to my principal supervisor, Prof. Stella Valenzuela, for believing in me and providing me this opportunity. I am grateful for your kindness, unlimited support, motivation and remarkable scientific guidance that has been given throughout my candidature. Professor Stella represents an excellent model for distinguished scientist women that have inspired me to grow as a good scientist in the future.

I am also grateful to my associate-supervisor, Dr. Charles Cranfield, for his help, support and guidance as well as invaluable advice, direction and inspiration that provided to me throughout the study.

Furthermore, I would also like to thank Prof. Bruce Cornell for his profound knowledge in the research field, his patient approach and rich teaching experiences that have helped me a lot and enabled me to accomplish the outcome of this project.

Additionally, I would like to thank Dr. Maryam Parviz for her valuable advice, encouragement and help at every time I encountered problems.

My gratitude also is extended to all academics, staff, lab managers, officers, technicians from the Life of Science faculty at UTS and from ANSTO for their supportive attitudes

and helpful comments during my study. Thanks to all my friends and colleagues inside and outside the university for their invaluable help.

Finally, I would like to deeply appreciate my beloved family for their continued love and support throughout these years.

All my love goes to my parents, my angels, mother and father, Wasfia El Kayali and Mousa Gharbieh, your blessing kept me going during this long and often challenging time. To my lovely sister Suzan, thanks for your humor and friendship. To my brothers, Fadi and Marwan, to my mother in law and father in law, Intesar El Shawwa and Amin Alghalayini, for their support and motivation.

I also want to pay my regards to my charming daughters Sarah and Dana, my lovely sons, Saed-Allah and Yousif for their love and providing a wonderful company during the stressful time along this journey. I feel blessed to have such an amazing family that, for me, is a source of inspiration, motivation and strength.

I extend my love and important big thanks to my husband Tariq Alghalayini, I am grateful and blessed having you in my life, without you, this journey was impossible. Thank you for your unconditional love, assistance and support through all of the years. You have always lifted me up through the stressful times.

Publications

Refereed journal publications

- **Alghalayini, A.**, A. Garcia, T. Berry, and C.G. Cranfield, *The Use of Tethered Bilayer Lipid Membranes to Identify the Mechanisms of Antimicrobial Peptide Interactions with Lipid Bilayers.* Antibiotics, 2019. **8**(1): p. 12.

Conference Presentations

- ## Conference oral presentations

  - **Amani Alghalayini**, Lele Jiang, Xi Gu, Guan Yeoh, Charles G. Cranfield, Victoria Timchenko, Bruce Cornell, Stella M. Valenzuela. Heat transfer characteristics of nanoparticles measured with tethered bilayer lipid membranes. 10th International Nanomedicine Conference. 2019 Pier One Sydney Harbour Hotel, Sydney, Australia

  - **Amani Alghalayini**, Lele Jiang, Xi Gu, Guan Yeoh, Charles G. Cranfield, Victoria Timchenko, Bruce Cornell, Stella M. Valenzuela**.** Study of heat transfer from laser-irradiated gold nanoparticles using tethered bilayer lipid membranes. Asian biophysics association symposium and annual meeting 2018 of the Australian society for biophysics. RMIT University, Melbourne, VIC, Australia

  - **Amani Alghalayini**, Lele Jiang, Xi Gu, Guan Yeoh, Charles G. Cranfield, Victoria Timchenko, Bruce Cornell, Stella M. Valenzuela. Real-time monitoring of heat transfer between gold nanoparticles and tethered bilayer lipid membranes. ICEAN 2018 the International Conference on Emerging Advanced Nanomaterials. Newcastle Exhibition & Conference Centre, Newcastle, NSW, Australia

  - **Alghalayini, Amani**; Parviz, Maryam; Cornell, Bruce A.; Cranfield, Charles G.; Valenzuela, Stella M. Cell-electrode interfaces and optimal architecture for cell detection. IDEAL-ARC Hub Annual Forum 2018. University of South Australia, Cancer Research Institute, Adelaide, Australia.

- **Conference poster presentations**

  - **Alghalayini, Amani**; Parviz, Maryam; Cornell, Bruce A.; Cranfield, Charles G.; Valenzuela, Stella M. Optimizing cell-electrode interface mimicking the natural environment. International Conference on Nanoscience and Nanotechnology ICONN 2018 the University of Wollongong, Wollongong, Australia

  - **Alghalayini, Amani**; Parviz, Maryam; Cornell, Bruce A.; Cranfield, Charles G.; Valenzuela, Stella M. Ion conduction recording of neuronal cell activity utilizing tethered lipid membrane. The 2017 annual meeting of the Australian Society for Biophysics. UTS, Sydney, Australia.

  - **Alghalayini, Amani**; Parviz, Maryam; Cornell, Bruce A.; Cranfield, Charles G.; Valenzuela, Stella M. Development of a cell-based sensor using functionalized tethered lipid bilayer membrane. The New Horizon, 2017. University of Sydney, Sydney, Australia

  - **Alghalayini, Amani**; Parviz, Maryam; Cornell, Bruce A.; Cranfield, Charles G.; Valenzuela, Stella M. Improving implantable technologies by optimizing specificity and efficiency between electrode-cell interfaces. The New Horizon 2016, Sydney, Australia.

Table of Contents

Extending the uses of lipid-membrane coated electrodes: Next generation of lipid membrane biosensors and smart implantable cell-electrode devices

Chapter 1

Literature Review

Chapter 2

The ionic to electronic interface: key challenge to improving implantable medical devices

Chapter 3

Developing ion-channel switch nano-biosensors for direct cell detection

Chapter 4

Real-time monitoring of heat transfer between gold nanoparticles and tethered bilayer lipid membranes

Table of Figures

Chapter 1

Literature Review

Chapter 2

The ionic to electronic interface: key challenge to improving implantable medical devices

Chapter 3

Developing ion-channel switch nano-biosensors for direct cell detection

Chapter 4

Real-time monitoring of heat transfer between gold nanoparticles and tethered bilayer lipid membranes

Appendix

List of Abbreviations

Å	Angström (10-10 m)
AC	Alternative current
AFM	Atomic Force Microscopy
Ala	Alanine amino acid
Alpha-IMS	Alpha-Institute for Microelectronics Stuttgart
AM199	Zwitterioninc lipids comprised 70% C20 diphytanyl-ether-glycero-phosphatidylcholine and 30% C20 diphytanyldiglyceride ether lipids
AM215	mobile lipids mixture of 3:7 molar ratio of GDPE: DPEPC
Arg	Arginine amino acid
Asn	Asparagine amino acid
Asp	Aspartate amino acid
BLM	Black lipid membrane
B-PE	1-oleoyl-2-(12-biotinyl (aminododecanoyl))-sn-glycero-3-phosphoethanolamine
BSA	Bovine serum albumin
C_m	Membrane capacitance
cRGDfK(B-PEG)	Cyclo [Arg-Gly-Asp-D-Phe-Lys (Biotin-PEG-PEG)]
CHO-K1	Chinese hamster ovary cells
Con-A	Concanavalin A
Cys	Cysteine amino acid
D_2O	Deuterated water
d31-POPC	Deuterated 1-palmitoyl-(d31)-2-oleoyl-sn-glycero-3-phosphatidylcholine
DAPI	4′,6-diamidino-2-phenylindole
DC	Direct current
DLP	Half-membrane is spanning
DMEM	Dulbecco's modified eagle's medium
DOTAP	1, 2-dioleoyl-3-trimethylammonium-propane (chloride salt)
DPBS	Dulbecco’s phosphate-buffered saline
DPEPC	diphytanyl ether phosphatidylcholine
DP-NGPE	1,2-dipalmitoyl-sn-glycero-3phosphoethanolamine-N-(glutaryl) (sodium salt)
ECIS	Electrical cell-substrate impedance sensors
ECM	Extracellular matrix
E-coli	Escherichia coli
EDC	1-(3-dimethylaminopropyl)-3-ethylcarbodiimide hydrochloride
EDTA	Ethylenediaminetetraacetic acid
EIS	Electrochemical impedance spectroscopy
f	Frequency

FBS	Fetal bovine serum
G418	Geneticin
gA5XB	biotinylated gramicidin
gAYYSSBn	tethered gramicidin
GDPE	glycerodiphytanylether
Gln	Glutamine amino acid
Glu	Glutamic acid amino acid
Gly	Glycine amino acid
G_m	Membrane conduction
GNPs	gold nanoparticles
GNUs	gold nano urchins
GRGDS	Glycine-arginine–glycine–aspartic acid-serotonin (GLY-ARG-GLY-ASP-SER)
Hz	Hertz
I	Current
ICS	Ion-channel switch
IKVAV	Ile-Lys-Val-Ala-Val
K	Kilo
laser	light amplified stimulated emission of radiation
LB	lysogeny broth
Leu	Leucine amino acid
Lys	Lysine amino acid
M	Molar
mg	Milligram
ml	milli-Litre
MLP	Mobile lipid phase
mM	milli-Molar
MSLa	Biotinylated tethered membrane-spanning lipid
MTSDDL	Met-Thr-Ser-Asp-Asp-Leu (Methionine-Threonine-Serine-Aspartate-Aspartate-Leucine)
mV	Millivolt
MΩ	Megaohm
nF	NanoFarad
NHS	N-hydroxysuccinimide
nm	Nanometer
nM	Nanomolar
NNEN	Asn-Asn-Glu-Asn (Asparagine Asparagine Glutamate Asparagine)
NR	Neutron Reflectivity
ºC	Degree Celsius
OEG	Oligo ethylene glycol
OmpF	Outer membrane protein
PBS	Phosphate buffered saline
PC	Phosphatidylcholine

PE	Phosphotidylethanolamine
PEG	Polyethylene glycol
PFA	paraformaldehyde
PHSRN	Pro-His-Ser-Arg-Asn
PLL	Poly-L-lysine
POEGA	Poly(oligoethylene glycol) acrylate
POPC	1-palmitoyl-2-oleoyl-sn-glycero-3-phosphatidylcholine
POPE	1-palmitoyl-2-oleoyl-sn-glycero-3-phosphatidylethanolamine
PS	Phosphatidylserine
Q	Momentum transfer
QCM	Quartz Crystal Microbalance
R	Resistance
RGD	Arginine–glycine–aspartic acid (Arg-Gly-Asp)
Rm	Resistance
RYD	Arginine–tyrosine –aspartic acid (Arg-Tyr-Asp)
SAMs	Self-assembled monolayers
SAMs	self-assembled monolayers
Ser	Serine amino acid
SFM	serum-free medium
SH-SY5Y	Neuroblastoma cell line
SiO_2	Silicon dioxide
SLB	Supported lipid bilayer
SLD	Scattering Length Density
SPR	Surface Plasmon Resonance
t	Time
T10	10 percent of tethering molecules
T100	fully tether molecules percentage
TAT	GRKKRRQRRRPQ
tBLM	Tethered bilayer membrane
TEG	Triethylene glycol
Triton-X100	Octylphenyl-nonaoxyethylene
Trp	Tryptophan amino acid
Tyr	Tyrosine amino acid
UV	Ultraviolet
V	Voltage
Val	Valine amino acid
YIGSR	Tyr–Ile–Gly–Ser–Arg
Z	Impedance
|Z|	The magnitude of the impedance
ΔA	Percentage surface area expansion
θ	Phase
λ	Wavelength
µg	Microgram

µl	micro-Litre
µM	Micromolar
µS	Microsiemens
σ	Roughness
2D	Two-dimensional
3D	Three-dimension

Abstract

The ability to combine both a functional sensing and signalling membrane-electrode interface system is crucial for developing new technologies that can directly connect the living biosphere with electrical devices. However, there is a considerable distinction between both the chemical and biomechanical properties of live cell membranes versus synthetic electrical prostheses, thus there remain significant challenges that must be overcome in order to establish stable and functionally predictable interactions between these different components. The sparsely tethered bilayer lipid membrane possesses the necessary skeleton onto which novel chemistries can be added in order to succeed in the first iteration of correctly integrating electronic coupling with biological tissue.

This dissertation presents an investigation into controlling the ionic and the electronic interface and then detecting ion fluxes arising from nearby biologically active cells at the nanometer scale, by using the detectable electrical signals derived from interfacing of membranes with a gold electrode. In it, the feasibility of implementing tBLMs as either an interface between biological systems and electrical devices or for continual sensing in real-time or for diagnostic purposes is investigated.

Commencing is a comprehensive review of variant artificial lipid membrane models and the impedance spectroscopy approach (Chapter 1). A demonstration of the intimate nanoscale contacts of cells with the surface of the electrode is presented in Chapter 2. The aim of this study was to examine the feasibility of applying tBLMs in bio-implantable devices to offer specific transmission of electrical signals to individual target neurons to improve signal fidelity. This was to be achieved by reducing leakage pathways, thereby minimizing electrophoretic ion currents being lost into the surrounding interstitial

medium. Chapter 3 describes how, instead of using the lipid membrane-covered electrodes to signal to cells, the electrode might be used to as a nano-biosensor for cell detection. Various approaches to increase sensitivity were explored to enhance this capability. The necessity for detection at the nanometer scale is explored in Chapter 4, recording in real-time the laser-generated heat pulses arising from laser-illuminated gold nanoparticles. Detection of these heat pulses required attachment of the gold nanoparticles to the membrane surface, while non-specific binding of gold nanoparticles failed to elicit a measurable response.

Conclusions and perspectives are presented in Chapter 5, sum up of the significant achievements presented in this dissertation, which has focused on extending our understanding of cell membrane interactions and exploring the feasibility of using these across a range of applications.

Chapter 1

Literature Review

Chapter 1

Literature Review

1.1 Introduction

Bilayer lipid membranes, tethered over gold substrates, provide us with new possibilities in the development of superior close-contact biomimetic electrodes. Cell membranes represent a critical part of living cells that define their outer perimeter, as well as creating specialised internal compartments in eukaryotic cells. They participate in cell protection, cell to cell recognition and are critical for creating and maintaining electrical and chemical signaling processes. Phospholipids are the main building blocks of cell membranes that self-assemble into bilayers, which, together with membrane proteins that are either embedded or attached peripherally, play essential roles in normal cellular functioning [1-3].

The amalgamation of biologically active elements, such as cell membranes and proteins, with electrodes that can detect bioelectrical signals, creates a functional biological electrode interface system, which can connect artificial lipid membranes, that mimics natural lipid membranes, with electrical devices. This combining of biocompatible materials with organic tissues is crucial for developing bio-implant devices that can compensate or replace missing body functions, by artificially stimulating neuronal or other body cells. Also, interfacing biocompatible functionalized electrodes with bilayer lipid membranes is also critical for the development of nano-biosensors. The artificial membrane-electrode interface can be used to examine the potential effects of newly-developed compounds as well as various stimuli *in vitro*. Variable functionalization or specific protein and/or ion channel insertion into artificial membranes is designed to

mimic the natural environment in order to study the signal responses. This, in turn, can reduce the usage of animal-based testing and improve specificity to identify unknown compounds.

This chapter delivers an outline of the various models of artificial lipid membranes, along with a discussion of the advantages and limitations of each model. Also, it discusses the key points of understanding the tethered bilayer lipid membrane (tBLM) approach. In addition, this chapter reviews the key studies and application that associate tBLMs technology, highlighting the significance of extending the uses of lipid-membrane coated electrodes for the development of an innovative generation of lipid membrane biosensors and smart implantable cell-electrode devices.

An explanation of the principles and applications of electrical impedance spectroscopy in investigating the membrane conduction and capacitance as well as the cell-electrode interface will be covered. As a final point, this chapter will highlight the main objectives of this dissertation.

1.2 Biological membranes: Significance within *in-vivo* systems and *in-vitro* models

Cellular bilayer membranes can be considered one of the most critical structures that have led to the existence of living cellular life on this planet [3]. As hydrophobic barriers, lipid membranes define the architecture of the overall cell, provide compartmentalization of intracellular biomolecules and serve as a scaffold for protein anchorage and organisation.

Cellular bilayer membranes are comprised of a complex combination of lipids and proteins. The hydrophobic interaction between individual lipid molecules creates and

drives, the self-assembled bilayer membrane [4]. Together with the lipids, the embedded proteins across the lipid bilayer support various cellular process such as conveying ions, intracellular signaling and transporting nutrients [5]. Natural cell membranes incorporate various lipids, whereas the artificial lipid membranes models can be produced from select, specific phospholipids [6]. The sophistication and variability of natural lipid membrane systems are one of the significant challenges in understanding the lipid-protein interactions in cells.

There have been various artificial membrane platforms developed to provide close bio-mimetic versions or copies of natural lipid membrane architecture and functionality. These biomimetic membranes match the two-dimensional membrane design of cellular membranes, avoiding the multilamellar structure present in many liposomal mixtures [7].

1.3 Development of artificial bilayer lipid membrane technologies

The various artificial lipid-based models that are currently available are described below.

1.3.1 Black Lipid Membranes

The first successful model membrane system developed for studying the electrical characteristics of planar bilayer lipid membranes are *black lipid membranes* (BLMs). BLMs were first reported in 1962 by Mueller et al., where a small aperture was used, over which a phospholipid bilayer could be partitioned, separating two chambers containing an aqueous solution [8]. A droplet of lipids dissolved in a hydrophobic solvent is introduced or painted, across the aperture within the hydrophobic partition. Salt solutions can be added to either side of the lipid-coated aperture. Lipid bilayers made this way

revealed themselves as black upon light reflection when they were unilamellar. The method for BLM formation is illustrated in Figure 1.1.

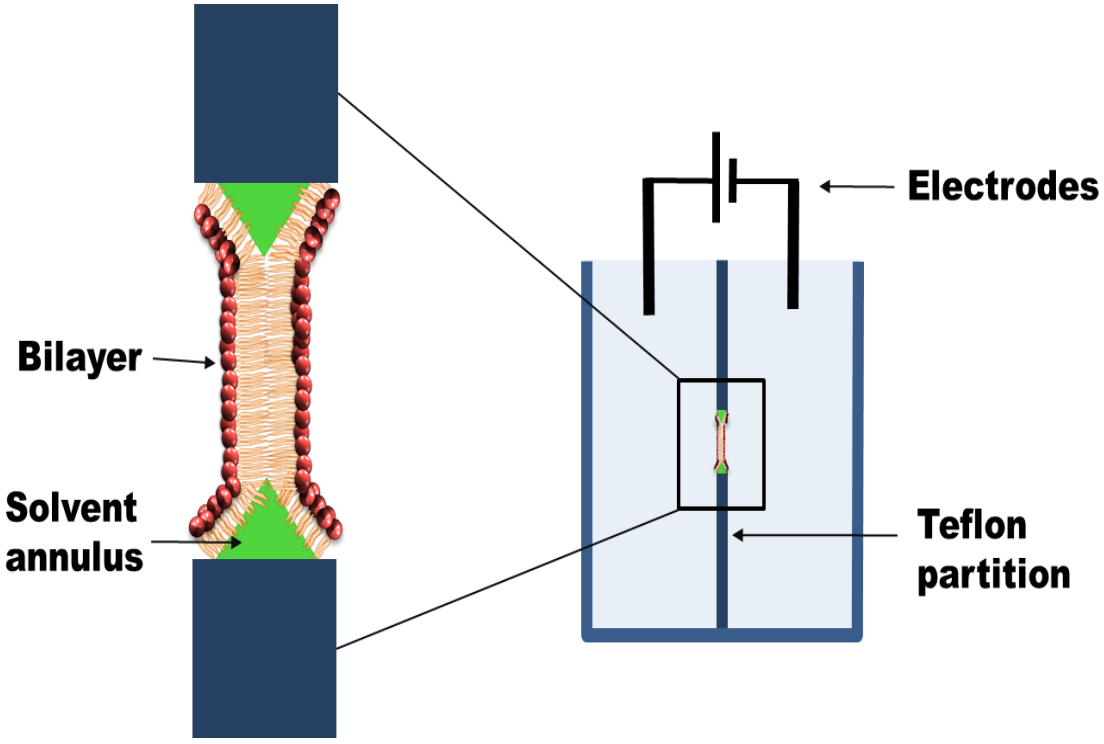

Figure 1.1: A schematic representation of Black Lipid Membrane (BLM) System. The system setup includes two chambers filled with an aqueous solution and linked to each other through a small hole in the Teflon partition. The electrical recording system is constituted of the applied voltage to electrodes in each chamber. The current-voltage amplifier utilized to investigate membrane conduction is caused by current passing through the painted membrane in the hole. This black lipid membrane is formed by inoculation of phospholipids that are dissolved in a hydrophobic solvent into the small aperture. This modified Figure based on [8].

Different biophysical processes have been investigated by use of the BLMs technique such as characterisation of ion channels, membrane proteins, antibiotic and pore-forming compounds [9-14]. For example, Tien et al. (1967) were able to compute the thickness of BLM by using dye compounds coupled with nonlinear optical microscopy [15]. Likewise,

Ries et al. (2004) derived BLM thickness by analysing reflected light intensity using second harmonic generation micrographs and scanning two-photon fluorescence microscopy [16]. Cheley et al. (2002) applied the pore-forming BLMs approach to examine cell signalling molecules. The introduction of phosphate anions demonstrated complete block of the α-hemolysin transmembrane pore, as well, they showed similar effects for several pores engineered to access other cell signalling molecules such as calcium [17]. The same methodology was employed by Braha et al. in order to sense divalent metal cations utilizing polyhistidine sequences[13, 14].

The absence of physical support in the BLM model, minimizes the interference between the membrane and support, moreover, provides a close mimic to the actual cell membrane. However, on the other hand, the lack of supporting substrate allows the transmembrane proteins to persist in their mobility within the membrane bilayer suspension [18]. In addition, BLM model membrane systems offer only limited stability and lifetime. This was primarily because they can be easily ruptured and removing residual solvent during the membrane formation process proved problematic [12]. The problem of residual solvent within the phospholipid bilayer meant that it could denature added proteins [19].

1.3.2 Supported Lipid Bilayer (SLBs) Membranes

In order to improve upon the drawbacks associated with BLMs such as residual solvent and limited stability, supported lipid bilayers (SLBs) were produced by Tamm and McConnell in 1985 whereupon a lipid bilayer was created over a solid substrate [20]. Since then, a variety of solid support substrates have been utilized such as glass, mica or silicon, as well as several methods established to employ the SLBs [21, 22].

The main methods applied to form the SLBs involve either the Langmuir-Blodgett technique [23], vesicle deposition [24] or an amalgamation of these techniques [25]. However, applying amphiphilic phospholipids to a solid substrate using the air-water interface method exposes the proteins to the air that, in turn, affects protein activity and leads to protein denaturation [25]. Also, this technique is not conducive to the integration of transmembrane proteins into the lipid bilayer, which could be due to air contact [25].

The vesicle adsorption and fusion method for forming solid SLBs can be prepared by a plethora of methods that use high pressure to extrude vesicles through polycarbonate porous membranes [26]. Also, techniques of sonication and ultracentrifugation of lipid molecules can be utilized to form the vesicles [27]. These mentioned approaches can enable the integration of transmembrane proteins into SLBs within a highly delicate process that is influenced by numerous conditions such as configuration, dimension, charge, surface roughness, pH and the osmotic pressure of the vesicle [28-30].

In SLBs as shown in Figure 1.2, the hydrophilic heads of one bilayer leaflet face the bulk aqueous solution while the corresponding inner membrane leaflet only has a very thin aqueous layer between it and the substrate, which is characteristically 10-20 Å [31, 32].

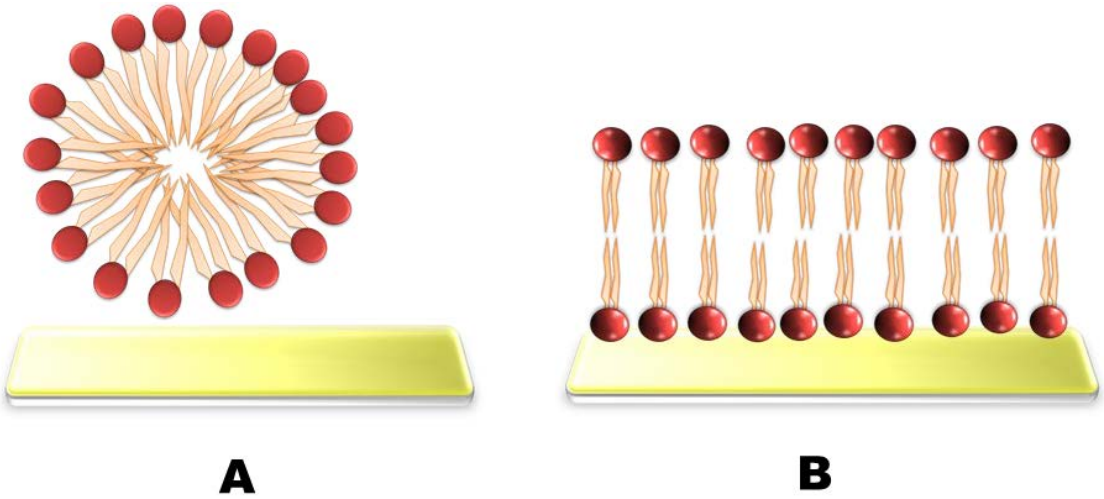

Figure 1.2: A Schematic representation of Supported Lipid Bilayer Membrane (SLB) System. Formation of an SLB can be approached through either vesicle fusion method or the Langmuir-Blodgett technique. In this scheme displayed vesicle fusion technique: (a) Small lipid vesicles introduced to the solid substrate following vesicle adhesion, rupture and fusion started spontaneously over the substrate; (b) Bilayer lipid membrane formed over the solid support. The bilayer lipid membrane separated by ~1 nm water layer over the solid surface. The modified figure was based on [33].

Extensive studies have employed SLB methods in order to examine various biophysical processes. For instance, Stelzle et al., (1993) investigated different protein-lipid membrane interfaces such as streptavidin and *Apismellifera* venom phospholipase A2 (PLA2) using an SLB membrane model. The streptavidin interface with the biotinylated lipids, while PLA2 enzymes interfere with the formation of the intact lipid bilayer membrane. They were able then to distinguish between ligands of pure adsorption and ligands interfaces producing membrane defects. Surface plasmon resonance and impedance spectroscopy were used to determine changes in electrical properties of the membrane. However, the detection sensitivity of this developed sensor was limited and relies on ligand formation over the full covered insulating dielectric layer [34].

Larsson et al. (2003) applied the SLBs approach to detect single DNA strand immobilization and subsequent hybridization by examining the variations in membrane thickness and water content using quartz crystal microbalance and surface Plasmon resonance techniques [35].

In order to better mimic the environment of the native cell, lipid membranes have been employed to coat abiotic surfaces for the enhancement of cell adhesion and spreading. The added advantage of this approach is the ability to efficiently regulate the concentration of incorporated transmembrane proteins and peptides in the bilayer lipid membranes. Hence, this method can provide an in-depth interrogation of the molecular interactions between cell-cell interfaces, for instance, investigation of the signalling and adhesion processes between cells [36]. A number of studies have employed lipid membrane coated electrode methods. Mostly SLB membranes have been utilized for this purpose.

A study by Groves et al. (2001) demonstrated that variable lipid membrane composition has a profound effect on cell binding affinity. For instance, phosphatidylserine lipids promote cell adhesion [37]. While further studies revealed a mixture of positively charged lipids with different percentages of unsaturated lipids as a component of the SLB membrane could improve neuronal cell adhesion [38, 39].

The work by Oliver et al. (2009) demonstrated that the fluidity of lipids has a significant role in cell adhesion induction, as fluid lipid bilayers mostly prevent cell adhesion. Alternatively, using a fixed monolayer lipid membrane promotes epithelial cell attachment and growth. [40]. Svedhem et al. clarified that SLB membranes could be selectively functionalized with an IKVAV peptide motif, that in turn, efficiently promotes

neuroblastic cell attachment and neurite outgrowth [41]. Similar work by Thid et al. revealed that 1% IKVAV peptide was the minimum required level for neural cell attachment and growth on SLB coated SiO_2 surfaces [42]. Bérat et al. shown that SLB can be functionalized by utilizing self-assembled Annexin-A5 peptides as a bridge to anchor peptides that promote cell attachment [43].

Sandrin et al. clarified that 10 nm RGD ligand spacing is the least appropriate spacing to observe attached cells on a substrate. 60 nm was found to be the optimum space between ligands, as mentioned by previous studies [44]. Huang et al. utilized collagen molecules conjugated via amide linkages to SLB, which enhanced cell attachment and reduced nonspecific binding [45]. Ananthanarayanan et al. demonstrated that functionalized bilayer membranes with distinctive design linking the RGD peptide motif supported neural stem cell growth and differentiation into mature neural cells [46]. Zhu et al. later confirmed Ananthanarayanan's et al. results utilizing quartz crystal microbalance [47]. Hu et al. functionalized SLB membranes through the incorporation of cyclic hexa-lipopeptide RGD, through the biotin-mediated anchorage. The authors found the RGD motif sites are highly selective to $\alpha_v\beta_3$ integrin receptors [48].

Pautot et al. found recombinant *glycosylphosphatidylinositol* (GPI) anchored neuroligin bound to flat SLBs induced adhesion of non-neuronal cells. [49]. Likewise, Baksh et al. explored silicon micro beads covered with fluid lipid bilayer membranes that included GPI-linked with the neuroligin, which triggered synapse formation by neuronal cells [50]. Furthermore, Ghosh et al. used SLB membranes functionalized with specific immunoglobulins and showed that this could also enhance neuronal cell adhesion and maintain neuronal viability [51]. Groves and colleagues further demonstrated that lipid

bilayer composition could control neural cell growth and synapses at specific regions on these artificial substrates [52-54].

In summary, the SLB technique permits the implementation of a variety of lipids to compose the membrane and enables the control of lipid asymmetry with insignificant residual solvent [23]. However, SLBs still have some significant drawbacks; these arise from the 10-20 Å thin layer between the bilayer lipid membrane and the underlying substrate surface. This can interfere with transmembrane protein or ion channel insertion as well as diminished protein functionality. Thus the supported substrate surface influences are dominant over lipid-protein interfaces [31]. Further, the volume between the bilayer and the substrate is so small as to reduce the ability of ions to accumulate in the presence of an applied electrical potential limiting the accuracy of impedance measures [55].

1.3.3 Hybrid Bilayer Membranes (HBMs)

Another group of planar bilayer lipid membrane models are the hybrid bilayer membranes (HBMs). A hydrophobic self-assembled monolayer (SAM) coats the substrate, which is followed by the second layer of phospholipids that adhere spontaneously upon introduction of vesicles [56]. This membrane model represents the most straightforward technique for the immobilization of half-membranes. The hydrophilic lipid head groups face the bulk aqueous solution, while the non-polar acyl chains of the lipids are directed toward the hydrophobic surface [57]. Nuzzo and Allara in 1983 were able to deposit methyl-terminated alkanethiols on a gold substrate to yield excellent stability of the designed HBMs [58]. An HBMs membrane model is demonstrated in Figure 1.3.

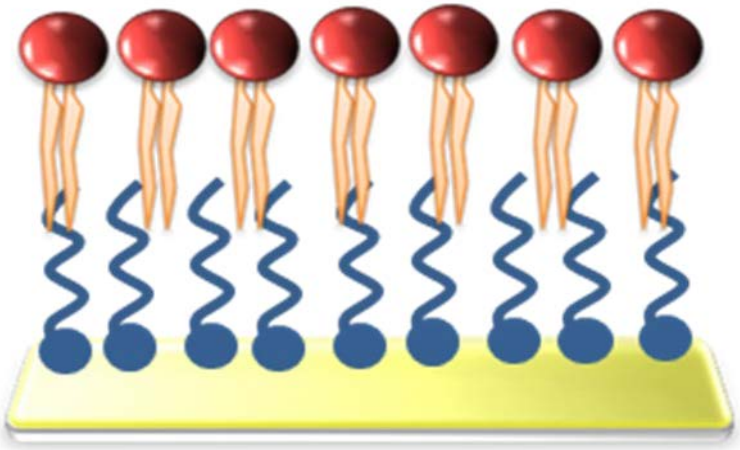

Figure 1.3: A Schematic representation of Hybrid Bilayer Membranes (HBMs) model. The inner layer is self-assembled on the electrode surface with an outer layer of lipid. The modified figure was based on [59].

The first depositing monolayer on the gold surface maintains outstanding mechanical stability and versatility of the HBM system. The major studies over this membrane model were to investigate the analytes that can bind to the outer phospholipid layer of the native membrane. For example, Katja et al. (2002) determined the calcium ion concentration via determining the rate constants and affinity constants of annexin A1 anchoring to phosphatidylserine lipids HBMs interface by means of the quartz crystal microbalance method [60]. Other work by Glazier et al. (2000) demonstrated the pore-forming activity of the protein α-hemolysin by using HBMs and the impedance spectroscopy and voltammetry techniques [61]. A combination of neutron reflectometry techniques with HBM model system was used to reveal the orientation of melittin proteins [62].

In addition, the HBM platform was utilized to develop the Hydrophobic Association Analysis (HBA) sensor chip. This sensor chip assists transmembrane protein examination on BIAcore systems. In this regard, the lipid monolayer included membrane proteins; for instance, variable bacterial selectivity was explored over lipopolysaccharides modified

supported monolayer HBA model by detecting various antibodies and measuring their dissociation rate [63].

However, HBM membrane models have some fundamental shortcomings; the integral component of this system prevents lateral membrane mobility. Consequently, there is a loss of membrane fluidity within the formed lipid monolayer; in turn, phospholipids are usually not sufficiently mobile to allow examination of various transmembrane proteins. Therefore, only limited lipid-protein investigations can be accomplished by employing HBM models [64, 65].

1.3.4 Polymer-cushioned lipid bilayer membranes

With the aim of creating a bio-membrane that can provide lipid mobility with adequate space between the substrate and the lipid bilayer, Sackmann et al. in 1996, established a polymer-cushioned lipid bilayer membrane system [66]. The polymers were employed to act as a 'cushion' between the lipid bilayer and substrate. Soft polymeric constituents provide a greasy layer that, in turn, increase the ability of protein insertion into the bilayer. The mechanism of forming conductive holes within the designed polymer-bilayer followed by spontaneous healing is still not clear. Wagner and Tamm et al. then hypothesized that this phenomenon was due to the polymer smoothed surface facilitating lipid vesicle spreading [67].

In this regard, the polymer cushion selection is a crucial key to this model stability. The tethered polymer required to provide thermodynamic and mechanical stability, in turn, can allow complete wetting amongst surface-hydrated polymer interface [68].

This combination of stability and adequate space between the membrane and substrate surfaces provide distinct advantages over the previous artificial lipid membranes model systems. The offered stability of recombinant proteins within the polymer-cushion lipid bilayers membrane model is a crucial feature replicating natural surroundings of a biological membrane. In this membrane model, ligand-receptor interface experiments are carried out by attaching transmembrane proteins directly to the solid substrate, followed by the introduction of lipid molecules in the surrounding extents [69]. A polymer-cushion lipid bilayers model is demonstrated in Figure 1.4.

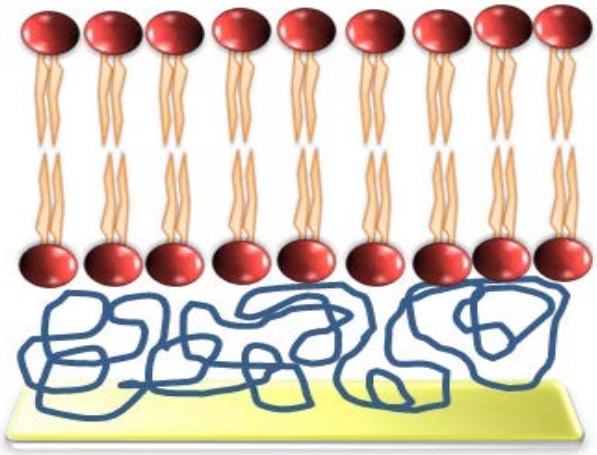

Figure 1.4: A schematic representation of the polymer-cushion lipid bilayers approach. Polymer molecules introduced over the substrate, which is then followed by the addition of lipid bilayer. The lipid bilayer and the polymer cushion are joined via covalent interaction. The modified figure was based on [70].

Several studies have now been published describing the use of polymer-cushion lipid bilayer membrane models to investigate lipid-protein interactions. For example, in 2004, Ataka et al. demonstrated improved stability of an embedded protein by means of employing surface tethered proteins into the lipid bilayer. In this work, cytochrome-C oxidase was immobilized on a chemically modified gold substrate. The chemical surface-tethering presented by the high affinity for Ni-nitrilotriacetic acid (NTA). Briefly, the first monolayer comprised succinimidyl propionate active esters that tethered over the gold

surface. Then, nickel- NTA chelating acid layer created, later histidine-tagged protein adsorbed over this patterned layer. In addition, the cyclic voltammetry technique used to assess the protein's functionality in the membrane model [71]. Further works revealed that diffusion coefficients of integrated protein over polymer-cushion lipid bilayers model were analogous to those assessed for corresponding proteins in actual cell membranes [68, 69]

In addition, polymer-cushion lipid bilayers membrane models have been applied in understanding cellular mechanosensitivity. The substrate stiffness was adjusted via a layer by layer assembly on artificial solid substrates. Ge et al. were able to functionalize a polymer-tethered lipid multi-bilayer with N-cadherin linkers to control the movement and function of anchored cells [72]. The polymer-tethered lipid multi-bilayers facilitate the diffusion of cadherin-based cell-substrate linkages when compared to traditionally used polymeric gel substrates and as a consequence, improved cell movement was achieved [72, 73].

A critical point in the success of this membrane model system has been the preservation of the lateral fluidity of the membranes. However, the main drawback of this system remains the chemical constitution of the polymer chains that likely interfere with transmembrane protein insertion and functionality [59].

1.3.5 Tethered Bilayer Lipid Membranes (tBLMs)

To avoid the previously mentioned drawbacks in planar lipid bilayer model systems, a distinctive approach was established that sought to anchor bilayer lipid membranes over a substrate via a set of tethers. Tethered bilayer lipid membranes (tBLMs) are therefore

considered an improvement on SLBs, where a reservoir is formed between the solid support and the lipid bilayer [74-76].

The tBLM approach can offer a closer mimic to natural lipid membranes in comparison to the other artificial lipid membrane models by virtue of their use of tethering anchors. This unique characteristic is due to the aqueous ionic reservoir expanse between the gold substrate and the subsequently formed membrane that provides sufficient space to incorporate membrane proteins, ion channels or other specific functionalization molecules [77-79]. tBLMs' architectural design avoids the direct attachment of integrated proteins to the solid substrate. Furthermore, this system offers stable bilayers with outstanding electrical sealing properties, which are equivalent to that of live cell membranes [79, 80].

The lipids incorporated in tBLMs can be comprised of a variety of native or synthetic lipids. Several research groups have demonstrated the competence of tBLMs in providing a valuable sensor to detect a variety of targets as well as study the biological processes of a living membrane. Formation via a self-assembly mediated method is revealed in Figure 1.5 below.

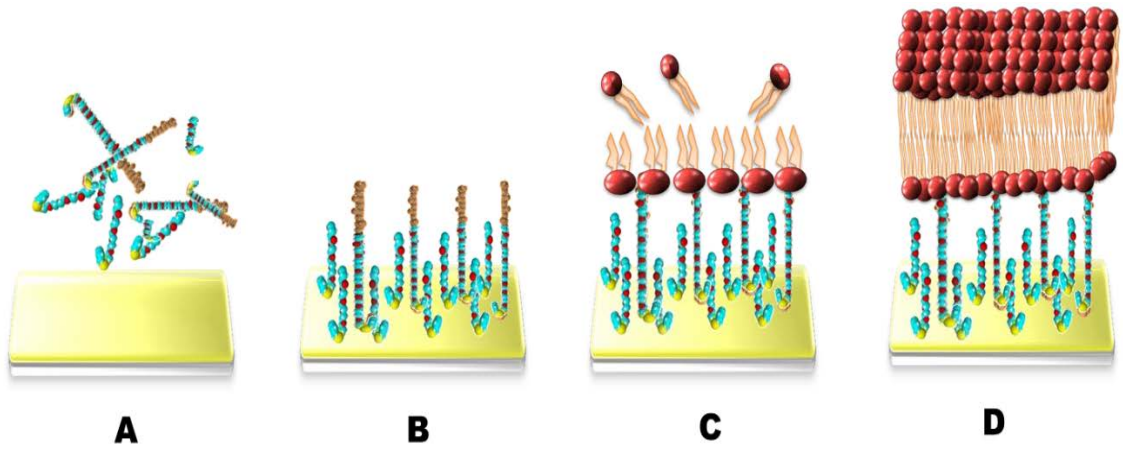

Figure 1.5: Schematic representation of the stepwise, self-assembly driven formation a tethered Bilayer Membrane (tBLM) on a gold substrate. The formation process of

tBLMs comprises several stages: (a) Dipping the gold substrate in an ethanol-mixture solution of spacer and tether molecules; (b) Incubation period allow the spontaneous reaction of benzyl disulfide mixture with gold and subsequently tethers to surface to form the first layer that includes the tether molecules (ethylene glycol groups ended with hydrophobic phytanyl chain) and spacer molecules (ethylene glycol chains ended with a hydroxyl group); (c) Introduction of non-tethered lipids that are dissolved in a solvent in order to form the second layer; (d) Washing the lipids with buffer to form t-BLM by the solvent-exchange method. The modified figure was based on [81].

The inner or bottom leaflet of the lipid bilayer is covalently attached to a surface via the tether molecules, while the upper bilayer leaflet self-assembles, resulting in the phospholipid polar head groups facing the liquid medium phase above the fully formed bilayer membrane. Spacer molecules in varying ratios can be included to create the reservoir, thus increasing the water content to better mimic cytosolic cell characteristics. Further expanding the reservoir area also reduces the frictional coupling between the solid substrate and the bilayer lipid membrane [82].

1.4 Biological applications of tethered bilayer lipid membranes

tBLM model membranes have been a successful platform allowing researchers to gain insights that help to unravel the physical and chemical features of membranes, along with investigating protein-lipid membrane interactions. In addition, they provide a system that can be adapted to serve as a detection sensor for a variety of pharmacological samples, biological molecules and analytes.

This model system maintains outstanding mechanical stability and offers distinct advantages over other artificial lipid membrane systems. A gold electrode is at the core architecture of the tBLMs platform. The chemical properties allow it to be readily

modified with desired biomimetic substrate ligands. Likewise, it provides the electrical impedance spectroscopy functional readout. Electrochemical variations in the tBLMs model such as resistance, conductance and capacitance are critical parameters revealing.any defects within the molecular design of the lipid membrane. This has opened the perspective to investigate the electrical properties and ionic transport phenomena across the developed artificial lipid membrane model. The reservoir area of the tBLM model delivers simultaneous access to the liquid phases by both sides of the membrane bilayer, providing an environment that replicates the actual cell membranes.

The tBLM system, therefore, provides information about several significant biological processes together with a broad range of applications. Below, is a concise review of some of these applications.

1.4.1 Transmembrane protein studies using tBLMs

The robustness, outstanding stability and ease of bilayer formation as well as protein insertion together offer a unique characteristic of tBLMs in order to study variable transmembrane proteins and molecular processes taking place in membranes. Several ion channels or transmembrane proteins have been examined by means of this tBLM approach, for example, voltage-gated ion channels [83-85] and ligand-gated ion channels [86-88] in an aim to investigate and further characteristics the activity of various pharmacological compounds, analytes and new therapies, in addition, to develop selective ion channel nano-biosensors.

Using tBLMs constituted of diphytanyl phosphodatidyl choline, Naumann *et al.* were able to determine the K^+ transport kinetics of valinomycin [89]. Because of its unique ability

to transport K^+ in preference to sodium ions (Na+), valinomycin has been an antibiotic of choice for control use with tBLM architecture function and usefulness [90-94].

In this context, Cornell et al. (1997) were able to incorporate gramicidin-A (gA) ion channels across tBLMs that were further functionalized with antibodies, in order to provide sensing tBLMs platform [79]. gA peptide represented the first ion channel tested using tBLMs. The gA biosensor platform was developed in order to detect variable bio-threats, for instance, detecting influenza virus [95, 96]. This ion channel switch (ICS) nano-biosensor determined by the variation of membrane conduction. Briefly, the architecture comprised two types of gA monomers: mobile within the upper leaflet of membrane bilayer and tethered gA monomers within the lower membrane leaflet, in addition to tethered membrane spanner lipids. The detection mechanism depends on trapping the introduced analyte by transient antibody fragment and stationary membrane spanner lipids, thus can be determined by a significant drop in membrane conduction [79].

Another approach illustrates the feasibility of conducting a single ion channel over tBLMs rather than using the relatively gA simple chemical structure. Keizer et al. were able to assess single ion channel potential and detect analytes in the micromolar range, due to the contribution of the high sealing properties offered by tBLMs membrane model. In this work, researchers integrated the big potassium (BK) ion channel across tBLMs. BK is a highly conductive single ion channel, that can be stimulated by calcium ions and/ or voltage introduction. The organic cation tetraethylammonium that can block BK currents was used to investigate the BK single ion channel activity [97].

In the following ion channel studies using lipid membranes that were tethered to gold electrodes, the activity of chloride intracellular ion channel (CLIC) family proteins was

revealed via evaluating membrane conductance. CLIC proteins represent a unique family of proteins that have dual action as ion channels and as enzymes. This is related to the ability of these proteins to exist as both soluble and membrane-bound forms. The work by Valenzuela and colleagues revealed the dependency of CLIC channel activity on the type and concentration of sterols within the phospholipid bilayer. Consequently, their findings demonstrated the importance of sterols in the lipid membrane to regulate the CLIC protein ion channel activity and membrane insertion [98, 99].

To understand in detail, cellular signal-transduction processes, a study of the gating phenomena (opening and closing) of ion channels were accomplished using tBLM models. Employing impedance spectroscopy and tBLMs technique offered the ability to determine the specific binding between the ligand receptors and targeted antibodies. For example, Stora and co-workers examined the Outer membrane protein (OmpF) porins gating channel that constitutes of trimeric ion channels over Escherichia coli membrane. Results demonstrated the firm binding between the colicinN toxin and OmpF channel. The membrane conductance diminished as a result of the increase of colicinN toxin amount then reached complete blocking of ion channels in values higher than 10μM toxin concentration [100].

Further work has been done to develop the membrane composition of tBLMs to mimic native *E.coli* membrane in order to improve porins stability. This has been achieved by increasing the density of the porins in the tBLMs interface. In the existence of R-domain of colicinN toxin impedance values increased, in turn, confirmed the ability of the embedded protein to bind to specific toxin domains [101].

Similar designs to those of Stora and co-workers were explored by Yin and co-workers, who used various channel blockers to assess alamethicin ion channels activity. Amiloride and other equivalents of channel inhibitors effects have been investigated over alamethicin ion channels incorporated across tBLMs. Electrical impedance spectroscopy results revealed the required concentration of the blocker and their effectiveness [102].

Significantly, α-hemolysin was chosen to be a model protein to compare to other ion channels activity across tBLM models. α-hemolysin from *Staphylococcus aureus* which is a high-resolution pore-forming toxin created an ion channel into tBLM. This can be identified by a distinct increase in membranes conduction [103-105].

A different strategy was conducted for measuring ion channel activity using channel-forming antibiotics or peptides. A study by Becucci et al. (2007) measured the kinetics of ion channel formation across tBLM utilizing the positively charged *monazomycin* antibiotic. Analysis of magnitude impedance vs. time data showed the peptide behavior is represented channel-forming peptides [106]. Similar designs to those experiments were used to evaluate the performance of Melittin molecules, the component of the honey bee venom [106].

1.4.2 Antibiotic and antimicrobial peptides studies using tBLMs

There have been various conventional methods developed to detect pathogenic bacteria. Most of these employ time-consuming strategies such as plating and counting bacterial cells. The tBLM sensing platform has been applied as a new technique that can provide a simple, effective detection method for pathogenic bacteria.

Of these, Tun and co-workers were able to significantly distinguished between bacterial strains that cause disease and non-pathogenic bacterial species by monitoring the electrochemical changes in membrane sealing. The pathogenic toxins of *Staphylococcus aureus* (MSSA476) and *Pseudomonas aeruginosa* (PAO1), also known as their virulence factors, interfere with the outer bilayer of lipid membranes, thus creating imperfections and membrane leakages. A decrease in membrane resistance and amplification of membrane capacitance reflected an impairment in the membrane related to the presence of pathogenic toxins at the bacteria-membrane interface that causes damage to the membrane. On the other hand, the addition of non-pathogenic bacteria such as *E. coli DH5α,* to the tBLMs demonstrated only slight discernible variance in membrane resistance reflecting intact membrane [107].

Another study by Spencelayh et al. (2006) investigated glycopeptide antibiotics such as vancomycin and ramoplanin interaction over tBLMs. These type of antibiotics interfere with the formation of peptidoglycan coatings that protect gram-positive bacteria from lysis. Significantly, the authors were able to use a natural *E. coli* membranes along with a synthesized peptidoglycan cell wall in order to form the lipid membrane. Surface plasmon resonance and impedance spectroscopy were used to determine changes in membrane thickness. The result revealed that the presence of vancomycin caused an increase in membrane thickness as it binds to the peptidoglycan layer [108].

tBLMs as artificial membrane models, provide a close mimic to various native bacterial membranes, thus enabling the examination of different antimicrobial peptide activity. This offers a rapid and sensitive screening technique for pharmaceutical testing and design, in turn, enhance our understanding of these molecular interfaces. Antimicrobial peptides are considered as novel substitutes for standard antibiotics, which also have been

widely studied using tBLM membrane models. For example, a tBLM model was developed to replicate the Gram-negative bacterial outer membrane in order to examine the performance of lipopeptaibol trichogin GA IV amphipathic antimicrobial peptide. The peptide was incorporated within the tBLMs, which permeabilized the lipid bilayer and formed an ion channel. The impedance results studied the ion transport process, which revealed a voltage-gated behavior of the antibiotic monomers upon developing dimers [109].

There have been several more tBLMs models developed to investigate a wide range of antimicrobial peptides. Of these, zwitterionic and negatively-charged lipids employed into tBLM architecture to determine how lipid head-group charges might alter the interaction properties of various biphenyl peptidomimetics. Amongst the studied peptidomimetics compounds, guanidine salt 35d displayed potency to cause membrane disruption due to increased membrane conduction values [110]. There are other small molecular antimicrobial peptidomimetics compounds researched similarly [111].

Likewise, the tBLM platform was used to determine the interface and performance of newly developed antimicrobial peptides. For instance, the interaction of N-sulfonylphenylglyoxamide-based antimicrobial peptides was explored using negative-charged lipids replicating bacterial cell membranes. EIS measurements of tBLM demonstrated an increase in membrane conductance recordings. Thus these compounds were suggested to perform as antimicrobial pore-forming molecules [112]. Recent work by Andersson et al. developed a unique configuration of lipid membranes that mimic the asymmetrical cell wall of gram-negative bacteria. These were used to investigate the colistin antimicrobial peptide-tBLMs interface and subsequent changes in lipid bilayer membrane structure [113].

Niu et al. employed the tBLM platform to investigate the influence of lipid membrane composition on antimicrobial peptide interactions. In this work, variable membrane structures were used that demonstrated the membrane interaction of the synthetic antimicrobial peptide V4, was dependent on the membrane structure. V4 showed an increased binding tendency towards negatively charged lipids, demonstrated by a decline in membrane resistance [114]. Another study by Valincius et al. investigated PLA2 protein interaction with lipid membranes utilizing a tBLMs approach combined with impedance spectroscopy and neutron reflectivity techniques. PLA2 enzymatic activity showed a dose-dependent relationship based on PLA2 and calcium concentrations. The results demonstrated that the destruction rate of tBLMs following injection of PLA2 was much greater in the case of tBLMs constituted with palmitoyloleoylphosphatidylcholine (POPC) lipids compared to tBLMs made with diphytanoylphosphatidylcholine (DPhyPC) lipids [115].

Furthermore, tBLMs has been used as sensor platforms to sense the activity of various pore-forming toxins. For example, the cholesterol-dependent cytolysins represented by *Vaginolysin* bacterial pore-forming toxin was detected utilizing a tBLM sensor [116]. The work demonstrated a distinguishable simple, rapid detection of the very low concentration of *vaginolysin* toxins. EIS recordings showed significant amplification of membrane conductance due to the introduction of *vaginolysin* toxins was cholesterol concentration-dependent. Consequently, the increase of ion permeability causes pore formation into a lipid membrane. However, the detection process occurred in the absence of human complement protein CD5; thus, the method needs further development before it can be used to assess real samples [116].

In other approaches, intensive work has been undertaken using the tBLM platform to examine membrane interactions by various damaging toxins. The adenylate cyclase (CyaA) bacterial toxin from *Bordetella pertussis*, has a unique protein translocation mechanism that inspired researchers to engineer a tBLMs on intracellular calmodulin amine grafted gold surfaces. In this work, researchers studied the CyaA toxin activity within the bilayer lipid membrane utilizing surface plasmon resonance technique. Notably, the results indicate that the translocation of toxin and its insertion into the membrane occurs under specific circumstances mainly: temperatures above 15˚C, particular membrane potential and the existence of calcium. The electrical field was also suggested to motivate the calcium-CyaA dependency towards complete translocation into the membrane [117-120].

1.4.3 Engineered nanomaterials investigations by means of tBLMs

An innovative engineered nanomaterial-lipid membrane interface that mimics the natural surroundings of cells could provide a better understanding of the nanoparticles' characteristics and biological systems. The integration of engineered nanoparticles in biomedical fields mainly arises from their unique properties include straightforward functionalization with specific target molecules, as well as, their suitability for the development of minimally invasive techniques [121]. In addition, they are also being implemented widely in drug delivery, biosensors and nanomedical prosthesis [122].

In order to study nanoparticle interactions with biological systems, the tBLM platform offers a useful platform by which to do this as it both replicates the native membrane components, as well as providing real-time monitoring of the lipid membrane-nanoparticle interactions under controllable and highly sensitive methods. In this regard,

various types of engineered nanoparticles such as silver, silica and polystyrene nanoparticles were investigated using a tBLM membrane model system [123-125].

The implementation of silver nanoparticles are well-known for their antibacterial characteristics [126, 127]. However, silver nanoparticle-mammalian cell interactions can lead to inflammation and protein denaturation [128]. Therefore, in order to investigate the safety of the silver nanoparticles for proposed medical applications, the tBLMs platform was an appropriate means to further investigate. Work by Goreham et al. demonstrated the feasibility of examining silver nanoparticles using a tBLM model combined with impedance spectroscopy and atomic force microscopy techniques. In this work, researchers found that the silver nanoparticles develop weak anchoring with the membrane bilayer without any real diffusion within the lipid bilayer membrane itself [123].

Likewise, the tBLM biomimetic membrane model was used to define the interaction between silica-core nanoparticles and lipid membranes. Silica nanoparticles are widely used in targeted drug delivery due to their versatility [129, 130]. Liu et al. used tBLM to study the silica nanoparticle-lipid membrane interface, in order to determine the mechanism and size of formed pores. In this work, the variable state of silica nanoparticles (amine modified, carboxyl modified and bare) were evaluated using the bilayer lipid membrane and monitored via impedance spectroscopy. All silica nanoparticles with different surface functional groups demonstrated a decrease in membrane resistance with slight discernible variations. In turn, the reaction reflected the disturbance across membrane bilayer owing to the presence of nanoparticle [131].

Similar to the work of Liu et al. described above, further studies conducted by Liu and co-workers [125], who instead used polystyrene engineered nanoparticles to evaluate nanoparticle-lipid membrane interface. In this work, effects of polystyrene nanoparticle (PNP) size and the surface functional group was revealed. Statistical analysis classification was able to discriminate between variable nanoparticle sizes via assessing membrane disturbance parameters; the exponential rate constant and fractional loss of membrane resistance. PNPs coated with amidine functional group prompted nanoparticle aggregation over the tBLM model, while COOH functionalized PNPs disturbed membrane structure with a marked decrease in membrane resistance [125].

In summary, these previously mentioned studies emphasize the versatility of uses for tBLMs. They provide a means by which in-depth investigations of different cell-cell communications, protein-lipid membrane interfaces and nanoparticle-lipid membrane interactions can be studied. Moreover, allow real-time recordings, which can assist in rapid detection methods to screen for various toxins and pharmaceutical compounds. The tBLM is a construct that provides a foundation for addressing most of the problems faced by the latest generation of implantable medical device electrodes. Fabricating and characterising these tBLMs introduces the essential nature of a well-sealed membrane to contain ion gradients. Leakage pathways between cells are in the order of a few Ω/cm^2 reinforcing the reality that in the absence of a well-sealed contact to a target cell, little or no ion gradient will be available to stimulate that cell. Similarly, the ion fluxes and gradients from a distant isolated cell will soon dissipate and be lost preventing detection at an electrode. tBLMs can be fabricated containing cell adhesion molecules, integrins, and cadherins selectins in their outer surface. Therefore, there remain enormous opportunities to use the tBLM approach to convert membrane binding events and

alterations in membrane structure into detectable electrical signals at the nanometer scale. Examples of such constructs are the major objective of this dissertation

1.5 Electrical Impedance Spectroscopy (EIS)

Electrical impedance spectroscopy is a common technique used to explore the characteristics of various substrates. The technique measures the total effective impedance that results from an alternating current (AC) signal [132]. The implementation of slight sinusoidal current or voltage (20-50 mV) provides a real-time and non-invasive versatile approach.

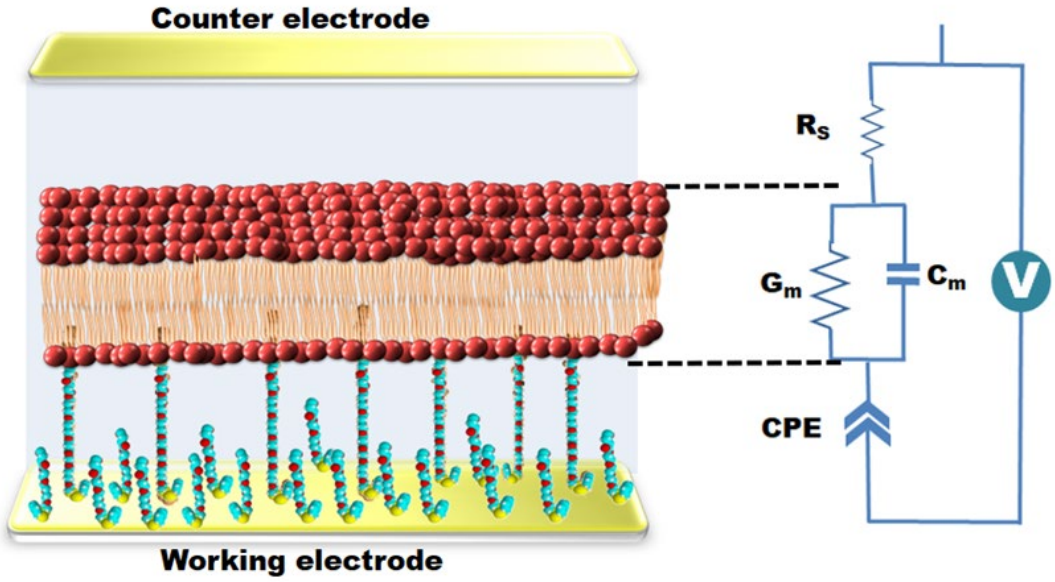

Figure 1.6: Representative model of the tBLMs equivalent circuit. AC voltage potentials, typically 20-50 mV peak-to-peak, are applied across a wide frequency range (typically 0.1 Hz-2000 Hz). The variable impedance parameter is fitted to an equivalent circuit such as the one depicted. In this equivalent circuit, the constant phase element (CPE) represents imperfect reservoir capacitance, which is a result of the impeded motions of the ions over the gold surface by the tethering chemistries. Membrane conductance is represented by G_m. C_m is the membrane capacitance, whilst R_s is the resistance of the electrolyte solution surrounding the membrane. The figure was modified from [93, 133].

EIS can be utilized to determine the membrane conduction and capacitance of artificial tBLMs when employing a relevant equivalent electrical circuit. Membrane conductance (G_m) studies provide information about the ability of membranes to pass ions (membrane permeability) as well as providing information on ion channel activity through ion channels proteins that are embedded within tBLMs. Membrane capacitance (C_m) is a measure of membrane thickness and/ or water content. An increase in G_m reflects a rise in ion transfer, in other words, an increase in membrane permeability, whilst rise in C_m indicates a *decrease* in membrane thicknesses; illustrated in Figure 1.6 [74, 134].

At low frequencies such as 1 Hz, the double-layer capacitance or Helmholtz capacitance is predominant, where there is a charge build-up at sulfur-gold interface. While at midrange frequencies such as 1 kHz, the membrane capacitance is predominant, where capacitance reflecting the tethered membrane capacitance and thus the membrane thickness. Whereas at high frequencies such as 100 MHz, the solution resistance is dominant, which represents the resistance to ion movement in the outside solution. Thus at very high frequencies, the capacitance is reduced because the ions have insufficient time to migrate between the electrode and cell membrane [133, 135].

In addition to being used for tBLMs investigations, EIS can be used in tissue culture conditions to monitor cell adhesion, and cell movement over time [136]. By introducing a relatively high-frequency AC potential to the electrodes and measuring the voltage change by a phase-sensitive impedance spectrometer, the magnitude of the impedance over a range of frequencies can be correlated to the amount of cells adhered to the electrode [137, 138]. Cells layer coverage over the modified electrode will impede the current and, in turn, increase the overall electrode impedance [137, 138]. An electrical cell-substrate impedance sensor (ECIS) was established three decades ago by the Giaever

and Keese in 1991 [139]. A schematic illustration of the ECIS measurement system is displayed in Figure 1.7.

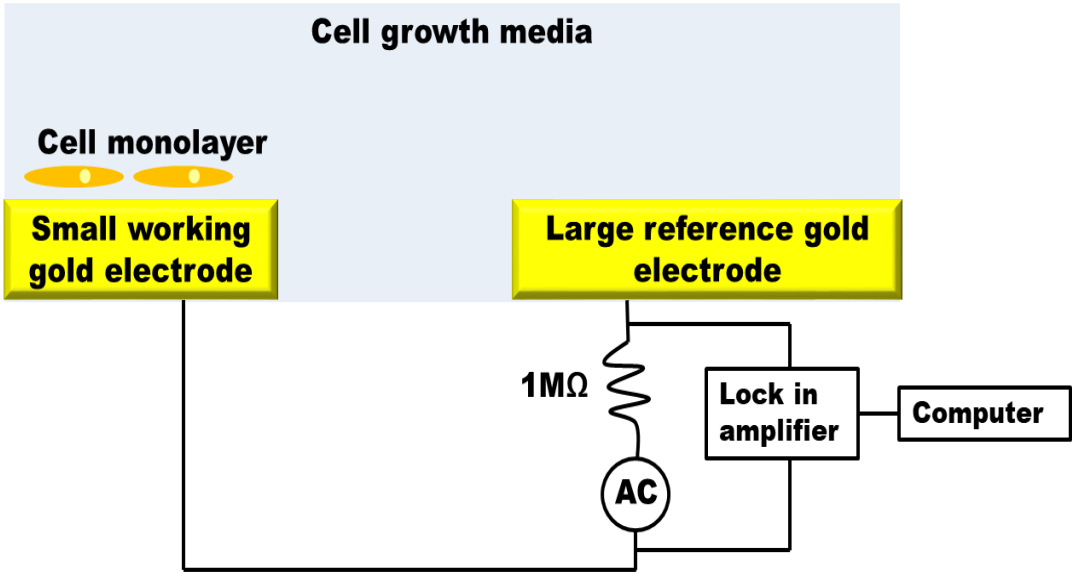

Figure 1.7: A representative figure of the ECIS measurement system. The adapted figure was based on [138].

ECIS provides quantitative evidence about morphological and locomotion characteristics of the cells illustrated in Figure 1.8.

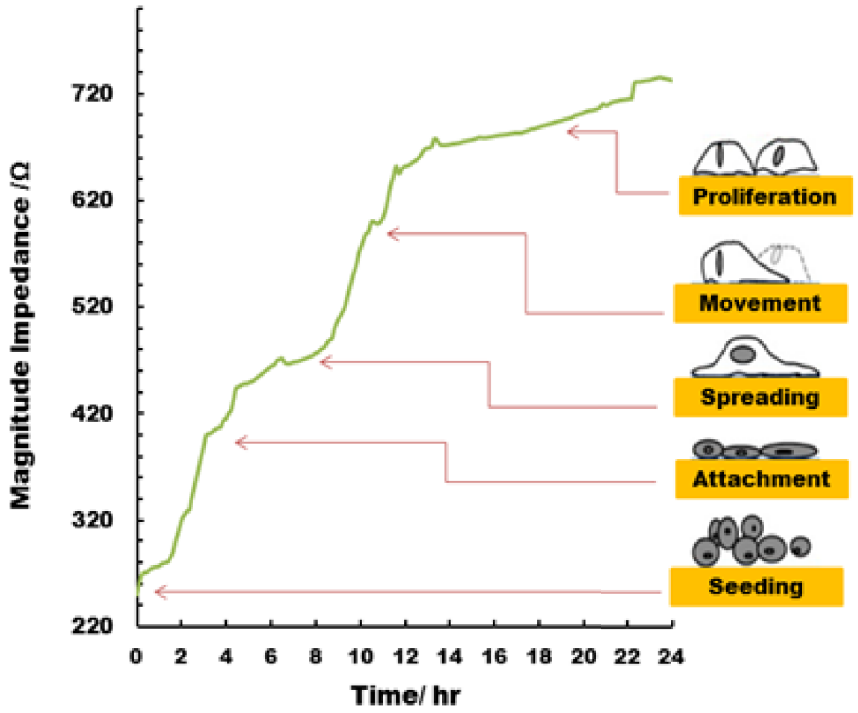

Figure 1.8: A typical magnitude impedance values of epithelial cell attachment and proliferation diagram. The time course of impedance spectroscopy is equivalent to

monitoring various stages of cells adhesion and spreading. Firstly seeding cells, then cell attachment, spreading, migration and proliferation. The modified figure was based on [140].

Using EIS techniques requires some understanding of basic electrical circuit theory. For direct current identification, Ohm's Law can be used to describe the relationship between resistance, current and potential [141]:

$$R_{(t)} = \frac{V_{(t)}}{I_{(t)}}$$

Here, R is the resistance, I the current, V the voltage; all as a function of time (t).

The complex *impedance* (Z) is assessing the tendency of an electric system to resist current movement in an alternating current (AC) circuit. In a perfectly resistive system, the current and voltage are in the same phase of AC circuits. However, in the ordinary AC circuits, the electric current components *reactance (X)* and resistance (R) lead to a shift in phase amongst the electric current and voltage. Therefore, magnitude impedance (|Z|) calculated by measuring the phase shift φ between these mentioned parameters, illustrated in Figure 1.9.

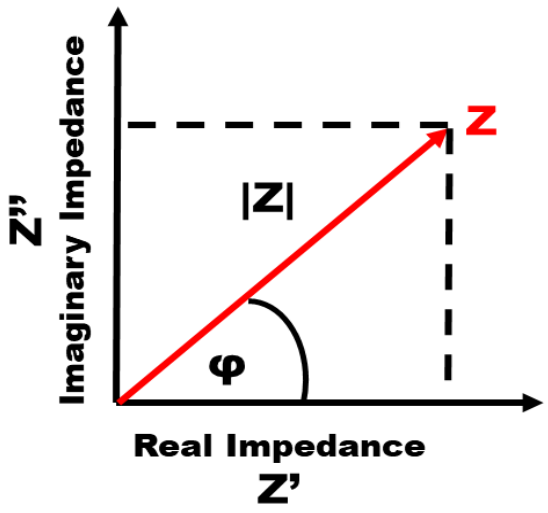

Figure 1.9: Arithmetical illustration of Z in a complex plane. X-axis represented a real impedance, while y-axis represented the imaginary impedance. The magnitude of

impedance $|Z|$ is determined by the length of the vector. The phase shift φ among voltage and an electric current is represented by the angle between $|Z|$ vector and the x-axis.

Hence, complex impedance Z can be determined by the sum of real and imaginary impedance as followed:

$$Z = Z' + {}_{i}Z''$$

Here, Z' is the *real* part of the impedance and ${}_{i}Z''$ the *imaginary* part; all as a function of frequency [142].

When measuring the impedance of cells populating an electrode, an equivalent electrical circuit model can be described using an amalgamation of resistors and capacitors. The transmembrane proteins and ion channels can be represented as a resistor, whereas the cell phospholipid bilayer membrane has properties of a capacitor in parallel to the aforementioned resistor. In series with this will be the capacitance of the gold electrodes [143, 144].

The circuit requires a reference electrode to close the circuit. However, the vast reference electrode impedance (Z_c) reading is insignificant in comparison to the small working electrode measurement [145]. This kind of electrode is called a *monopolar electrode*, as the impedance is calculated from the working electrode only, while the reference electrodes are large in size in comparison to the working electrodes in order to ensure no current limitations arise [146].

EIS signals are highly sensitive to any nonspecific adsorptions that diverge the current pathway above the electrode, which can arise from functionalized layer defects, in comparison to other methods such as *surface plasmon resonance* (SPR) [147]. Measuring

impedances over a range of frequencies can aid in the discrimination of junctional impedances and impedance initiated by cell-substrate interactions [148].

Also, the impedance value relies on the applied frequency and current behavior. The live cells intracellular spaces assumed to be a resistor in series with a lipid membrane of cells, which assumed to be a capacitor due to the accumulation of ionic species. Thus the changing of impedance is dominated by the cell membrane (the capacitor), whereas the cell-electrode interface represents the non-ideal capacitive behaviour which defined as a constant phase element (CPE) [149]. At a low frequency (less than 2 kHz), the current flow is strongly influenced by the high resistivity of cells capacitance components; thus the current mainly pass through the gaps between neighbouring cells and the medium, outlined in Figure 1.10 [150, 151].

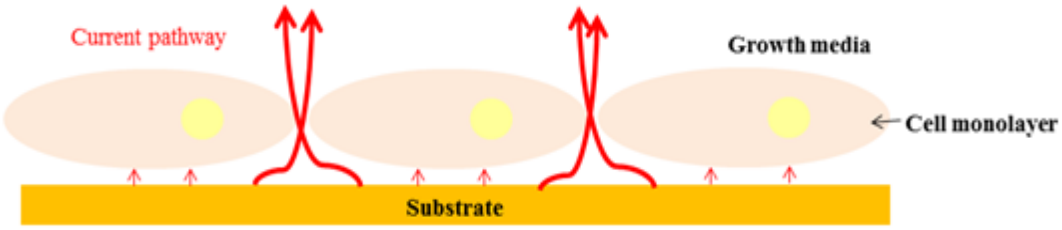

Figure 1.10: The AC current pathway at low frequencies within cell monolayer (EIS method). At low frequencies (such as ~100 Hz) the lipid membrane prevents the current to enter inside the cell, so the dominant influence on the current profile are the gaps between neighboring cells and any ion channels within cell membranes, symbolized by bold arrows. The adapted figure was based on [152].

At higher frequencies (~ 40 kHz), the measured impedance is dominated by resistive elements rather than capacitive elements, the membrane capacitance becomes negligible, and the current capacitively couples directly through the insulating cell membranes and consequently can enter the intracellular area by passing through the membrane. These higher frequencies can then be used to provide a simple measure of overall cell coverage over the electrode (Figure 1.11) [150, 151, 153].

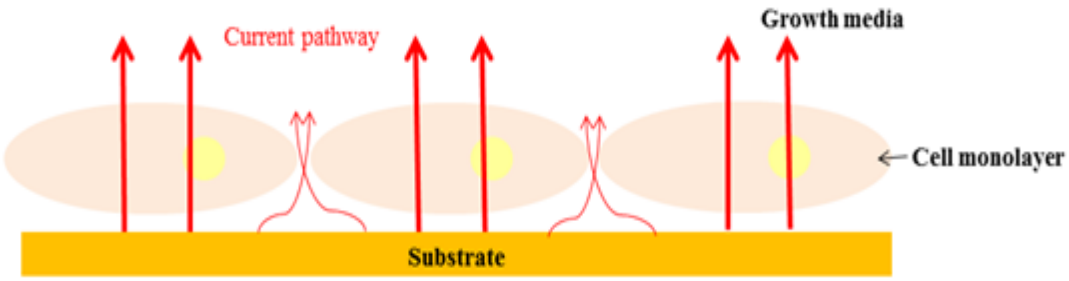

Figure 1.11: The AC current pathway at high frequencies within cell monolayer (ECIS method). At very high frequencies, such as 40 kHz, current crosses the cell membrane and pass in the intracellular space, so the current is considered to be more a measure of cell coverage across the electrode. The adapted figure was based on [152].

1.6 Aims and Significance of this thesis

Engineered lipid membranes are appealing to many research interests, particularly the sparsely tethered membranes constructs provide the closest analogues yet devised of natural biological membranes, in developing biosensors that provide close resemblance to natural cell membranes. In addition, tBLMs offer solutions to create a new generation of active implantable medical devices, such devices promise unprecedented advances in restoring or enhancing human capabilities and more significantly, in redesigning the maintenance of human health. Research into tBLMs address the nanometre-scale integration of external electronics with the medical diagnostics and pharmaceutical therapeutics which is at the core of this dissertation. Therefore, this thesis aims to integrate tBLMs technology beyond their typical utility as a peptide-membrane interaction assay system.

Here, three different studies were explored; namely:

1. Attempting to improve implantable technologies by optimizing the specificity and efficiency between electrode-cell interfaces.

2. The development of an ion-channel switch nano-biosensor for direct cell detection.

3. The development of a real-time monitoring device for the study of heat transfer between gold nanoparticles and lipid membranes, used in hyperthermia based treatments.

1.6.1 Improving implantable technologies by optimizing the specificity and efficiency between electrode-cell interfaces

Our first study was investigating the feasibility of tBLMs improving implantable technologies. Making the necessary close contact between the electrode and the cell plasma membrane has always been a challenge for existing procedures that aim to simultaneously stimulate while also detecting ionic currents from neuronal cells and other electrically active cells. Ideally, enhanced interfacial connectivity should diminish leakage pathways between target cells and the reading or stimulating electrode as well as between adjoining cells.

The hypotheses for this work were:

1. That intimate cell contact and targeted communication can improve the selectivity and sensitivity of the electrodes that are employed to stimulate and monitor cell activity *in vitro* and *in vivo*.
2. That this can be achieved via coating the gold surface electrode with novel tethered bilayer membranes (tBLMs) technologies. The tBLMs will provide more efficient cell-surface crosstalk points, by mimicking the natural cellular environment and thus improving cell-electrode attachment and interfacing.

Accordingly, the aims of this part of the research were to:

Aim 1: Prepare biocompatible and functional electrode coatings.

To achieve this aim, this project sought to create a range of coating modifications onto the gold electrodes for the subsequent selection of the most appropriate substrate functionalization, which significantly enhanced cell attachment and proliferation and biocompatibility.

Aim 2: Testing cell attachment and communication of electrode coatings.

To address this aim, the research investigated the cell and substrate interface and attachment, assessed by using impedance spectroscopy over a range of frequencies. Localized electrode-cell intimate contact and communication could then assist in effective cell action, potential stimulation and cell monitoring. Cell viability and proliferation was assessed. Imaging of cells was undertaken to check cell morphology and immunochemistry and Western blotting used to probe for any physiological changes.

Aim 3: Enhance electrode efficiency.

This aim sought to functionalize and modify the chemistry of tethered bilayer membranes to improve signal conduction for cell-based electrical devices. This aim also sought to discern the optimal surface modifications possible that would produce the minimal ion leakage pathway.

The ultimate significance of this part of the project would put us on the path to improving the quality of life for those individuals who are visually and/or hearing impaired. By developing an advanced interface that enhances efficiency and direct communication with

biological neuronal tissue, biomedical devices such as cochlear and retinal implants would be able to employ more localized electrodes without the risk of significant cross-talk, improving implant fidelity.

1.6.2 Developing ion-channel switch nano-biosensors for direct cell detection

The second study explored during this Ph.D. project was impedance sensors based on the tBLMs nanoswitch biosensor in order to detect specific cell types from within a heterogeneous cell population. In 1997 Cornell et al. were able to incorporate gramicidin-A (gA) molecules to act as a nanosensor switch [79]. Using this same technology, we aimed to study the characterization of ion-channel switch tBLMs in order to develop an anion channel switch nano-biosensor for cell detection. Developing the ion channel nano-biosensor approach for cell detection could provide a new label-free, a discriminative and sensitive technique for variable cell detection. This aim specifically sought to develop a highly sensitive nano-biosensor that could detect as few as 10,000 cells/ mL using a gramicidin-A ion sensor switch. Adherent and non-adherent cells would be identified by cell-specific functionalization that mimics biological sensory function.

Accordingly, the aims of this part of the research were to:

Aim 1: Identify and characterize the architecture of ion-channel switch tBLMs utilizing electrical impedance spectroscopy and neutron reflectometry approach method to determine their suitability for cell detection

This aim sought to investigate the streptavidin-biotin-gramicidin monomer interface.

Aim 2: Specifically functionalize the ion nanosensor switch and test for its capability of detecting cells.

This aim sought to employ cell-specific functionalizations to detect variant cell types such as adherent and non-adherent cells. RGD peptide and concanavalin-A polysaccharide were applied for the biosensing interface in order to provide close mimic to the natural environment of membrane-membrane contacts. In addition, this approach will offer promising outlooks for the study of complex cell populations, including the detection and identification of the specific type of cells, for example, cancerous cells.

1.6.3 Real-time monitoring of heat transfer between gold nanoparticles and tethered bilayer lipid membranes

The third study tested the hyperthermia phenomena from irradiated gold nanoparticles (GNPs) over tBLMs, given that assessing the direct consequences of the laser-induced heating phenomena of embedded GNPs in biological tissues is challenging. An innovative nanomaterial-electrode interface that mimics a cell's membrane and the natural surroundings of cells, serves as a model to better understand the heat transfer characteristics of irradiated gold nanoparticles within biological systems.

Accordingly, the aims of this part of the research were to:

Aim 1: Create a platform by which laser-irradiation of gold nanoparticles could occur simultaneously with electrochemical impedance spectroscopy recordings.

In order to investigate the induced hyperthermia responses by nanoparticles at a lipid bilayer interface, a suitable platform that enabled nanoparticles to be irradiated when added to preformed tBLMs, needed to be developed.

Aim 2: Obtain real-time measurements of localized heating from GNPs irradiated by lasers using various tBLM architectures.

This aim used tBLMs of differing architectures that can differentially induce the attachment of gold nanoparticles to the membrane surface. Such architectures include ion channel and varying lipid composition. Using these architectures, experiments were undertaken and results compared to thermal predictive mathematical models to demonstrate the utility of the technique for measuring heat transfer characteristic.

Chapter 2

The ionic to electronic interface: key challenge to improving implantable medical devices

Chapter 2

The ionic to electronic interface: key challenge to improving implantable medical devices

2.1 Introduction

The interface between natural biologically active cells such as neurons, with electronically conductive electrodes is a major challenge to detecting and stimulating the sensing and signaling pathways in the body. The challenge is to devise biocompatible materials that are capable of selectively binding to specific cell surfaces and to permit the measurement of ionic fluxes at the cell surface or alternatively to generate ion fluxes at that surface to trigger an action potential in an active cell. This capability is crucial for developing implanted devices such as cardiac pacemakers, cochlear implants, retinal implants and any other device aimed at compensating or replacing missing cellular functions, through artificially monitoring and stimulating neuronal or other body cells. The field remains in its infancy with there being few examples of a bio interfacial architecture that remotely equates to the efficiency of natural intercellular communication [154, 155]. There remain many significant challenges to overcome in order to establish stable and functionally predictable interactions between these distinct components.

The interface between the cell and the electrode should aim to mimic the natural biochemical environment of the target cells, by offering proper transmission of electrical signals to specific neurons in the brain [156]. Accordingly, the interface relies on the ability of electrodes to transduce sensitive, stable stimuli and transfer efficient charges as electrical patterns to the relevant cells. Furthermore, electrodes should be soft,

biocompatible, non-toxic, mechanically-matched interface and stable and preserve the physiological properties of the target tissue, while at the same time, encourage cellular attachment, cell survival and cell proliferation [157, 158].

There are still various challenges that need to be overcome before the effective application of electrode bio-implants is achieved. For instance, obtaining the necessary contiguous contact between the electrode and the plasma membrane of cells has always been a challenge to existing procedures for stimulating and reading ionic currents in neurons and other electrically active cells.

An appropriate interface should reduce leakage pathways between target cells and electrode as well as among adjoining cells to avoid electrophoretic ion currents being lost into the interstitial medium before arriving at the reading electrode [159]. A biocompatible electrode coating that permits localized electrode-cell intimate contact and communication will improve the selectivity and sensitivity of electrodes that are employed to stimulate and monitor cell activity *in vitro* and *in vivo*.

This chapter delivers an outline of the history and development of retinal and cochlear implant technologies. In addition, the key points of understanding the interfacing and adhesion of neuronal cells as well as describing variable abiotic surfaces and the feasibility to regulate cell attachment and growth onto these modified electrodes are discussed.

Experiments were employed to examine the effect of various coatings, namely fibronectin, PEG-RGD, POEGA-RGD and bare tBLMs on promoting cell growth, attachment and biocompatibility. During these experiments, impedance spectroscopy along with imaging of cells was undertaken to define the efficacy of coatings.

Furthermore, this chapter studies the feasibility of using the tBLMs coated onto gold electrodes to enhance electrode-cell localized contact and communication.

2.1 Development of implants and recent applications

2.1.1 Retinal implant technologies

Retinal implants were designed to restore missing photoreceptor cell function in people who have lost their vision due to degenerative eye conditions, for example, age-related macular degeneration and retinitis pigmentosa [160]. The prosthesis is implanted in one eye and operates by inducing activity in any remaining undamaged retinal ganglion cells [161]. Retinal electrode arrays deliver intense electrical pulses at various sites within the retina. These pulses correlate with the brightness of the scene at that location. As a consequence, visual perceptions can arise via the surviving retinal cells that become stimulated. This serves to provide the implanted person with a sense of light intensity but no fine visual definition [162-164].

Different sites of electrode implantation have also been trialed in order to provide improved visualization. These include suprachoroidal (between the sclera and choroid), subretinal (under the retina), and epiretinal (on the top surface of the retina), each with varying levels of success (Figure 1.1) [165, 166].

In 1956, Tassicker outlined the first retinal prosthesis [167], which was followed by Brindley and Lewin in 1968, who found that direct electrical stimulation of the visual cortex introduces visual percepts [168]. In the 1990s, retinal implant research expanded rapidly, including studies where electrical current pulses were applied to stimulate the implanted multi-electrode array on the retina of blind subjects [169, 170]. Humayun and

colleagues demonstrated that electrical stimulation of specific sites at the retina in healthy and blind persons could produce steady visual sensation [169, 171, 172].

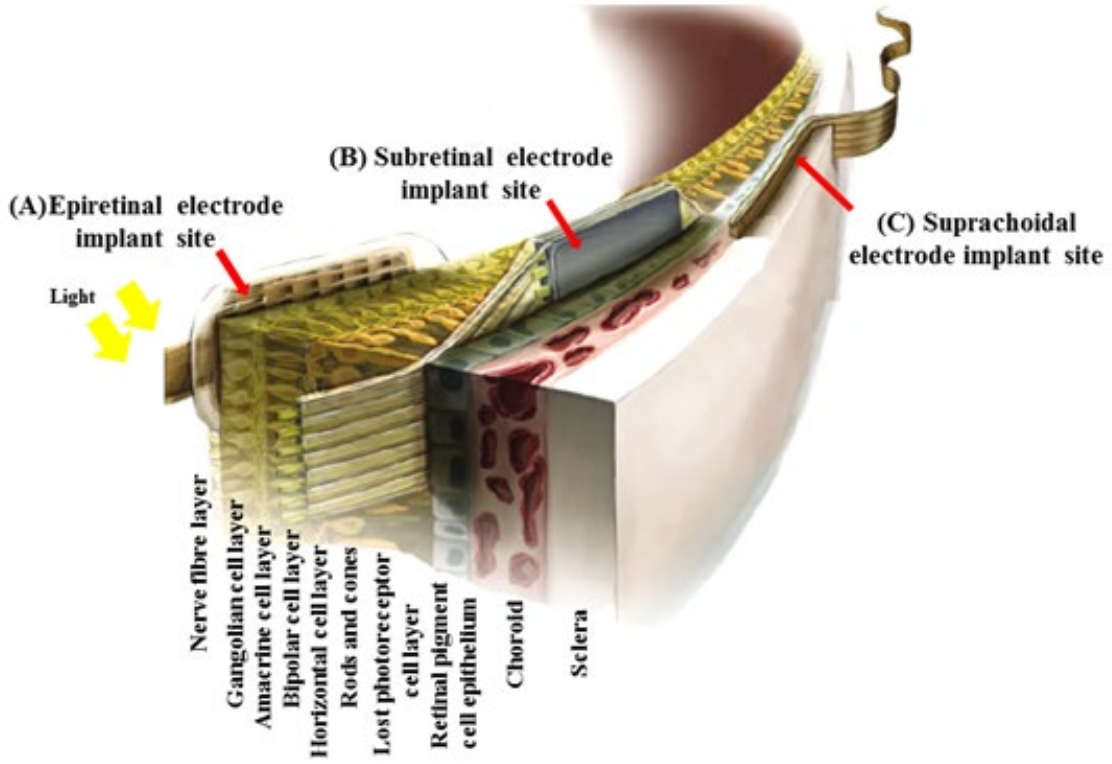

Figure 2.1: Overview of the diverse sites of retinal electrode implantation locations. (A) The epiretinal implant electrode site between in fibers of the inner retinal ganglion cells and nerve fiber layer; (B) Subretinal placement positioned on the retinal pigment epithelium at the contacting side of the lost photoreceptor cells. Photodiodes respond to the light signal, which triggers electrodes to stimulate bipolar cells, which, in turn, induce the optic nerve to process the signal; (C) Suprachoroidal electrodes are present in the posterior part of the eye between the choroid and sclera; thus, electrodes directly stimulated retinal ganglion cells. The modified figure was based on [173].

In 2002, the first retinal prosthetic implants termed *Argus I* began with 16 implanted electrodes at the epiretinal site, relying on the direct ganglion cell stimuli in addition to an external digital camera [174]. This digital camera with special sensors mimics the photoreceptor arrangements of the retina, which gives rise to the possibility of extracting meaningful artificial three-dimensional data from the captured pictures [173, 175]. Later, in 2011, the next generation of platinum-coated epiretinal electrodes, *Argus II*, with 60

stimulating electrodes were approved for marketing after effective implantation in thirty subjects [176, 177]. In 2012, diamond-based suprachoroidal 20 stimulating electrode array retinal implants were developed by Bionic Vision Australia [175, 178]. In 2013, the subretinal Alpha-Institute for the Microelectronics Stuttgart (Alpha IMS) prosthetic device was approved. Alpha IMS implants target the photoreceptor cells that keep the regular eye movement intact. This included 16 stimulating electrodes and 1500 units of a multi-photodiode array with the amplifier. The light-sensing microphotodiode captures images instead of the external camera, unlike other current utilized devices [179-181].

Stimulator implantable metal electrodes are facing a thin membrane between electrode and nerve cells [182]. Further, electrodes are typically fabricated from noble metals such as iridium, platinum or gold. This is related to their fundamental resistance to corrosion and destruction. However, the use of noble metals means there is capacitive coupling at the electrode surface which limits their utility with regards to being able to apply extended DC potentials in comparison to redox metals such as silver or silver chloride [74, 183].

Importantly, electrodes should provide robust electrical pulses to induce action potentials by the targeted neuronal cells, while at the same time preserving the electrode constituent and surrounding neuronal tissue [184].

Noteworthy though, the temporal resolution is much less in implanted persons (less than 3 Hz) in comparison to normal vision (nearly 20 Hz). This reduced resolution is related to direct membrane depolarization instead of releasing an ordinary neurotransmitter to stimulate the remaining retinal cells [173, 185].

The key critical parameters to consider when assessing the spatial resolution of implanted electrodes are electrode dimension, topography, arrangement, and the expanse gap

between the target cell and the electrode. Mathematical modeling has demonstrated the three-dimensional resolution of electrodes, in particular, will decrease in the case where there is a significant distance from the electrode site to the target cells [186]. There are inventive attempts to improve the temporal resolution using the repetitive frequency of electrical implants to mimic the native rod and cone cell frequency of the human eye [173, 187]. Using three-dimensional electrodes is also promising in the improvement of spatial resolution to enhance the visual angle. The 3D architecture will increase the surface area of the electrode at the same time attempt to keep diameter comparative with the original cone-diameter [173, 188].

At present, all current retinal implants provide little improvement in the vision of the subjects who use these prosthetic devices. The provided benefit to the subject is largely to allow them to detect objects and improve their orientation to assist with mobility [176].

Innovative studies are currently being designed to deliver extremely precise and accurate electrical induction toward the targeted cells. This is within improved safety frameworks to protect the surrounding sensitive retinal neurons from damage in order to achieve a greater degree of functional vision [182, 187]. These continuing studies include exploiting new novel electrode materials with the aim of achieving a close mimic to natural vision. For instance, the semi-conductive nanocrystalline diamond used to improve the biocompatibility, safety, and durability of implanted devices [182].

There, therefore, remain essential outstanding challenges to be overcome in currently implementable retinal technologies, in order to enhance the visual acuity of visually impaired patients.

2.1.2 Cochlear implant technologies

Cochlear implants were proposed to restore hearing functions by compensating for hair cells loss and spiral ganglion cell degeneration in people who are severely hard of hearing or are totally deaf [189, 190]. An introduced electrical current can directly stimulate surviving spiral ganglion neurons of the cochlear nerve creating an auditory sensation [191, 192].

The mechanism and process of natural hearing relies on the transformation of sound waves into nerve impulses and, as a consequence, translated by the brain into understandable sound. Briefly, sound waves pass the outer part of the ear to inside the ear canal until they arrive at the eardrum. The tympanic membrane will vibrate according to the sound frequency delivering airwaves to middle ear bones. These airwave vibrations convert into fluid waves when passing through the oval window membrane that, in turn, induces liquid wave tension inside the cochlea. At this point, movements of fluid in the cochlea prompt outer hair cells to bend in response to the fluid pressure, which will amplify the fluid vibration into specific frequencies. The inner hair cells are tethered to mechanoreceptors that will transform this mechanical vibration into graded action potentials according to the amount of fluid tension. As a consequence, it will induce electrical signals within the auditory nerve that are then interpreted by the brain as sound [193-195].

In the late 18th century, the first documented electrical stimulation experiment of the auditory system was performed by Alessandro Volta. The author applied a large voltage from a battery connected to two metal rods across his ears. This led to the generation of auditory sensation, which was described as crackling or bubbling [196]. Much later,

cochlear implant research extended to improve sound quality and efficiency. In the 1970s, patients were implanted with a single-channel cochlear implant that was only of benefit to the profoundly deaf. This early design implant performed by sending electrical impulses to a single area within the cochlea that resulted in stimulation of all nerve fibres.

The persons implanted with single-channel electrodes could distinguish one word from a small word set (less than three words) [197, 198]. In the 1980s multichannel cochlear implants were developed with the ability to convey electrical induction to multiple sites of the cochlea. This has benefited both profoundly deaf and severely hard of hearing individuals [199]. The multichannel cochlear implants were able to produce open-set word identification. As a result, people with an implant could recognize more than three words from speech. Multiple electrodes also enhanced the number of distinct frequency bands in comparison to single-channel devices [200, 201]. In the 2000s speech processor, electronics, and other strategies were developed and improved. Speech processors have become much smaller in size, more convenient and convey higher electrical pulses with variable frequency bands [202]. The currently used cochlear implant devices principally consist of a multi-channel electrode with variable implant numbers, an audio processor and an implanted receiver-stimulator [203]. Figure 1.2 illustrates the cochlear implant electrode components.

Current studies are focusing on achieving enhanced implanted electrodes that can keep implants without the need for replacement after a period of time [204]. Diverse surface biotechnology approaches are being developed for the cochlear implants as are strategies to improve the frequency resolution, induction of neurite expansion toward bone structure, and the implant-tissue interface [205-207]. Tan et al. recently summarized the evolving surface biotechnology of cochlear implants. These new technologies include

modification of the electrode surface coating by using variable electrical conductive polymer and anti-scarring agents. They also include mechanical electrode topography alterations; for instance, increased electrode surface roughness was demonstrated a significant reduction on bacterial adherence to the modified surface in comparison to smooth surfaces [208-210]. Moreover, modifying an implanted surface with a polypyrrole conductive polymer improved neurite outgrowth and at the same time, minimized spiral ganglion neuron degradation, which results from the lost hair cell protection. Polypyrrole polymers serve to store neurotrophins, and their discharge can occur via electrical stimulus [211, 212].

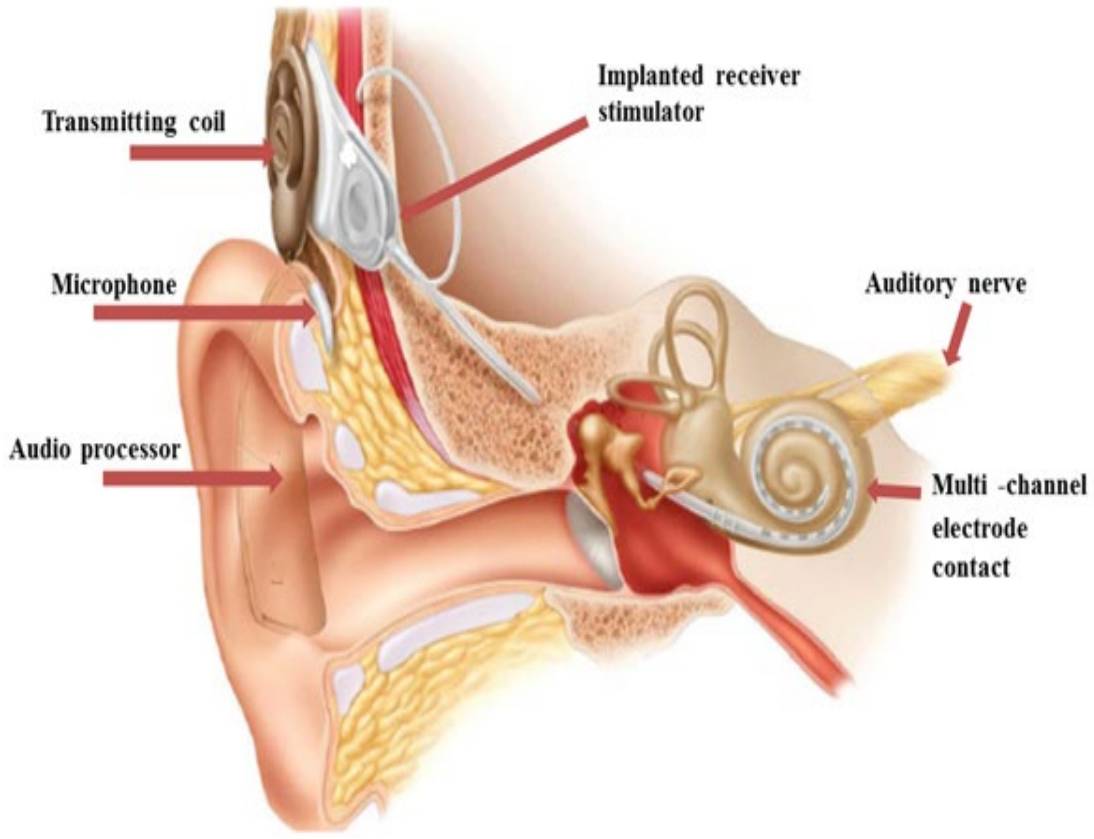

Figure 2.2: Schematic representation of multiple-channel cochlear implant electrode components. The multiple-channel cochlear implant electrode includes a microphone that gathers the sound from the surroundings and an audio processor that collects sounds and transforms it into a digital frequency signal. A transmitting coil sends the electrical

current and transmits the data to the internal implant. The implanted receiver-stimulator translates the wireless frequency signals conveyed from the audio processor into electrical induction, which then induces the auditory nerve. The multi-channel electrode changes signals to electrical energy that make contact with the cochlea. This electrode is usually implanted at the *modiolus* in the scala tympani adjacent to the targeted spiral ganglion cells. The modified figure was based on [203].

Bohl et al. have made a promising development by using cochlear implanted electrodes that improve spiral ganglion cell growth and diminished fibrosis. This was achieved *in vitro* by specific functionalization of the electrode surface. Included was a poly4-hydroxybutyrate biodegradable polymer layer, that can dispense anti-inflammatory drugs and nerve growth factors in order to enhance nerve cell proliferation [213].

A noteworthy new direction in cochlear implantation is the utilization of electrodes that act via optical stimulation. As an alternative to electrodes that depolarize the remaining spiral ganglion cells through electrical current induction, optical induction stimulates auditory neurons mainly via infrared laser light [214]. This permits more concentrated and accurate stimulation of spiral ganglion cells, and as a consequence, could produce improved spectral and temporal resolution via having more controllable channels [215]. Light-emitting semiconductors that use light to expose the remaining spiral ganglion cells in hearing affected patients is one example of optical cochlear implantation [216].

2.2 Neuronal cells signalling, communication and interfacing with the surrounding environment

2.2.1 Mechanisms of neuronal cell signalling

Cell signalling allows cells to communicate with each other. In nature, an action potential is stimulated via depolarization of the cell membrane. Nonetheless, depolarization of the cell membrane can be stimulated artificially through introducing electrical current utilizing the implanted electrodes [217]. Normal neuronal cell communication and signalling mechanisms involve the amalgamation of electrical signalling and chemical signalling [218]. Neuronal cells ordinarily have the ability to conduct signals by producing chemical messengers for chemical signalling induction. However, at the same time, neuronal cells can generate the signal electrically [219].

Chemical signalling is considered as the most common signalling pathway in neuronal cells [220]. Predominantly governed through presynaptic neurons, the release of the chemical neurotransmitters leads to signals being detected and amplified by the targeted cell [221]. While, the electrical signalling represents the highly rapid response signal that is needed for the neuronal cell communication [220, 222]. Electrical signalling is governed via gap junction channels that transmit ionic current and small molecules over the neuronal cell membrane. There are other diverse pathways that deliver electrical signals, for example, production of electrical fields in order to stimulate other neuronal cells [219, 222].

However, there are also other mechanisms for communication between neuronal cells; for instance, volume transmission of diffusion and wiring transmission [223, 224].

Volume transmission is considered as a new type of significant neural communication, which depends on the diffusion of chemical molecules. Notably, the signals diffuse through the extracellular fluids across a greater distance, resulting in less signal "safety' or accuracy in comparison to other types of neuronal communication transmission [221, 225]. Wiring transmission, which derived its name from its similarity to transmit signals through a wire, utilizes cellular chain channels [224, 225]. These wire channels link the signal message between both origin and target neuronal cells with higher signal safety in contrast to volume transmission. The plasma membrane tunneling nanotube is an example of wiring transmission achieved through tiny nanotube wires, which create the intracellular neuronal linkage utilizing actin constituents [226-228].

2.2.2 Neuronal cells communication and interface with the surrounding environment and the impact on neurite outgrowth

Neurons and neuronal stem cells have the ability to respond selectively to their physical, chemical and topographical surroundings [229, 230]. Significantly, neuronal stem cells have the potential to regenerate new neurons. This regeneration of neurons can substantially modify the neuronal shape, structure, and flexibility [231-233]. Moreover, neuronal cell sensing of the surrounding environment can stimulate their migration, either repulsively or attractively [234]. This stimulation is related to several cues such as chemotaxis cues, durotaxis cues, mechanotaxis cues - associated with direct sensing of the mechanical properties of the cell surrounding - galvanotaxis cues attended by electrostatic potential, and phototaxis cues influenced by the light strength [235-237].

For instance, in chemotaxis, cells sense the concentration gradients of soluble factors in the extracellular environment, via specific cell membrane receptors [235]. Target cells

can release chemoattractants or growth factors to trigger the migration of cells towards the vicinity as well as attract or repel axon growth [238]. Stromal cell-derived factors, netrin-1 and vascular endothelial growth factor are examples of critical chemoattractants guidance cues of neuronal cells [239-241].

Durotaxis cues can alter cell behaviour and differentiation according to the reaction between the cell surface and substrate rigidity [242, 243]. Researchers have found that the differentiation of mesenchymal stem cells is influenced by the rigidity of the growth substrate. On soft elastic surfaces, these cells differentiate into myocytes, while on rigid surfaces, they differentiate into osteocytes [244]. Furthermore, Lee et al. found that by using only nanometer groove arrangement modifications on the surface without any other chemical or physical addition can prompt human embryonic stem cells to differentiate into neuronal cells [245].

It is also known that neurite outgrowth stimulation is regulated by endogenous soluble proteins, for example, nerve growth factor, and extracellular matrix (ECM) glycoproteins [246, 247]. Neural cell adhesion molecules also have significant roles in the enhancement of the neurite outgrowth and branching [248, 249]. Matsumoto et al. reported a method using carbon nanotubes coated with neurotrophins to promote and stimulate the neurite outgrowths of neurons [250]. Paviolo et al. exposed that laser exposure could promote neurite outgrowth [251]. Nakano et al. revealed that neural and thymus-derived activators, also known as neuregulin-2, promoted neurite outgrowth *in vitro* [252]. In this context, laminin is considered as one of the ECM glycoproteins that promotes neurite outgrowth [253, 254]. Garcia et al. have shown that laminins associate in axonal guidance in vivo [255]. More recently, Zhou et al. explored the combination of ECM components such as laminin, fibronectin and collagen and the electrical stimulation to promote nerve

regeneration and repair, in turn, improve neural cell adhesion, neurite growth and extension [256].

Significantly, introducing stem cell differentiation and neurite outgrowth guiding along with electrode surface modifications can improve the quality of implanted technologies. For instance, implanting electrodes modified with stem cells could substitute for the lost cellular functions in the visually and hearing impaired [257].

However, this kind of intimate electrode-nerve interface implants would raise other challenges, for instance, the reconfiguration of native tissue architecture such as glial cells, myelin cells, epineurium cells and perineurium cells and their relative positions [258]. Thus using new technologies, such as a tBLM coated electrode interface that was investigated in this chapter, might provide more intimate contact with the nerves.

2.3 Adhesion of cells to their surrounding environment

Cell adhesion is crucial in cell communication, differentiation, and development [259-261]. As such, any dysfunction or reduction in the cell-cell adhesive process can disorder the cells in term of morphology and structure and, in turn, promote the manifestation of abnormal cells [262, 263]. Cell adhesion on electrodes *in vitro* commences when functionalized electrode surface elements are recognized by the cell. This initial cell binding and attachment process to the electrode substrate is crucial and should be sufficiently durable to diminish any gap between cells and abiotic surfaces, which can consequently induce unwanted current leakage between cells hindering the accuracy and fidelity of recorded signals [264].

Stable and specific adhesion achievement requires a complex binding event involving different adhesion molecules, such as transmembrane protein receptors, ECM molecules, and peptide ligand binding in addition to the abiotic surface design [261].

2.3.1 Transmembrane adhesion receptors

Transmembrane adhesion receptors have an important role in attaching cells to their surrounding environment through cytoplasmic adaptor proteins such as talin, focal adhesion kinase, vinculin, α-actinin, the kindlins and paxillin [265]. Each receptor embedded in the cell membrane is linked to a particular cellular biochemical pathway [266]. Each also has a significant role in regulating signal transmission via coupling the actin cytoskeleton to cell-matrix [267-269]. Moreover, adhesion receptor mobility in membranes controls the internal forces that induce the growth of focal adhesion domains, which, in turn, affects intracellular signal transduction events [270, 271].

Cells express distinct cell surface adhesion receptors including integrins, cadherins, syndecans and other proteoglycans and cell adhesion molecules [272]. Integrin and cadherin families are the most commonly studied adhesion receptors [269]. The integrin family has been shown to promote focal adhesion-mediated cell adhesion to the ECM on modified artificial surfaces such as gold, glass, silicon, diamond and platinum [273]. Integrin family receptors include fibronectin receptors, collagen receptors, laminin receptors and vitronectin receptors [268, 269, 274, 275]. In particular, the neural cell adhesion molecules is one of the most significant cell surface glycoproteins that acts as a receptor and mediates cell-cell adhesion and intracellular downstream signaling in the nervous system [276, 277].

2.3.2 Extracellular matrix adhesion molecules

ECM molecules *in vivo* and *in vitro* promote adherence and spreading of cells through their interaction with other matrix components and with cell surface receptors [278]. A high molecular weight characterizes ECM molecules, so they are relatively difficult to synthesize in comparison to peptides [279]. Different types of ECM adhesion components are utilized to modify the substrate surface to support cells adhesion. These include laminin [280], fibronectin [151, 281-283], collagen [284], gelatin [148] and poly-lysine [285].

Laminin is a critical trimeric glycoprotein of the basal lamina of peripheral nerve cells. Laminin's importance is related to the enhancement of neurite outgrowth and cell adhesion, proliferation, and migration [286]. Yu et al. combined laminin and a particular nerve growth factor and demonstrated significant improvement in nerve regeneration [287]. Collagen and fibronectin ECM molecules also support significant neuronal cell attachment and improved neurite expansion. Wegener et al. have shown that fibronectin-coated surfaces enable rapid cell spreading in comparison to other examined proteins such as laminin, vitronectin, and bovine serum albumin [151]. However, laminin functionalized surfaces showed significant cell attachment in contrast to other ECM elements [288, 289]. Diverse cell types have different responses with variable ECM modified surfaces. For instance, a Poly-L-lysine (PLL) modified surface shows the minimum stem cell adhesion and proliferation number in comparison to a laminin-modified surface [290].

2.3.3 Peptide ligand-binding motifs

There are many kinds of ligands, including peptide ligand binding motifs, neurotransmitter, hormones, toxins, and pharmaceutical drugs [291]. Peptide ligand-binding motifs are small peptide molecules (3-10 amino acid) found in the ECM that are naturally secreted by cells. ECM are now also artificially manufactured to improve cell adhesion processes *in vitro* [278]. They provide a secure attachment of cells to other cells or surfaces via the formation of focal adhesion that links the cell surface layer with ECM components [278]. Peptide ligands have certain benefits over the ECM derived molecules, including increased selectivity, enhanced stability, and improved cell adhesion [292].

One of the frequently used peptide ligand binding motifs in cell adhesion techniques is the short amphiphilic tripeptide, arginine-glycine-aspartic acid (RGD), which exists in fibronectin, laminin and other ECM proteins [293, 294]. Pierschbacher et al. revealed that RGD is an essential sequence within fibronectin, which is known to promote cell adhesion [295]. Like RGD, contemporary studies indicate that the cysteine extended GRKKRRQRRRPQ (TAT) peptide ligand also improves cell attachment on artificial surfaces [296].

The YIGSR ligand on the β1 chain of laminin is another example of how peptide ligand binding modifies and stimulates neural cell adhesion and outgrowth [297, 298]. Also, the synergistic effect of the motif Pro-His-Ser-Arg-Asn (PHSRN) found in fibronectin ECM molecules increases the affinity of RGD [299]. Recently, combinations of two different ligands, RGD and Tyr–Ile–Gly–Ser–Arg (YIGSR), have been shown to progressively enhance initial endothelial cell adhesion and migration [300, 301]. Peptide ligand-binding

motifs can be classified into mobile and immobile ligands. Mobile ligands are free to move through the surface, such as ligands on lipid bilayer modified surfaces [36]. Immobile ligands are anchored to the surface [302].

2.3.4 Abiotic surfaces

The interface between abiotic surfaces and biotic cells are critical for cell adhesion stimulation. Abiotic surfaces represent the nonliving substrate on which live cells can grow. The most common materials for the microfabrication of abiotic substrate surfaces are based on polystyrene, silicon, and glass, all known for their stability and low toxicity [303, 304].

The ideal abiotic surfaces should provide significant cell adhesion, proliferation, and differentiation [305]. Additionally, the surface should be electrically conductive for implementation purposes and for *in vitro* cell-based research electrical measurements such as impedance spectroscopy [306]. Control of chemical and physical coating is essential to enhance the performance of substrates. Notably, additional coatings might lead to current leakage from the culture medium or other cells, which in turn may result in increased extraneous noise [307].

2.4 Regulation of cell adhesion

From the moment the cell membrane surface touches the electrode surface, direct interfacing commences. Hence, control and design of the substrate surface constituents are essential for cell adhesion and proliferation. In the natural and artificial environments, cells respond to a group of chemical, physical and mechanical signals that regulate the

cell's function and fate [308-310]. This section will discuss the cellular effects of such influences derived from the artificial electrode substrates.

2.4.1 Chemical cues

Soluble chemical cues are one of the most critical signals in regulating cell adhesion onto artificial surfaces, via modulation of focal adhesion composition and intracellular signaling which in turn, controls cell function, and fate [311]. To pattern the chemical molecules on the electrode surface, there are different applied methods such as lithography and microcontact printing [312-315].

Commonly a chemical gradient technique is employed in the chemical modification of electrode surfaces, such as for self-assembled monolayers (SAMs) and for modifying culturing substrate chemical interactions [316]. SAMs are characterized by their simplicity to functionalize by altering terminal functional groups with moieties like carboxylic acid, hydroxyls and amine groups [317-320]. Adjusting culturing substrate chemicals can also control cell behavior [321]. For example, functionalization of reactive polymer films with azlactone has an influence on the immobilization of other amine chemical elements that, in turn, can stimulate or inhibit cell attachment. However, functionalization with the hydrophilic carbohydrate D-glucamine prevents cell attachment and proliferation [322].

The use of strong cross-linking binding molecules on electrode surfaces can also enhance cell adhesion. One example being the biotin-avidin binding system, which is considered as one of the strongest non-covalent interactions occurring in nature [323, 324].

2.4.2 Physical cues

Physical cues include a variety of factors that regulate cell rigidity and arrangement dynamics to promote cell adhesion. The density of a hydrogel group is one critical factor in determining surface stiffness from an exceedingly soft substrate to a solid one. The rigid surfaces have presented an increase in target cells adhesion in comparison to less rigid modified surfaces [244, 325, 326]. Equivalent to these findings, seeded cells on a surface with varying levels of stiffness were demonstrated where cells migrated towards the region of highest stiffness [242, 327].

The arrangement of integrins and other ECM molecules on artificial surfaces can also be a critical factor to control cell adhesion [275, 281]. The precise modification of integrins can alter the cell adhesion process [328]. Further, nanoscale discrepancies in the spacing among adhesive ligands and/or their density can control cell spreading, relocation, and focal adhesion dynamics [329]. For instance, Geige et al. investigated that variations in the ligand spacing of a few nanometers can influence cell adhesion [270]. They demonstrated that cell adhesion is optimal when the average ligand spacing is smaller than 70 nm [330]. Notably, there is no difference between well-arranged space arrays or randomly distributed arrays when the ligand spacing is less than 70 nm. On the other hand, ligands that are ordered have an enhanced cell adhesion affinity when there is a greater than 70 nm spacing as does the density of ligands [331, 332].

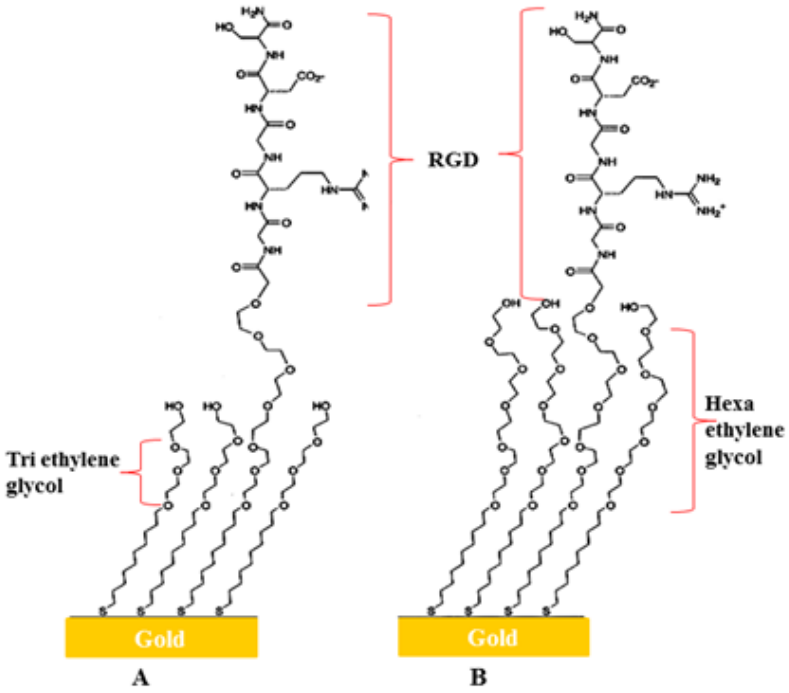

Figure 2.3: Comparison between different OEG lengths modified on a gold surface and functionalized with RGD. The cell attachment to the RGD peptide is dependent on the length of the ethylene glycol carbon chain. (A) The tri-ethylene glycol group readily binds the RGD motif and has a significant improvement in cell adhesion in comparison to longer hexa-ethylene glycol chains (B). The modified figure was based on [332].

Researchers have developed a spontaneous monolayer enclosing oligo ethylene glycol (OEG) that can be functionalized with specific peptides on the electrode surface. This OEG monolayer can eliminate the adsorption of non-specific proteins [333]. Notably, the lengths of OEG groups influence ON cell attachment and spreading when compared to using a constant density of the attached peptides. OEG alkanethiol, with a very long carbon chain, considerably reduces the efficacy of cell attachment and spreading. Alternatively, decreasing the length of OEG alkane thiol carbon chains improves cell adhesion (Figure 2.3) [332].

2.4.3 Mechanical cues

The steric interaction between integrins and cadherins on surfaces controls the three-dimensional distribution of receptors, signal networks and the actin structure within cells [269]. The topography of surface ligands regulates the arrangement of natural and artificial features such as the size, shape, and spacing of nanometer-scale structures. Therefore, this influences cell adhesion, morphology, migration, orientation, and differentiation [310, 334, 335]. For example, topographical roughness can increase the total electrode reaction area that can come in direct contact with cells [336]. Topographical configurations also play a crucial role in promoting neuronal axon and neuronal dendrite length and branching via mimicking the natural *in vivo* environment [337].

There are diverse nano- to micro-topographic designs that have been developed *in vitro* for culturing neuronal cells, which include altering anisotropic groove depth that align fibres and channels [338] and incorporating isotropic topographies such as pillars or posts and holes [339]. Yim et al. have shown that a 350 nm wide groove pattern improves neuronal cell regulation in comparison to un-patterned ones which, in turn, enhance human mesenchymal stem cells to differentiate into neuronal cells [335]. Wieringa et al. utilized various ridge widths for modifying focal adhesion formation and hence, changed the cell-substrate interface. They found that, under suitable culturing conditions, cells displayed enhanced extensive neurite outgrowth [340].

Creative approaches incorporating both mechanical and chemical adjustments can improve cell attachment and proliferation. Recent studies found that combinations of the appropriate roughness and mechanical modifications can be made using hydrofluoric acid

on silicon substrates, which can efficiently enhance neural cells to adhere and spread [341, 342].

In this regard, the overall aim of this study is to elaborate on the possibility of applying the tBLMs system to improve implantable technologies. Therefore, a range of coating variations onto the gold substrates was undertaken firstly. Consequently, a comparison of the variable substrate modifications in terms of their ability to improve cell attachment, proliferation and biocompatibility were assessed.

As such, this chapter will examine:

- Determining the effect of different gold electrode modifications, namely fibronectin, PEG-RGD, POEGA-RGD, compared to bare tBLM activity.
- Assessing the functionalized-tBLM coatings ability to enhance electrode-cell localized contact and communication.
- Evaluating the consequences of different working electrode size on the magnitude of impedance measurements due to cell growth and adhesion.

2.5 Materials and Methods

2.5.1 Chemicals

All chemicals used to perform the experiments, unless mentioned otherwise, were of analytical grade and used as advised. 100% pure ethanol, phosphate buffer saline (PBS), 1-(3-dimethylaminopropyl)-3-ethylcarbodiimide hydrochloride (EDC), N-hydroxysuccinimide (NHS), anhydrous dimethyl sulfoxide (DMSO), Bovine serum albumin (BSA), streptavidin and GLY-ARG-GLY-ASP-SER (GRGDS) peptide were purchased from Sigma- Aldrich (Sydney, Australia). Cyclo [Arg-Gly-Asp-D-Phe-Lys (Biotin-PEG-PEG)] c (RGDfK(Biotin-PEG-PEG)) where PEG = 8-Amino-3,6-Dioxaoctanoic Acid were obtained from Peptides International (Louisville, USA). Phospholipids: 1-palmitoyl-2-oleoylsn-glycero-3-phosphocholine (POPC), 1,2-dipalmitoyl-sn-glycero-3phosphoethanolamine-N-(glutaryl) (sodium salt) (DP-NGPE), 1, 2-dioleoyl-3-trimethylammonium-propane (chloride salt) (DOTAP), and 1-oleoyl-2-(12-biotinyl (aminododecanoyl))-sn-glycero-3-phosphoethanolamine (B-PE) were purchased from Avanti Polar Lipids (Alabaster, USA) and used as received. Benzyldisulfide-TEG-OH, Phytanyl bis-tetra-ethylene glycol, Diphytanyletherphosphatidylcholine, and Glycerodiphytanylether were a kind contribution from Surgical Diagnostics (SDx Tethered Membranes Pty Ltd, Australia). Thiol-PEG12-acid were purchased from Broadpharm (San Diego, USA).

16% paraformaldehyde (PFA), Triton x 100, Dulbecco's modified eagle's medium (DMEM), Dulbecco's phosphate buffer saline (DPBS), nutrient mixture F-12, PBS, fetal bovine serum (FBS), TryPLE, 0.5 M Ethylenediaminetetraacetic acid (EDTA), Penicillin / Streptomycin solution, Geneticin (G418), 4′,6-diamidino-2-phenylindole (DAPI), Alexa

Fluor 568 Phalloidin and Alexa Fluor 647 Phalloidin were obtained from Life Technologies Australia Pty Ltd (Sydney, Australia).

Poly oligo ethylene glycol acrylate (POEGA) synthesized polymer was a gift from Dr. Maryam Parviz (Institute for Biomedical Materials and Devices School of Mathematical and Physical Sciences, University of Technology Sydney, Australia).

2.5.2 Electrodes

Gold electrode slides are an in-kind contribution from Surgical Diagnostics (SDx Tethered Membranes Pty Ltd, Australia) (Figure 2.4). Slides are made of 25mm x 75mm x 1mm polycarbonate with patterned gold arrays for electrodes. A polyethylene cartridge defines six measuring wells; in addition, cartridges include the counter gold electrode. The large counter electrode is situated opposite to the tethering electrodes, instead of being in the plane on the same slide in order to minimize the surrounding noise effect. Each well is designed as a flow cell chamber has the maximum capacity 600 µl solution with a 2.1 mm^2 active tethering electrode area.

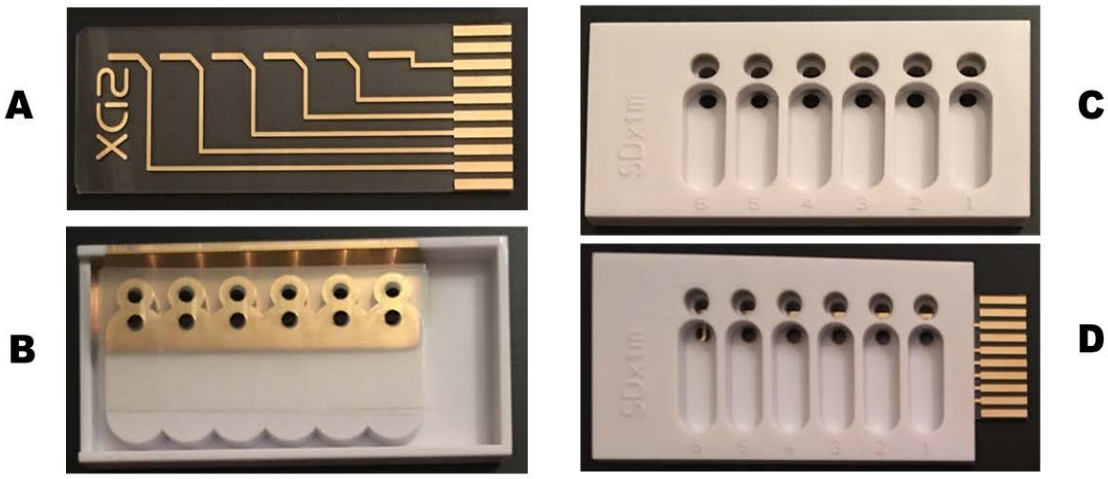

Figure 2.4: Photographs of SDx electrode array. (A) Slide array with six working electrodes; (B) Counter electrode at the bottom of the cartridge; (C) 6 well flow cartridge; (D) Assembled cartridge.

Small working electrode (8W1E) (0.049 mm^2 working electrode area) slides were purchased from Applied Bio-Physics (Troy / New York, USA). The bases are also prepared from a polycarbonate, following which a gold deposition by sputtering and photolithographic methods (http://www.biophysics.com). The polystyrene chamber constitutes of eight measuring wells using the maximum capacity of 400µl media (Figure 2.5).

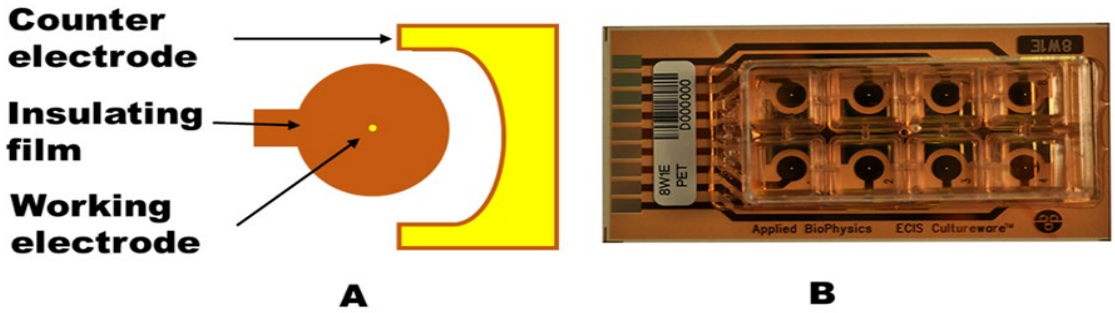

Figure 2.5: Photograph of Applied Bio-Physics 8W1E electrode array. (A) Schematic top view of one well. Gold working and the counter electrode are on the same array, small working electrode defined by photopolymer insulating film; (B) Eight wells assembled cartridge. Adapted photographs were based on [152].

2.5.3 Cell culture procedures

2.5.3.1 Cell lines

Adherent cell lines CHO-K1 (Chinese Hamster Ovary) epithelial cells and the neuronal cell line SH-SY5Y human neuroblastoma cells, were utilized in this work.

2.5.3.2 Cell sub-culture

All cell culture procedures were performed under sterile environments within a Class II laminar flow cell culture cabinet. All materials utilized for cell culture were wiped clean with 80% ethanol prior to employing them in the safety cabinet. CHO-K1 cells were

cultivated to confluence in culture flask (25 cm^2, polystyrene easy flask, filter cap, Nunc, Thermo Fisher, Australia) in Dulbecco's Modified Eagle Medium mixture F-12 (DMEM- F12) (Life Technologies, Australia) culture media complemented with 5 % heat-inactivated fetal bovine serum (FBS) (Life Technologies, Australia). SH-SY5Y cells were grown to confluence in DMEM-F12 culture media supplemented with 10 % FBS. Briefly, cells were checked daily for contamination and growth and every 3−4 days; the cells were passaged.

For adherent cell detachment procedure, 1ml of TryPLE (Gibco recombinant cell-dissociation enzymes reagent) was added to a 25 cm^2 flask of adherent cell monolayer and incubated for 2-3 minutes inside the 37 ˚C incubator. Cells were dislodged by a single hit of the flask with the flat part of the hand. FBS free medium was used for subsequent cell washing steps. The collected cell suspension was centrifuged at 1200 rpm for 5 minutes. Following this, the supernatant was discarded and the cell pellet was re-suspended in FBS free medium. Cells were re-plated into sterile 25 cm^2 tissue culture flask in the total volume of 8 ml medium with 5 or 10 % FBS and incubated in the 5% CO_2 incubator at 37 °C.

In order to seed the cells on the modified surfaces, the cells were diluted to final concentration 10×10^5 cells/ml in fresh corresponding complete growth media in addition to penicillin-streptomycin antibiotic (used concentrations: 100 u/ml for penicillin and 100 µg/ml streptomycin.).

2.5.3.3 Transfections of mammalian cell lines with H2B-GFP Plasmid DNA

H2B-GFP plasmid DNA was purchased from Addgene plasmid (H2B-GFP from Geoff Wahl - Addgene plasmid # 11680; http://n2t.net/addgene:11680; RRID: Addgene_11680) handling and preparation methods of plasmid carried out following the supplier's information. Briefly, upon receipt of the H2B-GFP bacterial stabs, bacteria were streaked onto lysogeny broth (LB) agar plate. Single colonies were isolated using a sterile stick, which was then used to inoculate growth medium (LB broth) containing 50 µg/mL kanamycin selective antibiotic (Sigma Aldrich) was incubated overnight at 37 ºC, 200 rpm shaking incubator. Following plasmid amplification glycerol stocks were prepared and DNA purified for use in subsequent transfections [343]. QIAGEN Plasmid Maxi Kit (QIAGEN, Hilden) was used for plasmid DNA isolation following the manufacturer's instructions.

CHO-K1 cells and SHS-Y5Y cells were transfected with H2B-GFP Plasmid DNA and were carried out using Lipofectamine 2000 (Invitrogen, Darmstadt) following the supplier's information [344].

Briefly, the day before transfection, cells were detached and counted. Cells were seeded into 6-well plates (35 mm^2) at a density of 3- 4 x 10^4 cells per well in 1ml of complete growth medium (DMEM-F12 + FBS). On the day of transfection, cell density was between 50 to 80% confluent. Individual transfection mixtures were prepared, each containing 1 µg plasmid DNA plus 9 µl Lipofectamine in 100 µl serum-free medium (SFM), and gently mixed. These mixtures were incubated for 45 minutes at room temperature to permit DNA- Lipofectamine complexes to form. To each of these

mixtures, a final volume of 1 ml was achieved by adding serum-free media (SFM). The cells in 6 well plate were washed twice with SFM; next 100 µl of the prepared transfection solution was applied to the cells. After 24 hours of incubation, the SFM medium was exchanged to FBS holding medium. The transfected cells were assessed by epifluorescence microscopy after 24 hours. To create an individual stable cell clone, cells were cultured in the presence of 1000 µg/ml of the selection antibiotic geneticin (G418) (Life Technologies Australia Pty Ltd) and single clones selected as outlined below.

The technique of limited dilution isolated stably transfected cell clones. Transfected cells were screened for fluorescence; stable positive fluorescent clones were cultured into 96 wells plates in a dilution of one cell per well in an aim to achieve single colonies. This procedure was repeated several times by choosing the cell populations that exposed the highest percentage of fluorescence transfected cells. Subsequent stable positive clones were expanded into larger culture flasks and frozen stocks were stored in liquid nitrogen.

2.5.3.4 Cells visualization and imaging procedure

The cells electrode surfaces were rinsed three times with PBS. 200 µl of 4% (v/v) PFA in PBS was introduced over the surface and was incubated for 15-30 minutes inside the incubator at 37 ˚C in order to attempt to fix cells to the electrode surfaces. Following the incubation period, wells were washed three times with 200 µl PBS each time. 200 µl of 0.1% Triton x 100 in PBS was placed on the surface and was kept warm for 5 minutes at room temperature in order to permeabilize the cells. The substrate was then rinsed three times with 200 µl PBS. Cell-electrode interfaces were incubated with 1 mg/ml BSA in PBS for 1hour at room temperature with the purpose of minimizing nonspecific binding and improve staining quality.

The non-transfected cells were stained for actin with Alexa Fluor 647 Phalloidin (excitation/emission: 650/668 nm, red) and the cell nucleus with DAPI (blue). 1:200 phalloidin solution in PBS were employed on the fixed cell interface. The dish was covered with aluminum foil, followed by 20 minutes of incubation time at room temperature. To identify nuclei, 1:1000 DAPI solution in PBS was placed on the well-plate and was incubated for 5-10 minutes at room temperature in dark condition. For long-term storage of cells, a 1-3 drop of mounting media dressed over the stained fixed cell-electrode slide and cover glass slip was placed on the top. In order to visualize cells and confirm cells adhesion, an upright fluorescence phase-contrast microscope (Nikon, Tokyo, Japan) was used.

2.5.4 Electrode surface modification

A variety of coatings were applied to the gold electrodes, as shown in Figure 2.6 below. These modifications were aimed at enhancing the adhesion, spreading and growth of the various cells types on the gold electrode arrays, which could then be monitored in real-time by recording the changes in impedance. In addition, several working electrode sizes were investigated, including 2.1 mm^2 gold electrodes and 0.049 mm^2 electrodes.

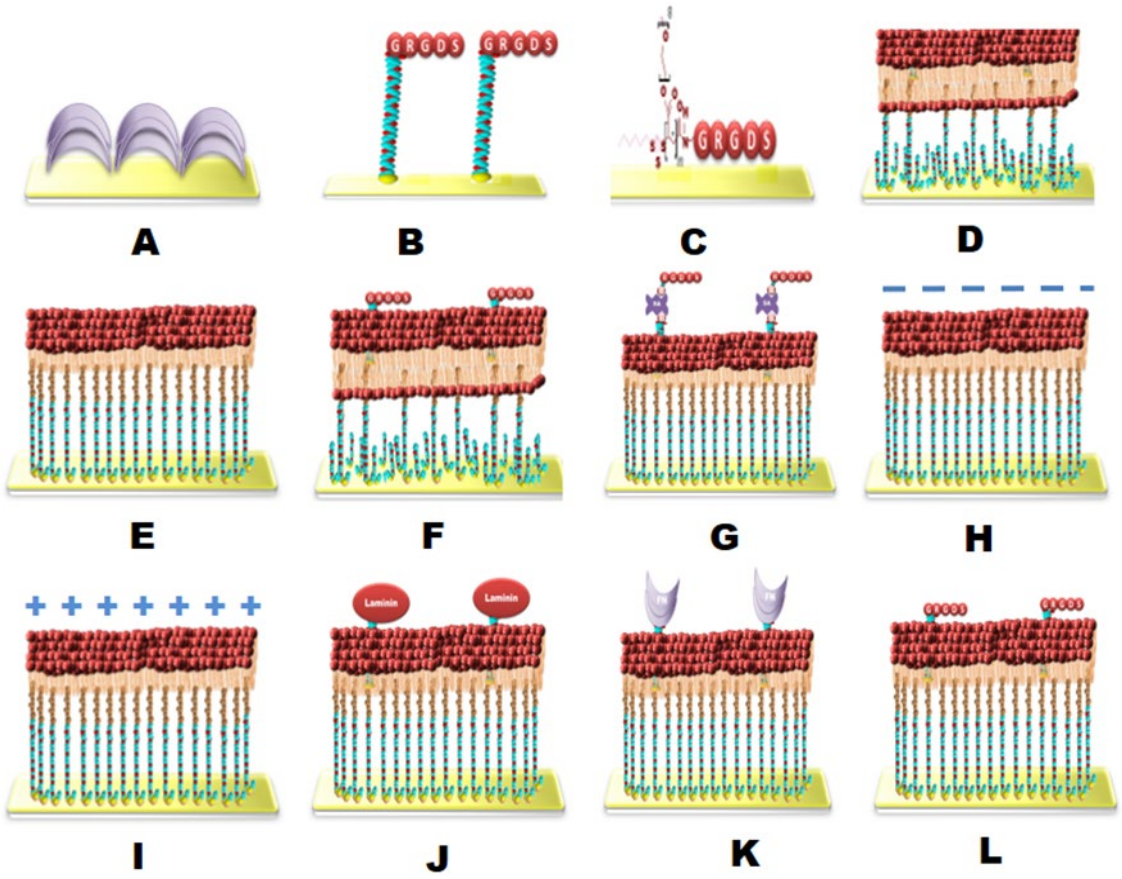

Figure 2.6: Cartoons of the various coating modifications made to the gold electrode surfaces (A) Fibronectin; (B) Thiol-PEG12-acid-RGD; (C) POEGA Polymer-RGD ; (D) non-functionalized tBLM T10; (E) non-functionalized tBLM T100; (F) GRGD- tBLM; (G) cRGD-PEG-B tBLM (H) negative tBLM; (I) Positive tBLM; (J) Laminin tBLM (k) fibronectin tBLM (L) GRGD-tBLM T100. Electrical impedance spectroscopy was employed to compare the interfacial interaction and coverage with live cells.

2.5.5 Coating and modification of the gold electrodes

For the fibronectin coating, all wells of the SDx gold electrode array were incubated with 50 µl of a sterile solution of 10 µg/ml fibronectin in PBS for 1 hour at 37 ˚C. Next, the excess protein on the substrate surface was removed by rinsing the substrates three times

with 100 µl of deionized water. The fibronectin-coated substrates were held in deionized water for subsequent application.

For thiol-PEG12-acid-RGD gold surface functionalization, the freshly prepared gold slides were immersed directly in the thiol-PEG12-acid solution for at least one hour with slight agitation at room temperature. The thiol-PEG12 acid-coated substrates were kept under pure ethanol until use. For experiment use, slides were dried from ethanol then the slide was assembled with the appropriate sterile cartridge. The carboxylic acid terminal groups of the thiol-PEG12-acid monolayer were stimulated with 50 mM EDC and 50 mM NHS in an aqueous water solution for 2 hours with continuous shaking in a sterile condition, illustrated in Figure 2.7.

Carboxyl activated gold slides were washed three times with PBS. Then, 100 µl of 40 µM that equivalent to ~ 20 µg/ml of GRGDS (Sigma- Aldrich, Australia) peptide dissolved in PBS was placed over the carboxyl modified gold slides and were incubated for 30 min at room temperature. Following the modified gold surfaces were rinsed with PBS and were utilized within the same day to culture the cells on. Modifying the surface and seeding cells were done in a biological safety cabinet.

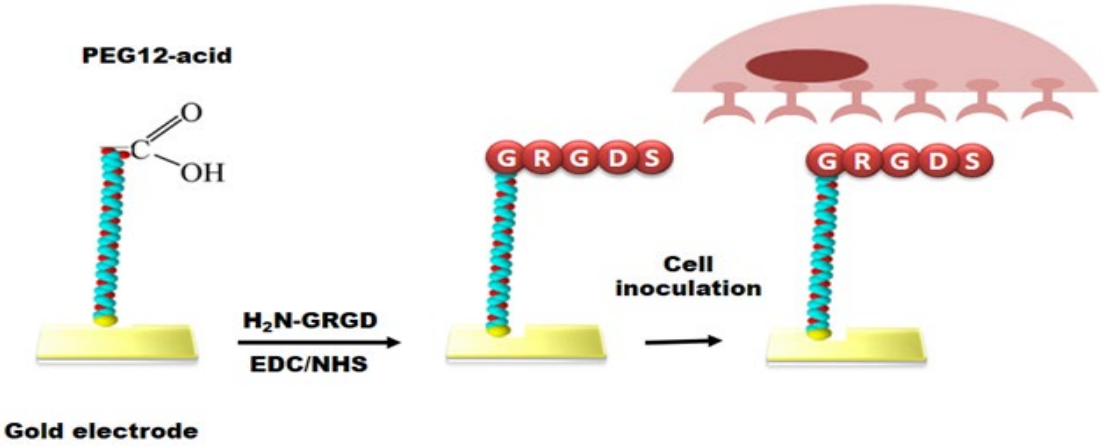

Figure 2.7: Schematic illustration of RGD-gold electrode fabrication. Thiol-carboxy-terminated poly (ethylene glycol) (HS-PEG12-COOH) self-assembled monolayer over

gold electrode was produced via spontaneous thiol-gold coordination. EDC/NHS crosslinkers were introduced to activate the carboxy terminate and form an NHS ester. GRGDS was attached to the amino-group via the amide bond. Cells were inoculated after concluding RGD surface modification.

10 mM thiol-POEGA polymer layer (homemade synthesized polymer) thiol-gold interactions was cross-linked by incubation over the assembled gold electrodes with a cartridge for 18 hours under high humidity conditions at 37 °C. High humidity chamber made using a 150 mm sterile Petri dish (Thermo Fisher, Australia) with wet tissues and small wells filled with sterile water, in order to control the atmospheric humidity as well as to deliver a mechanically stable polymer layer on the electrode surface. Extra polymer molecules were removed by rinsing the substrates carefully three times with PBS. The modified substrates were kept suspended in PBS until utilized. The carboxylic acid terminal groups of the POEGA polymer was activated by adding 100 µl of 50 mM EDC and 50 mM NHS mixture to each well for 2 hours with continuous shaking under sterile conditions. Carboxyl activated gold slides were rinsed three times with PBS. Next, the carboxyl modified gold slides and was incubated for 30 min at room temperature with 100 µl of 40 µM of GRGDS peptide dissolved in PBS. The coated gold surfaces were then rinsed with PBS and were utilized by seeding and culturing the cells within the same day.

2.5.6 Tethered Bilayer Lipid Membranes model

The gold patterning and first monolayer of coating tether molecules were prepared by SDx Tethered Membranes Pty Ltd [345]. The gold electrodes were then immersed in a solution comprised of 9:1 ratio of spacer molecules (benzyl disulfide comprised a four oxygen-ethylene glycol spacer, terminated with an OH group), and hydrophobic tethering

molecules (benzyl disulfide with eleven oxygen–ethylene glycol linker group with a single C20 hydrophobic phytanyl chain). These immersed gold electrodes are incubated for at least 1 hour with shaking, then washed 3 times with pure ethanol. The gold electrode with the first monolayer is then either used directly or stored in pure ethanol.

The second layer is made by adding 8 µl of 3mM mobile lipid phase (MLP) that is comprised of 70% zwitterionic C20 diphytanyl-ether-glycero-phosphatidylcholine and 30% C20 diphytanyldiglyceride ether lipids (AM199) dissolved in 100% pure ethanol. 8 µl of these mobile lipids are introduced to each assembled electrode and incubated for 2 minutes at room temperature. Each electrode is then washed 3 times with 100 µL of PBS buffer. Displacing the ethanol solvent with the aqueous solution in this way (the *solvent exchange method*) enables the formation of a lipid bilayer surrounding the tethering molecules. Formation of a stable tBLM is confirmed by EIS, this is achieved by monitoring the membrane capacitance range is between 0.8 - 1.2 µF/cm2 for 10 % tethering chemistries [74, 346]. For instance, the 0.7 µF /cm^2 membrane capacitance values are very low, thus would indicate a very thick membrane, whereas membrane capacitance values up near 1.5 µF /cm^2 are very thin and/or have too much water associated with them [346, 347]. Also, the phase versus frequency profiles reveals the integrity and fluidity of the tethered membrane which reflect lipid-analyte interactions. For instance, incorporating ion channels such as gramicidin–A in the membrane would shift the frequency at the minimum phase to higher frequencies [347].

Gold electrodes were coated with a variety of molecules including fully tethered (100%) (T100) or down to 10% of tethering molecules (T10), as well as a range of lipid compositions. These architectures were embedded along with several functionalizations to enhance cell adhesion and growth over the bilayer lipid membranes, as illustrated in

Figure 2.6 (D-L). Chemical structures of phospholipids used in this study are presented in Figure 2.8.

For T10 tBLM functionalization, the second layer of lipid membrane was modified in composition. This layer constituted 80:20 equivalent amount of AM199: DP-NGPE lipids. DP-NGPE lipids are carboxy-terminated lipids that can be utilized to couple RGD peptides via EDC/NHS chemistry amine activation. The density of RGD peptide employed as previously used for thiol-PEG acid modification that equivalent to 19 μg/ml.

For fully tBLM T100 functionalization, the second layer of the lipid membrane is comprised of mixture AM199: B-PE lipids equivalent amount of 80:20. 10 nM streptavidin incubated with the bilayer such that they would bind to the biotinylated lipids, which was followed with three wash steps to remove unbound streptavidin molecules. Following, 100 nM cRGD-PEG-B peptide was introduced that would be attached to the free binding site of streptavidin.

Further fully tBLM T100 model functionalization, the second layer of the lipid membrane is comprised of mixture AM199: DOTAP lipids or AM199: phosphatidylserine (PS) equivalent amount of 80:20. In addition, other layers constituted of 80:20 equivalent amount of AM199: DP-NGPE lipids. Following by functionalization with laminin, or fibronectin or GRGDs.

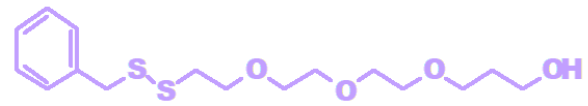

Benzyldisulfide-TEG-OH

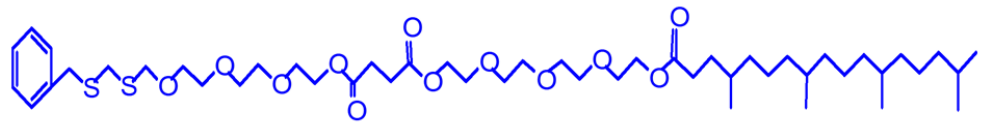

Phytanyl bis-tetra-ethyleneglycol

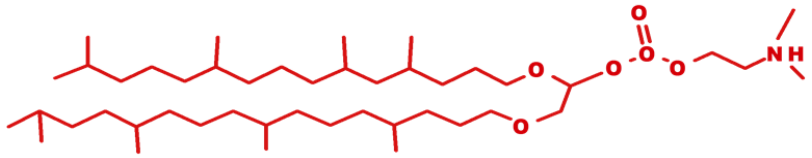

Diphytanyletherphos PC

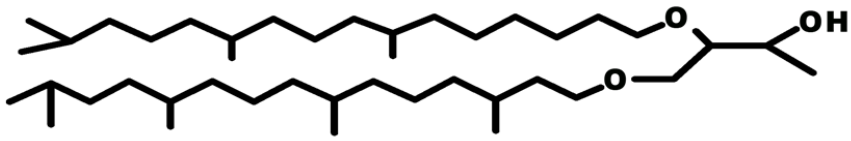

Glycerodiphytanylether

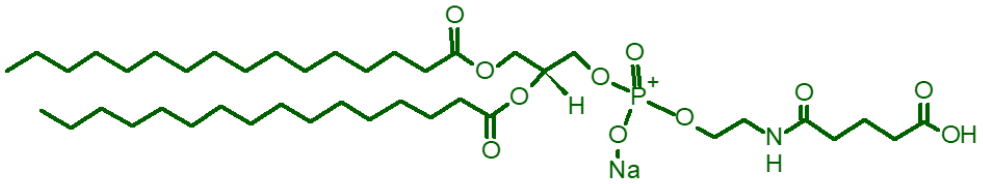

DP-NGPE

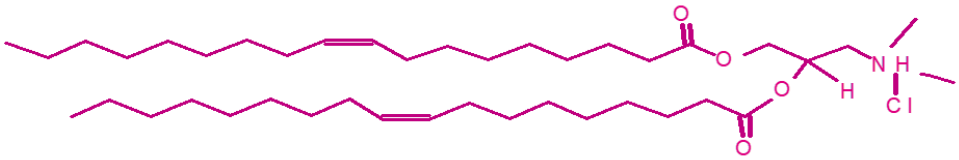

DOTAP

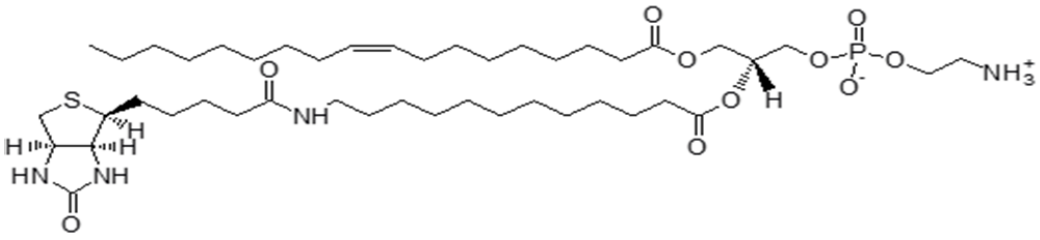

B-PE

Figure 2.8: Chemical structure of lipids employed in this study. The displayed structures are: Benzyldisulfide-TEG-OH, Phytanyl bis-tetra-ethyleneglycol,

Diphytanyletherphosphatidylcholine, Glycerodiphytanylether, 1,2-dipalmitoyl-*sn*-glycero-3phosphoethanolamine-N-(glutaryl) (sodium salt) (DP-NGPE), 1, 2-dioleoyl-3-trimethylammonium-propane (chloride salt) (DOTAP), and 1-oleoyl-2-(12-biotinyl (aminododecanoyl))-sn-glycero-3-phosphoethanolamine (B-PE).

2.5.6.1 Cartridge sterilization

All cartridges in advance to assembling with the electrode were sterilized by first rinsing with 80% ethanol, then allowed to air dry. The cartridges were then exposed to UV light in a laminar flow hood for 15-30 minutes.

2.5.6.2 Electrical impedance spectroscopy sensing

Electrical monitoring of cell growth was done using methods described previously [138, 139]. A non-invasive weak amplitude sinusoidal AC voltage signal (25 mV) within a frequency range of 0.1 - 25000 Hz was applied to the gold electrodes. The real-time increase in impedance magnitude, was the recorded measure of cell growth, attachment and spreading, following seeding of cells and monitoring for 24-48 hours. A representative illustration of the experimental setup for impedance measurements is illustrated in Figure 2.9. The normalized magnitude of the electrode surface impedance, onto which cells had been added, was compared with the interfacial interaction of a cell-free surface, at a selected frequency.

The impedance magnitude of the modified cell-free gold surfaces was determined as baseline data. The magnitude of the impedance measurements was then normalized by dividing the impedance measured while cells were growing over the baseline impedance. All measurements were taken while the electrode was inside a temperature-controlled humidified incubator at 37 °C in the presence of 5% CO_2. Cells were initially added at a

concentration of 10^5 cells/ml unless otherwise stated. Cell seeding was completed after 30-60 minutes after the creation of the coated electrodes in order to confirm the stability of impedance measurements as well as exclude the interference of the introduced culture medium.

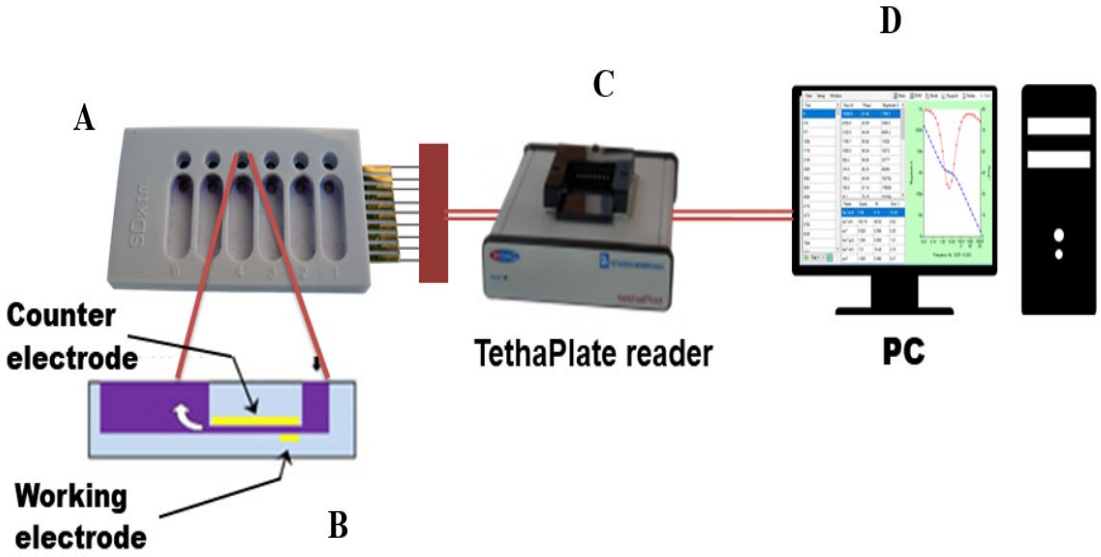

Figure 2.9: Representative illustration of the experimental setup for impedance recordings. Components of impedance spectroscopy measurements system; (A) A cartridge assembly with six electrodes (kept inside an incubator with controlled temperature and CO_2); (B) the electrodes design scheme; (C) tethaPod^{TM} reader (impedance analyzer and frequency generator) (kept outside incubator); (D) a personal computer.

2.5.7 Statistical analysis

Results are displayed as mean standard error (±SE) of three independent experiments replicates unless otherwise indicated. Results were analyzed and graphs created using the GraphPad Prism software version 7.04 (GraphPad Software, Inc.).

Statistically, significant differences between each group of data were determined using two-way ANOVA followed by Bonferroni post hoc multiple comparison tests. Bar graph comparing average impedance values recorded over a 24 hour period, per electrode area (cm^2). One-way ANOVA was conducted to analyse the bar graphs, followed by Tukey multiple comparison tests. P-values obtained that are less than 0.05 (*$P < 0.05$) were considered statistically significant.

2.6 Results

2.6.1 Optimization of electrode surface to develop a real-time monitor of cell growth via impedance measurements

A range of coatings were applied to the gold electrodes, as described previously in Figure 2.6. For these various gold surface modifications, the aim was to observe the influence of each modification on the growth and adhesion of the cells by examining electrical impedance variation and by fluorescence imaging. In addition, several working electrode sizes were investigated, including 2.1 mm^2 gold electrodes and 0.049 mm^2 electrodes.

2.6.2 Impedance measurements of CHO-K1 cells grown on fibronectin functionalized gold electrodes

It was important to investigate the effect of various surface electrode coatings on the adhesion and growth of the cells prior to the introduction of artificial tBLM membrane surface coatings. Therefore, we studied the effects of various coatings on cell proliferation. In order to investigate cell attachment and growth on the gold electrode surfaces, CHO-K1 cells were initially utilized due to their ease of culturing and robust growth. The cells' growth was monitored through real-time measurements, as well as by visual inspection, using light and fluorescence microscopy.

As discussed previously, fibronectin is an important ECM molecule that supports cell attachment significantly as well as improved neurite expansion [151, 281-283]. Therefore, fibronectin was the main ECM of interest in our initial study. Electrodes coated

with fibronectin demonstrated cell attachment and cell spreading as reported by an increase in impedance magnitude over time (Figure 2.10 C). This was also confirmed via fluorescence microscopy (Figure 2.10 B) showing a confluent CHO-K1 cell monolayer. One-way ANOVA followed by Tukey multiple comparison tests for average impedance values recorded over a 24 hour period also confirm there was a significant effect of fibronectin surface coatings on cell growth and attachment (obtained p values obtained are less than 0.05) as seen in Figures 2.10 (D), below.

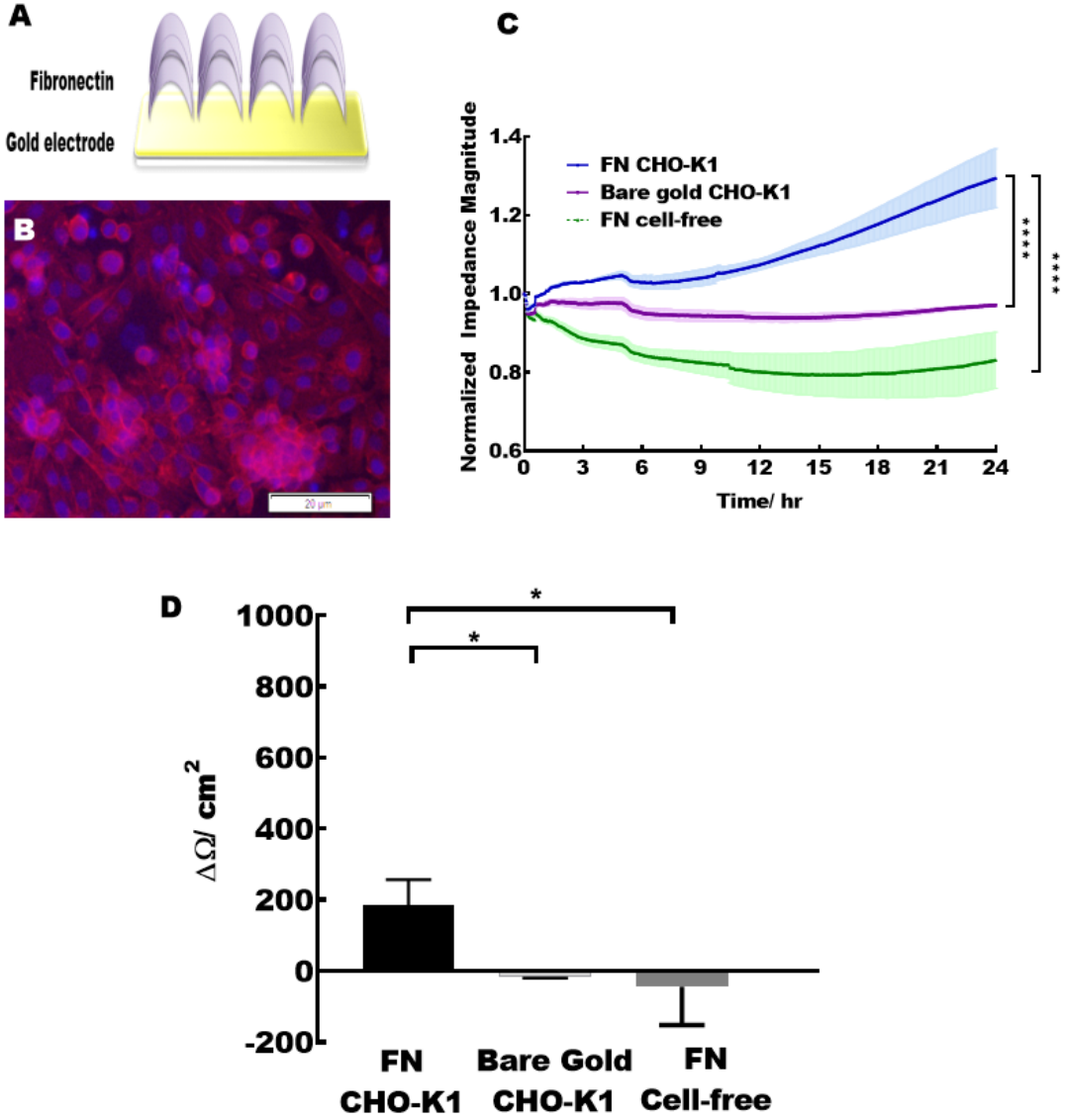

Figure 2.10: CHO-K1 cells attachment investigation on the fibronectin-modified surface. (A) Electrode surface coated with 10 µg/ml fibronectin; (B) CHO-K1 cells were stained for actin with Alexa Fluor 647 Phalloidin (red) and for the cell nucleus with DAPI

(blue); (C) Impedance of the modified and as-received surfaces was investigated and was compared with the interfacial interaction with live cells. Increase impedance values of CHO-K1 cells grown on fibronectin functionalized gold electrodes were considered as a positive control for cell spreading and attachment onto the electrode surface; (D) Bar graph comparing average impedance values recorded over 24 hours, per electrode area (cm^2). One-way ANOVA was conducted, followed by Tukey multiple comparison tests (*P< 0.05 and ****P< 0.0001). The error bars indicate the average standard error of three replicate independent impedance magnitude measurements (n = 3).

2.6.3 Evaluating electrical impedance parameters

The different applied frequency ranges (0.1-25000 Hz) were evaluated in order to identify the most sensitive and significant frequency corresponding to cell growth and adhesion using CHO-K1 seeded onto RGD-coated electrodes. Impedance real-time measurements were recorded over time. Normalized magnitude impedance values were derived by dividing the measured impedance magnitude values by the last reading before the cell introduction that are equivalent values from the cell-free coated surfaces. Thus, the normalized values of impedance magnitude provide better inter-experimental comparability.

The frequency of 3125 Hz was found to be the most sensitive frequency corresponding to the highest cell coverage in comparison to other frequencies, as shown in Figure 2.11. One-way ANOVA analysis followed by Tukey multiple comparison tests for an average mean of the impedance values for each frequency recorded over 8 hours resulted in significant changes between the variable frequencies, obtained p values obtained are less than 0.05.

The frequency of 3125 Hz (around 4 kHz) was chosen for analysis of cell growth and coverage in all subsequent experiments. 3.125 kHz frequency was used due to the tethaPod™ impedance reader frequencies setup. This finding was also supported by Giaever and Keese's ECIS study, that demonstrated 4000 Hz frequency provides significant information that reflects cell adhesion and growth events [138, 139].

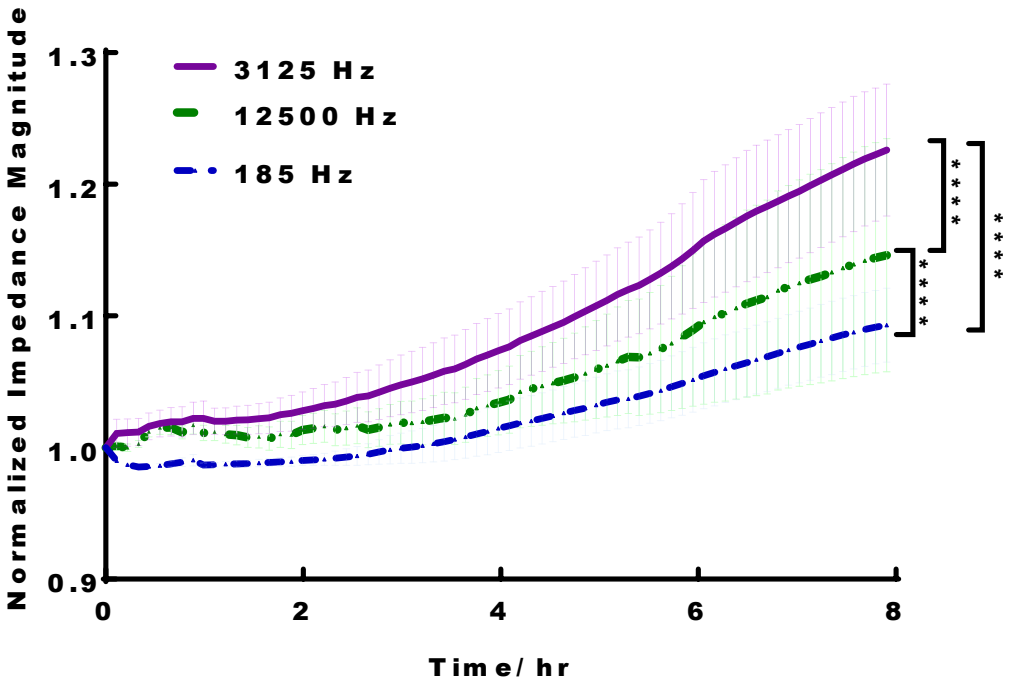

Figure 2.11: Normalized impedance magnitude changes over time to CHO-K1 cells at different frequencies. Frequency ranges of 185 Hz, 3125 Hz and 12500 Hz were explored. Normalized magnitude impedance values are displayed with the most sensitive frequency = ~4 kHz (solid line); Line graph comparing average impedance values recorded over 24 hours, per electrode area (cm^2). The error bars indicate the average standard error of three independent impedance magnitude measurements (n = 3). One-way ANOVA was conducted to analyse the bar graphs, followed by Tukey multiple comparison tests (****P< 0.0001).

2.6.4 Detachment of adherent cells using the calcium chelating agent EDTA while monitoring changes in impedance

The EDTA agent is known to chelate calcium and magnesium ions, resulting in cell rounding and detachment from adherent surfaces [348]. The divalent cations calcium and magnesium have a critical impact on the adhesion behavior of live cells through the integrin-mediated mechanisms and cation bridging interactions between the cell binding sites and the substrate surface [349, 350]. A possible mechanism of divalent cations functions as bridging between carboxyl or other negatively charged groups that are present on the substrate [351].

Using a chelating agent provides a simple real-time investigation method for monitoring cell detachment versus adhesion events. As seen in Figure 2.12 (A), the formation of a confluent CHO-K1 cells monolayer is represented by an increase in impedance magnitude measurements over the 24 hours real-time monitoring of cells growth.

Figure 2.12 (B) displays the response of a growing and attached CHOK-1 cell monolayer compared to an equivalent sample whereupon EDTA was introduced. The cell monolayer response was monitored via impedance magnitude measurements at ~4 kHz. For the cell layer exposed to EDTA, a dramatic decrease in the normalized impedance was detected, indicating cell detachment as the likely reason. In comparison, the untreated CHO-K1 cell monolayer showed stabilize impedance magnitude measurements over time. Also, statistical analysis of the average impedance values recorded over 10 hours using one-way ANOVA analysis followed by Tukey multiple comparison tests confirmed the significant difference in the results, as the obtained p-value is less than 0.05, as seen in Figure 2.12 (C).

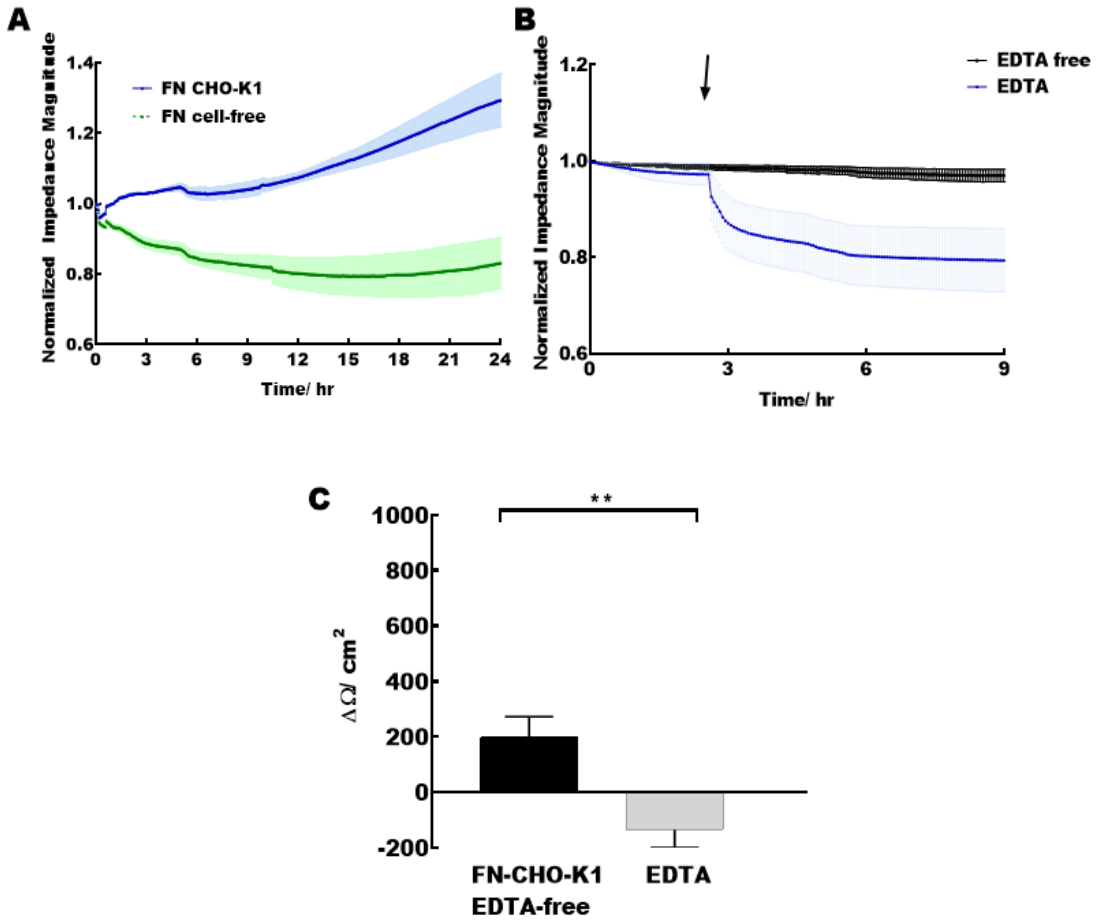

Figure 2.12: Treatment of attached CHO-K1 cells by EDTA. (A) Variations in impedance magnitude as CHO-K1 cells spread and attach onto fibronectin-coated gold electrodes; (B) Typical time course of the normalized impedance magnitude at ~4 kHz of EDTA treated and untreated CHO-K1 cells cultures on fibronectin modified gold electrodes. A gradual drop in impedance magnitude occurs following the introduction of EDTA cells detachment agent (arrow). Measured impedance magnitudes were normalized to the last value before the introduction of 100 µl of 5 mM EDTA; (C) Bar graph comparing average impedance values recorded over a 24 hour period, per electrode area (cm^2). One-way ANOVA was conducted to analyse bar graphs, followed by Tukey multiple comparison tests (**P< 0.01). The error bars indicate the average standard error of three independent impedance magnitude measurements (n = 3).

2.6.5 Impedance measurements of CHO-K1 cells and SH-SY5Y cells grown on RGD functionalized gold electrodes

To further mimic the extracellular matrix (ECM) as a means of regulating cell adhesion, we tested the effect of small peptide coatings over the gold surface electrodes using thiol-PEG-RGD peptide. The peptide sequence RGD is a well-known tripeptide that was originally identified from fibronectin ECM molecules. This RGD sequence is abundantly common in ECM molecules and is recognised by various types of integrin receptors [293]. Consequently, RGD ligands can greatly enhance cell adhesion and proliferation as well as provide a well-controlled environment for studying cell surface interactions [352, 353]. The density of the applied GRGDS peptide was around ~ 20 µg/ml, which was intended to improve the dynamic of cell adhesion and spreading [354].

According to our results, as seen in Figure 2.13, increasing impedance magnitude over time indicated cell attachment and cell spreading over the RGD monolayer modified surface. Two different cell types were investigated to assess the effect of RGD functionalized surface on their cell growth and attachment. Epithelial cells represented by CHO-K1 and neuronal cells represented by SH-SY5Y cells. Over the first 10 hours of recording, both cell lines showed similar impedance changes on the RGD peptide-modified surface (Figure 2.13 B). However, beyond 10 hours, the impedance continued to increase for the CHO-K1 cells while the SH-SY5Y cell impedance plateaued. Fluorescence microscopy results supported this, where we see a fully confluent CHO-K1 cell monolayer coverage, while SH-SY5Y fluorescence-stained cells showed patchy and only partial cell coverage (Figure 2.13 C, D). The real-time impedance measurements of SH-SY5Y cultured cells reflect the lower cell coverage over time compared to CHO-K1 cells, when cultured on the same modified surface.

Further statistical analysis was performed by carrying out One-way ANOVA followed by Tukey multiple comparison tests for average impedance values recorded after a 20 hour period. These results also confirmed that there was a highly significant effect seen in CHO-K1 cell growth and attachment on RGD monolayer coatings in comparison to the cell-free electrode (obtained p values are less than 0.01). Comparison of CHO-K1 to SH-SY5Y cell growth and attachment over the RGD monolayer coating resulted in less significant changes with p values less than 0.05. While, SH-SY5Y cell growth and attachment over RGD monolayer coatings in comparison to cell-free coated electrode also demonstrated lower significant changes, with p values less than 0.05, as shown in Figures 2.13 (E), below.

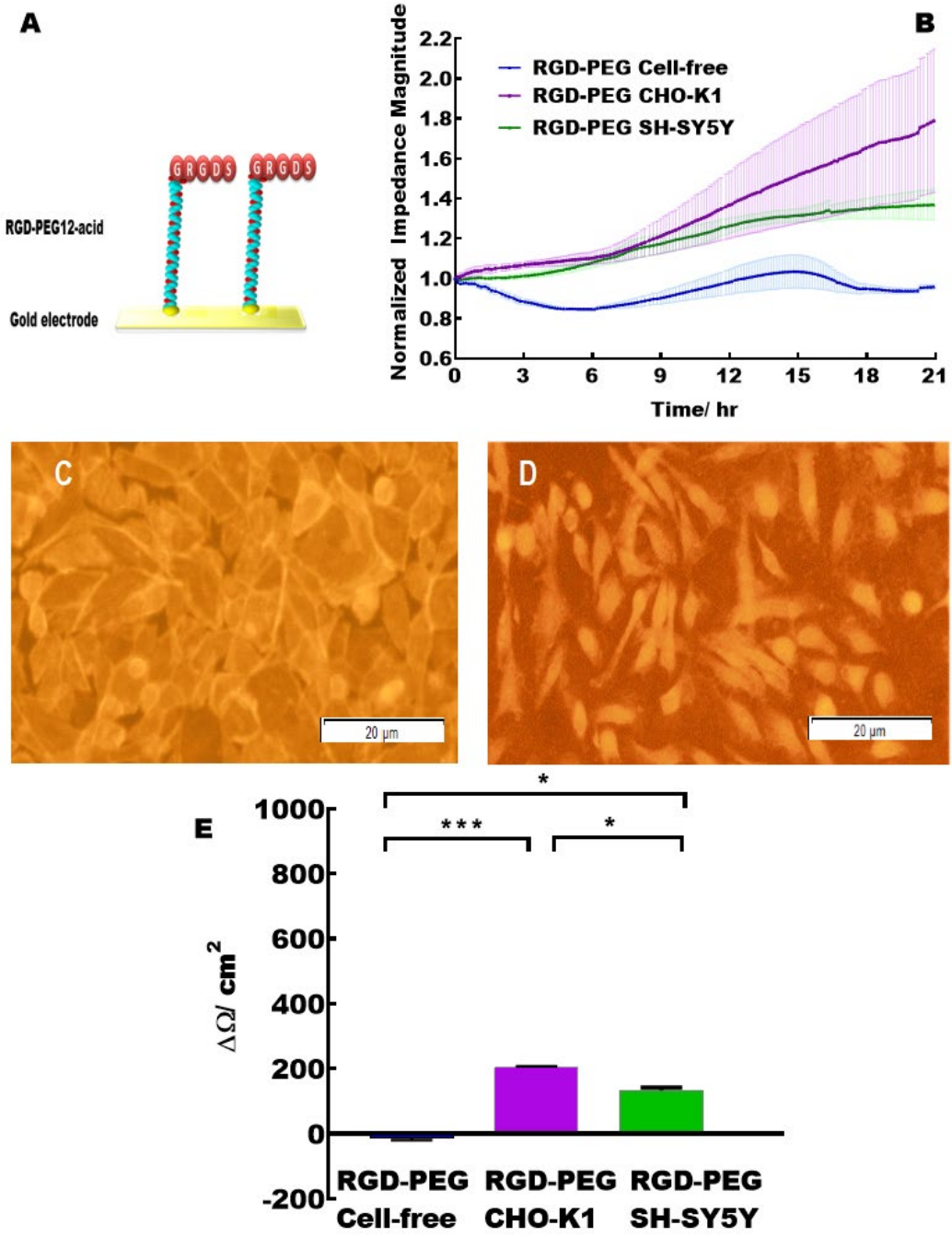

Figure 2.13: Variable cells attachment investigation on RGD modified surface. (A) Electrode surface modified with thiol-PEG-RGD; (B) Impedance measurements of the modified and as-received surfaces compared the interfacial interaction with live cells. The increase was considered as a demonstration of the cells spreading and attachment onto the electrode surface. The error bars indicate the average standard error of three independent impedance magnitude measurements (n = 3); (C) CHO-K1 cells were stained for actin with Alexa Fluor 568 Phalloidin (red-orange); (D) SHSY-5Y cells were stained

for actin with Alexa Fluor 568 Phalloidin (red-orange); (E) Bar graph comparing average impedance values recorded after a 20 hour period, per electrode area (cm^2). One-way ANOVA was conducted to analyse bar graphs, followed by Tukey multiple comparison tests (*P< 0.05 and ***P< 0.001).

2.6.6 Coating the gold surface with RGD using POEGA polymer as a linker

The behavior of cell attachment, spreading and interfaces are significantly affected by any slight alteration of RGD configurations, such as linker organization [355], spacing [329] and the surrounding molecules [332]. Therefore, it was important to investigate the RGD peptide effect on the cell adhesion and growth improvement using linker molecules of different lengths. As previously described in Section 2.5.5, thiol-PEG-acid was used to link the RGD peptide to the electrode surface. Here, we employed POEGA polymer as the first layer of the surface coating. POEGA polymer surface modification provides a different architecture that results in a reduced distance between the coupled RGD peptide and the gold electrode surface compared to the PEG-RGD.

CHO-K1 cell growth on these RGD peptide-functionalized surfaces was investigated. Two different gold electrode modifications were employed: thiol-PEG-acid and POEGA polymer. Thiol-PEG-acid gives a greater distance between the coupled RGD peptide and the electrode surface, while POEGA polymer represented the shorter distance between the attached RGD peptide and the electrode. Both of these different first layers fabricated over the gold electrode, terminated in a carboxy acid. EDC/NHS chemistry was used to activate the COOH terminate, which will allow GRGDS peptide coupling.

Normalized impedance magnitudes of CHO-K1 cell proliferation on RGD-POEGA polymer-coated gold electrodes revealed higher impedance values in comparison to RGD-thiol-12 PEG-modified gold electrode. Visual Imaging of CHO-K1 cells confirmed cell attachment and coverage (Figure 2.14). One-way ANOVA followed by Tukey multiple comparison tests for average impedance values recorded over 24 hours also confirmed higher significant CHO-K1 cell growth and attachment over POEGA-RGD monolayer coatings, compared to CHO-K1 cell growth and attachment over PEG-RGD monolayer coating (obtained p values are less than 0.05), as shown in Figures 2.14 (F).

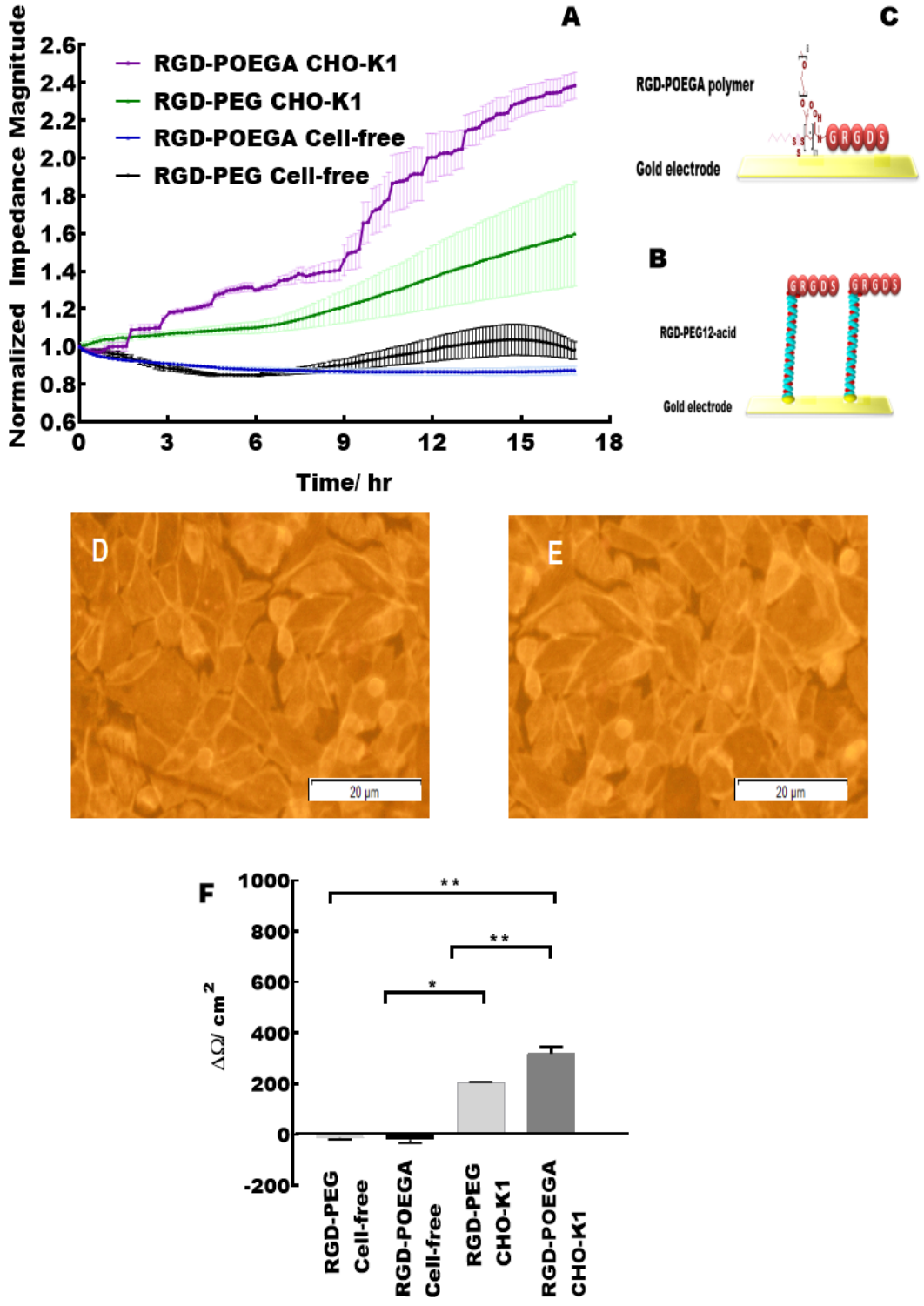

Figure 2.14: Comparison of CHO-K1 cell growth on the two types of RGD surface modification. (A) Normalized impedance magnitude of the POEGA-RGD and thiol-PEG-RGD modified surfaces were investigated and compared upon addition of CHO-K1 cells. Increases in impedance values of CHO-K1 cells grown on POEGA functionalized gold electrodes were higher than thiol-PEG acid-modified surface; (B) Cartoon of an

electrode surface coated with POEGA-RGD; (C) Cartoon of an electrode surface modified with thiol-12 PEG-RGD. The error bars indicate the average standard error of three independent impedance magnitude measurements (n = 3); (D) CHO-K1 cells grown over RGD-POEGA polymer-coated gold electrodes were stained for actin with Alexa Fluor 568 Phalloidin (red-orange); (E) CHO-K1 cells grown over RGD-thiol-PEG monolayer-coated gold electrodes were stained for actin with Alexa Fluor 568 Phalloidin (red-orange); (F) Bar graph comparing average impedance values recorded after 16 hours, per electrode area (cm^2). One-way ANOVA was conducted to analyse bar graphs, followed by Tukey multiple comparison tests (*P< 0.05 and **P< 0.01).

2.6.7 Impedance measurements of CHO-K1 cell attachment on non-functionalized tBLMs (T10)

As outlined previously, in order to assess cell adhesion and spreading, a comparison of impedance magnitudes of cells grown on a range of coatings applied directly to the gold substrates was initially undertaken. In this next section, we investigated the effect of incorporating a tBLM system as a means by which to improve cell attachment, proliferation and biocompatibility.

Therefore, the gold electrode was coated with a tBLM with 10% tethering chemistry using AM199 lipids. Tethered bilayer lipid membranes provide full coverage of the surface that would minimize ion leakage pathways. Cells were then added following the formation of stable sealed tBLMs. Impedance values showed that the membrane was not conductive following the addition of cells, while visual fluorescence images confirm the absence of cell growth and adhesion (Figure 2.15).

One-way ANOVA analysis followed by Tukey multiple comparison tests for average impedance values recorded after 8 hour period resulted in no significant changes between

the variable frequencies, obtained p values obtained are greater than 0.05, as seen in Figures 2.15 (D), below.

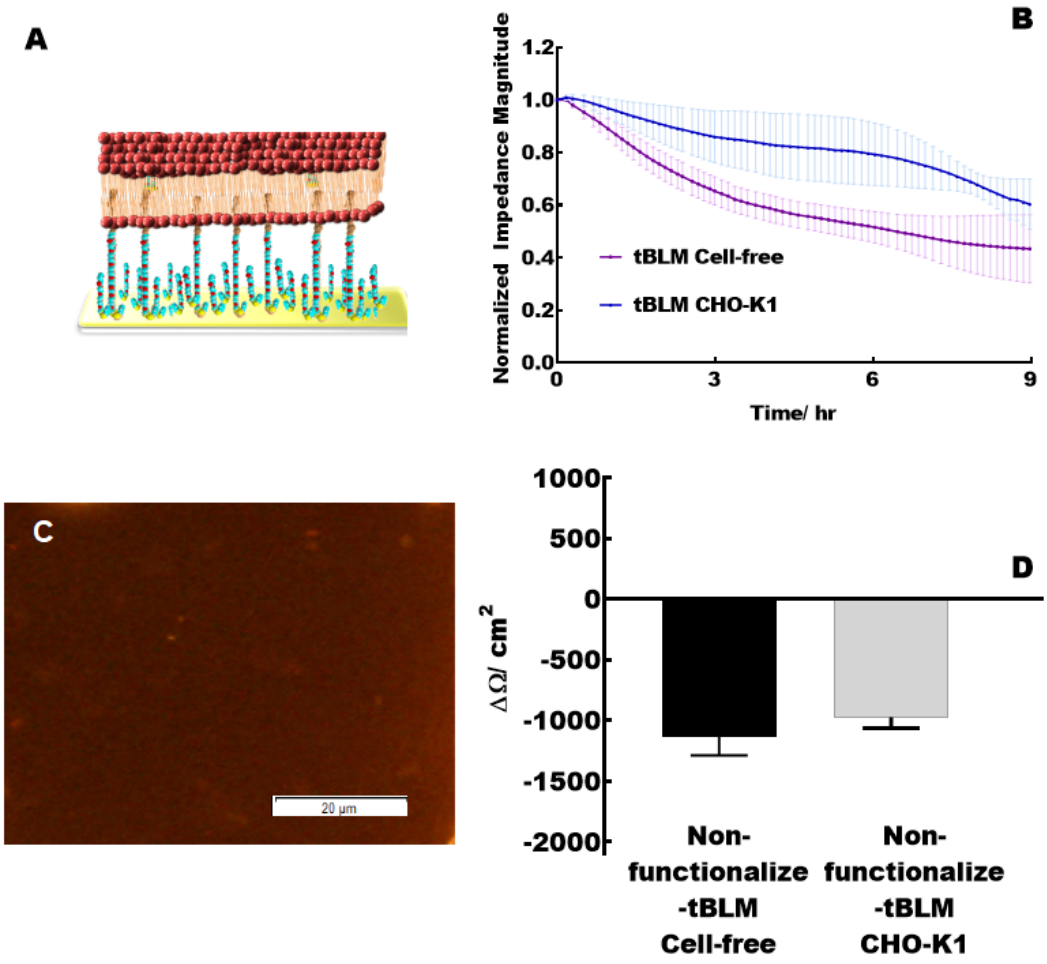

Figure 2.15: CHO-K1 cells growth investigation onto tBLMs modified surface. (A) Electrode surface coated with tBLMs; (B) Normalized impedance magnitude of modified surfaces was investigated and was compared with the interfacial interaction with and without the injection of live cells. Impedance values of CHO-K1 cells grown on tBLMs were nonsignificant. The error bars indicate the average standard error of three independent impedance magnitude measurements (n = 3); (C) CHO-K1 cells were stained for actin with Alexa Fluor 568 Phalloidin (red-orange); (D) Bar graph comparing average impedance values recorded after a 8 hour period, per electrode area (cm^2). One-way ANOVA was conducted to analyse bar graphs, followed by Tukey multiple comparison tests (*P< 0.05).

2.6.8 Impedance measurement of CHO-K1 Cell attachment on RGD-functionalized tBLMs (T10)

Following the negative result from the tBLM coating as a means to enhance cell attachment and spreading, a chemically functionalized-tBLM coating was created in an attempt to improve electrode-cell localized attachment, contact and communication.

Given the previous enhancement of cell attachment and growth using the thiol-PEG and POEGA linkers added directly onto the gold substrate, it was decided to now incorporate these and create functionalised tethered lipid bilayer membranes. The functionalised tBLMs were formed, as explained in Section 2.5.6. Impedance magnitude of the functionalized surfaces was investigated and was compared in the presence and absence of CHO-K1 cells. The increase in measured impedance signals confirmed the effectiveness of RGD-tBLMs to create a suitable electrode-cell interface, while visual fluorescence images confirm the ability of cells to grow and attach over RGD-functionalized tBLM surface (Figure 2.16).

Further, one-way ANOVA analysis followed by Tukey multiple comparison tests for average impedance values recorded after 12 hours revealed significant variations between the functionalized and non-functionalized-tBLM upon cell introduction, obtained p values obtained are less than 0.05, as shown in Figures 2.16 (D), below.

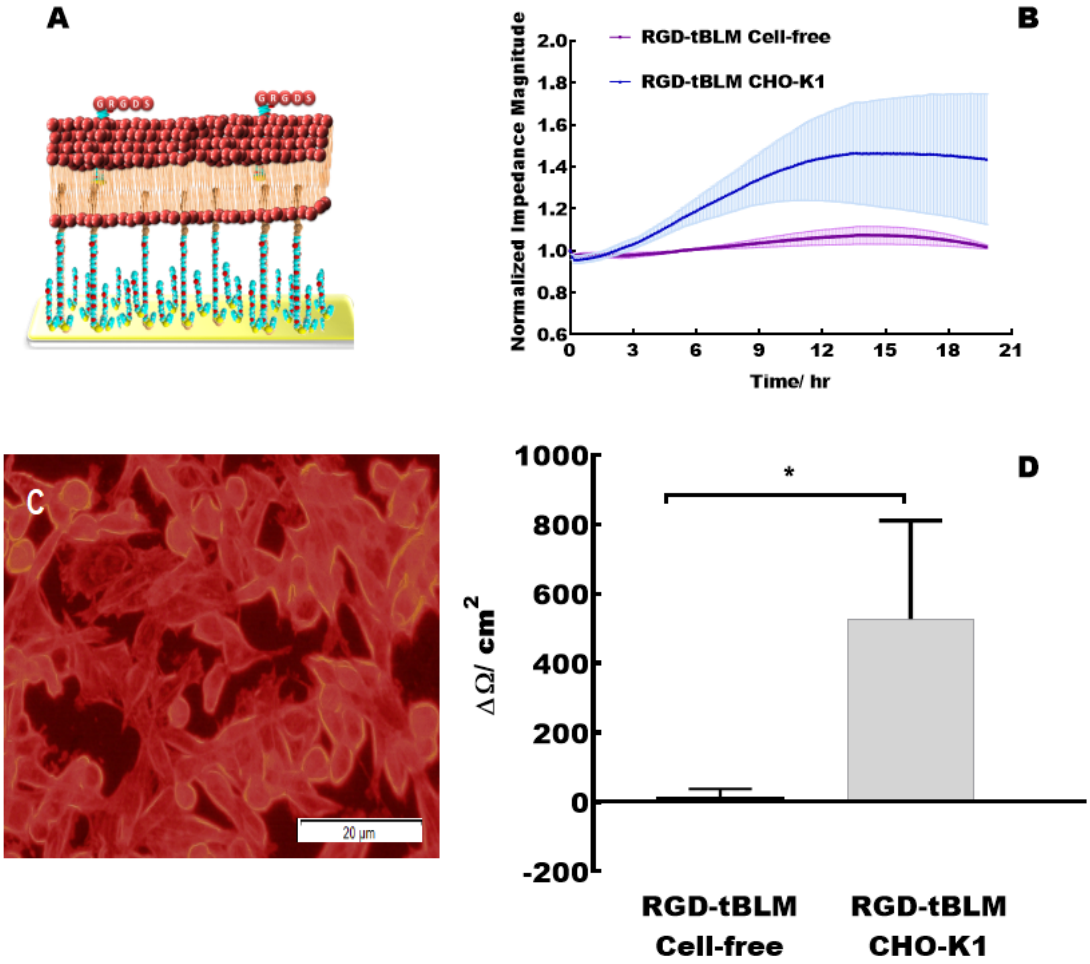

Figure 2.16: Impedance measurements of CHO-K1 cell attachment on RGD functionalized tBLMs (T10). (A) Electrode surface coated with tBLMs functionalized with RGD peptide; (B) Normalized impedance magnitude of RGD-tBLMs modified surfaces was investigated and was compared with the interfacial interaction with and without the inoculation of live cells. Increase normalized impedance values of CHO-K1 cells grown on functionalized tBLMs were displayed. The error bars indicate the average standard error of three independent impedance magnitude measurements (n = 3); (C) Fluorescent images of CHO-K1 adhered onto a gold surface modified with RGD peptide-functionalized tBLM. CHO-K1 cells were stained for actin with Alexa Fluor 568 Phalloidin (red-orange); (D) Bar graph comparing average impedance values recorded after 12 hours, per electrode area (cm^2). One-way ANOVA was conducted to analyse bar graphs, followed by Tukey multiple comparisons tests (*P< 0.05).

2.6.9 Impedance measurement of CHO-K1 cell attachment on RGD-functionalized tBLMs that were fully tethered (T100)

The different architecture of coupling was implemented utilizing a fully tethered lipid membrane (T100) in order to provide robust modification for subsequent cells introduction. Therefore the following experiments were designed to assess the relative effectiveness of cell adhesion and growth, over different membrane rigidity architectures.

As mentioned previously in Section 1.3.3, this type of tBLM membrane is very stable and provides vigorous coating [64, 65]. Variable lipid modifications were conducted, for instance, the high-affinity binding between biotin and streptavidin compounds by functionalizing fully tethered tBLMs with cyclic RGD peptide coupled to biotin (cRGD-PEG-PEG-Biotin), as seen in Figure 2.17 (A). tBLMs could be formed, as explained in Section 2.5.6. Impedance magnitudes of the functionalized surfaces were investigated and compared in the presence and absence of CHO-K1 cells.

The impedance results did not show any constancy when repeated numerous times. However, visual imaging of CHO-K1 cell displayed some cell attachment and growth over cRGD-functionalized tBLMs (T100) gold electrodes (Figure 2.17 C).

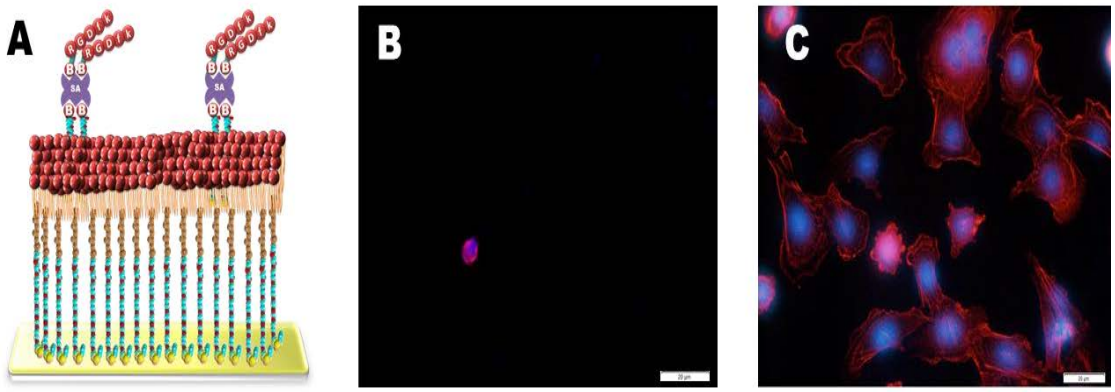

Figure 2.17: Visual imaging of CHO-K1 cell attachment on non-functionalized tBLMs and cRGD-functionalized tBLMs (T100) gold electrodes. (A) Electrode

surfaces coated with tBLMs that functionalized with Biotinylated-PE-Streptavidin-Biotin-PEG_PEG-RGD; (B) Fluorescent images of CHO-K1 adhered onto a non-functionalized tBLMs gold surface. CHO-K1 cells were stained for actin with Alexa Fluor 647 Phalloidin (red) and for the cell nucleus with DAPI (blue); (C) Fluorescent images of CHO-K1 adhered onto a gold surface modified with a cRGD-PEG-PED-Biotin functionalized tBLM. CHO-K1 cells were stained for actin with Alexa Fluor 647 Phalloidin (red) and for the cell nucleus with DAPI (blue).

Further fully tBLM model functionalization was employed: positively charged tBLM (DOTAP lipids), negative charged tBLM (PS lipids), RGD-tBLM, laminin-tBLM and fibronectin-tBLM as illustrated in Figure 2.6 (J- L). Our results demonstrated insignificant variation in magnitude impedance measurements. Besides, the visual imaging of CHO-K1 cell and SH-SY5Y showed only slight cell attachment and growth over various fully tethered (T100) tBLM coatings.

2.6.10 Comparison of diverse gold surface modifications using 2.1mm^2 working electrodes on CHO-K1 cell growth and adhesion

The ability of the modified surfaces to enhance cells growth and attachment was examined by average impedance values recorded over time, per electrode area (cm^2). The impedance magnitude was determined using electrical impedance spectroscopy. The normalised mean value provides a quantitative comparison of the relative amount of cell coverage on the differently functionalised surfaces, as seen in Figure 2.18. This comparison provides evidence that RGD-tBLM gold surface modification shows more impedance magnitude value in comparison to other surface modification, namely fibronectin, PEH-RGD and POEGA-RGD.

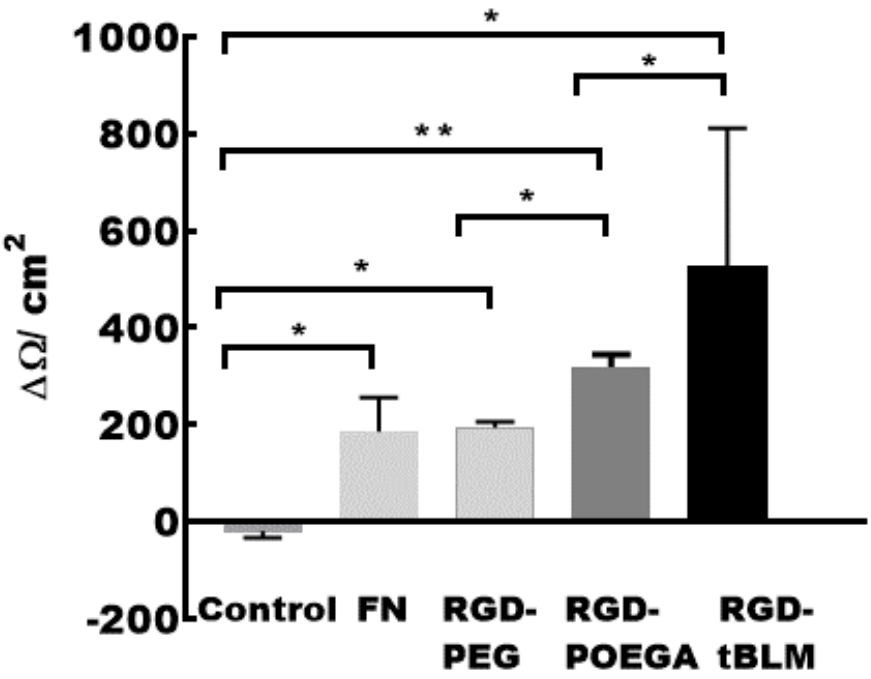

Figure 2.18: Comparison of impedance measurement of CHO-K1 cell growth and adhesion using various gold surface modifications on 2.1mm^2 working electrodes area. Gold working electrode surfaces (2.1 mm^2) coated with fibronectin, thiol-PEG-RGD, thiol-POEGA-RGD and tBLM-RGD. The impedance of the modified and as received surfaces was investigated and was compared with the interfacial interaction with live cells. Increase impedance values of CHO-K1 cells grown on tBLM-RGD functionalized gold electrodes were the highest. The error bars indicate the average standard error of three independent impedance spectroscopy conductance measurements (n = 3). Bar graph comparing average impedance values recorded after 18 hour period, per electrode area (cm^2). One-way ANOVA was conducted to analyse bar graphs, followed by Tukey multiple comparison tests (*P< 0.05 and **P< 0.01).

2.6.11 Impedance measurement of CHO-K1 cell attachment and growth on diverse gold surface modifications on small electrodes

In order to investigate the consequences of different working electrode size on cell growth and adhesion by assessing the magnitude of impedance measurements, small working electrodes (0.049 mm² area) were explored and their impedance compared with those for the larger working electrodes (2.1 mm² area) using the same surface modifications in the presence and absence of cells.

As described in material and method Sections 2.5.6, we used a variable surface modification for the cell growth and adhesion improvement. An electrode array comprising eight individual wells, as seen in Figure 2.5 (B), was placed in cell culture incubator at 37 °C with 5 % CO_2. Gold electrodes were interfaced to the tethaPod^{TM} impedance reader located outside the incubator by a home-made setup. CHO-K1 cells were seeded onto electrodes of size 0.049 mm² that were coated with either fibronectin, thiol-PEG- RGD or thiol-POEGA-RGD.

We monitored the growth and attachment of the cells by impedance magnitude recordings and fluorescence imaging. The result is presented in Figure 2.19 (A), is the representative impedance magnitude of CHO-K1 cell coverage demonstrating the fibronectin gold surface modification over two different working electrode size 0.049 mm² and 2.1 mm², along with the negative control of modified surface in the absence of cells. From these results, it was evident that the 0.049 mm² working electrode size modified with fibronectin coating, demonstrated higher impedance magnitude values in comparison to the 2.1 mm² working electrode size modified with the same coating.

Further statistical analysis was carried out using Graph pad prism, according to ANOVA statistical test analysis comparing the impedance magnitude values obtained for CHO-K1 cell adhesion and spread. The analysis demonstrated that there was a significant difference in the impedance magnitude of the modified 0.049 mm^2 surfaces in comparison to 2.1 mm^2 modified surfaces as indicated by one way ANOVA followed by Tukey's multiple comparisons statistical test, where the p-value obtained is below 0.05, as shown in Figure 2.19 (F).

The data suggests that using a commercially supplied smaller gold electrode gives improved impedance measurements of CHO-K1 cell growth on fibronectin functionalized gold surfaces, as seen in Figure 2.19.

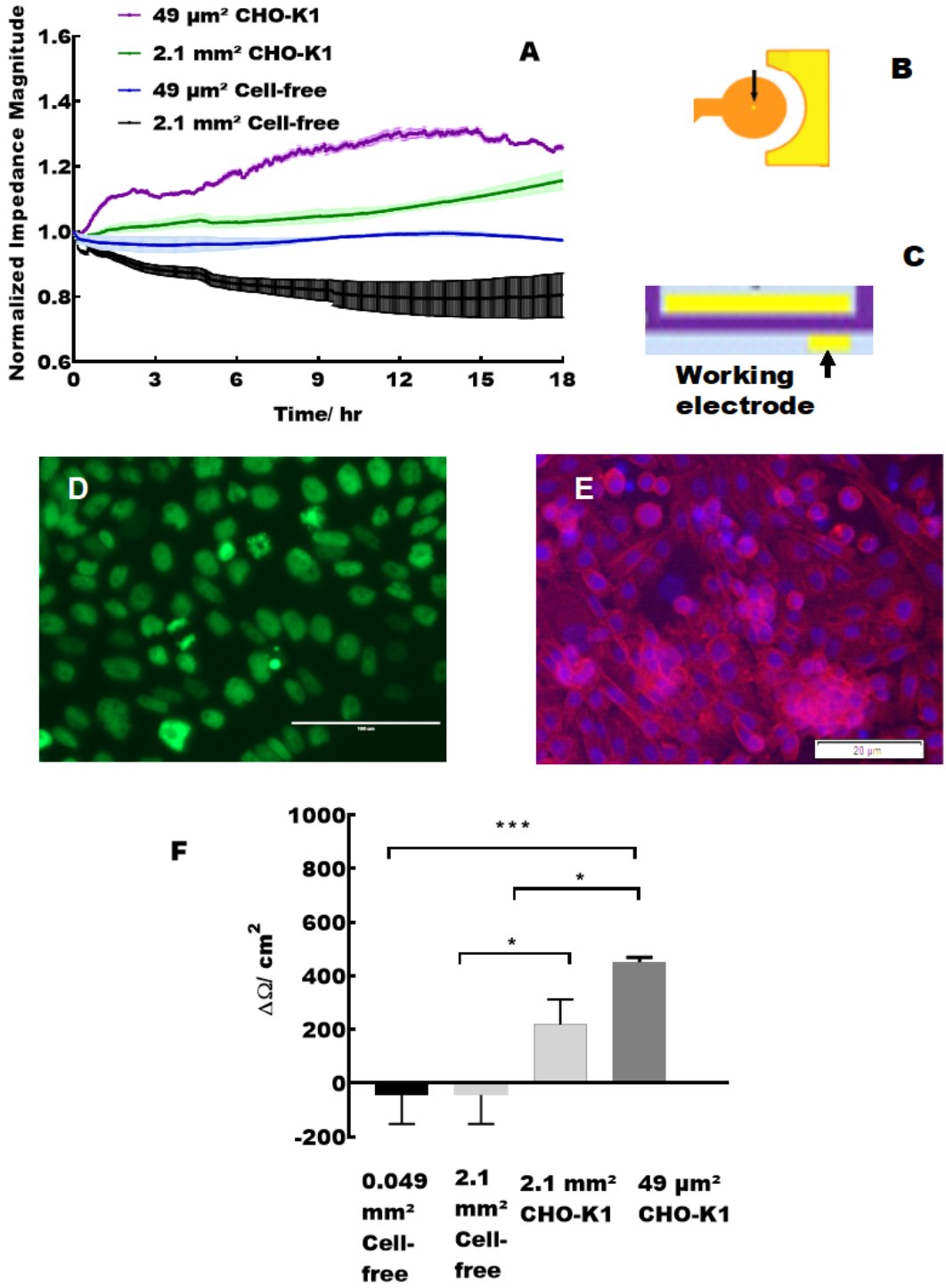

Figure 2.19: Comparison of impedance measurements using the variable working electrode size on fibronectin functionalized gold electrodes. (A) Electrode surfaces coated with 10 µg/ml fibronectin. The impedance of the modified and non-modified surfaces was investigated and was compared with the interfacial interaction with live cells. The error bars indicate the average standard error of three independent impedance magnitude measurements (n = 3); (B) Small working electrode 0.049 mm² in area; (C)

Large working electrode 2.1 mm² in area; (D) Fluorescence image of transfected CHO-k1 cells in the presence of GFP histone plasmid DNA (H2B-GFP); (E) cell nucleus with DAPI (blue); (F) Bar graph comparing average impedance values recorded over 16 hour period, per electrode area (cm^2). One-way ANOVA was conducted to analyse bar graphs, followed by Tukey multiple comparison tests (*P< 0.05 and ***P< 0.001).

CHO-K1 cell growth and adhesion were investigated using various gold surface modifications on 0.049 mm² area electrodes by comparing the impedance measurement values, as shown in Figure2.20. The 0.049 mm² gold electrodes were functionalized with fibronectin, thiol-PEG-RGD and thiol-POEGA-RGD. Then a comparison of impedance measures of CHO-K1 cell growth and adhesion using various gold surface modifications on 0.049 mm² small electrodes with the growth of the CHO-K1 cells on same gold surface modification while using 2.1 mm² large working electrode. Within these variable electrode modifications, POEGA polymer functionalized with RGD demonstrated the highest impedance values corresponding to the highest cell coverage.

Further statistical analysis was conducted. The analysis revealed that there was a noteworthy difference in the impedance magnitude of the 0.049 mm² modified surfaces in comparison to 2.1 mm² corresponding modified surfaces, as indicated by one way ANOVA followed by Tukey's multiple comparisons statistical test, where the p-value obtained is below 0.05, as seen in Figure 2.20 (B).

In this regards, the various gold electrode modification revealed improved impedance magnitude values using a smaller working electrode (0.049 mm^2) in comparison to the same modification using a larger 2.1mm^2 area working electrode.

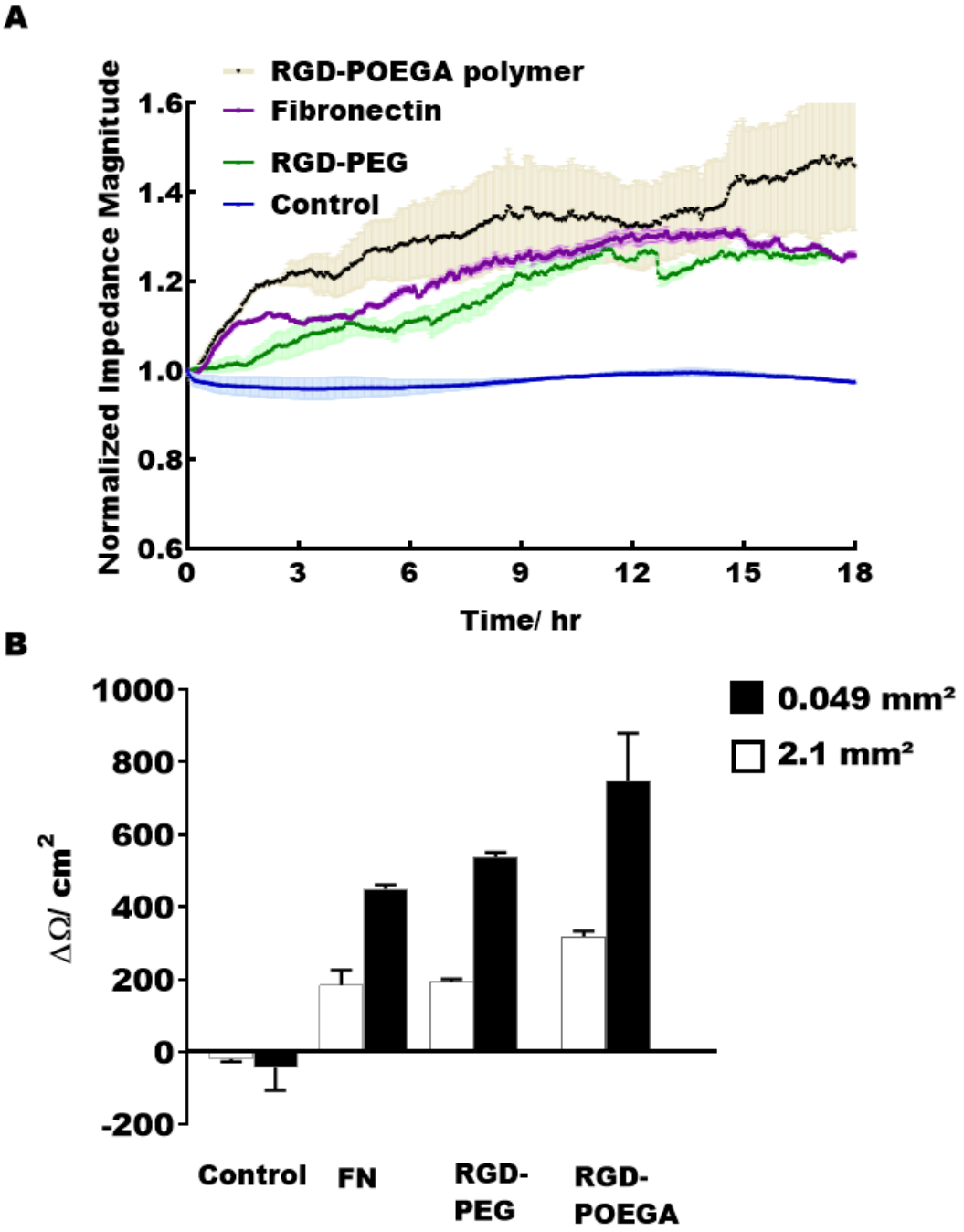

Figure 2.20: Comparison of impedance measurement of CHO-K1 cell growth and adhesion using diverse gold surface modifications on small electrodes with the growth of the CHO-K1 cells over RGD-tBLMs (T10). (A) Small working electrode surfaces (0.049 mm^2) coated with RGD-POEGA, fibronectin and RGD-thiol-PEG. The impedance of the modified and as received surfaces was investigated and was compared with the interfacial interaction with live cells. Increase impedance values of CHO-K1 cells grown on RGD-POEGA polymer functionalized gold electrodes were the highest. The error bars indicate the average standard error of three independent impedance

magnitude measurements (n = 3); (B) Bar graph comparing average impedance values between small (0.049mm^2) and large (2.1mm^2) working electrode using same surface modification, recorded over 18 hour period, per electrode area (cm^2). One-way ANOVA was conducted to analyse bar graphs, followed by Tukey multiple comparison tests (*P< 0.05).

Unfortunately, due to the incompatibility of small (0.049mm^2) working electrode with the tBLM coating modifications, it was not possible to examine the cell growth and adhesion using RGD-tBLM-0.049mm^2 gold surface. This was mainly related to the architecture of 0.049mm^2 working electrodes that are defined using a wax layer, which was easily destroyed with the ethanol component of the first layer of the tBLM coating.

2.7 Discussion

The goal of this study has been to make advances in electrode-cell technologies that can ultimately improve the quality of life for visually and hearing-impaired patients. The aim has been to develop an advanced interface that enhances efficiency and direct communication between electrical devices and biological tissues. As such, forming the necessary direct contact between the electrode and cell plasma membranes remains a key challenge in existing procedures for stimulating and reading ionic currents arising from neurons and other electrically active cells.

Combining impedance spectroscopy with fluorescence microscopy gives a unique investigational system for the study of cell adhesion, proliferation and compatibility. Impedance spectroscopy allows for monitoring cell coverage, electrical signal transfer and the cells' electrical properties, while fluorescence microscopy confirms cell growth and adhesion as well as providing information as to the compatibility of the modified surface adhesive.

Various coatings, along with different dimensions of gold electrode surfaces were explored to identify the impedance spectroscopy setup that creates an optimized, localized electrode-cell with close contact and communication.

2.7.1 Determining the effect of different gold electrode modifications, compared to bare tBLM on cell-electrode interactivity

Several studies have shown that ECM components such as fibronectin can be implemented to improve abiotic surface modification for cell adhesion and spreading

[151, 356]. In view of that, fibronectin is considered as one of the significant coatings that can induce cell adhesion and spreading. Our data support this, as seen in Figure 2.10, the fibronectin coating promoted cell attachment and growth. These findings supported our original hypothesis and acted as our proof-of-principal that gold-coated electrodes provided by our industry partner SDx, can be successfully tailored to monitor cell attachment and growth via impedance spectroscopy. Furthermore, fluorescence microscopy could be used in parallel (Figure 2.10, B) to demonstrate cell growth and attachment and thus support and complement our impedance data.

The frequency parameter selection for the impedance magnitude measurements is one of the critical parameters that represents the sensitivity of these experiments. In this study, three critical frequencies were examined, namely 185, 3125 and 12500 Hz. The change of the cells' monolayer magnitude impedance value was superior at the intermediate frequency of around 4 kHz, as seen in Figure 2.11. This finding is consistent with previously published studies of other groups at which this frequency displayed the most sensitive frequency that can mirror cell growth and adhesion changes [138, 139].

A possible explanation for this may be that at frequencies of around 4kHz, the impedance magnitude is heavily influenced by the resistive contributions from the intercellular and subcellular spaces, thus it can detect any alteration within the tightness of the cell-cell contact area and cell-substrate area [139, 357]. Whereas at frequencies of higher range, the impedance magnitude is heavily influenced by the capacitive contributions arising from the cell membranes [357]. This (4kHz) optimal frequency was therefore employed for the experiments in this study.

Impedance spectroscopy measurements are highly sensitive to cell growth and adhesion variations. For cell-cell and cell-substrate interface monitoring over the time course, detachment compounds were applied. EDTA, the detachment agent, was introduced over the confluent cells layer of coated electrode. Impedance spectroscopy recordings have revealed a decline in measured magnitude impedance. In other words, when the cell coverage layer was disrupted due to cell detachment agent addition, the impedance reduced, due to the absence of impeding layer which caused a previous increase in measured impedance, as shown in Figure 2.12. These results further confirmed that the impedance changes we were observing were, in fact, directly related to the attachment and spreading of the cells.

Several studies have been undertaken in order to understand the effect and mechanisms of RGD peptide on cell adhesion that is known as the main binding site for cells in ECM molecules [295]. For instance, the spacing between RGD molecules is a critical factor in cell-surface interface [153, 227].

In this regards, our comparative study using different linker lengths indicated that close contact between the RGD peptide and the electrode surface has a more potent effect on promoting cell adhesion and spread. These results are similar to the findings obtained by Houseman et al., 2001 [332]. In another study, Attwood et al. (2016) used three different lengths of PEG linkers that were functionalized with RGD motif in order to investigate cells behavior. They found the human foreskin fibroblasts cells focal adhesion progressions were mature, long and wedge-shaped when short linker surfaces were used, while on longer linker surfaces the focal adhesions were immature, smaller and more circular shaped. Thus cells adhesion and proliferation is directly enhanced by the reduction of the functionalized linker length [358].

In this study, a comparison between dodeca-OEG lengths and POEGA polymer-modified on a gold surface and functionalized with RGD demonstrated that POEGA polymer di-ethylene glycol group readily binds the RGD motif and has a significant improvement in cell adhesion in comparison to longer dodeca-ethylene glycol chains, as illustrated in Figure 2.14.

In addition, based on RGD studies, the epithelial cell growth showed a higher density of cells over RGD functionalized surfaces in comparison to neuronal cells. Both electrochemistry impedance measurements and fluorescence microscopy data supported RGD-cell adhesion (Figure 2.13). This is in agreement with studies by other researchers examining the ability of RGD peptide to enhance adhesion of variable cell types to modified surfaces [359, 360].

Various studies have shown that the adhesion and growth of different types of cells behaved differently when seeded on diverse functionalized surfaces, for example, glass surfaces that modified with laminin showed neurites extension of seeded neuronal cells, while poly-ethyleneimine surfaces modified with laminin displayed random neuronal cells growth [361]. Thus, cells adhesion and differentiation are controlled by numerous factors, for instance, the interaction of cells with the corresponding adhesive binding sites on the ECM [362]. In this regards, a recent study by Farrukh et al. (2017) was found the surfaces that modified with specific neuronal receptor-mediated such as Ile-Lys-Val-Ala-Val (IKVAV) ligand enhanced neuronal cells growth and spreading [363]. Likewise, Ehteshami et al. have observed that when using neuronal cells, adhesion was minimal with RGD peptide in comparison to IKVAV, a laminin-based peptide [359]. IKVAV ligand has also been shown to promote neurite outgrowth [364].

This enhancement of neuronal cells growth was due to the existence of IKVAV mimetic peptide, which is a short ligand of the adhesive site on laminin [365]. The laminin is a well-known protein of ECM that abundantly exist in brain tissues and have a critical role in neuronal spreading and growth improvement as well as extending neurites extension enhancement [366, 367].

On the other hand, the RGD tripeptide is derivative from various ECM proteins such as fibronectin and laminin, that promote and support cell adhesion, however RGD peptide possess high affinity and specificity for $\alpha_v\beta_3$ integrin that widely found on the epithelial cells surfaces such as CHO-K1 in comparison to neuronal cells such as SH-SY5Y [360, 368].

2.7.2 Assessing the functionalized-tBLM coatings ability to enhance electrode-cell localized contact and communication

Using non-functionalized tBLMs in association with electrical impedance spectroscopy, it was revealed that these coatings are unlikely to promote cell adhesion. Our initial study displayed the repellent characteristics of non-functionalized tBLMs towards cell adhesion (Figure 2.15). This finding matched earlier studies that indicated natural fluid lipid bilayer membranes were protein and cell repellent. As shown by Andersson et al., in the presence of SLB membranes, there was no notable cell adherence or growth in comparison to a control surface. The authors indicated that phosphatidylcholine bilayers are resistant to protein adsorption and as a consequence, resist cell attachment [369].

Further, Kam and Boxer demonstrated fetal bovine serum (FBS) components in the culture media had similar cell repellent influences [370, 371]. However, later studies do

not support this and have demonstrated cell attachment and proliferation on lipid membranes in the presence of a variable percentage of FBS (1-20%). It is likely that proteins from the FBS itself contributed to the cell adhesion and growth noted on these membrane coated surfaces [45, 372].

Furthermore, a study by Groves et al. displayed that different lipid membrane compositions has a profound effect on cell binding affinity. For instance, phosphatidylserine lipids can induce cell adhesion [37]. While further studies revealed a mixture of positively charged lipids with different percentages of unsaturated lipids as a component of the SLB membrane could improve neuronal cell adhesion [38, 39].

It is well-known that cellular behaviour is in response to the surrounding microenvironment via the various physical and chemical cues controlling such activities as cell adhesion, spread, differentiation and death [373-375]. Cells naturally form linkages to the ECM proteins using transmembrane integrin receptors [272]. The RGD motif is the minimal adhesive ligand within various ECM proteins that connects and promotes cells adhesion [376, 377]. In this study, the tBLM (T10) was functionalized with RGD peptides in order to provide a close mimic of natural cell membranes as well as to the natural surrounding microenvironment.

It was demonstrated previously that artificial lipid membrane represented by SLB, when functionalized with RGD ligands, resulted in notable improvements in cell attachment and growth over these RGD functionalized membranes [46, 47]. According to our results (Figure 2.16), functionalized RGD-tBLMs provide an increase of impedance magnitude values demonstrated cell growth and proliferation when compared to the same functionalized membrane in the absence of cells. However, there was a high fluctuation

between different repeats that was demonstrated by wide standard error range. Statistical analysis of functionalized-tBLM with or without cells revealed the significant variance in impedance magnitude measurements. The fluorescence microscopy images suggested RGD-tBLMs compatibility for cell growth, though there was less amount of cells density over RGD-tBLM, as shown in Figure 2.16 (B).

The results of the present study indicate the sensitivity of cells-RGD-tBLMs (T10) interactions that provide enhancement of cells impedance profile in comparison to the other surface functionalization; this is clearly illustrated by the comparison column graph in Figure 2.18. Also, the results in this study presented less cell density coverage of RGD-tBLM (T10) surface, as seen in Figure 2.16 (C), in comparison to other modified surfaces in this study, which would interfere with the principal aim of this study to use tBLM in implantable technology.

One of the explanations that may account for the absence of complete cell coverage is the properties of the lipid bilayer membranes that cause cell repellent [369]. This, in turn, directly reduce the number of the attached cell over the surface of the bilayer lipid membrane. This finding points to the critical role of the RGD tripeptide in cell adhesion. Such types of RGD-tBLM functionalization would facilitate the close adhesion of cell surface receptors to RGD tripeptides, thereby improving the induction of cell growth. The distance between the RGD functionalized phospholipids molecules (COOH terminate) would also affect the amount of cell adhesion and spreading over the modified surface. As mentioned previously, several studies have been revealed that the variation in RGD tripeptide density of promote cell adhesion and spreading differently, which is most likely due to variations in number and strength of integrin-ligands bonds [354].

In view of that, cell growth and spreading over the implanted surface is one of the critical interfaces for implementable technology improvement. This interface between specific cell types such as specific neuronal cells populations and modified electrode enables specific cell attachment and growth as well as eliminate the growth of other invading cell types such as macrophages that directly affect implantable electrode integrity and functionality [378]. Indeed, mimicking the normal function of neuron cells *in vitro* is a crucial step towards developing implantable technologies. Thus, despite the enormous studies and gains in implementable technology, the delivery of high-selective modified electrode that provides close contact between the cell and electrodes in addition to minimize ion leakage pathways remains largely unfulfilled. Therefore, these findings presented here need further experiments in the future in order to strengthen the proposal for *in vitro* modified electrode that cell attachment and growth could be enhanced.

Further experiments were performed in this study by using different lipid compositions (previously considered) and lipid functionalization. The T10 tBLM was comprised of 10% tethering molecules and 90% spacer molecules, while T100 tBLM was comprised of 100% tethering molecules [379]. In comparison, the T10 tBLM provides a closer mimic to natural lipid membranes by allowing sufficient space for water content at both sides of the membrane. In contrast, T100 tBLM provides a highly rigid artificial membrane with water content restricted mainly to the exterior side of the membrane [57].

This study was conducted using two different tBLM membrane models, namely T10 (10% of tethering chemistry) and T100 (100% of tethering chemistry). In this regards, based on the obtained result using the fully tBLM model (T100) that modified with different functionalization, as seen in Figure 2.6 (J-L), it becomes clear that both modified and unmodified fully tBLM demonstrate insignificant impedance magnitude values upon

cell seeding, while the visual imaging of cells (Figure 2.17) revealed a slight cell growth and spreading on these coatings.

Thus, from this, we can postulate that the reasons for poor cell growth and adhesion of cells over fully tethered tBLMs could be due to the membrane architecture, which is highly rigid and which restricts lateral membrane mobility. As such, there is a loss of membrane fluidity within the fully tethered tBLMs [64, 65]. Oliver et al. (2009) demonstrated that the fluidity of lipids has a significant role in cell adhesion, as excessively fluid lipid bilayers mostly block cell adhesion. Alternatively, when the same author used a fixed monolayer lipid membrane; results demonstrated the promotion of epithelial cell attachment and growth [40]. This suggests that the architecture, and in particular the fluidity of lipid membranes, has a high impact on cell growth and adhesion. Further, it suggests that the fluidity of the RGD-tBLM (T10) better mimics native cell-ECM as well as cell-cell interfaces.

2.7.3 Evaluating the consequences of different working electrode size on the magnitude of impedance measurements due to cell growth and adhesion

Several studies confirmed the influence of working electrode size on the detection sensitivity to reflect cell adhesion and growth events [138, 380]. The work of other groups has confirmed that smaller-area working electrodes improve the sensitivity in impedance relative to cell density variations as well as generating higher impedance magnitude values. This observed higher sensitivity of smaller-radius working electrodes is related to its higher impedance magnitude values that consequently provide an improvement of

signal-to-noise ratio, as well as a reduction in solution resistance from the surrounding medium [138].

From this point of view, it was essential to investigate the various surface modifications using smaller-radius working electrodes and establish if this could improve detection of cell adhesion and spread. Therefore, the small size of 0.049 mm^2 electrodes was employed and compared with magnitude impedance values of larger 2.1 mm^2 working electrodes. Our real-time measurements demonstrated that the small dimension working electrodes displayed higher sensitivity in comparison to larger working electrodes. This is in agreement with studies by other groups [138]. Among the examined interfaces, POEGA Polymer-RGD demonstrated the most improved localized electrode-cell intimate contact and communication (Figure 2.20).

Another point of view is that are being directed towards using smaller implanted electrodes. Though the choice of the electrode metal and size is a critical issue when trying to stimulate excitable tissue and minimize the cascade formation around the implanted electrode, the so-called capsule [381]. For instance, Campbell et al. showed that very small diameter implants are associated with a thin capsule [382]. However, the implanted electrode size of currently used devices, such as cochlear implants, is mainly limited by current injection.If a high current is injected, heat would be generated; thus, as a consequence electrochemical reactions in the tissue would be driven [383, 384].

2.8 Prospective future implantable electrode model

In regards to the previous results, cell attachment and growth over modified surfaces was found to be enhanced by various microenvironment factors: First, the distance between

adhesion ligand and the surface. It was found that smaller distances between the adhesion ligand and the membrane surface, provide a more potent effect in improving cell adhesion and spreading. Second, owing to neuronal cell surface interaction with the adjoining modified surface, modifying surfaces with specific ligands such as IKVAV pentapeptide would most likely enhance neurite outgrowth and attachment on the modified electrodes. Third, using fluid and functionalized tBLMs (T10) as a coating provides fewer leakage pathways between cell-surface interface as well as minimizing non-specific cell binding due to cell membrane repellent properties. It would be appropriate that future studies determine more precisely the optimal distance between the ligand and functionalized phospholipid heads to ensure the cell adhesion enhancement. It would be appropriate that future studies compare the functionalized tBLM coating with standard implant surfaces such as silicon, platinum, titanium or ceramics. Fourth, using a group of multiple nanoscale electrodes side by side would increase the intensity of the delivered electrical signal to specific neuronal cells, for instance using Multiparous surfaces would increase the surface area within the overall nanoscale dimension.

Accordingly, based on these criteria, we postulate that a combination of different parameters would improve implantable electrodes technology, as illustrated in Figure 2.21. Basically:

- Receptors that capture specific cells in order to achieve the intimate contact between the tBLM at the electrode surface and the membrane of the sequestered cells.
- A biocompatible surface, to protect the sequestered cell from contacting the driving metal electrode. This is to minimize tissue scarring at the electrode surface.
- Ion channels embedded within the tBLM permit the passage of a high flux of ions from the reservoir space to the sequestered cell surface. This can increase the

specificity by providing specific target signals towards specific types of cells that are attached to the tBLM.

- An ionic reservoir area between the tBLM and the tethering gold electrodes capable of storing sufficient ionic charge which when driven through the ion channels embedded in the tBLM will be sufficient to trigger an action potential in a sequestered cell.

Thus, in the future, such an electrode coating model constructed using the findings from this study could lead to significant improvements, ultimately resulting in the use of these surfaces as effective implantable electrodes.

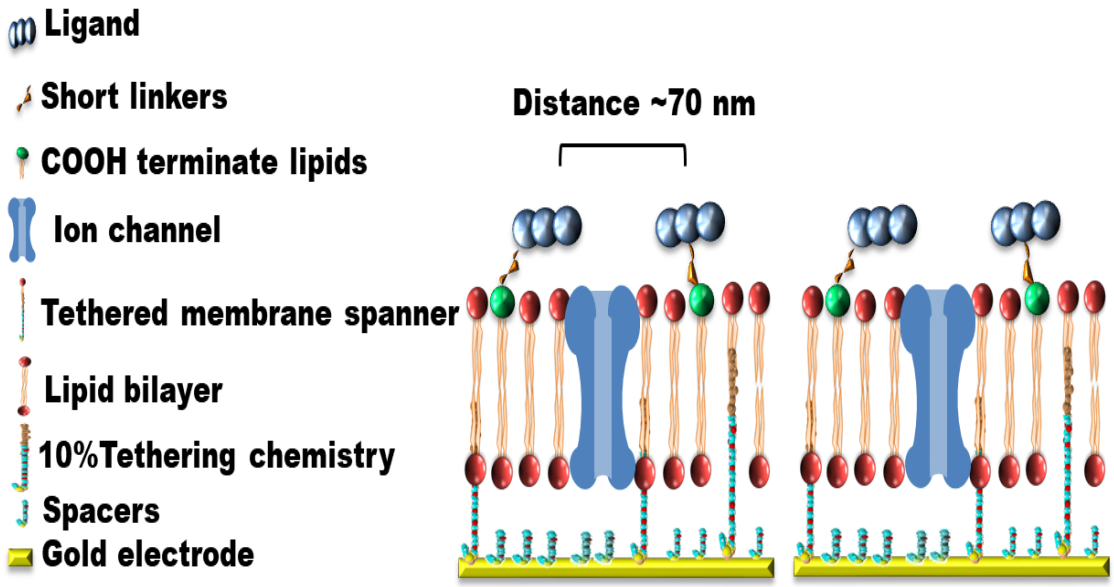

Figure 2.21: A schematic model representing an ideal coated electrode for enhanced implantable technologies. The gold electrode surface combines with the tethering chemistry and spacer forming the tBLM membrane model (T10). Large ionic reservoir area to store ions. Inserted specific ion channels to drive ion passage through these channels. The phospholipid bilayer is shown a mixture of zwitterionic mobile lipids and COOH terminate phospholipids with percentage corresponding to distance between COOH phospholipid head group around ~70nm. A schematic model of short linkers

between the phospholipid head group and ligand. Specific ligand conjugate would enhance specific cell type adhesion and growth.

In conclusion, the amalgamation of the biologically active elements with biocompatible electrodes is critical to stimulate and monitor cell activity *in vitro*. A biocompatible electrode coating that permits localized electrode-cell intimate contact and communication would improve the selectivity and sensitivity of electrodes that are employed to stimulate and monitor cell activity *in vitro* and *in vivo*. The designed model, as seen in Figure 2.21, is based on our findings from this study and presents a possible future implantable electrode that would improve the cell-electrode interface. Overall, these findings highlight the importance of adhesive cues in the improvement of electrode-cell contact efficiency.

Chapter 3

Developing ion-channel switch nano-biosensors for direct cell detection

Chapter 3

Developing ion-channel switch nano-biosensors for direct cell detection

3.1 Introduction

There is an increasing demand for improving discriminative and sensitive biosensors that are able to detect different cell types amongst heterogeneous cell populations. Widespread studies have been established in order to develop a label-free and real-time cell detection biosensor. The usual methods for direct cell detection typically involve labelling [385]. Moreover, currently used techniques lack the ability to address mixed samples. In order to overcome the limited applied cell detection methods, novel methods are required.

The main objective of this study was to develop new approaches for the detection, and isolation, of cells at very low concentrations within a mixed population. Here, this chapter describes the attempt to develop and to provide label-free, real-time cell isolation and detection. This will be accomplished by applying a new modification onto the ion nano-sensor switch technology established by Cornell et al. in 1997 [79].

Likewise, this chapter studies the attempt to identify streptavidin coverage in the membrane architecture and characterize the ion-channel switched tBLM utilizing electrical impedance spectroscopy and neutron reflectometry methods. Along, with the assessment of the feasibility of cell detection by using the direct gramicidin biosensor system using different binding motifs. Besides, investigating the development of an RGD competitive assays of the ion channel nano-biosensor switch. Furthermore, this chapter

outlines the background of gramicidin peptide and gramicidin nanosensor switch architecture and mechanisms.

3.2 Gramicidin peptide

Gramicidins are hydrophobic linear pentadecane peptide ion channel that have the ability to passage cations through membranes [386, 387]. Gramicidin antibiotics were originally isolated from the bacteria *Bacillus brevis*. Unlike most identified proteins and peptides, gramicidin isoforms possess an alternating sequence of *L* form and *D* isomer amino acid, this, in turn, allows gramicidin to form a hydrogen bond helix [388]. There are various forms of gramicidin peptide; namely A, B and C that consist mainly of 15 amino acid residues. The differences between the various isoforms are related to the peptide residue at position 11 [389].

Amongst these different isoforms, gramicidin A (gA) represent the most hydrophobic peptide due to the existence of four tryptophan residues in their structure [390-392]. Tryptophan residues influence gA structure and function; as a consequence, improve the integral component of the channel activity and conductivity [390-392]. gA includes a tryptophan residue at position 11, which is fundamental to the gA ion channel structure and function [393-396]. Substituting tryptophan with other amino acid leads to the reduction of gA ion channel cation conductivity [397-399]. gA amino acid sequence and structure is illustrated in Figure 3.1.

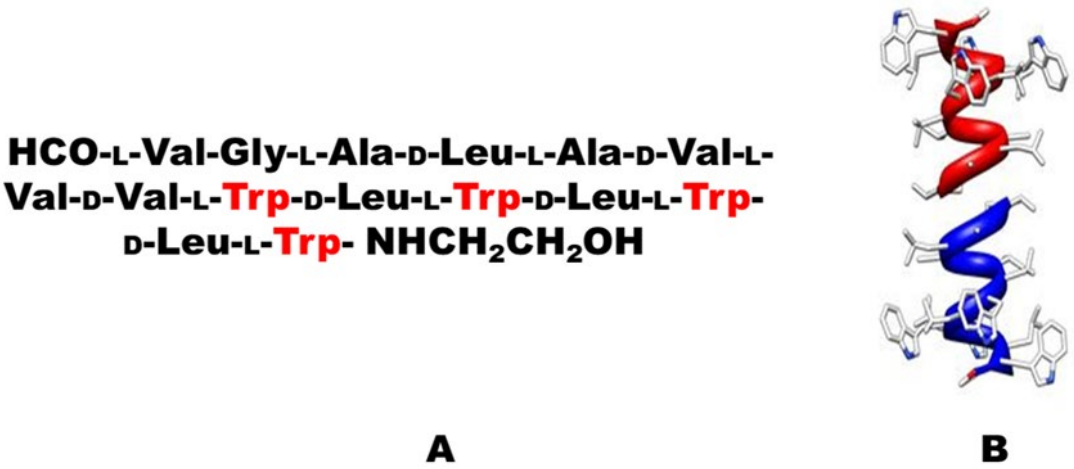

Figure 3.1: Gramicidin A transmembrane ion-channel sequence and structure. (A) gA amino acid sequence. Ala, Leu, Val amino acid side chains are hydrophobic, Trp amino acid from a side chain is amphipathic and the N-terminal is replaced with a formylated valine, while the C-terminal is replaced with the ethanolamine [388, 400]; (B) gA ion channel structure. Alternating L, D-amino acid sequences enables gA to fold as a right-handed β-helix stabilized by a hydrogen-bonding pattern. Within the lipid bilayers, the C-terminus is directed towards the membrane surface as a consequence of hydrogen bonds between tryptophan and phospholipid head groups, while N-terminus is aligned with the internal hydrophobic components of the lipid membrane. The gA structure figure was taken from the Research Collaboratory for Structural Bioinformatics (RCSB) of Protein Data Bank (PDB) (RCSP-PDB) (code 1GRM) [401].

A membrane ion channel is formed from coupling the two gA monomers by hydrogen bonding. This occurs when each monomer of the dimeric complex resides in opposing leaflets of a lipid bilayer. The full gA channel width is nearly 4 Å and about 25 Å in length, giving it a selectivty for monovalent cations [402, 403]. Each gA ion channel can conduct ~ 10^6 ions per second for cationic complexes of less than 2 Å diameter, such as the K^+ and Na^+, while the bigger cations are excluded, such as tetramethylammonium ($(CH_3)_4N^+$) or ammonium (NH_4^+) [402, 404]. Thus gA channel has a cationic conductance specificity as well as dimerisation dependancy.

3.3 Association and dissociation of gramicidin-A ion alters channel gating

Several studies were carried out to determine the dissociation and association events of gA dimer with the aim of exploring the gating of the gA ion channel [405-408]. The hydrocarbon thickness of the membrane, membrane voltage and ion occupancy were demonstrated as important factors that directly affect the rate of gA dissociation and association. Rudnev et al. (1981) revealed that the concentration of salt in the aqueous solution surrounding the bilayer lipid membrane alters the bilayer surface tension [409]. Elliott et al. (1986) found the lifetime of each single gA channel was increased as the mono-acylglycerol lipid monolayer membrane thickness decreased until, at ~2.2nm, the lifetime of the channel was constant [407]. Ring et al. (1992) found that the lifetime of the gA channel is dependent on the ion occupancy levels [406].

Another study, conducted by Sandblom et al. (2001), demonstrated that the proportion of gA channel dimers formed escalates with an applied voltage of up to 50 mV [405]. Wanasundara et al. (2011) disclosed that the dissociation of gA dimers ensues through the lateral movement of gA monomers within the lipid bilayer [408]. Further, the dissociation energy of gA dimers in a dimyristoylphosphatidylcholine bilayer membrane was approximately equivalent to the energy cleavage of six intermolecular hydrogen bonds [408]. Through these studies, and others, it became clear that gA ion channel gating is dependent on dimerisation of monomers in opposing leaflets of the bilayer (Figure 3.2).

3.4 Gramicidin-gated ion channel nano-switch biosensor

Gramicidin ion channel switch (ICS) biosensors were first conceived by Cornell et al. in 1997, inspired by the distinctive electrical conductive characteristics of gramicidin dimers [79]. The gramicidin biosensor platform was initially developed in order to detect variable bio-threats, for instance, detecting influenza virus [95, 96].

The ICS biosensor architecture is built on a gold surface, employing sulfur-gold bonds and polar linkers. The first layer is constituted of mercaptoacetic acid disulphide (MAAD) or ethylene disulphide (EDS) spacer molecules and half-membrane-spanning tether molecules, as discussed previously (Chapter 2).

Moreover, the first layer includes tethered gramicidin monomers embedded within the inner leaflet of the membrane bilayer, as well as immobile tethered membrane-spanning lipids (MSLa), tethered to the gold substrate functionalized with a biotin termination. The second layer is completed with mobile gA monomers and transient half-membrane-spanning lipids. These mobile gramicidin monomers possess a 5-aminocaproyl linker molecule [410] which is terminated with biotin. Thus, subsequent functionalization relies on streptavidin-biotin strong coupling affinity. In turn, the detector molecules (e.g., antibodies) are biotinylated and also bound to the streptavidin molecules. The ICS system architecture illustrated in Figure 3.2.

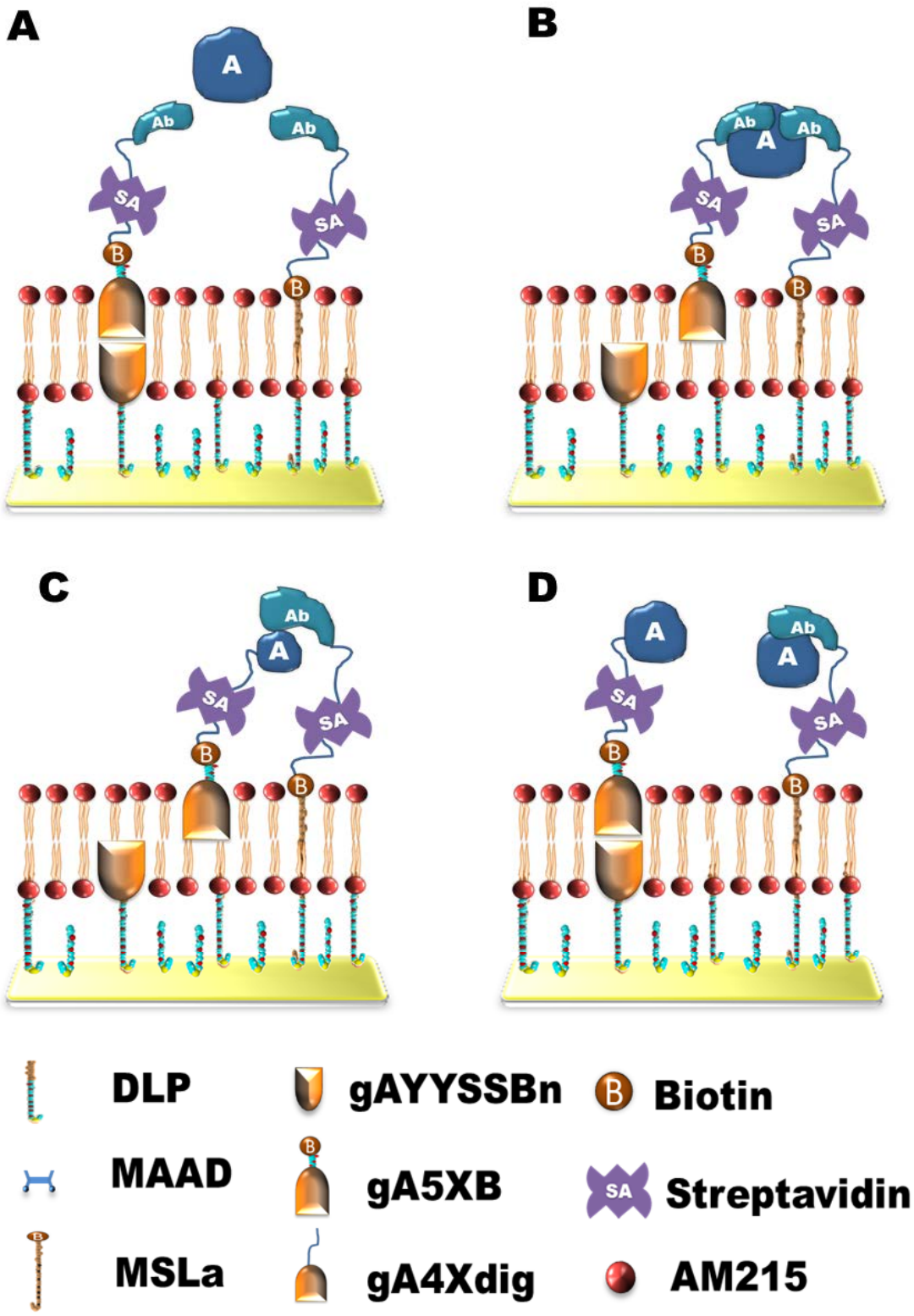

Figure 3.2: Representative schematic illustration of ion-channel switch (ICS) biosensor. The MAAD and tether molecules over the gold electrode offer a reservoir area that enables the unimpeded current flow. Figure (A) and (B) represent the direct ICS assay. (A) The reactive site of the freely mobile gramicidin monomers and tethered

membrane spanner are coupled to the antibody fragment. The gA ion channel is conductive due to the regular formation of dimers between mobile and immobile gA monomers; (B) In the presence of an analyte, the mobile gA channel within the outer leaflet of the membrane and MSLa are inter-bound with the analyte. Thus, the mobile gA channel is unable to dimerize with its immobile gA monomer partner. As a result, the ionic current across the membrane is reduced and the overall measured membrane conduction will drop. Figure (C) and (D) represent the competitive ICS assay; (C) Ion channel are kept in their monomeric form prior to the introduction of the analyte. The mobile gA monomer is immobilized due to its interactions with molecules that mimic the sample; (D) The introduction of the sample of interest will compete with the previously attached analyte mimic for the antibody-binding site. This, in turn, will release the mobile gA monomer permitting it to dimerise with the immobile gA monomer. This modified Figure was based on [79].

3.4.1 The direct two-site sandwich ICS sensor

In the gramicidin-A biosensor direct assay, the concentration of biotinylated gA molecules /cm^2 in the membrane second layer is equivalent to 3.0 x 10^9 molecules /cm^2, biotinylated membrane-spanning molecule density is less than the biotinylated gA density which is equivalent to 6.7 x10^8 molecules/cm^2, while the concentration of introduced streptavidin ~ 1 pM [79]. The dual functionalization of the mobile gramicidin monomers and MSLa utilize whole antibodies or antibody fragments. In the absence of an antigen analyte, the biosensor freely permits the dimerisation between the mobile and immobile gA monomers giving relatively high membrane conduction reading across the tBLM. The introduction of the target analyte causes the antibody fragments to bind to the analyte. When this happens, the mobile gA monomers are prevented from dimerising with the tethered gA monomers and overall membrane conduction drops.

3.4.2 The competitive ICS sensor

In the competitive assay version of the ICS sensor (Figure 3.2 C and D), the tethered MSLa compounds are functionalized with a targeted analyte mimic. In the absence of the analyte, an antibody-linked gA (gA4Xdig) molecule will couple with the analyte mimic preventing the development of gA dimers. In this case, the overall membrane conduction is minimal. The addition of the target analyte will compete with the previously coupled analyte mimic, permitting the analyte-mobile gramicidin to diffuse freely, enabling the dimerisation between it and the immobile gramicidin monomers, which amplifies membrane conduction.

3.5 Outline of this research study

Here, we hypothesized that instead of using the gA-biosensor for analyte-antibody detection, the biosensor might be used to as a nano-biosensor for cell detection. Thus the overall aim of this study is to examine the feasibility of cell detection using direct gramicidin biosensor system.

3.5.1 Study streptavidin coverage on biotinylated gA monomers

The initial employment of streptavidin as an intermediate coupling component was for its high binding affinity towards biotin molecules (K_d~10^{-13} M) [411]. There are several forms of streptavidin derivatives from in *S. avidinii*. However, the C-terminus streptavidin form displays a superior binding affinity for biotin molecule [412, 413].

However, previous electrical impedance spectroscopy studies have shown that the introduction of streptavidin as an intermediate coupling component induces a reduction

in membrane conduction [79]. Streptavidin is commonly used as a coupling agent due to its extremely high binding affinity to biotin molecules, in addition, to its ability to perform efficiently in environments such as extreme temperature, pH, solvents and enzymes [414]. Questions still remain, however, regarding the mechanisms that are involved in the interaction of streptavidin with biotinylated lipids or biotinylated gramicidin monomer components within lipid bilayers.

Therefore, the first part of this project aimed to examine streptavidin interaction with biotinylated gramicidin monomers across lipid membranes, as well as to assess streptavidin coverage over lipid membranes in order to determine the concentration of possible binding sites. This will be done by using different techniques, namely: electrical impedance spectroscopy and neutron reflectometry methods.

The electrical impedance spectroscopy studies will be undertaken using a tBLM system using different streptavidin concentrations. The tBLM-ICS biosensor and EIS will provide direct information on the streptavidin at various concentrations of interaction with the freely mobile biotinylated gramicidin monomers and will allow understanding the factors that regulate the gA channel activity. Neutron reflectivity assays will elucidate any structural changes of the tBLM system that will provide direct information whether streptavidin binding also induces any membrane morphological changes

3.5.2 Development of direct two-site sandwich ICS biosensor

Cells naturally possess the ability to sense and react to their surrounding environment; this is governed by binding of various cell membrane receptors (integrins) to the extracellular matrix (ECM) proteins [415]. ECM protein-integrin binding at the

membrane surface plays a crucial role in various biological processes, such as maintaining tissue structural integrity and cell transduction [416].

In this study, different binding motifs were examined in order to enhance sensor efficiency. These binding motifs can recognize specific receptors at the cell membrane surface. As described below, the motifs chosen for this study were RGD peptide, streptavidin and concanavalin A.

3.5.2.1 Development of RGD direct two-site sandwich ICS biosensor

RGD (Arg-Gly-Asp) binding motifs provide biomimetic properties for cell attachment and growth and, as a consequence, various studies have used RGD peptide to form a well-packed layer for inducing cells adhesion over different surfaces, that were then subsequently used as sensors for specific pharmaceutical compounds on cells [354, 417, 418]. RGD peptides can be recognized by almost half of all known integrins embedded into cell membranes [293]. The RGD-integrin interface creates cell adhesion recognition sites called *focal adhesions* and also mediated intracellular signalling pathways [376, 419, 420].

The direct ICS nano-sensor was functionalized with biotinylated cyclic RGD (cRGD) utilizing the high binding affinity of streptavidin-biotin molecules. Studies have reported a higher cell attachment to cyclic RGD peptides in comparison to linear peptides [421]. For this reason, we utilized cRGD peptide to functionalize the gA-ICS sensor to attract cell surface recognition sites in order to couple and interface with it.

Traditional cell detection approaches usually employ antibodies and labelling techniques, such as the use of exogenous fluorophores [385]. Challenges still remain to build a label-free nano-biosensor capable of distinguishing individual cells types in a heterogeneous cell population. Here, as a proof of principle, we aim to construct a label-free, real-time and biomimetic functional nano-biosensor that can detect low cell concentration by functionalizing the ICS-tBLM biosensor with RGD binding motif, as seen in Figure 3.3. However, there is a risk of a reduction of the binding affinity between the binding motifs such as RGD and cell integrins in comparison to the binding affinity of specific antibodies to cell membrane surface [422].

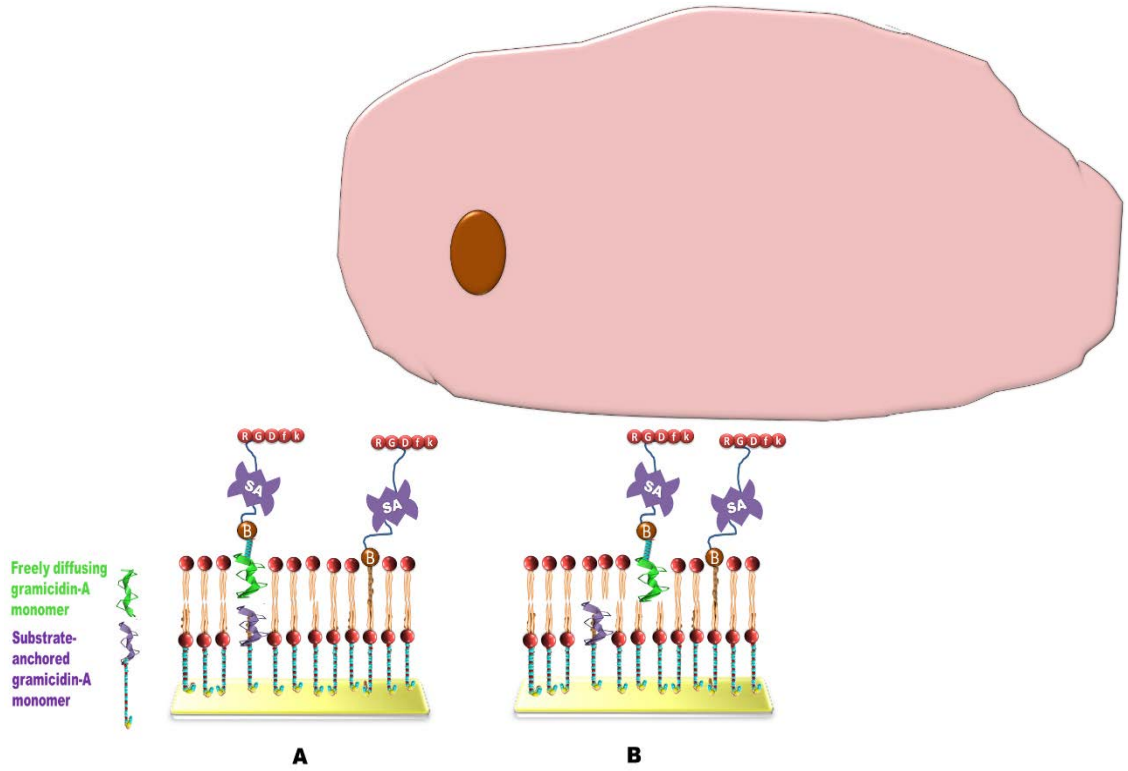

Figure 3.3: Representative schematic illustration of RGD ICS biosensor modification. The inner membrane leaflet is comprised of fully tethered phytanyl lipids (T100) incorporating tethered gA monomers. The outer leaflet consists of freely diffusing cyclic RGD (cRGD) linked-streptavidin-biotinylated gA monomers. Interspersed in this tBLM architecture are cRGD linked-streptavidin-biotinylated full-membrane spanning lipids. (A) RGD direct ICS assay, the reactive site of the freely biotinylated mobile

gramicidin monomers and tethered membrane spanner are coupled to the cRGD motif via biotin-streptavidin linkage; (B) In the presence of cells, the mobile channel within the outer leaflet of the membrane and MSLa are interbond with the cells and, as a result, the ionic current is switched off (Drawing is not to scale).

3.5.2.2 Development of streptavidin direct two-site sandwich ICS biosensor

Streptavidin itself contains an RYD (Arg-Tyr-Asp) binding motif, which shares similar binding properties to the RGD motif's ability to bind to integrin receptors [423]. Thus, streptavidin itself might be employed as a cell-binding motif equivalent to those of natural ECM proteins in order to elicit cell adhesion events (Figure 3.4) [424].

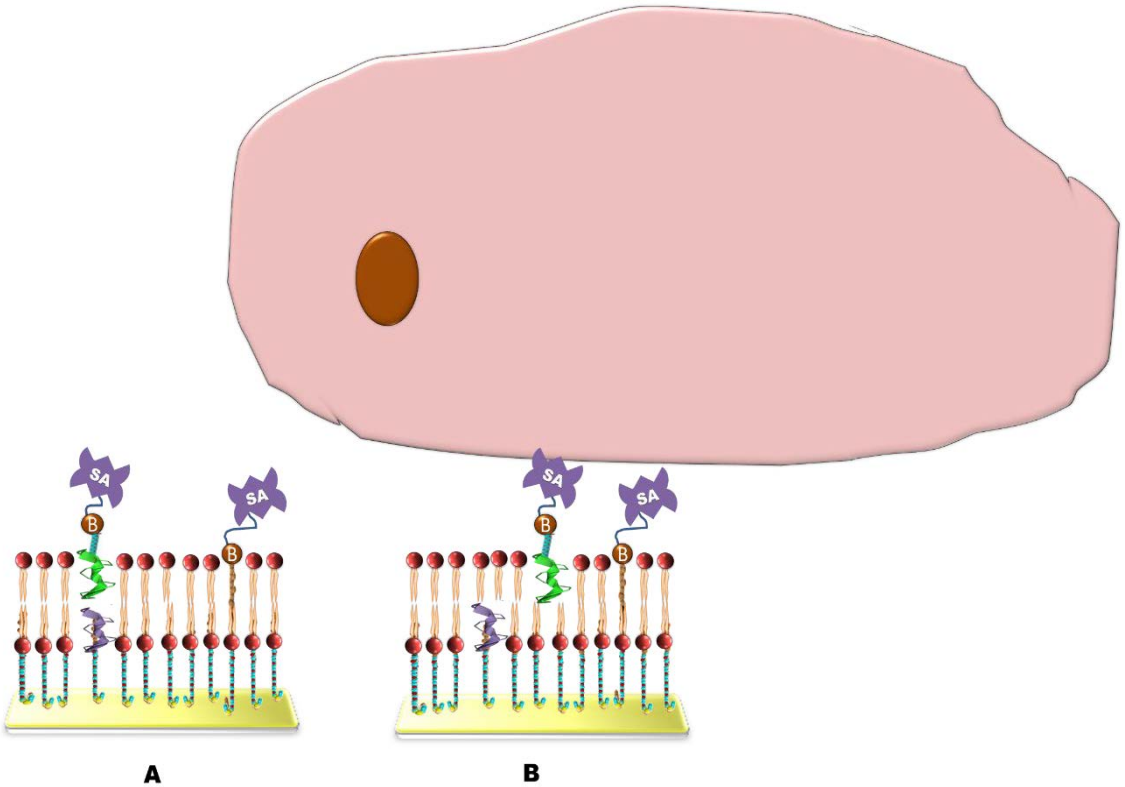

Figure 3.4: Representative schematic illustration of streptavidin ICS biosensor modification. The inner membrane leaflet is comprised of fully tethered phytanyl lipids (T100) incorporating tethered gA monomers. The outer leaflet consists of freely diffusing streptavidin-biotinylated gA monomers. Interspersed in this tBLM architecture are streptavidin-biotinylated full-membrane spanning lipids. (A) When the reactive site of

the freely mobile steptavidin-biotinylated gramicidin monomers and tethered membrane spanner coupled to the streptavidin are not sandwiching a cell analyte, the ionic current is switched on; (B) In the presence of cells, the mobile channel within the outer leaflet of the membrane and MSLa are interbond with the cells and, as a result, the ionic current is switched off (Drawing is not to scale).

However, the RYD binding motif within the streptavidin structure might have a smaller binding affinity towards cells integrins than RGD binding, which may directly affect the efficiency of any developed biosensor. Nevertheless, we will need to test the ability to use a streptavidin only nano-biosensor architecture and compare it to RGD containing architectures, as this will also provide information as to background cell binding in situations where RGD has been poorly conjugated.

3.5.2.3 Development of Concanavalin A direct two-site sandwich ICS biosensor

Polysaccharides are one of the most abundant biological recognition sites through protein-carbohydrate interactions. Also, it is well known that the protein-carbohydrate interface performs critical roles in a variety of critical biological events, such as cell-surface recognition and adhesion [425, 426]. Concanavalin *A*, from *Canavalia ensiformis*, belongs to a family of proteins called *lectins,* which possess binding motifs to saccharide molecules that can identify the trimannoside sequence of glycan structures [427, 428]. In addition, concanavalin A can anchor to the various glycoproteins via protein-carbohydrate interactions [427, 428]. The employed concanavalin A (Con-A) biosensor modification in this study is illustrated in Figure 3.5. However, the binding specificity would be reduced by using the generic binding motif, namely Con-A.

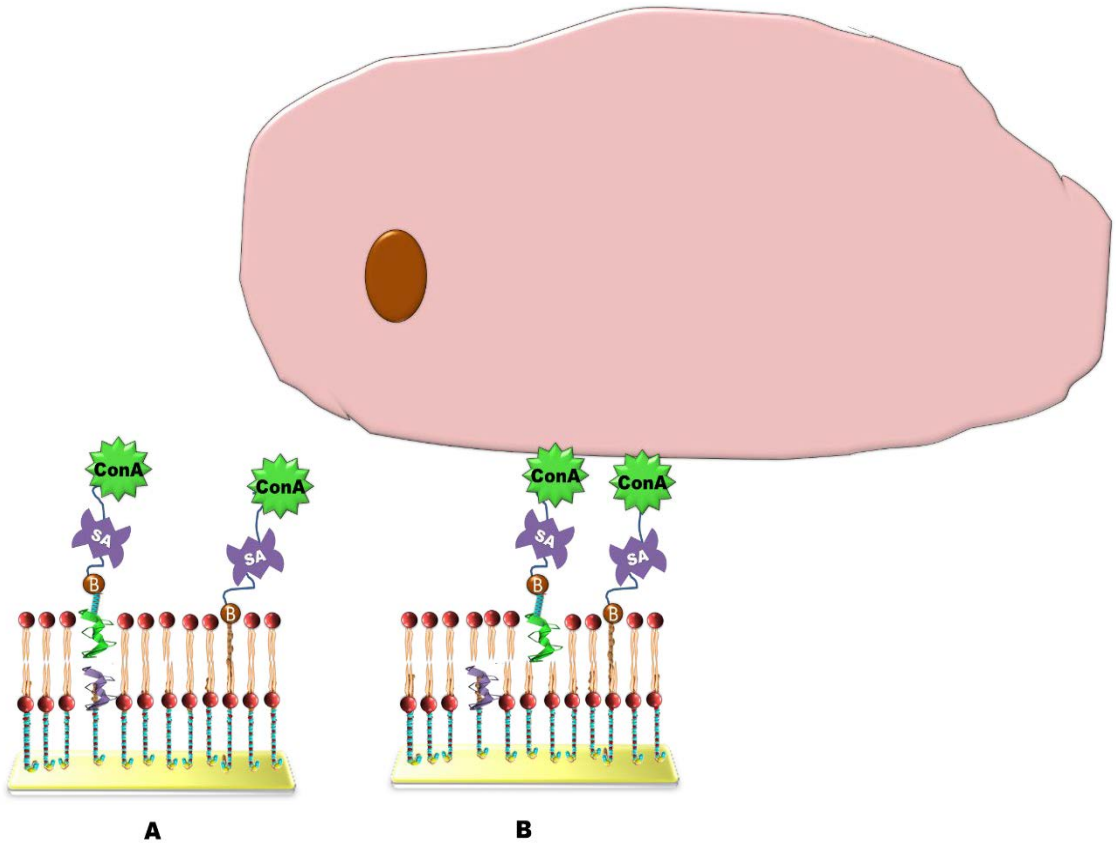

Figure 3.5: Representative schematic illustration of Concanavalin A ICS biosensor modification. The inner membrane leaflet is comprised of fully tethered phytanyl lipids (T100) incorporating tethered gA monomers. The outer leaflet consists of freely diffusing Con-A linked-streptavidin-biotinylated gA monomers. Interspersed in this tBLM architecture are Con-A linked-streptavidin-biotinylated full-membrane spanning lipids. (A) When the reactive site of the freely mobile Con-A-steptavidin-biotinylated gramicidin monomers and tethered membrane spanner coupled to the streptavidin *are not* sandwiching a cell analyte, the ionic current is switched on; (B) In the presence of cells, the mobile channel within the outer leaflet of the membrane and MSLa are interbond with the cells and, as a result, the ionic current is switched off (Drawing is not to scale).

Other studies have used microarray systems to study the carbohydrate-bacterial cell interface, and they found that the polysaccharides epitopes could be employed to detect pathogens within heterogeneous populations [429, 430]. The employing of Con-A as a binding motif in this study could allow a variety of glycoproteins on the cell surface to be recognized by Con-A when it is incorporated into the biosensor. The percentage of

glycoproteins expressed on the cell surface varies depending on the cell-type. For instance, bacterial cells, such as E.coli and blood cells, contain higher amounts of cell surface glycoproteins [431-433]. Thus, Con-A could be used as a recognition site nano-biosensor to detect various bacterial cells.

3.5.3 Development of an RGD competitive ICS biosensor

The gA ion channel competitive ICS biosensor was originally applied to the detection of small analytes, as illustrated previously in Figure 3.2 (C and D) [79]. In this study, an RGD competitive assay was investigated in order to investigate that the sensor could be improved by using small molecules that could compete with cell binding, as illustrated in Figure 3.6 below. In this version of the competitive assay, we tried to use a low molecular weight component using the minimal integrin structure that can bind to RGD peptide, which comprises the six amino acid *MTSDDL*. The hexapeptide MTSDDL (Met-Thr-Ser-Asp- Asp-Leu) has a similar structure to that found in β integrin subunits [434, 435].

Here, the introduction of bespoke MTSDDL dimers would compete with the MTSDDL monomer for the RGD binding motif, liberating the mobile gA monomer and increasing the overall membrane conductance. The inclusion of MTSDDL *dimers* that includes two MTSDDL peptides linked by an NNEN (Asn-Asn-Glu-Asn) amino acid chain represents the short dimer or, NNENNNNENNNNENNN amino acid that represents a longer-linked dimer. The selection of the polar N (Asparagine) amino acid and the negatively charged E (Glutamate) amino acid as linker residues was to minimize any interference by the amino acid with the lipid bilayer membrane. When monomer and dimer configurations are introduced to the developed ICS biosensors, it was hypothesised that they would provide significant evidence of the binding affinity to cRGD binding motif.

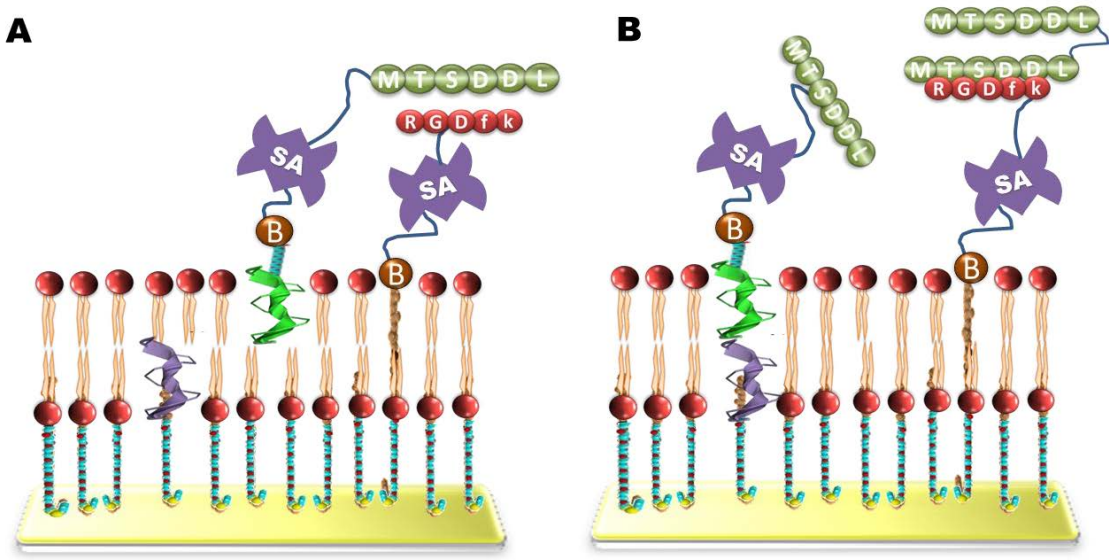

Figure 3.6: Representative schematic illustration of RGD competitive ICS biosensor mechanism. The inner membrane leaflet is comprised of fully tethered phytanyl lipids (T100) incorporating tethered gA monomers. The outer leaflet consists of freely diffusing MTSDDL linked-streptavidin-biotinylated gA monomers. Interspersed in this tBLM architecture are cRGD linked-streptavidin-biotinylated full-membrane spanning lipids. (A) When the reactive site of the freely mobile MTSDDL-streptavidin-biotinylated gramicidin monomers and cRGD linked-streptavidin-biotinylated tethered membrane spanner are coupled, the ionic current is switched off; (B) In the presence of MTSDDL dimer, competition with the previously attached MTSDDL peptide occurs, then the mobile channel within the outer leaflet of the membrane are released as MSLa is interbond with the dimer and, as a result, the ionic current is switched on (Drawing is not to scale).

3.6 Aims of this research study

The overall aim of this study was to investigate the feasibility of developing nano-biosensor for cell detection using the gA-biosensor.

As such, this chapter will:

- Attempt to identify streptavidin coverage in the architecture and characterize the ion-channel switched tBLM utilizing electrical impedance spectroscopy and neutron reflectometry methods.
- Assess the feasibility of cell detection using the direct gramicidin biosensor system and enhance sensor efficiency using streptavidin, concanavalin A and RGD binding motifs.
- Investigate the development of an RGD competitive assays of the ion channel nano-biosensor switch to enable cell detection.

3.7 Materials and Methods

3.7.1 Chemicals

All chemicals used in experiments, unless mentioned otherwise, were of analytical grade and used as advised. 100% pure ethanol, chloroform, phosphate buffer saline (PBS), perdeuterated 1-Palmitoyl-2-oleoyl-sn-glycero-3-phosphocholine (d82-POPC), concanavalin-A-biotin conjugate**,** streptavidin Alexa Fluor 488 and streptavidin were purchased from Sigma- Aldrich (Sydney, Australia). Cyclo [Arg-Gly-Asp-D-Phe-Lys(Biotin-PEG-PEG)] or c(RGDfK(Biotin-PEG-PEG)); where PEG = 8-Amino-3,6-Dioxaoctanoic acid were obtained from Peptides International (Louisville, USA).

Benzyldisulfide-TEG-OH, tethered gramicidin (gAYYSSBn), biotinylated tethered membrane-spanning lipid (MSLa), (AM215) includes mobile lipids mixture of 3:7 molar ratio of glycerodiphytanylether (GDPE): diphytanyl ether phosphatidylcholine (DPEPC) and biotinylated gramicidin (gA5XB) monomers, full-membrane-spanning lipids (MSL) and double-length reservoir half-membrane-spanning phytanyl lipids (DLP) were a kind contribution from Surgical Diagnostics (SDx Tethered Membranes Pty Ltd, Australia).

16% paraformaldehyde (PFA), Triton x 100, Dulbecco's modified eagle's medium (DMEM), Roswell Park Memorial Institute medium (RPMI-1640 medium), Dulbecco's phosphate buffer saline (DPBS), nutrient mixture F-12, PBS, fetal bovine serum (FBS), TryPLE, 0.5 M Ethylenediaminetetraacetic acid (EDTA), Penicillin/ Streptomycin solution 4′,6-diamidino-2-phenylindole (DAPI) Alexa Fluor 568 Phalloidin and Alexa Fluor 647 Phalloidin were obtained from Invitrogen (Sydney, Australia).

Synthesized chemical peptides: Biotin- NNENMTSDDL peptide (10 amino acid) (Purity: >90%), short dimer MTSDDLNNENMTSDDL Peptide (16 amino acid) (Purity: >90%) and more extended dimer MTSDDLNNENNNNENNNNENNNMTSDDL Peptide (28 amino acid) (Purity: >90%) were purchased from GeneScript (Central, Hong Kong).

3.7.2 Electrodes

The electrode formation and setup are detailed in Section 2.5.6.

3.7.3 Streptavidin coverage examination on biotinylated gA tBLMs ICS sensor

3.7.3.1 Streptavidin-ICS-tBLM electrical impedance spectroscopy measurements

ICS sensor is illustrated in Figure 3.2. Following the formation of the lipid layer using AM215 lipids, four concentrations (1 nM, 10 nM, 50 nM, and 100 nM) of streptavidin were introduced to the liquid phase above the membrane. 0 nM represents the introduction of an equivalent amount of buffer (PBS).

3.7.3.2 Neutron reflectometry measurements

Neutron reflectometry measurements were performed using a fully tethered tBLM comprising a hydrogenated inner leaflet and a deuterated outer leaflet at the Australian Nuclear Science and Technology Organization (ANSTO), Lucas Heights, Australia. The PLATYPUS, time-of-flight reflectometer instrument at the 20 MW OPAL research

reactor was used to collect neutron reflectometry data. In this regards, neutron bandwidth ranging between 2.5 and 18 Å were used, as well as measurements collected at two incident angles, namely 0.85 ° and 3.8 °, in order to give a Q-range from 0.006 to 0.25 $Å^{-1}$.

Fully tBLMs were formed (as mentioned previously in Section 2.5.6) on gold-coated 50 mm diameter, 7 mm thick, conductive silicon disks (Melbourne Centre for Nanotechnology). DLP, the half-membrane spanning lipid anchors, was hydrogenated, while a mixture of a 3 mM of perdeuterated DOPC and ~ 150 pM of biotinylated gA monomer comprised the outer monolayer. The hydrogenated and deuterated lipid tails were used to provide sufficient neutron contrast between the two leaflets. Further contrast was created by bathing solutions of PBS in either D_2O or H_2O. Variable streptavidin concentrations were injected into the aqueous phase above the tBLM membrane, namely 1 nM, 10 nM, 100 nM.

The reflection of neutron reflectometry experiments is often described in terms of a momentum scattering vector (Q) that describes the ratio of the reflected beam and incident beam after reflection from a thin film.

$$Q = \frac{4\pi \sin\theta}{\lambda}$$

Here; θ is the scattering angle and **λ** is the wavelength of incident radiation.

Data fitting was accomplished using the RasCAL software within the MATLAB environment [436]. Scattering length density was modeled assuming that the tBLM-gA-streptavidin surface was comprised of a series of parallel layers.

3.7.4 Cell culture procedures

3.7.4.1 Cell lines

Adherently growing cell lines CHO-K1 (Chinese Hamster Ovary) epithelial cells as well as nonadherent cell lines U937 (human leukemic monocyte lymphoma) were utilized in this work.

3.7.4.2 Cells sub-culture

CHO-K1cells were seeded in DMEM-F12 culture media complemented with 5% fetal bovine serum as discussed in more detail in Section 2.5.3.2.

Cell subculture of non-adherent cells (U-937) was done using the same technique as adherent cell seeding, excluding the wash and cells detachment steps. U-937 cells were cultivated to confluence using RPMI-1640 (Life Technologies, Australia) culture medium in addition to 10% of heat-inactivated FBS (Life Technologies, Australia).

Cells, prior to addition to the ICS sensor, were washed at least 3 times with 15 ml of PBS and between each wash, cells were centrifuged for 5 minutes at 1200 rpm with the supernatants discarded in order to eliminate the interference of FBS protein residues.

3.7.4.3 Visualizing cell-epitope-ligand binding

Determination of cell-epitope-ligand binding was undertaken by staining cells with streptavidin Alexa Fluor 488 dye.

3.7.4.3.1 Visualizing surface-attached cell-epitope-ligand binding

CHO-K1 cells were cultured on glass coverslips at 1 x 10^5 cells/ml in the suitable culture medium conditions. Labelling of the cells was accomplished by incubating them with binding motifs: 10 µM (≈ 10 µg/ml) of cRGD-Biotin conjugate, 10 µg/ml of streptavidin or 10 µg/ml of Con-A-Biotin conjugate in PBS for 30 minutes at 37 °C and under 5% CO_2, followed by washing three times with buffer. 10 µg/ml of streptavidin Alexa Fluor 488 was added and incubated for 30-90 minutes at 37 °C then viewed under the fluorescence microscope to confirm the cells were labeled. Negative controls included the incubation of binding motif conjugates with the cells in the absence of streptavidin Alexa Fluor 488. More information about cell fixation and staining has been presented in Section 2.5.3.3.

3.7.4.3.2 Visualizing floating washed cell-epitope-ligand binding

Visualization of detached and pre-washed cells was carried as follows: after washing the cells three times with PBS; cells were counted and diluted to final concentration 10’000 cell/ml. CHO-K1 cells or U-937 cells were employed over glass coverslip inside 6-well plate. Later, 50µl of 10 µM cRGD-Biotin in 1ml PBS or 1ml of 10µg/ml concanavalin A-Biotin conjugate was added and the cells incubated for 30 minutes in the 37˚C incubator. Then, cells, were washed three times with PBS, was added to each well in order to rinse the unbound molecules. Next, of 100µl of 10 µg/ml, Streptavidin Alexa Fluor 488 in PBS was added and incubated for 30-90 minutes at 37˚C. Then the surface was rinsed three times with PBS. Mounting media was placed over the coverslip and cells were imaged utilizing fluorescence microscope.

3.7.4.3.3 Relative fluorescence images intensity analysis

Cells were studied using an upright fluorescence phase-contrast microscope (Nikon, Tokyo, Japan). Slides were imaged using a 40x objective and a 488 nm laser wavelength. At least three samples were prepared for each experiment, and each treatment was imaged in at least three separate areas. The obtained images were processed using ImageJ (1.46r) analysis software with appropriate plugins for diameters and fluorescence intensity measurements [437].

3.7.5 Two-site sandwich assay for preparation ICS biosensor experiments

The different modifications employed for the sandwich assays used in this study are illustrated in Figure 3.3, 3.4 and 3.5. The tethered ion channel, tethered membrane-spanning lipids, spacer chemistries and DLP, were coupled over the gold substrate to form the first layer. Lipid bilayer formation was by the solvent exchange technique previously mentioned in Section 2.5.6.

3.7.6 RGD two-site sandwich assay for preparation ICS biosensor experiments

RGD-ICS sensor is illustrated in Figure 3.3. To create this, 50 µl of 100 nM streptavidin molecules were introduced to the liquid phase above the membrane and incubated for 15-20 minutes and followed by three rinses with 200 µl of PBS. Next, 200 µl of 10 µM Biotinylated-cRGD was incubated with the tBLM for at least 30 minutes; then the

unbound biotinylated-RGD was rinsed three times with 200 µl of PBS. To this, a volume of 10,000 cells/ml was added.

3.7.7 Streptavidin two-site sandwich assay for preparation ICS biosensor experiments

Streptavidin-ICS sensor is illustrated in Figure 3.4. Following the formation lipid layer using AM215 lipids (refer to Section 3.7.1), 50 µl of 100 nM streptavidin molecules were introduced to the liquid phase above the membrane and incubated for 15-20 minutes and followed by three rinses with 200 µl of PBS. To this, a volume of 10,000 cells/ml was added.

3.7.8 Concanavalin A two-site sandwich assay for preparation ICS biosensor experiments

The Con-A-ICS sensor is illustrated in Figure 3.5. To create this, 50 µl of 100 nM streptavidin molecules were introduced to the liquid phase above the membrane and incubated for 15-20 minutes and followed by three rinses with 200 µl of PBS. Next, 200 µl of 1µM Biotinylated-Con-A conjugate was incubated with the tBLM for at least 30 minutes; then the unbound biotinylated-Con-A was rinsed three times with 200 µl of PBS. To this, a volume of 10,000 cells/ml was added.

3.7.9 The RGD competitive assay for preparation ICS biosensor experiments

The RGD-competitive ICS biosensor modification employed in this study is illustrated in Figure 3.6. To create this, the first layer formation technique was similar to previously mentioned in Section 2.5.6. Second layers were formed as previously mentioned without mobile biotinylated gramicidin monomers.

The membranes were left for 10-15 minutes until they displayed stable G_m values. Later, 50 µl of 1nM streptavidin molecules were introduced to the lipid bilayer membrane and incubated for 15-20 minutes so that they can conjugate to the MSLa biotinylated full-membrane spanning tether molecules. This was followed by three times rinsing with 100 µl of PBS. Next, 200 µl of 50 nM Biotinylated-cRGD was incubated with the streptavidin-conjugated tBLM for at least 30 minutes; then the unbound biotinylated-cRGD was washed three times with 100 µl of PBS.

Finally, 2µl of 7.5 nM gA5XB (refer to Section 3.7.1) was introduced directly to the 100µl liquid phase over the lipid membrane in order to have nearly ~ 150 pM gA5XB mobile monomer final concentration. Later, each well in the cartridge was washed at least three times with 100 µl of PBS. Then, as before, 50 µl of 1nM streptavidin molecules were introduced and incubated for 15-20 minutes. The surface was rinsed three times with 100 µl of PBS. As illustrated in Figure 3.6 (B) 50 µl of 50nM of the NNENMTSDDL-Biotin peptide was then applied. This was washed 3 times with 100 µl of PBS and 50 µl of the short dimer MTSDDLNNENMTSDDL peptide (16 amino acid) or MTSDDLNNENNNNENNNNENNNMTSDDL peptide (28 amino acid) 50 nM as a dimer, was added to be the competition epitope, as shown in Figure 3.6 (B).

3.8 Results

3.8.1 Study streptavidin coverage on biotinylated gA tBLMs ICS sensor

3.8.1.1 Study of the interaction of streptavidin with biotinylated gramicidin in tBLMs

In order to study the interaction of streptavidin with biotinylated lipids and biotinylated gramicidin monomer components within lipid bilayers, as well as to assess the efficiency of streptavidin coverage across the lipid membranes, electrical impedance spectroscopy was employed to measure gA ion channel dimer conductivity. In particular, various streptavidin concentrations were applied over the liquid phase of the lipid bilayer, namely 1 nM, 10 nM, 50 nM and 100 nM. The membrane conduction values were normalized to the corresponding value of membranes prior to the addition of streptavidin.

The tBLMs and impedance spectroscopy results demonstrate that the conductance of gA is highly sensitive to the streptavidin across the membranes with as little as 1 nM inducing a dramatic drop in membrane conduction as seen in Figure 3.7 below.

The variations in conductance for the different streptavidin concentrations investigated in this study were not significant. Though marginal, the 100 nM streptavidin concentration gave the largest switching activity compared to streptavidin free membranes. For this reason all subsequent experiments, the 100 nM streptavidin concentration was employed. It should be noted that this addition of streptavidin immobilises a proportion of gramicidin ion channel switches (~70% of membrane conduction drop upon streptavidin introduction, while ~30% of membrane ion channels are still conducting and allow ion

passage), but this still leaves a significant population of freely mobile switches to act as sensor moieties [79].

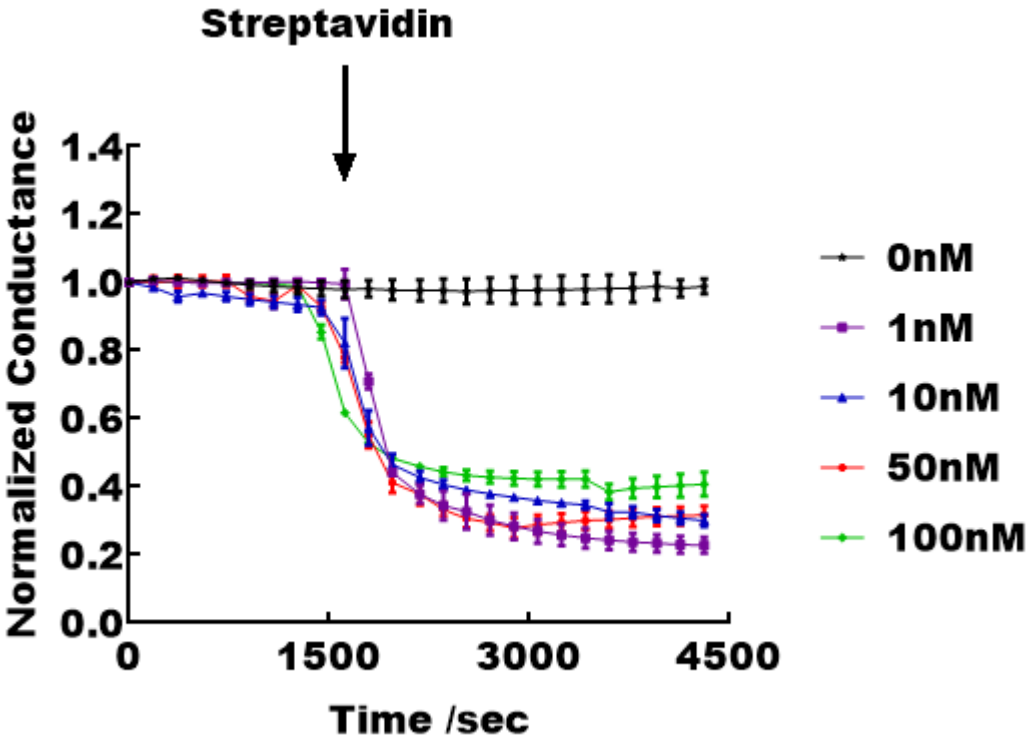

Figure 3.7: Interaction of streptavidin with biotinylated gramicidin incorporated into tBLM-ICS. The addition of streptavidin (at the time pointed arrow) prevents the formation of gramicidin channel dimers that, in turn, leads to a reduction in G_m. The membrane conduction values were normalized to the corresponding value of membranes before the introduction of streptavidin. The error bars demonstrate the standard error of three independent replicated samples measurements (n = 3).

3.8.1.2 Study the interaction of streptavidin with biotinylated gramicidin lipid bilayers by employing neutron reflectometry

To further examine streptavidin coverage and the architecture characterization of ion-channel switch tBLMs, neutron reflectometry was employed. In this regards, we can investigate the streptavidin and biotin gramicidin monomers interface and attachment

over a range of streptavidin concentrations. The neutron reflectometry results are presented for each introduced streptavidin concentration, as shown in Figure 3.8.

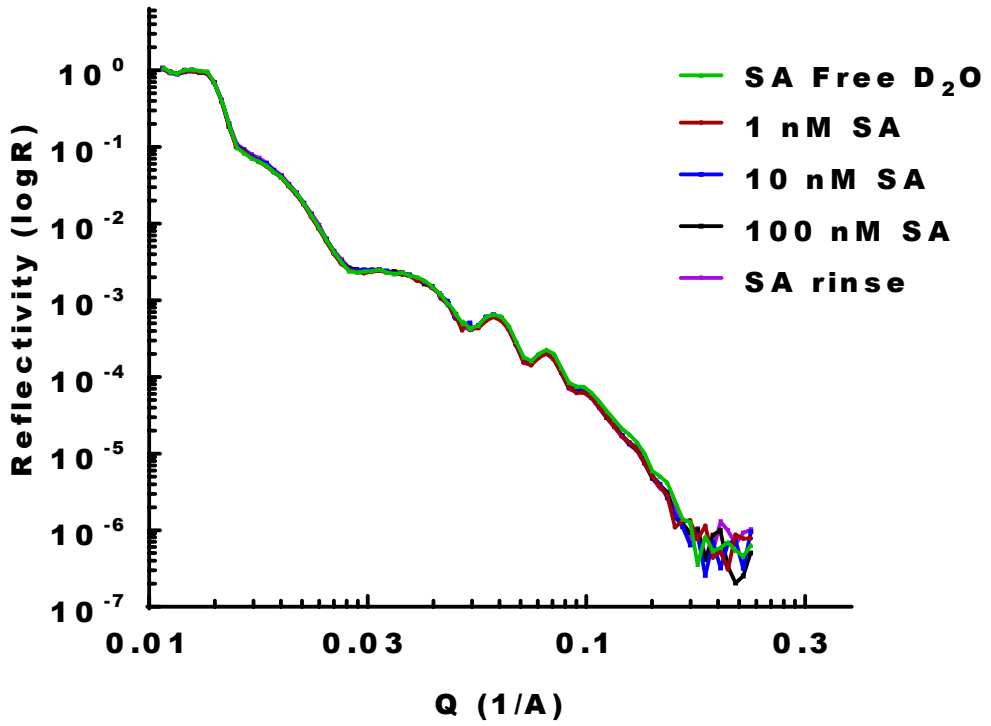

Figure 3.8: Comparison of neutron reflectometry profiles describing the interaction between streptavidin with biotinylated gramicidin monomers inserted within the fully tBLM. Profiles for different streptavidin concentrations, namely: 1 nM, 10 nM and 100 nM streptavidin and D_2O buffer negative control.

The comparison of the scattering length density of streptavidin-coated versus non-coated tBLMs revealed no distinguishable difference, indicating a low binding population of streptavidin. In addition, neutron reflectometry data shows that the introduction of various streptavidin concentrations over biotinylated gA monomers within fully tBLM results in an insignificant variance in neutron reflectometry profiles. This could be due to the shortage of sufficient contrast between the different streptavidin concentrations. It was concluded that it was not possible to elucidate the structural changes of the tBLM

membrane phospholipids thickness nor the effect of the streptavidin-gA interface using this neutron reflectometry technique.

3.8.2 Fluorescence imaging of cell epitope – ligand binding

In order to establish that the different proposed functionalizations used in this study, namely RGD, streptavidin and Con-A, are binding efficiently to the cell surface, a fluorescence microscopy investigation was employed to visualize cell labeling. Therefore, the first part of this fluorescence imaging study was aimed at investigating the possible binding sites of the employed binding motifs, as illustrated in Figure 3.9.

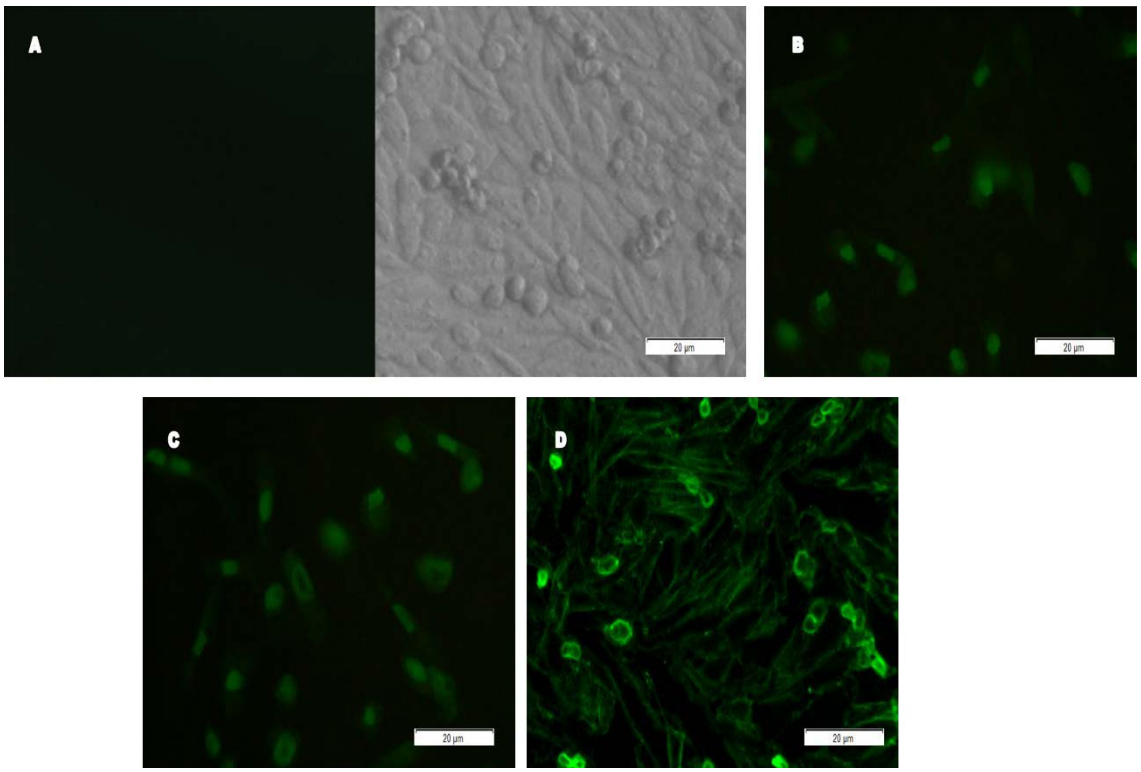

Figure 3.9: Fluorescence visualization of streptavidin, RGD and Con-A labeling. CHO-K1 cells incubated with the binding motif, followed by another incubation with Alexa Fluor 488 streptavidin with equivalent concentration (10µg/ml). (A) Light microscope image (Right image) fluorescence image (Left image) of untreated CHO-K1 cells which were used as a control; (B) Fluorescence image of CHO-K1 cells tagged with streptavidin Alexa Fluor 488; (C) Fluorescence image of CHO-K1 cells preincubated

with cRGD-Biotin and labeled with streptavidin Alexa Fluor 488; (D) Fluorescence image of CHO-K1 cells pre-incubated with Con-A-Biotin and labeled with streptavidin Alexa Fluor 488.

Green fluorescent staining from Alexa Fluor 488 labeling on the streptavidin was observed at the surface of the attached CHO-K1 cells, indicating that the RYD binding sites within streptavidin, cRGD and Con-A recognized the corresponding binding sites over the cell membrane surface.

3.8.3 A fluorescence imaging study of RGD labelling

Following labelling of Cho-K1 and U-937 cells using the techniques described in Section 3.7.4. cRGD-PEG-Biotin labeling was employed in order to confirm the presence of the corresponding binding sites for RGD motif over the cells membrane surface. Negative control staining was carried out using BPS buffer with cells as well as the incubation of cells with biotinylated RGD binding motif conjugate in the absence of streptavidin Alexa Fluor 488, as illustrated in Figure 3.10 below.

Green fluorescent staining from Alexa Fluor 488 labeling on the streptavidin was observed at the surface of the CHO-K1 cells and U-937 cells, indicating that the cRGD-PEG-Biotin recognized with the corresponding integrin over cell membrane as well as attached selectively to the streptavidin.

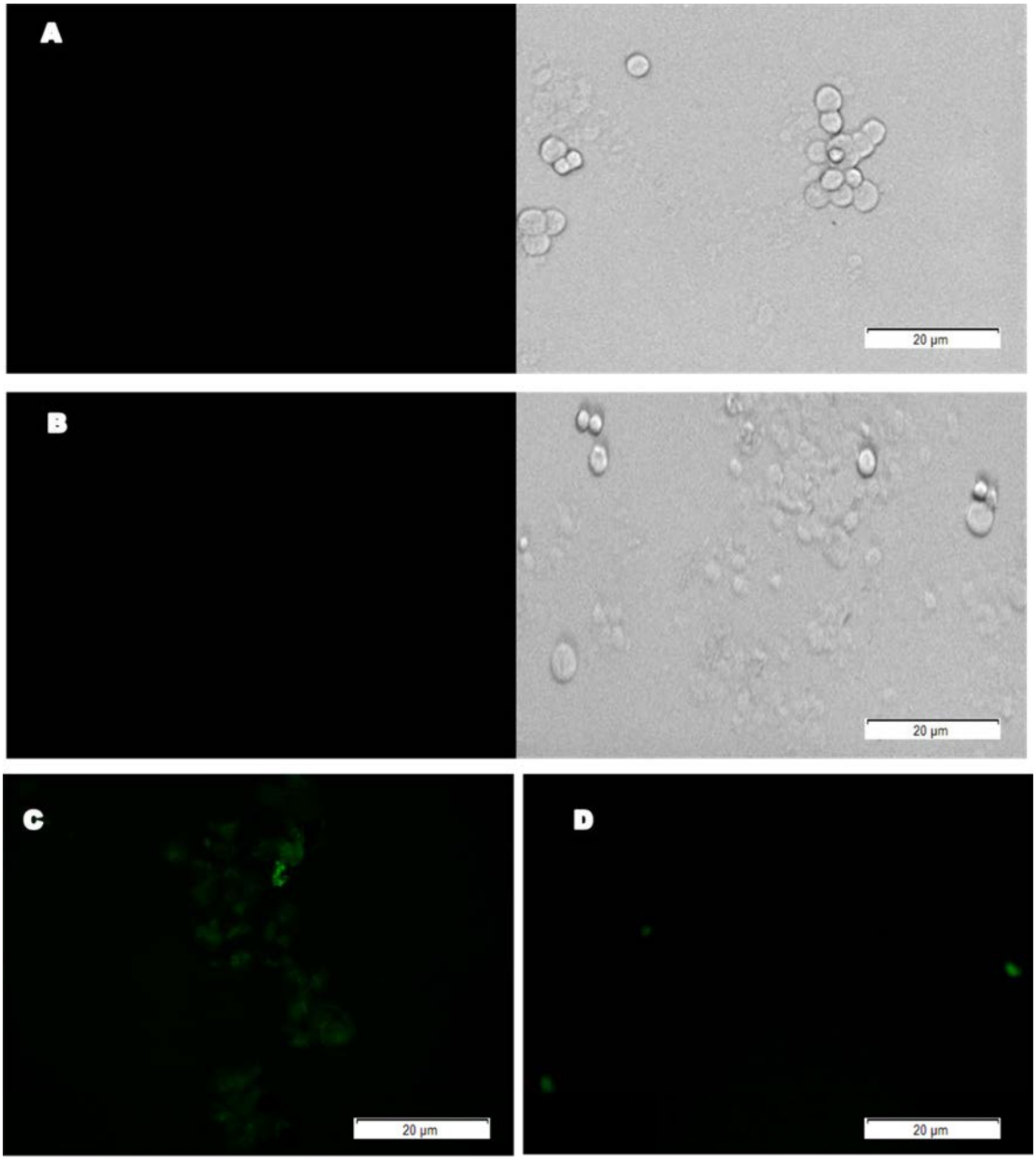

Figure 3.10: Fluorescence visualization of 10 µg/ml RGD labeling. (A) Light microscope image (Right image) fluorescence image (Left image) of CHO-k1 cells over glass surface in the absence of cRGD-Biotin and streptavidin Alexa Fluor 488; (B) Light microscope image (Right image) fluorescence image (Left image) of CHO-k1 cells treated with cRGD-Biotin conjugates over glass surface in the absence of streptavidin Alexa Fluor 488; (C) Fluorescence image of CHO-K1 cells tagging with streptavidin Alexa Fluor 488 and cRGD-Biotin over glass substrate; (D) Fluorescence image of U-937 cells tagging with streptavidin Alexa Fluor 488 and cRGD-Biotin over a glass substrate.

3.8.4 A fluorescence imaging study of streptavidin labeling

Streptavidin Alexa Fluor 488 labeling was employed in order to confirm the presence of the corresponding binding sites for RYD motif over the cells membrane surface. Negative control staining was carried out using BPS buffer only as well as the addition of fluorescence free streptavidin, as illustrated in Figure 3.11 below. Green fluorescent staining from Alexa Fluor 488 on the streptavidin was observed at the surface of the CHO-K1 cells and U-937 cells, indicating that the streptavidin recognized with cell membrane receptors.

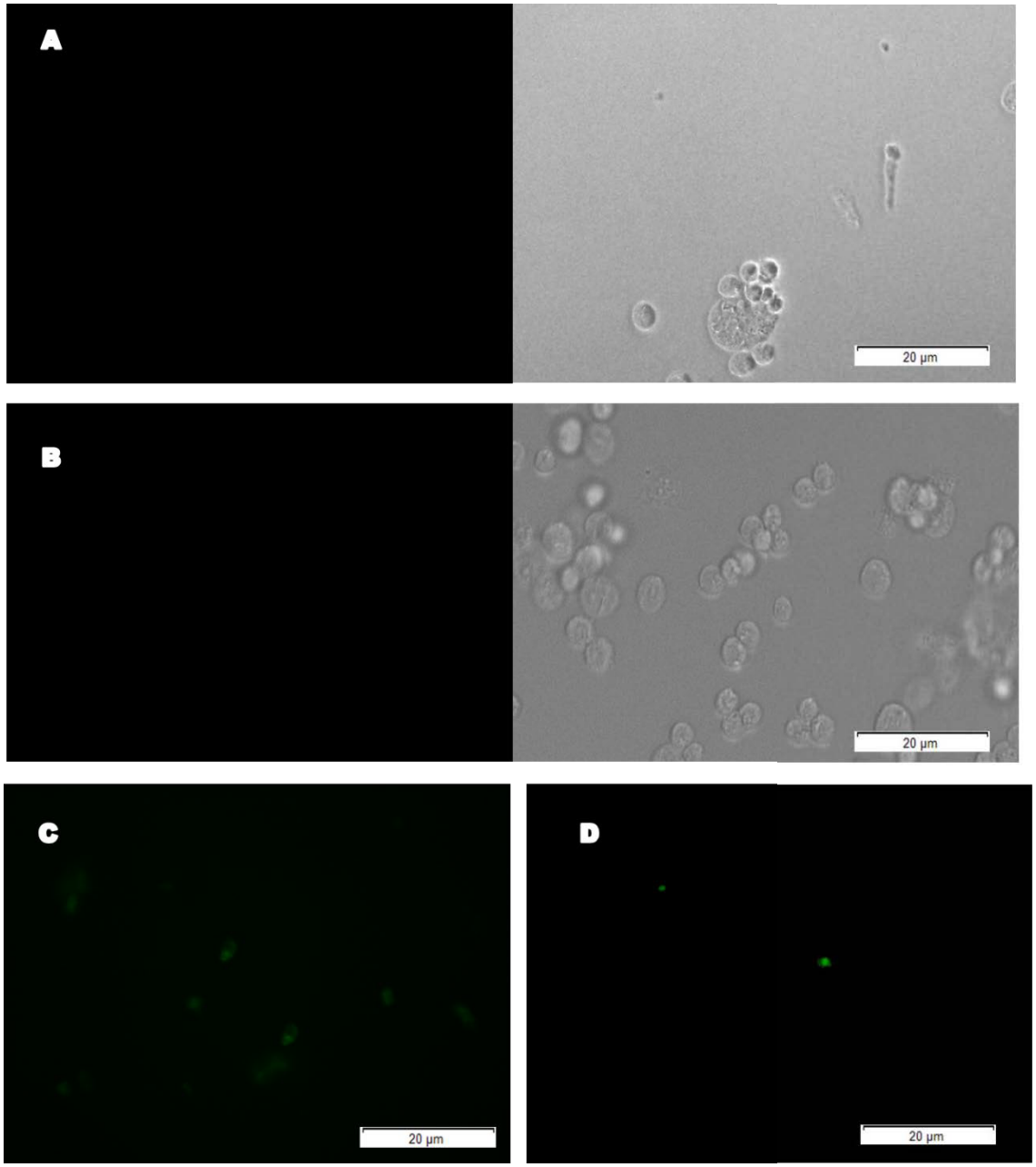

Figure 3.11: Fluorescence visualization of 10 µg/ml streptavidin labeling. (A) Light microscope image (Right image) fluorescence image (Left image) of CHO-k1 cells fluorescence image over glass surface in the absence of streptavidin Alexa Fluor 488; (B) Light microscope image (Right image) fluorescence image (Left image) of CHO-k1 cells-streptavidin (florescence-free) conjugates fluorescence image over glass surface in the absence of streptavidin Alexa Fluor 488; (C) Fluorescence image of CHO-K1 cells tagging with streptavidin Alexa Fluor 488 over glass substrate; (D) Fluorescence image of U-937 cells tagging with streptavidin Alexa Fluor 488 over a glass substrate.

3.8.5 A fluorescence imaging study of Con-A labeling

Following the introduction of biotinylated Con-A over washed cells, streptavidin Alexa Fluor 488 labeling was then applied in order to confirm the presence of the corresponding binding sites for Con-A over the cells membrane surface. Negative control staining was carried out using BPS buffer as well as incubated cells with Con-A binding motif conjugate in the absence of streptavidin Alexa Fluor 488, as illustrated in Figure 3.12 below. Green fluorescent staining from Alexa Fluor 488 on the streptavidin was observed at the surface of the CHO-K1 cells and U-937 cells, indicating that the Con-A recognized cell membrane receptors.

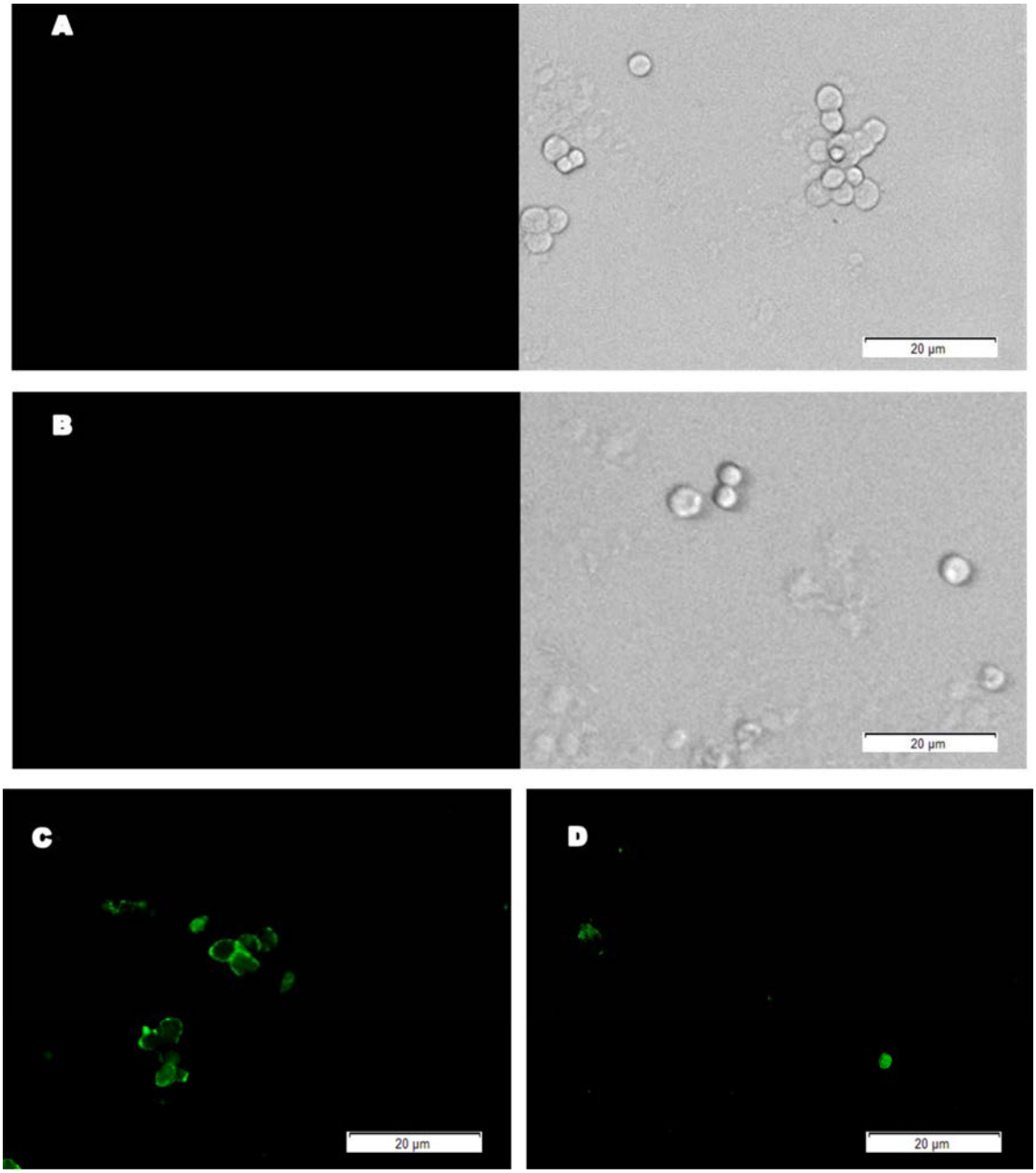

Figure 3.12: Fluorescence visualization of 10 µg/ml Con-A labeling. (A) Light microscope image (Right image) fluorescence image (Left image) of CHO-k1 cells fluorescence image over glass surface in the absence of streptavidin Alexa Fluor 488 and biotinylated Con-A; (B) Light microscope image (Right image) fluorescence image (Left image) of CHO-k1 cells- biotinylated Con-A conjugates fluorescence image over glass surface in the absence of streptavidin Alexa Fluor 488; (C) Fluorescence image of CHO-K1 cells tagging with streptavidin Alexa Fluor 488 and biotinylated Con-A over glass substrate; (D) Fluorescence image of U-937 cells tagging with streptavidin Alexa Fluor 488 and biotinylated Con-A over glass substrate.

3.8.6 Relative fluorescence intensity imaging of cell epitope – ligand binding

Overall, fluorescence imaging revealed cell labeling and adherence to the RGD peptide, RYD binding sites of streptavidin and concanavalin A. The relative fluorescence intensity levels were determined from the corresponding fluorescence microscopic images for the Alexa Fluro labelled streptavidin-conjugated on the treated cells with binding motifs under 40x magnification and compared with the untreated cells. It can be seen that significant Con-A binding motif binding was observed at the surface of both CHO-K1 cells and U-937 cells in comparison to the other binding motifs (RGD and streptavidin) and negative controls, as shown in Figure 3.13 below.

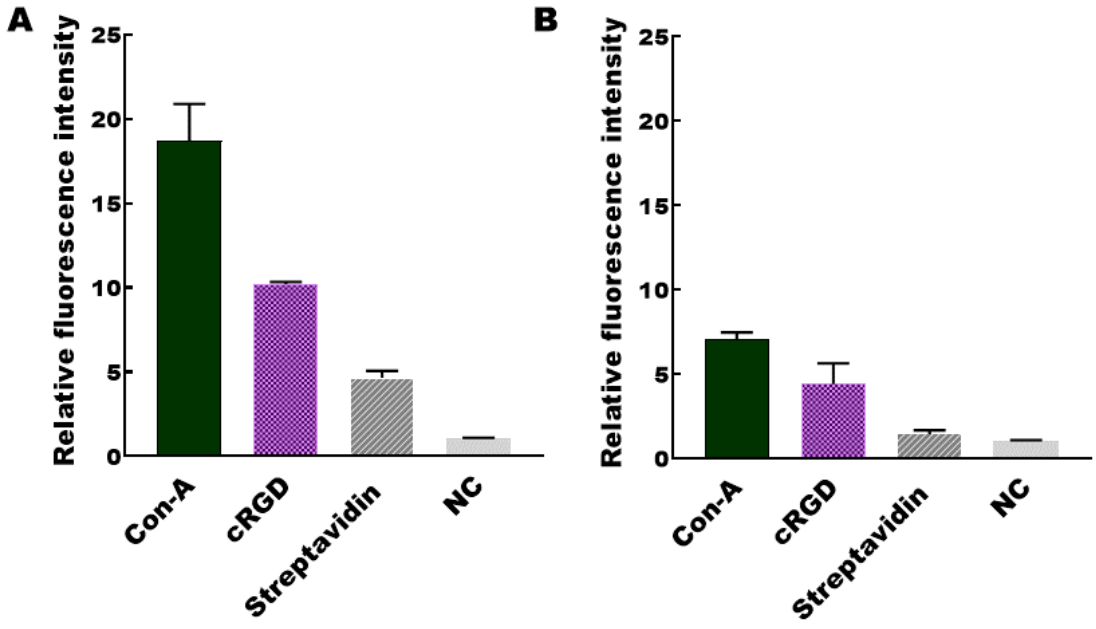

Figure 3.13: The relative level of fluorescence intensity of streptavidin Alexa Fluor 488-labelled. (A) The relative fluorescence intensity of CHO-K1 cells that treated with the different binding motifs (Con-A, cRGD and streptavidin) and untreated cells; (B) The relative fluorescence intensity of U-937 cells that treated with the different binding motifs (Con-A, cRGD and streptavidin) and untreated cells. The error bars indicate the average standard error of three independent images intensity measurements (n = 3).

3.8.7 Cell detection by measuring conductance Gm using variable functionalization of direct-ICS sensor

In the aim of examining the feasibility of cell detection using direct gramicidin biosensor system, we have employed different functionalizations of biotinylated mobile gA monomers and a biotinylated spanner in order to enhance sensitivity to cells.

3.8.7.1 Cell detection using a dual RGD peptide-functionalized ICS sensor

Here, a small number of adherent cells (10’000 cell/ml, CHO-K1) were introduced to the functionalized biosensor. The addition of streptavidin displayed a 60% reduction of membrane conduction as a result of some gA-Biotin-Streptavidin-MSLa-biotin cross-linking, as expected (Figure 3.14 A). It is expected then that residual mobile gA-SA-RGD molecules, when bound to cells, would cause a further significant decrease in membrane conduction [79]. However, as seen in Figure 3.14 (B), there was only a very slight drop in membrane conduction upon addition of the cells.

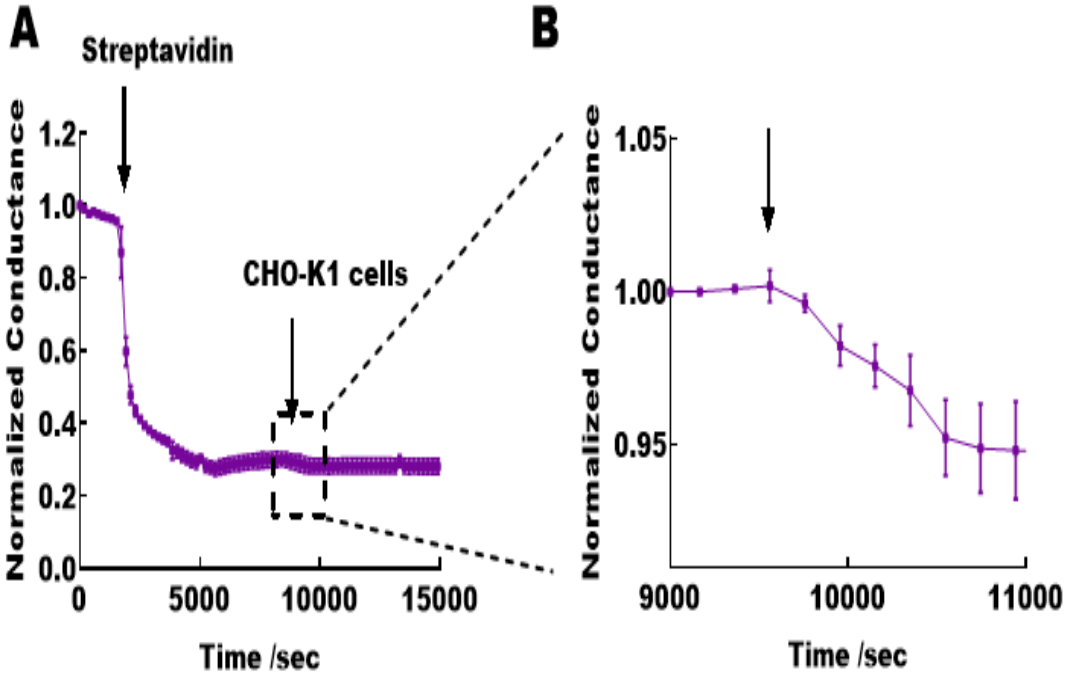

Figure 3.14: Direct cell detection using RGD-ICS biosensor. (A) Addition of streptavidin molecules demonstrated a significant decrease in G_m; (B) Introduction of 10'000 cell/ml of washed CHO-k1 cells showed slightly diminished G_m. The error bars indicate the average standard error of three independent impedance spectroscopy conductance measurements (n = 3).

We attempted to further investigate RGD-nanosensor efficiency using lymphoma cells that are smaller in size in comparison to CHO-K1 cells. It is known that the RGD binding motif binds specifically to the U-937 monocytic cells line [438]. In place of selective RGD epitopes such as α5β1 and αIIbβ3 integrins are abundant on the surface of these cells. As shown in Figure 3.15, there was only a slight decrease in membrane conduction upon introduction of these cells to overall gA channel gating.

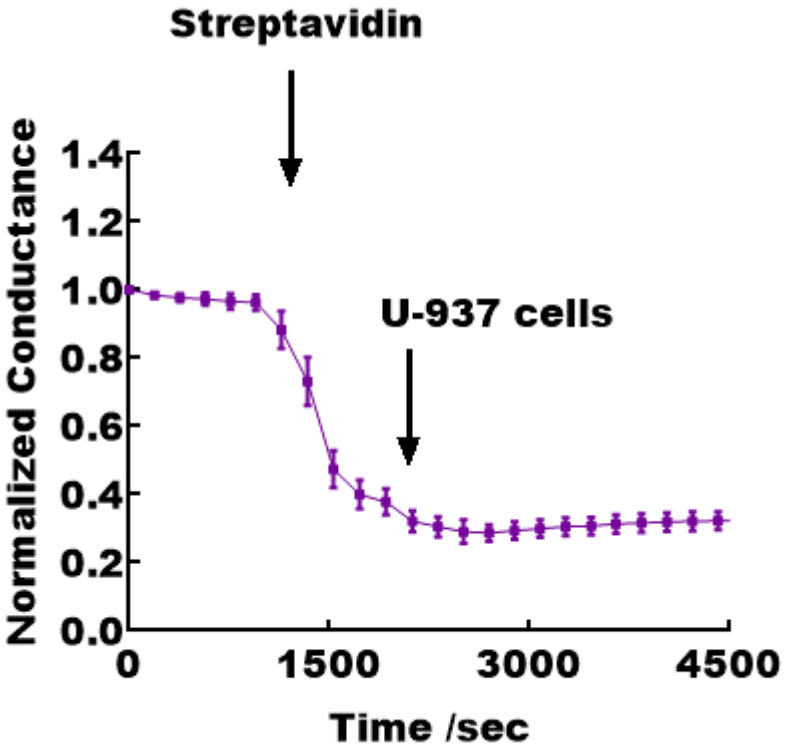

Figure 3.15: Direct non-adherent U-937 cell detection using RGD direct-ICS biosensor. Introduction of 10'000 cell/ml of washed U-937 cells was showed an insignificant variation in G_m when using the RGD-ICS biosensor. The error bars indicate the average standard error of three independent impedance spectroscopy conductance measurements (n = 3). Arrow indicates cells introduction.

3.8.7.2 Cell detection using a dual streptavidin functionalized ICS sensor

Upon an unsuccessful trial to improve the efficiency of the RGD-nanosensor, streptavidin was employed as a ligand for cell attraction. The selection of streptavidin as biosensor modification relates to its RYD motif that mimics the RGD motif binding sites [423]. The membrane conduction real-time measurements demonstrated a very slight variation upon the introduction of the CHO-K1 cells, as seen in Figure 3.16. This behavior is in the same line with the RGD binding results and can be considered to be insignificant.

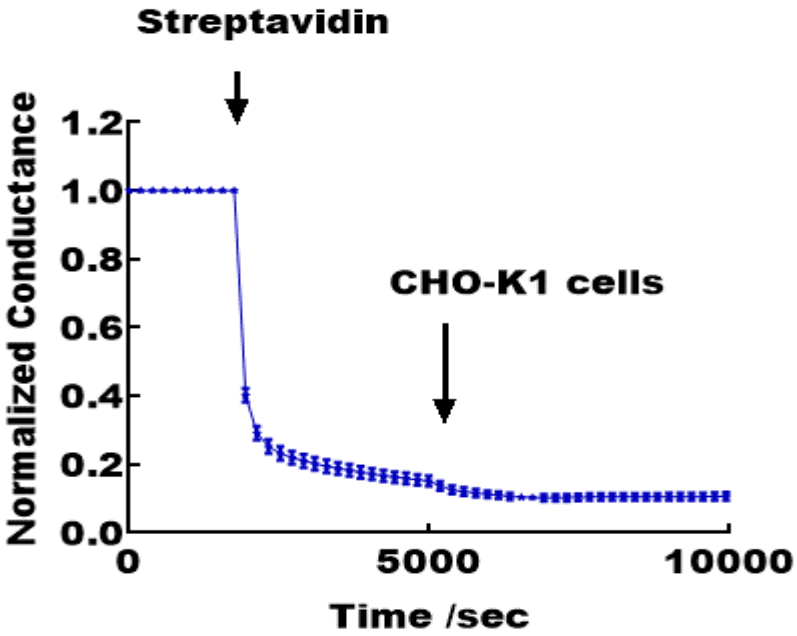

Figure 3.16: Direct cell detection using direct streptavidin-ICS biosensor. Addition of streptavidin molecules demonstrated a significant decrease in G_m, while the introduction of 10'000 cell/ml of washed CHO-k1 cells showed slightly diminished G_m. The error bars indicate the average standard error of three independent impedance spectroscopy conductance measurements (n = 3). The second arrow indicates the washed cells introduction.

3.8.7.3 Cell detection by measuring conductance Gm using dual Con-A functionalized direct-ICS biosensor

After the unexpected failed trials in improvement nanosensor efficiency, another cell-binding site was used to functionalize the direct-ICS sensor, namely Con-A. Results using a Con-A incorporated biosensor architecture with U-937 and CHO-K1 cells are shown in Figure 3.17.

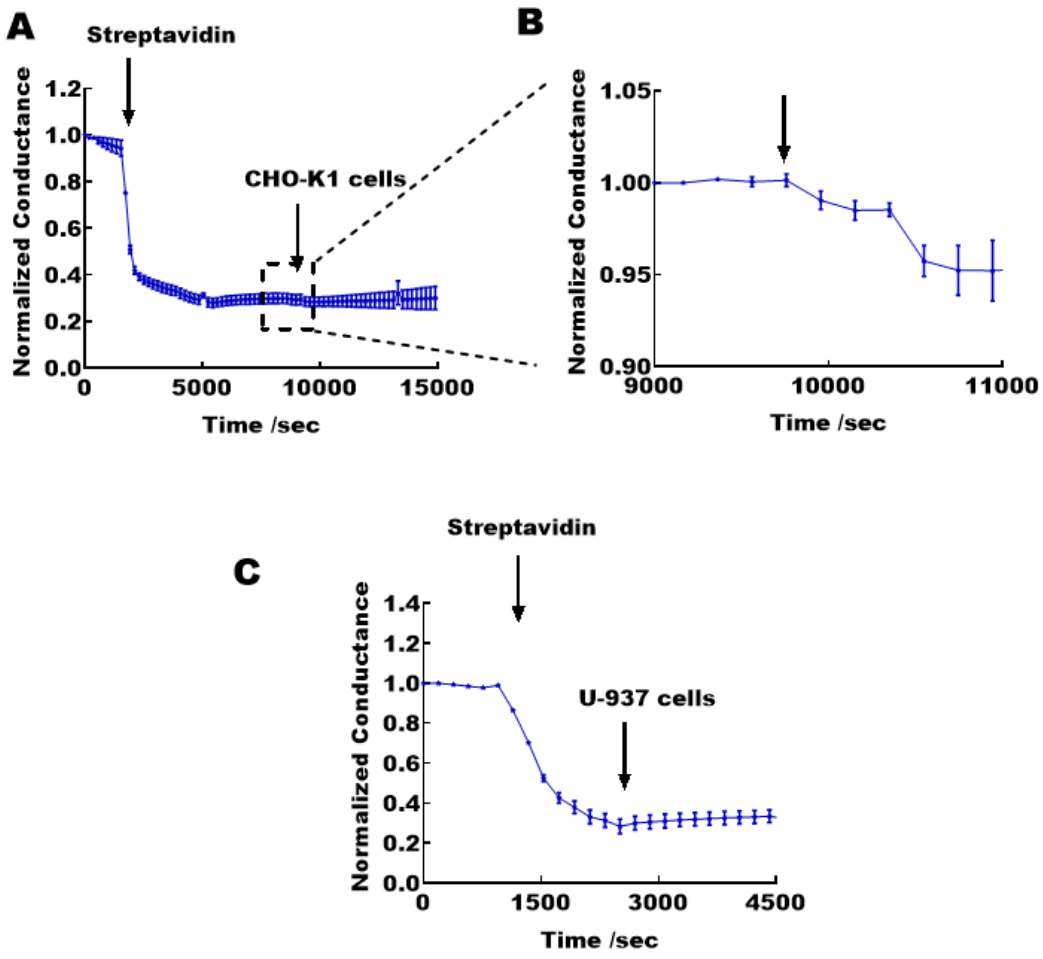

Figure 3.17: Direct cell detection using ConA-ICS biosensor. (A) Addition of streptavidin molecules demonstrated a significant decrease in G_m; (B) Introduction of 10'000 cell/ml of washed CHO-k1 cells showed slightly diminished G_m; (C) Introduction of 10'000 cell/ml of washed U-937 cells also exhibited a slight transient reduction in G_m. The error bars indicate the average standard error of three independent impedance spectroscopy conductance measurements (n = 3).

The results revealed a minor drop in the recorded normalized membrane conduction when the adherent CHO-K1 cells or U-937 cells were introduced. As with the RGD and streptavidin alone binding motifs, this small decline in G_m is considered insignificant.

3.8.7.4 MTSDDL dimer detection using a dual RGD peptide-functionalized ICS sensor

After unsuccessful detection of different cell types using the dual RGD sandwich assay, we aimed to investigate the improvement in the biosensor detection by using the MTSDDL dimer (which represents integrin-binding sites of RGD motif) when coupled to anchored cRGD and the diffusing cRGD. This would provide the opportunity to create a competitive dual RGD – hexapeptide dimer assay in order to simulate cell binding to dual RGD peptide-functionalized ICS sensor.

Firstly, we examined the designed MTSDDL dimers (18 amino acid and 28 amino acid long, including linker) binding affinity to cRGD using same designed biosensor as illustrated previously in Figure 3.3. The binding of MTSDDL dimers to cRGD binding motifs is assumed to prevent gA dimerization and thus drop the overall amplitude membrane conduction. The introduction of our designed dimers demonstrated insignificant variation in membrane conduction, as shown in Figure 3.18. Unfortunately the MTSDDL dimer- dual cRGD ICS sensor did not work efficiently, which prevented us from continuing the planned experiment to introduce cells that would compete with the previously added MTSDDL dimer, and subsequently release the mobile gA monomer and increase the overall membrane conduction. This can be explained either due to the designed dimer configuration that prevents the simultaneous attachment of anchored cRGD and mobile cRGD binding motifs, or could be due to the low binding affinity between the RGD and MTSDDL peptides.

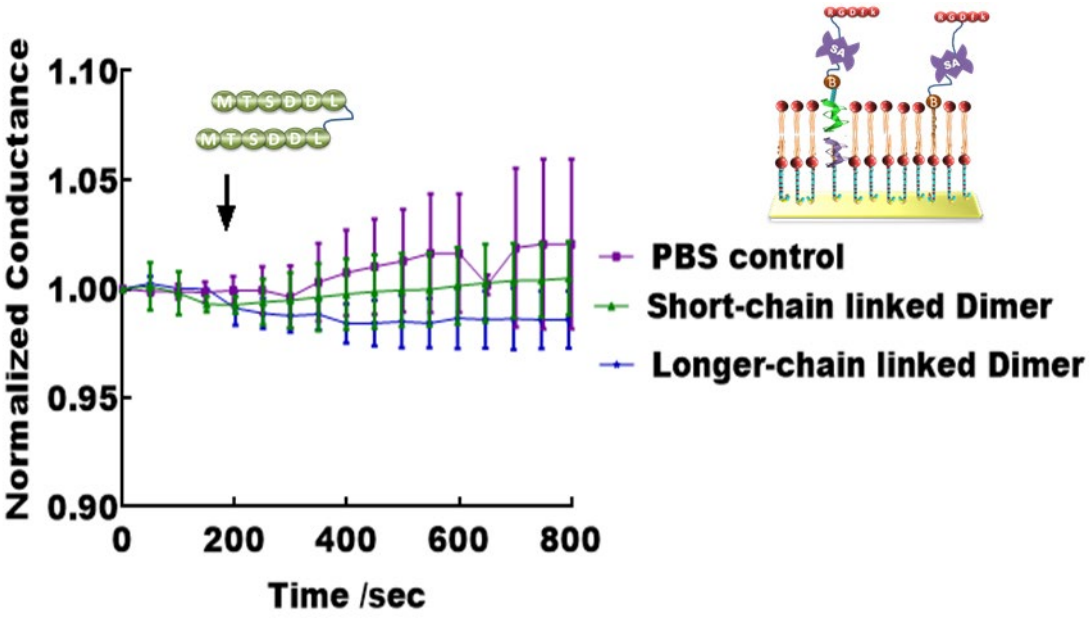

Figure 3.18: MTSDDL dimer-cRGD binding over direct ICS biosensor. Addition of 100 nM of the short-chain linked MTSDDL dimer (18 amino acid) or longer-chain linked MTSDDL dimer (28 amino acid) displayed insignificant variation in membrane conduction in comparison to the negative control (PBS buffer). The error bars indicate the average standard error of three independent impedance spectroscopy conductance measurements (n = 3).

3.8.8 Small peptide detection using RGD functionalized competitive-ICS biosensor

After the unsuccessful trials using our developed gA sensor to detect cells, MTSDDL hexapeptide *monomers* were employed instead of cells represented, by functionalization of the competitive ICS biosensor with RGD, as illustrated in Figure 3.19 (A), using the techniques described in Section 3.7.9.

To create a competitive sensor, we designed a biotinylated-NNEN-linked-MTSDDL monomer that, when bound to streptavidin bound-biotinylated mobile gAs, can directly attach to the tethered cRGD peptide. Then, we aimed to study subsequent non-

biotinylated MTSDDL molecule (using the designed dimers) competitive binding to cRGD peptide.

Our results showed a very slight drop in G_m after the introduction of the biotinylated-NNEN-linked-MTSDDL compound, as shown in Figure 3.19 (B). Though the decline was very minimal, it was concentration-dependent, and the experiments revealed that we need to introduce at least 5 nM of the biotinylated MTSDDL to observe the slight gating, as seen in Figure 3.19 (C).

For interest's sake, we then tested if the long-chain dimer would compete with the previously added MTSDDL monomer. The addition of the MTSDDL dimer peptide competes with the biotinylated MTSDDL for the anchored RGD motif, showing a very slight increase in the recorded G_m as seen in Figure 3.19 (D).

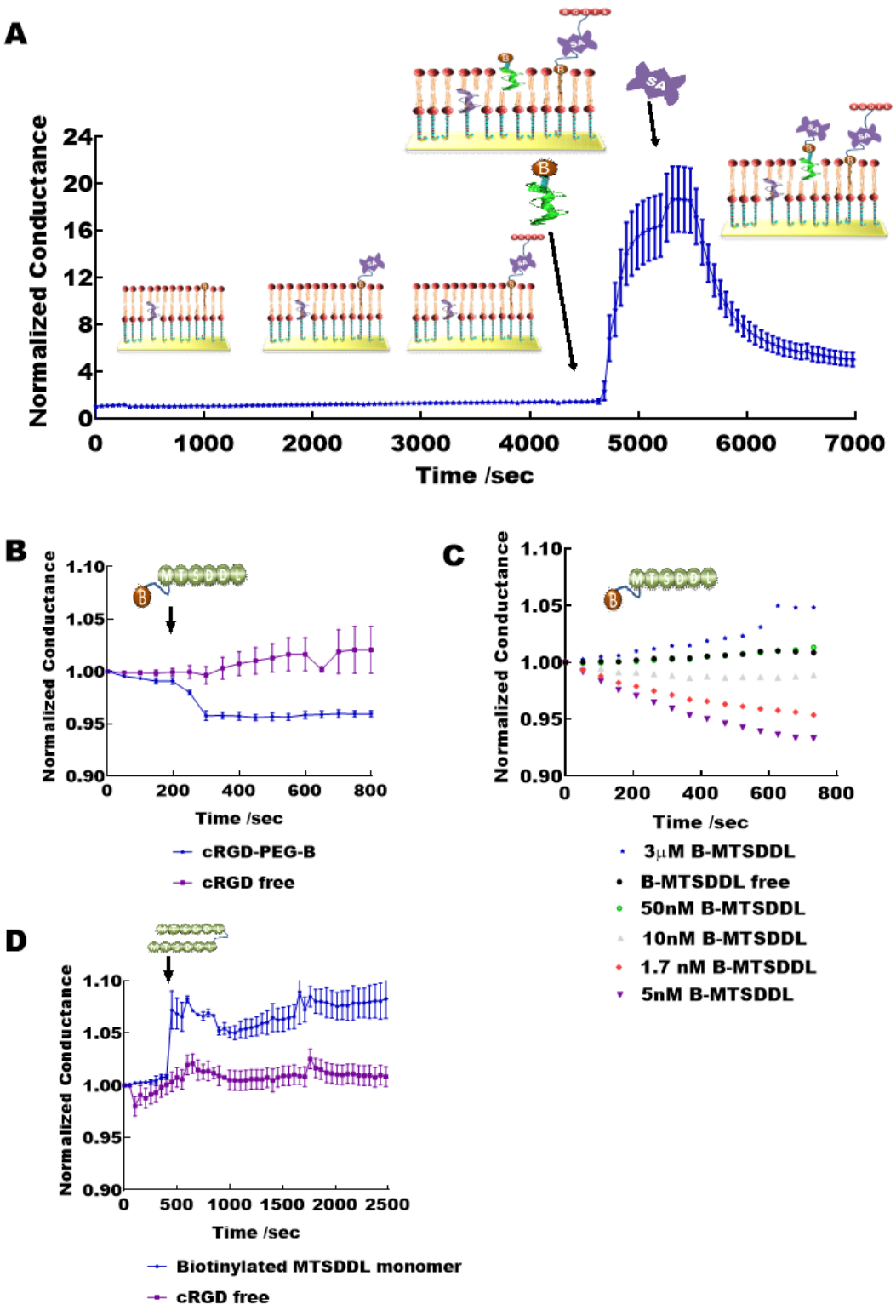

Figure 3.19: Competitive RGD-ICS biosensor. (A) The introduction of mobile gA monomer showed a dramatic increase in G_m that was followed by a significant decrease in G_m due to the addition of streptavidin; (B) Addition of biotinylated-NNEN-linked-MTSDDL molecules showed a very slight reduction in G_m; (C) The slight reduction in

G_m demonstrated a concentration dependency of biotinylated-NNEN-linked-MTSDDL molecules; (D) The subsequent addition of long-chain MTSDDL dimer demonstrated a small increase in G_m. The error bars indicate the average standard error of three independent impedance spectroscopy conductance measurements (n = 3).

3.9 Discussion

The ion channel gA switch nano-biosensor described by Cornell et al. (1997) provided an innovative biosensor architecture that can deliver rapid and precise detection of *analytes using antibody binding motifs* Figure 3.2 [79, 96, 439]. The detection mechanism of molecules of interest depends on the trapping of these molecules to the previously designed antibody fragments over the transient gramicidin fragments and tethered membrane-spanning molecules. Here, instead of antibodies, we attempted to utilize ligands for universal recognition sites extant in the cell membrane; namely RGD peptide, streptavidin and Con-A, in order to attempt to identify cells at low concentrations.

3.9.1 Investigation of Streptavidin and gA-ICS sensor interaction

The introduction of streptavidin as an intermediate coupling component displayed a significant reduction in membrane conduction. In other words, the decrease in membrane conduction in the gA-ICS sensor ought to have resulted from switching some of the gA ion channel off. This is due to streptavidin protein coupling to the biotinylated mobile gA monomers and tethered biotinylated membrane-spanner that prevent gA dimerisation with the immobilized gA monomer within the lower tBLMs leaflet [79].

How many streptavidin in fact bind to the surface of the sensor is unknown, so for this reason, we aimed to investigate the streptavidin interface and coverage across the gA-ICS sensor utilizing various techniques including impedance spectroscopy and neutron reflectometry. For this purpose, a range of streptavidin concentrations, namely: 1 nM, 10 nM, 50 nM and 100 nM were introduced to the liquid phase over the designed sensor.

The results were used to estimate the average streptavidin coverage and, in turn, reflect the number of the gA ion channels turning off that lead to a reduction in the overall membrane conduction. The coupling efficiencies of the attachment of streptavidin to the biotinylated molecules of the gA-ICS sensor were approximated from membrane conduction values to be between 50% to 80%, as seen in Figure 3.1. The results revealed slight variation among the different streptavidin coverage.

The neutron reflectometry profiles of streptavidin interactions with biotinylated gramicidin monomers (Figure 3.8) did not show any notable change in the deuterated POPC lipid layer of the fully tBLM membrane.

A possible explanation for our impedance and neutron reflectometry results is that increasing the amount of streptavidin affected the kinetic of the biosensor, and thus affected the rate of crosslinking streptavidin to biotinylated gramicidin-A and the biotinylated membrane spanner. Streptavidin used in the range of 1 to 100 nM would be 1000 times more than the number of biotinylated molecules at the biosensor surface and each individual streptavidin can be coupled to two biotin molecules.

3.9.2 Investigation of fluorescence imaging of cell epitope-ligand binding

The fluorescence imaging investigation of various cell epitope-ligands binding confirmed that RGD peptide, RYD binding sites of streptavidin and the concanavalin A motifs can be recognized by cell adhesion recognition sites (Figure 3.9, 3.10 and 3.11). The results suggest that Con-A has a higher binding affinity and/or more binding sites in CHO-K1 cells and U-937 cells over streptavidin and RGD (Figure 3.12). This is supported by other

research works that demonstrated that CHO-K1 cells express large amounts of glycoproteins on their surfaces [440]. On the other hand, other studies showed some epitopes for RGD over CHO-K1 cells such as $\alpha_v\beta_6$ [441], however, their surface lack other epitopes for RGD binding sites such as $\alpha_v\beta_8$ and $\alpha_v\beta_3$ integrins [442]. U-937 cells showed similar results to CHO-K1 cells, which express more significant amounts of glycoproteins on their surfaces compared to epitopes for RGD [443-446].

This would suggest that, of all the motifs, Con-A should have worked best for the sensors described here. However, this proved not to be the case and could be due to the fact that the cells are overly large with too many binding sites, preventing the lateral diffusion of any mobile gAs in a direct ICS sandwich assay architecture, which prevents the movement of mobile gA monomers. In this regards, using the direct gA ICS sensor, it was assumed that binding the analyte to functionalized gA mobile monomer and tethered functionalized spanning molecules at the same time, would release the mobile gA monomers, thus prevent the dimerisation of tethered gA monomer and mobile gA monomer, which can be detected by the drop of G_m. However, a population of mobile gA monomers would also be rendered immobile in the dimerised form with tethered gA monomers. Thus, there would be unnoticeable variation in the G_m before or after the introduction of the analyte. This is supported by Ryu et al. (2015), who revealed that the lifetime of gAs dimer increases when introducing different ionic liquids [447]. This could be the case here when we introduced cells that include different ionic liquids that are used in cell homeostasis, which might prolong the gA channel dimer lifetime and, consequently, account for any slight variation in the overall membrane amplitude conductance.

3.9.3 Direct functionalized-gA-ICS sensor functionalization

RGD, streptavidin and Con-A were attached to gA-ICS nanosensor in order to provide adhesive points for variable cell membrane-incorporated receptors, subsequently for development cell surface recognition, label-free and real-time biosensor. Though, there is a risk of reduction of the binding affinity between the binding motifs such as RGD and cells integrins in comparison to the extraordinary binding affinity of specific antibodies to cell membrane surface [422].

The hypothesized developed modified gA-ICS direct sensor was aimed to provide a gating in the gA ion channel of at least more than 5%. However, the EIS measurements failed to demonstrate cell detection, in contrast to the fluorescence microscopy investigation that confirmed RGD, streptavidin and Con-A motifs could be identified by cell adhesion recognition sites. The real-time measurements of membrane conduction were revealed a very slight reduction in normalized G_m. Thus, the functionalization of the direct gA nano-biosensor with the various employed binding motifs showed insignificant variation in amplitude membrane conductance upon the addition of low concentration of different cell types.

These unexpected results of RGD-ICS direct biosensor (Figure 3.14) may be due to the incidence of some non-attached RGD motifs that are still floating in the liquid above the tBLMs that are well known to prevent cell binding [294, 444, 448]. Also, the streptavidin-ICS biosensor, as shown in Figure 3.16, displayed similar insignificant results to RGD-ICS biosensor that could be mainly due to the low binding affinity between RYD binding motif within streptavidin molecules and introduced cells. As the previous mentioned developed biosensors, Con-A ICS direct biosensor (Figure 3.17) presented a minor

reduction in membrane conduction recordings, this insignificant drop in the overall membrane conduction measurements of tBLM compared to streptavidin coupling can be due to the low binding affinity of Con-A motif and cells (CHO-K1 and U-937 cells). In addition, a possible impediment employing carbohydrate-binding motif to detect cells is the lack of specificity to target specific types of cells amongst heterogeneous cells population.

Cell detection was hoped to be improved by using a competitive binding assay. An MTSDDL hexapeptide dimer was then used to simulate cell-binding and compete for the RGD binding sites (Figure 3.18). Unfortunately, the differently designed dimers (the short and the longer amino acid linker) demonstrated an insignificant change in membrane conduction, which revealed that the dimer could not couple to multiple RGD binding motifs, resulting in low detection signals.

The results suggest that cRGD and the MTSDDL hexapeptide dimers did not bind, efficiently. This is supported by Gersthagen et al., who displayed that there is different parameter affect binding affinity between artificial RGD receptors and RGD peptide, for instance, the distance between arginine and aspartate recognition amino acid is a critical factor in achieving a higher binding affinity [449].

Furthermore, the configuration of the dimers could be one of the causes that prevent the coupling of more than one cRGD peptide to switch off the gA-ICS sensor. The purity of used dimers (>90%) also might affect the binding affinity between the hexapeptide and the RGD motif, as usually the higher the purity of the peptide the more efficiently it interacts [450-452].

3.9.4 Indirect RGD-gA-ICS sensor functionalization

Using the competitive ICS version, as illustrated in Section 3.7.9, we were able to *streptavidinise* the biotinylated membrane spanner before forming the second membrane layer. However, streptavidinising the freely diffusing biotinylated gA monomer before forming the outer membrane leaflet would be challenging because of the difficulties in obtaining a monomeric gA - streptavidin complex. The tetrameric streptavidin could bind to multiple biotins monomers causing target aggregation and thus affect the gA monomer function to dimerize with the tethered gA monomer of the biosensor. This procedure would also add multiple purification steps [453].

The MTSDDL monomer binding to cRGD binding motif demonstrated a minor drop in membrane conduction (Figure 3.19 B). This is most likely due to the monomer having a different configuration to the previously tested dimers. This consequently confirms the conclusion that MTSDDL peptide has a low binding affinity towards RGD ligand, which could have resulted from various factors. Lee et al. (1995) demonstrated the significance of divalent cations on diverse motifs' binding affinity, for instance, there is metal ion-dependent adhesion site within integrin domains that affect their interaction to other molecules [454]. Cierniewski et al. (1999) showed that the RGD peptide binding to artificial integrin receptors is promoted at 0.1 mM Ca^{2+}, but not at higher amounts such as 1 mM Ca^{2+}. This suggests that the Ca^{2+} amount within the solutions should be optimized in the future [455]. This is supported by Rensing et al. (2001) that revealed the binding affinities of RGD-artificial receptors is small in aqueous solutions due to a reduction in the hydrogen bonds and electrostatic interactions [456].

Pasqualini et al. (1995) revealed that the cyclic motif conformation of RGD demonstrated a higher binding affinity to cyclic DDL binding sites in comparison to linear DDL synthetic motifs, which could be another factor that reduces the binding affinity between our cRGD and the MTSDDL hexapeptide [434].

A review by Gersthagen et al. (2010) displayed the challenges in developing an artificial receptor for RGD binding motif with high binding affinity [449]. For instance, the distance between arginine and aspartate amino acid needs to be optimized by including spacer in between in order to minimize self-association of the complementary binding epitopes. This suggests that the different artificial peptide receptor configuration could be further investigated in the future in order to improve the binding affinity that directly affects the sensitivity and efficiency of a biosensor.

3.10 Conclusion

This study provides an overview of the different attempts to develop ligand-ICS biosensor. The use of gA ion biosensor switches as cell detectors is a greater challenge than assumed. The limitation is mainly thought to be associated with the reduction of binding affinity between the artificial binding motifs and cells in comparison to natural cell-binding microenvironments and epitopes.

In the future, further investigation is needed about the configuration and distance between different motifs binding sites, as well as divalent cation concentration for improvement of ligand-based biosensors.

Chapter 4

Real-time monitoring of heat transfer between gold nanoparticles and tethered bilayer lipid membranes

Chapter 4

Real-time monitoring of heat transfer between gold nanoparticles and tethered bilayer lipid membranes

4.1 Introduction

Irradiated gold nanoparticles (GNPs) are increasingly being explored for use in biomedical applications due to their unique optical resonance absorption properties [457, 458]. Gold nanomaterials have been integrated into a broad range of biomedical applications, mainly for imaging and therapeutic purposes [459]. The therapeutic applications include targeted treatment of infections and tumors, as well as for the controlled release of drugs *in situ* [460]. In particular, irradiated GNPs have shown great potential as a means whereby laser-induced targeted hyperthermia treatments can be achieved [461].

However, assessment and understanding of the molecular interaction between GNPs and bio-membranes as well as the direct consequences of the laser-induced heating phenomena of embedded GNPs in biological tissues are yet to be fully elucidated. This is in large due to the complexity of native cell membranes. Therefore, a thorough understanding of the hyperthermia process of irradiated GNPs remains a challenge. As such, development of a nanomaterial-electrode interface that mimics the natural surroundings of cells with a precise composition could provide means by which to undertake an in-depth investigation of the heat transfer characteristics of irradiated gold nanoparticles within biological systems. Using artificial membranes represented by

tBLMs offers such a possibility, thus reducing the experimental challenges via their stability, sensitivity and defined parameters.

This chapter describes the employment of lipid membrane-coated electrodes as a sensor for assessing gold nanoparticle and lipid membrane interactions. This is critical for refinement of emerging photo-thermal therapies, as well as offering valuable information for detailed mechanisms of heat transfer within biological systems. In addition, this chapter reviews biomedical applications of GNPs.

The experimental setup was designed and created to allow simultaneous laser-irradiation of gold nanoparticles in the solution above or bound to the tethered membrane while monitoring changes in the membrane's properties via electrochemical impedance spectroscopy (EIS) recordings. The effect of various irradiated GNPs was examined over different tBLM architectures. During these experiments, EIS was used to evaluate the heating effects on the tBLMs via a thermally induced change in basal membrane ionic conduction.

Likewise, this chapter studies the efficiency of using the direct attachment of GNPs to adjacent tissue in enhancing heat transfer phenomena. Along with the assessment of the various tBLM architectures that can differentially induce the attachment of gold nanoparticles to the membrane surface. Furthermore, this chapter outlines the thermal predictive mathematical models to demonstrate the utility of the technique for measuring heat transfer characteristic.

4.2 Properties of gold nanoparticles

Gold is one of the main inert noble metals used in the biomedical and electronics sector due to its low toxicity and its significant thermal and electrical conductivity [462, 463]. Generally, the inert characteristic of bulk gold prevents any catalytic performance of this metal [463]. However, within the nanoscale gold size range, gold can perform as a catalyst in specific circumstances [464].

Gold in the nanoparticle scale has different physical and optical characteristics to larger gold aggregates. Moreover, the small size of GNPs offers a high surface area to volume ratio, allowing for subsequent functionalization [465, 466]. The usefulness of GNPs in therapeutic fields and imaging techniques mainly arises from their distinctive surface plasmon resonance [467, 468]. In this regards, each GNP can be excited by an electromagnetic fields at specific resonance wavelengths which produces an intense absorption, as illustrated in Figure 4.1. A consequence of this is a collective oscillation of electrons occurring on the surface of the nanoparticles which leads to a distinct elevation of temperature [469].

There are variable incident energies that can be used to excite the nanoparticles from sources such as near-infrared lasers [470], induced radio waves [471] or induced magnetic fields [472].

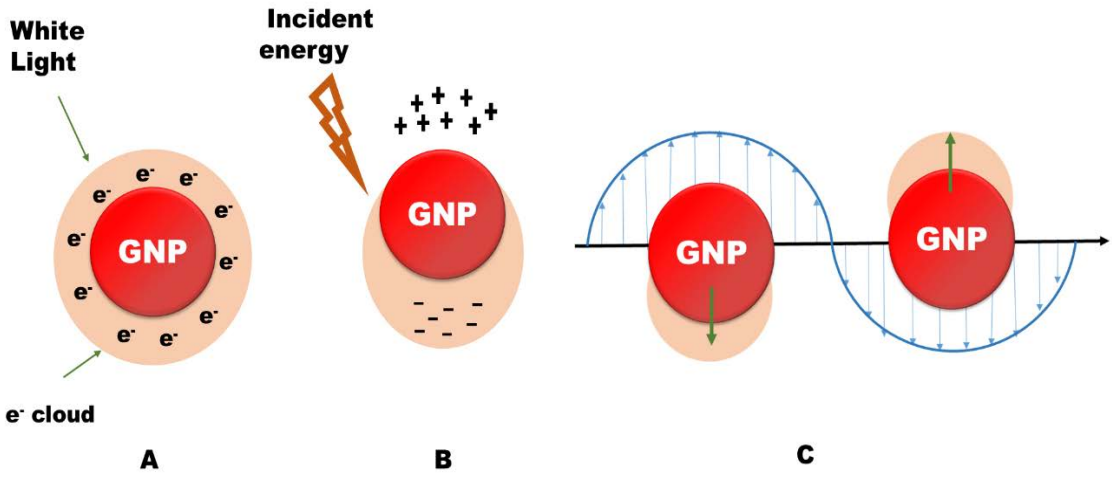

Figure 4.1: Schematic illustration of particular surface plasmon resonance. (A) White light excited electron cloud around the nanomaterial, then absorbed energy display color depending on particle size and shape; (B) Incident energy such as near-infrared laser light, radio waves and magnetic fields leads to excitation of nanomaterials in their plasmon resonance wavelength lead to an excitation of electrons, which in resonance with the frequency of visible light. Consequently, dipole band electrons conducted with particular to the positively charged metallic core; (C) Electrons cloud starts to oscillate; thus plasmon resonance force arises. As a consequence of electron oscillation, the temperature elevation occurred. Modified Figure was based on [473].

The light-scattering properties or surface plasmon resonance of nanomaterial suspensions are coupled to their size, shape and composition [474]. For nanoparticles sized more than 20nm, the plasmon resonance relies on the particle size, where the plasmon bandwidth and the size of the particles are directly proportional to each other [475]. On the other hand, for nanoparticles less than 20nm, the plasmon bandwidth and the size of particles are inversely related, this is related to surface electron scattering [476].

The selection of the laser wavelength was according to the absorption peak of each nanoparticle in order to yield the most efficient excitation, which consequently leads to heating. For example, the visible ruby red colour of spherical 30 nm GNPs indicates their ability to absorb light efficiently in the ~530 nm spectrum (blue-green light), while reflecting the red light, as seen in Figure 4.2. Thus, optical excitation of spherical, 30 nm gold particles at a frequency close to their surface plasmon resonance results in the hyperthermia phenomena. On the other hand, spherical 100 nm GNPs have a peak absorption at ~600 nm and thus have a pale blue color. They therefore would not generate significant levels of heating when exposed to the lower wavelength laser.

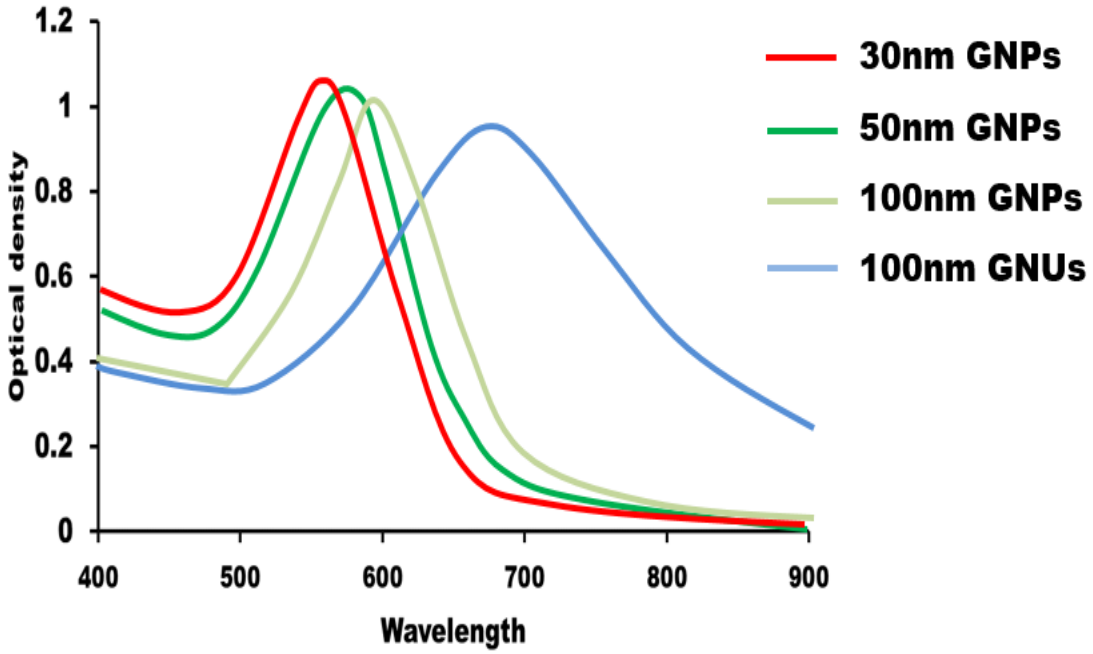

Figure 4.2: Optical absorption spectra of variable gold nanoparticles size and shape. Spectra of different size gold nanoparticles (GNPs) 30nm, 50nm and 100nm in diameter. Also, spectra of 100nm gold nano urchins (GNUs). Modified Figure was based on [475, 477].

4.3 Gold nanoparticles in biomedical applications

GNPs have been used in many diagnostic biological applications due to their unique optical resonance absorption in the so-called therapeutic window, simplicity of synthesis and to that can be added also the straightforwardly ability to modify them with various biomolecules [457, 458, 478]. The hyperthermia performance of irradiated gold nanomaterials also offers a new class of minimally invasive, selective, targeted treatment for infection and tumors.

Likewise, irradiated gold nanomaterials can combine in visualizing the structural characteristics of cellular and subcellular structures [461, 479, 480]. The main contribution of gold nanomaterials in bioimaging techniques is to perform as a robust contrast agent that enhances the detection quality of the target area, for instance, in cancerous cell detection [481].

GNP based biomedical therapeutic treatments rely on their ability to be easily modified and thus targeted to a specific antigenic site. Unlike many drug-based therapies that suffer from a lack of specific targeting and are instead distributed to several locations within the body. In addition, irradiated GNPs are considered minimally invasive and selective treatment [461, 479, 480]. Therefore, the employment of nanoparticles heated by a laser has been used in selectively heating and destroying diseased cells as well as selective drug delivery [482, 483]. Numerous other applications have used the plasmonic heating of particles in photo-thermal therapy, for example, in the stimulation the action potentials in nerve cells in order to control neuronal functions [484-486], kill cancerous cells [461], gene transfection [487] and the controlled release of drugs *in situ* [488]. A consequence of the photothermolysis phenomena of these heated plasmonic nanoparticles is damage

of cell membranes. The fluid lipid bilayer membrane is considered a particularly vulnerable site within a cell by such treatments, as well as denaturation of proteins within cells, which can lead to cell destruction [489].

Significantly, the permeability of ions across cell membranes is crucial to control cell function. Various investigations have aimed to understand the mechanisms of the heat effect on bilayer lipid membranes [490-493]. Phospholipids movements in the presence of heat are one mechanism that causes phase transitions within the bilayer membranes [494]. Though this mentioned transition has a dependency on the composition of the lipid layers [495]. Moreover, nanopore formation has been demonstrated as a consequence of adequate plasmonic heating of nanorod or nanoparticle aggregates that exceed the physiological tolerance of cell membranes [491].

However, assessing the direct consequences of the laser-induced heating phenomena of embedded GNPs in biological tissues is still problematic. There is a necessity to discuss the fundamental mechanism of how heat transfer occurs between GNPs and adjoining cells, as well as to understand the fundamental effects of the heating on membrane structure and electrical properties, as well as ion channels. An innovative nanomaterial-electrode interface that mimics the natural surroundings of cells could provide a better understanding of the heat transfer characteristics of irradiated GNPs within biological systems.

In this work, we have developed a real-time dynamic non-invasive approach to investigate the nanoscale heat stability of artificial bilayer lipid membranes due to irradiated GNPs. The immediate objective of this study was to establish a method by which laser-induced gold nanomaterials in conjunction with real-time EIS recordings could be performed

simultaneously over an artificial lipid membrane model represented by tBLM. Our study has resulted in the establishment of such a system that allows us to achieve the aforementioned objective, by using transversal focusing of a laser beam light.

Significantly, this approach is unique in that tethered membranes can withstand substantial damage, unlike other systems (such as membranes formed by patch-clamp or liposomes) in which only a small amount of damage results in a catastrophic failure of the membrane which prevents further investigation.

Accordingly, this chapter will examine:

- Development of a novel platform by which laser-irradiation of gold nanoparticles could coincide with electrochemical impedance spectroscopy recordings.

- Investigation of real-time measurements of localized heating from GNPs irradiated by lasers across the tBLM membrane model.
- Evaluation of the consequences of direct GNPs attachment on the membrane permeability.
- Assessment of diverse architectures that can differentially induce the attachment of gold nanoparticles to the membrane surface.
- Outlining of thermal predictive mathematical models to demonstrate the utility of the technique for measuring heat transfer characteristics.

4.4 Materials and Methods

4.4.1 Chemicals

All chemicals implemented to perform the experiments, unless mentioned otherwise, were of analytical grade and used as advised. 100% pure ethanol, phosphate buffer saline (PBS), cholesterol, streptavidin and spherical bare gold nanoparticles with 30 nm diameter were purchased from Sigma- Aldrich (Sydney, Australia).

30 nm diameter streptavidin-conjugated gold nanoparticles, and 100nm diameter Streptavidin conjugated gold nano-urchins were obtained from Cytodiagnostics, Canada. Cholesterol-PEG-Biotin (MW1000) were purchased from NANOCS, USA. Standard mobile lipids [70% zwitterionic C20 Diphytanyl-Glycero-Phosphatidylcholine lipid: 30% C20 Diphytanyl-diglyceride-OH ether] were kindly provided from SDx Tethered Membranes Pty. Ltd., Australia.

Laser light sources irradiation from a HeNe laser or a solid-state diode laser functional at λ = 530 nm was from (Melles Griot 05-LGR-151). Laser light sources λ = 650 nm was from (M-16A648-150-LZ) MTO Laser, Inc., China.

4.4.2 Electrodes

Direct exposure of laser beam lights towards the tBLM experimental concepts required to work in the absence of solid 6-well defined polyethylene cartridges (Chapter 2, Figure 2.4). As a consequence, for combining GNPs irradiation with EIS measurements, unique electrode arrays (SDx Tethered Membranes Pty Ltd, Australia) (Figure 4.3) were used that have been further modified for this purpose.

Coplanar gold electrodes are made from 25 mm x 75 mm x 1 mm polycarbonate base substrate with patterned gold arrays layout. A transparent adhesive layer defines the six individual measuring chambers. The coplanar gold electrode allows the direct exposure of the laser beam light to the tBLM membrane. Each well of the electrode array contains a circle-shaped working electrode (area: 0.707 cm^2) and half-circle shaped counter electrode or coplanar electrode (area: ~ 0.725 cm^2), which were separated by a gap of ~2 mm. The transparent adhesive layer insulates the rest of the deposited gold from the bulk electrolyte, while the underlying gold layout connects the working electrodes to contact areas outside the measuring chambers in order to provide the electrical connection to the tethaPod^{TM} reader for EIS measurements.

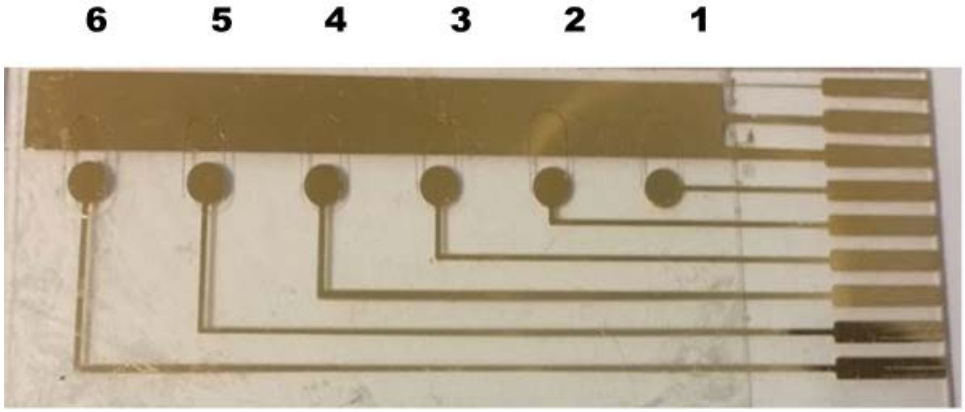

Figure 4.3: SDx coplanar electrode. Six wells defined by the transparent adhesive layer.

4.4.3 Tethered lipid bilayer membranes (tBLMs) formation

Solvent exchange methodology has been employed to form tBLMs as described previously in detail in Section 2.5.6.

The lipid mixture for all demonstrated experiments, unless otherwise stated, was 3 mM mobile phase lipids, that were themselves comprised of 70% zwitterionic C20 diphytanyl-

ether-glycero-phosphatidylcholine and 30% C20 diphytanyldiglyceride ether lipids (a mixture referred to as *AM199*) mixed with 3 mM cholesterol-PEG-Biotin in a 50:1 ratio.

4.4.4 Preparation of the tBLM with variable cholesterol composition

3 mM cholesterol was dissolved in pure ethanol. Mobile lipids were prepared by mixing different percentage (30:70; 1:10; 1:100; 1:1000) of non-functionalized cholesterol with the first mixture of standard mobile lipids and cholesterol-PEG-Biotin (50:1).

4.4.5 Electrical impedance spectroscopy (EIS) measurements

Measurements were carried out using the impedance analyzer SDx tethaPod™ equipment controlled by SDx tethaQuick™ software (SDx Tethered Membranes Pty Ltd) for data acquisition and analysis. Using a 25 mV peak-to-peak AC excitation at frequencies between 0.1 and 10,000 Hz with two steps per decade. Membrane conduction (G_m) and membrane capacitance (C_m) variation were assessed using EIS swept-frequency electrical equivalent circuit that mirrored ionic permeability over the membranes.

4.4.6 Laser irradiation

Two types of lasers, green and red, were used in this study depending on the size (30 nm, 100 nm) and shape (sphere or urchins) of gold nanoparticles, as explained below.

4.4.6.1 Green Laser

A 532 nm green laser (OBIS LS/OBIS CORE LS, China) was used to study the heat transfer of 30 nm spherical GNPs. The power of the laser was ~135 mW (which

equivalent 350.8 mW/cm² irradiance). Laser burn paper (Lastex) was used to assess the ability of laser power to burn the paper.

4.4.6.2 Red laser

100nm GNUs plasmon absorption at a wavelength around 650 to 700 nm; therefore, a red laser at a wavelength of ~ 650 nm (150 mW red laser, 648 nm, M-16A648-150-LZ, China) was used for this nanomaterial. The power of the laser was 150 mW (which equivalent 389.8 mW/cm² irradiance) and operating current 210 mA.

4.4.7 Alignment of laser and gold electrodes

Initial experiments were performed using a vertical laser beam light focusing set-up. Custom made a holder for the laser (λ = 530 nm and λ = 650 nm, Laser Quantum) was built. A 10× immersion objective was used for focusing the laser in order to focus the beam on the formed tBLM using the vertical alignment only, illustrated in Figure 4.4 (A).

Subsequent experiments were performed using horizontal laser beam light focusing set-up. The laser beam and the angle of electrode were adjusted such that a uniform track of light from laser passing through the liquid above the electrode was just visible evenly at the gold surface. The alignment process was performed manually, using a very substantial metal support with gearing from microscope in order to achieve the appropriate precision. The impedance reader, electrodes as well as laser beam source were settled on separated XYZ stage, allowing positioning of the setup relative to the laser beam light, illustrated in Figure 4.4 (B).

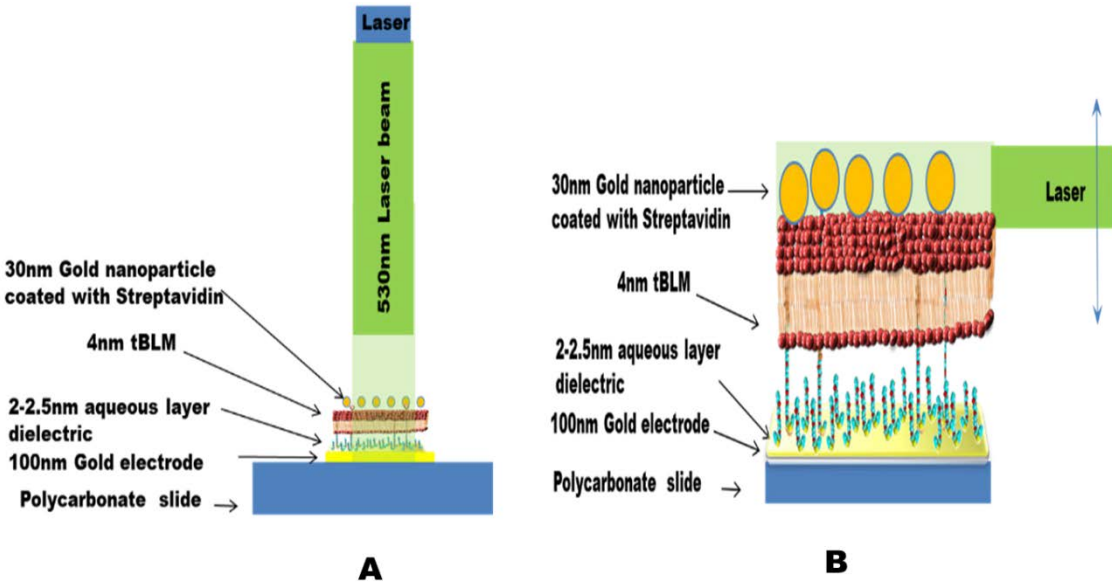

Figure 4.4: Schematic of tBLMs and heated gold nanoparticle (GNP) interface system. The tBLMs were formed directly on a gold electrode. Functionalized gold nanoparticles were added to the liquid phase surrounding the bilayer membrane. The laser light was aligned with the lipid-buffer interface. (A) vertical laser alignment; (B) horizontal laser alignment.

Functionalized or bare gold nanoparticles were added to the liquid phase sitting above the bilayer membrane. The laser beam light was aligned within the lipid-buffer interface using the following steps: the laser beam light was focused horizontally. The tBLM position relative to the laser was adjusted for each experiment by raising or lowering the slide while observing changes in membrane conductance. Correct alignment of the laser beam with respect to the tBLM was set when no conductance changes were arising from the laser interacting with the underlying bulk gold. GNPs were added to the buffer above the tBLM and the laser beam switched ON and OFF manually. Each experiment consisted of turning the laser ON for exactly 105 seconds, followed by 105 seconds OFF. This was then repeated for a further two rounds.

Nanoscale heating was manipulated by irradiating gold nanoparticles in solution located above and/or directly attached to the t-BLMs, with a laser beam of set wavelength coupled

to the GNPs plasmon resonance frequency. Electrical impedance spectroscopy was utilized to assess the heating effects on the tBLMs via measuring membrane conductance.

4.4.8 Statistical analysis

The statistical examination was carried out utilizing GraphPad Prism software (GraphPad Software, Inc.). The error bars indicate the average standard error of three independent impedance spectroscopy conductance measurements, both repeats and replicates. Each experiment was performed at least three times. For various groups comparison, P-value was calculated according to the one-way ANOVA test.

4.5 Results

4.5.1 Developing a platform by which an irradiated nanomaterial-electrode interface could be investigated in real-time

4.5.1.1 Vertical laser alignment combined with electrochemical impedance spectroscopy recordings

As described in material and method Section 4.4.7, two methods were used for laser beam alignment. A series of experiments were trialled to observe the effect of irradiating tBLMs with and without gold nanoparticles under vertical laser light focusing (Figure 4.4 A). Using a corresponding laser wavelength of 530 nm and streptavidin-coated spherical 30 nm GNPs, the following membrane conductance recordings were observed, shown in Figure 4.5. When the laser was turned ON, there was an almost 2-2.5 fold increase in membrane conductance both in the absence and following the addition of GNPs.

Various combinations and concentrations of GNPs were trialled; however, there was no observable, nor significant difference between samples with or without GNPs. It was clear that exposure of the membranes to laser alone led to a significant increase in membrane conductance, which either masked any effect that may come from the addition of GNPs or there was no discernible heating effect from the irradiated GNPs.

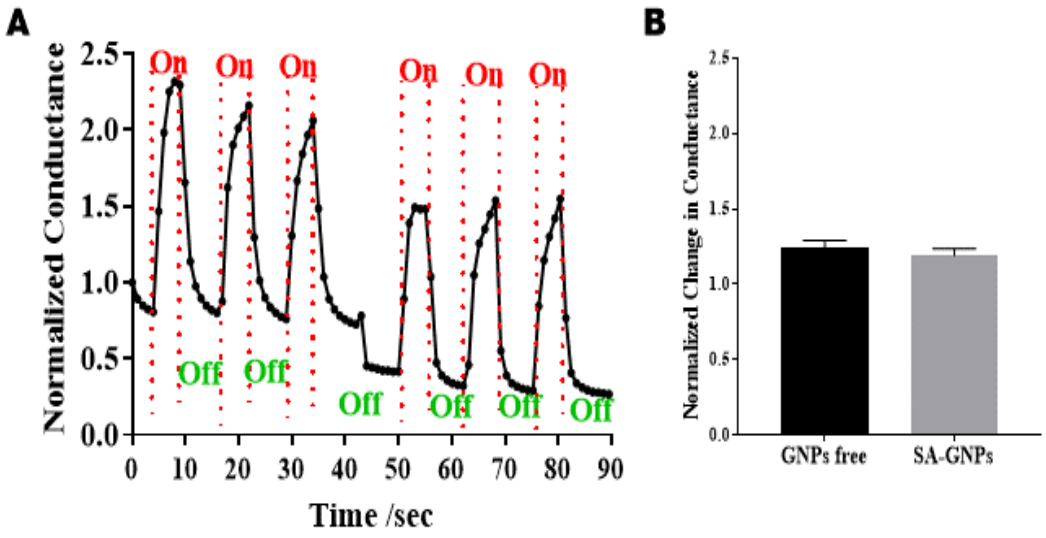

Figure 4.5: Irradiated GNPs investigation on the tBLM gold modified surface using vertical laser irradiation. (A) The period when the laser was turned ON is indicated in red. Streptavidin conjugated 30 nm spherical GNPs introduced. The membrane conduction values were normalized to the initial value of membranes conduction. Results are representative of at least three independent experiments. (B) The peaks of membrane conduction variation while the laser beam light is ON, with and without the introduction of 30 nm SA-GNPs, compared to conductance values in the absence of laser illuminating. The error bars indicate the standard error of three independent impedance spectroscopy conductance measurements.

4.5.1.2 Developing horizontal laser alignment combined with electrochemical impedance spectroscopy recordings

Given the tBLMs are formed by attachment to a substrate layer of bulk gold, it seemed likely that the effects seen above were as a result of heating coming from interactions of the laser with nanostructures within the sputtered bulk gold layer. Therefore, it was decided to adopt a new approach, using a horizontal light beam focusing to eliminate interaction between the laser light and the bulk gold substrate found below the tBLMs.

As outlined in Section 4.4.7, the laser was positioned and aligned in a manner where it was interacting with the tBLMs and liquid buffer above, but not with the gold substrate below. This was easily determined via vertical raising and lowering of the laser until the correct position was established, just at the point when no changes in membrane conductance could be observed.

In the current experiments, continuous-wave radiation from a green HeNe laser at a wavelength of 530 nm with a laser output power value of ~ 135 nW/μm^2, was applied for 105 seconds. The tBLMs were comprised of the standard mobile phase lipids (AM199), as well as incorporating 3mM biotinylated cholesterol.

A schematic of the experimental setup is presented in (Figures 4.6 A, B and C). Baseline recordings were first established, then the sample was added. Addition of buffer revealed negligible variation to the membrane conductance recordings during both periods of laser ON and laser OFF (Figure 4.6 D). Using the same tBLMs that contained biotinylated cholesterol, 30nm spherical bare gold nanoparticles were added. This resulted in minimal changes to the membrane conductance between the laser ON and laser OFF phases (Figure 4.6 E). In contrast, when streptavidin-conjugated 30 nm gold nanoparticles were added (Figure 4.6 F), there was a clear difference between the laser ON and OFF periods, with distinct increases in conductance amplitude during the laser ON phase.

This result indicated that in order for photothermal heating of the gold nanoparticles to result in membrane perturbations, close contact with the adjoining membrane was necessary.

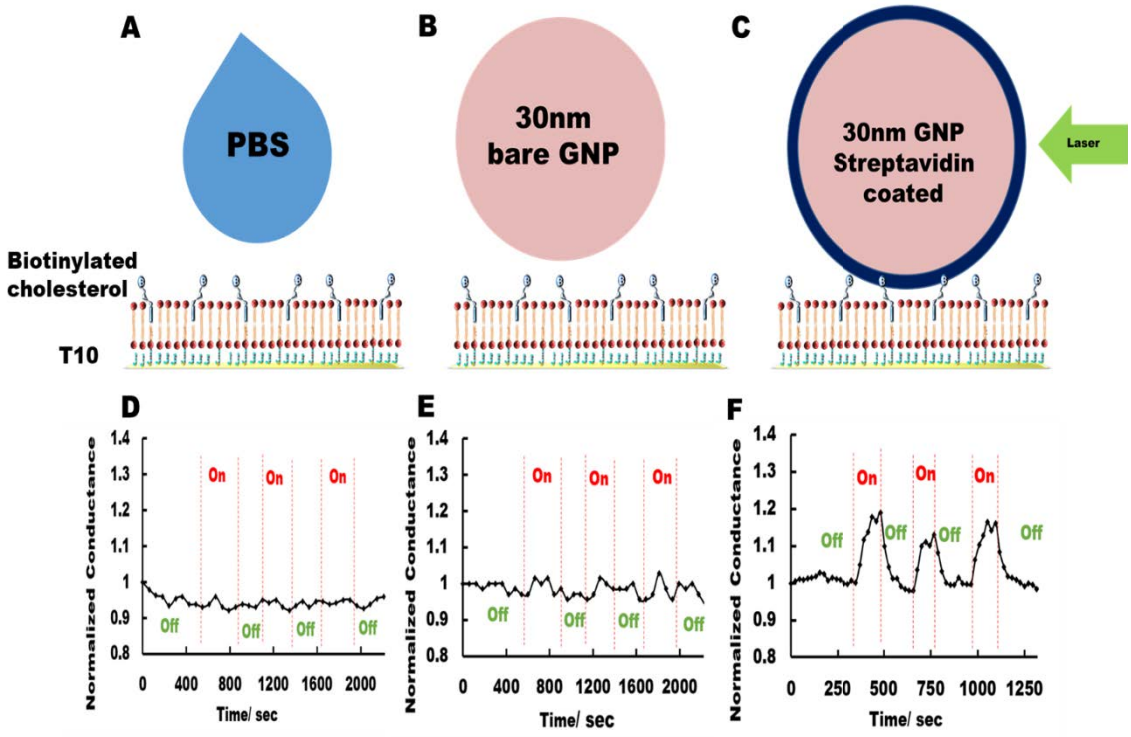

Figure 4.6: (A-C) Illustration of the assay set-up for measuring membrane conductance changes across tBLMs arising from 30nm spherical GNPs and laser illumination (λ = 530 nm). Samples were added above the tBLMs: (A) PBS buffer control; (B) Bare 30nm spherical GNPs; (C) Streptavidin-coated GNPs; Panels (D- F) Normalised conductance recordings over time. The period when the laser was turned ON is indicated in red: (D) Reference measurement of tBLM conductance in the absence of GNPs; (E) Non-functionalized bare 30nm spherical gold nanoparticles; (F) Streptavidin conjugated 30nm spherical GNPs. Results are demonstrative of at least three independent experiments.

The membrane capacitance was also examined for all the formed tBLMs in order to confirm the stability and thickness of the membrane bilayer [79] (Figure 4.7).

Overall, the obtained membrane capacitance measurements revealed a negligible variation in membrane capacitance. The membrane capacitance values are consistent with values characteristic of an intact 10% tethered tBLM membrane capacitance, which is 10.5 ± 0.7 nF [496].

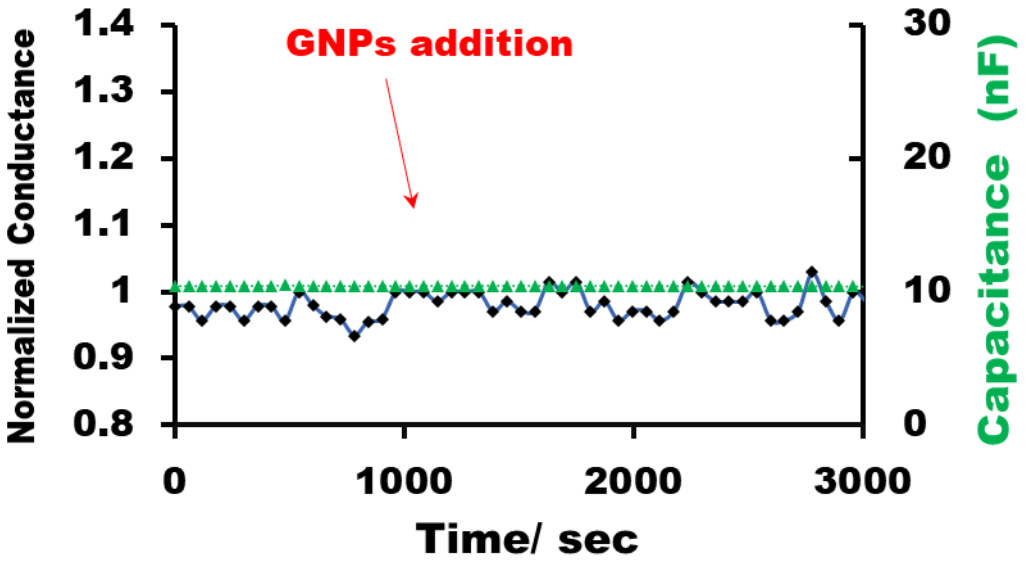

Figure 4.7: Capacitance changes across tBLMs arising from 30nm spherical GNPs and laser illumination (λ = 530 nm). GNPs samples were added above the tBLMs. Measurement of tBLM capacitance during both periods of the laser ON and laser OFF is indicated in green. Measurement of tBLM conductance during both periods of the laser ON and laser OFF is shown in black. Results are demonstrative of at least three independent experiments.

4.5.2 Effect of gold nanoparticle concentration on thermal disruption over lipid membrane

After achieving a definite increase in membrane conduction as a consequence of laser irradiated streptavidin-coated gold nanomaterials, we then have investigated the effect of hyperthermia phenomena delivered by laser irradiation at different concentrations of gold nanoparticles. Four concentrations (~$2.6X10^{9}$/ ml, $5.3X10^{9}$/ ml, $2.6X10^{10}$/ ml, and $2.6X10^{11}$/ ml GNPs/ml) of 30nm GNPs streptavidin-conjugated, using the same tBLMs that incorporated biotinylated cholesterol. 0% represents the unconjugated 30nm GNPs that were also exposed to laser light under the same conditions.

The same laser dosage of ~ 135 nW/mm^2 was applied and was also aligned to laser light under the same conditions using 530nm laser beam light. After laser irradiation,

normalized membrane conduction values in each treatment were analysed. Figure 4.8 displayed the increase of normalized membrane conduction measurements in each condition during the laser ON phase. The membrane conduction of highest GNPs concentration ($2.6X10^{11}$ GNPs/ml) after laser exposure had the highest conductance in comparison to the other employed GNP concentrations. Conversely, unconjugated spherical GNPs at the highest concentration ($2.6X10^{11}$ GNPs/ml) showed no significant increase in the membrane amplitude conductance. At the low concentration of streptavidin-coated 30nm GNPs, it seemed there were less amount of GNPs conjugates to bind on the surface of biotinylated tBLM as a result of a less increase in membrane amplitude conduction values in comparison to a higher concentration of GNPs conjugates. These results indicated that the amount of generated heat depended on the concentration of bound nanoparticles onto the interface.

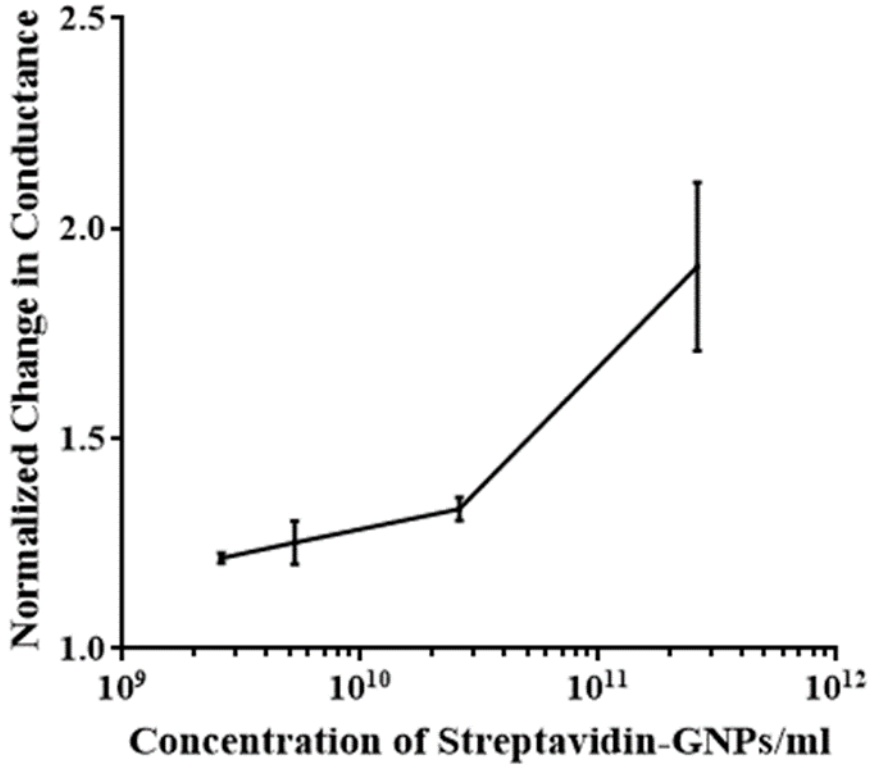

Figure 4.8: Normalized membrane conduction response for various streptavidin-conjugated GNP concentrations. The variable GNP concentrations: 2.6x109/ ml, 5.3x109/ ml, 2.6x1010/ ml, and 2.6X1011/ ml (diluted with PBS buffer) compared to conductance values in the absence of GNPs. The error bars indicate the standard error of three independent impedance spectroscopy conductance measurements.

4.5.3 Effect of irradiated GNPs on tBLMs with variable membrane-binding motif

The tBLM membrane model is known for providing a close mimic to different types of natural lipid membranes. Likewise, various studies have demonstrated that cholesterol in biological membranes improve membranes stabilization and provides variable transition phases [497]. In this regards, we have studied various combinations of mobile lipids and biotinylated cholesterol binding motif, as well as a mixture of biotinylated gramicidin monomers binding motif and the mobile lipids, in addition to pure mobile lipids without

any membrane-binding motif, as described in the schematic representative of the experimental setup, Figure 4.9 (A, B and C). Streptavidin-coated 30nm GNPs combined with the horizontal laser continuous-wave radiation alignment from a green HeNe laser at a wavelength 530 nm with a laser output power value of ~ 135 nW/mm^2, was applied for 105 seconds. Following the addition of streptavidin-coated 30nm GNPs a distinct variation in membrane conductance amplitude between the laser ON and OFF phases, with a definite increase in membrane conductance amplitude during the laser ON periods was obtained, as seen in Figure 4.9 (E and F). While using the tBLMs in the absence of biotinylated molecules, resulted in minimal changes to the membrane conductance between the laser ON and laser OFF phases (Figure 4.9 D).

As seen in Figure 4.9 (F), tBLMs designed with biotinylated gramicidin monomers in the absence of cholesterol, membrane conductance amplitude recordings revealed a distinct increase during the laser ON phase. This result indicated that cholesterol insertion within membrane bilayer is not essential for membrane perturbations as a result of photothermal heating events of the irradiated gold nanoparticles. Rather it confirms that the close contact of the GNPs to the membrane is critical.

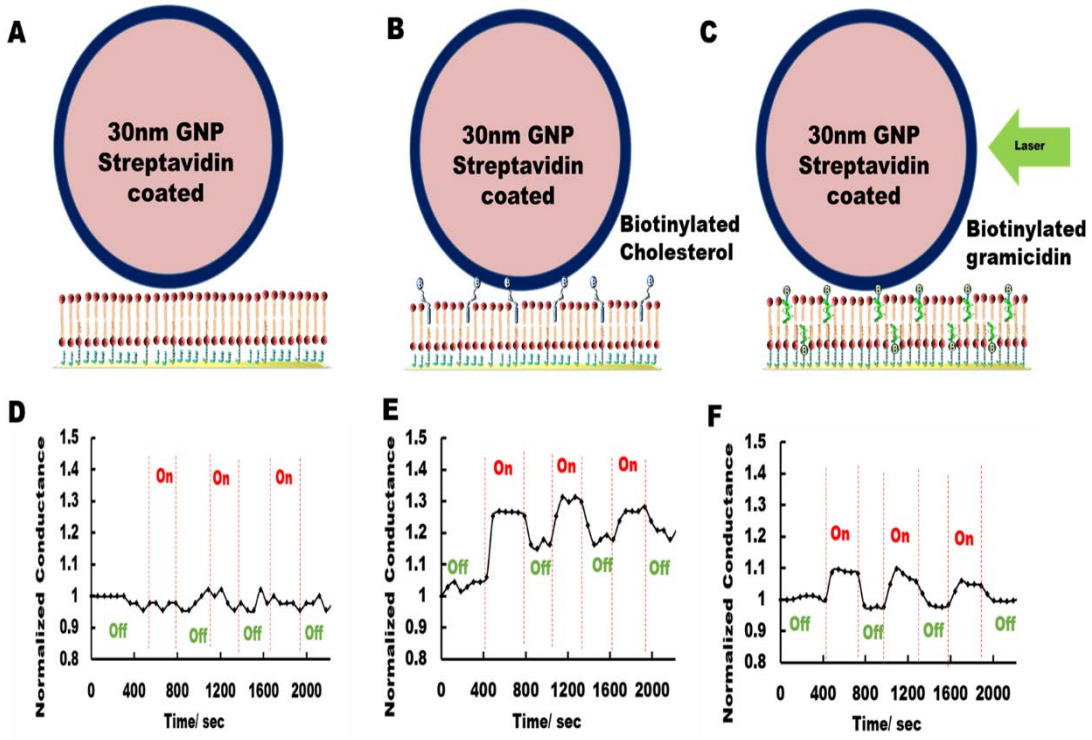

Figure 4.9: (A-C) Illustration of the assay set-up for measuring membrane conductance changes across tBLMs arising from streptavidin-conjugated 30nm GNPs and laser illumination (λ = 530 nm). Samples were added above the tBLMs: (A) tBLMs constituted of mobile lipids without any functionalizations; (B) tBLMs functionalized with biotinylated polyethylene-glycol cholesterol; (C) tBLMs functionalized with biotinylated gramicidin monomers; Panels (D-E) Normalised conductance recordings over time. The period when the laser was turned ON is indicated in red. Streptavidin conjugated 30nm spherical GNPs. Amplified ion membrane conduction recordings of tBLM were distance and laser dependent over time. Results are demonstrative of at least three independent experiments.

4.5.4 Effect of varying cholesterol concentration within the lipid membrane composition

Of the well-known functions of cholesterol in biological membranes is its role in membranes stabilization and variable transition phases [497]. For this reason, we have investigated the effect of cholesterol incorporation within tBLMs on the thermal heat distribution over the bilayer lipid membrane.

To undertake this study, different percentage of cholesterol molecules of 32%, 12%, 3%, 2% and 0% were chosen and incorporated within mobile lipids in order to form the bilayer lipid membrane. For cross-comparability, all conduction recordings were normalized to the GNPs response during the initial laser OFF phase.

Based on the normalized membrane conduction results during the laser On phase, discernible changes in membrane electrical properties were revealed. As seen in Figure 4.10, comparing the different percentage of cholesterol in the tBLMs while using the same amount of introduced streptavidin-coated-GNPs, it is evident that the lowest percentage of cholesterol (0%) showed the highest increase in membrane conduction, which indicates a greater heat sensitivity in comparison to other cholesterol percentages.

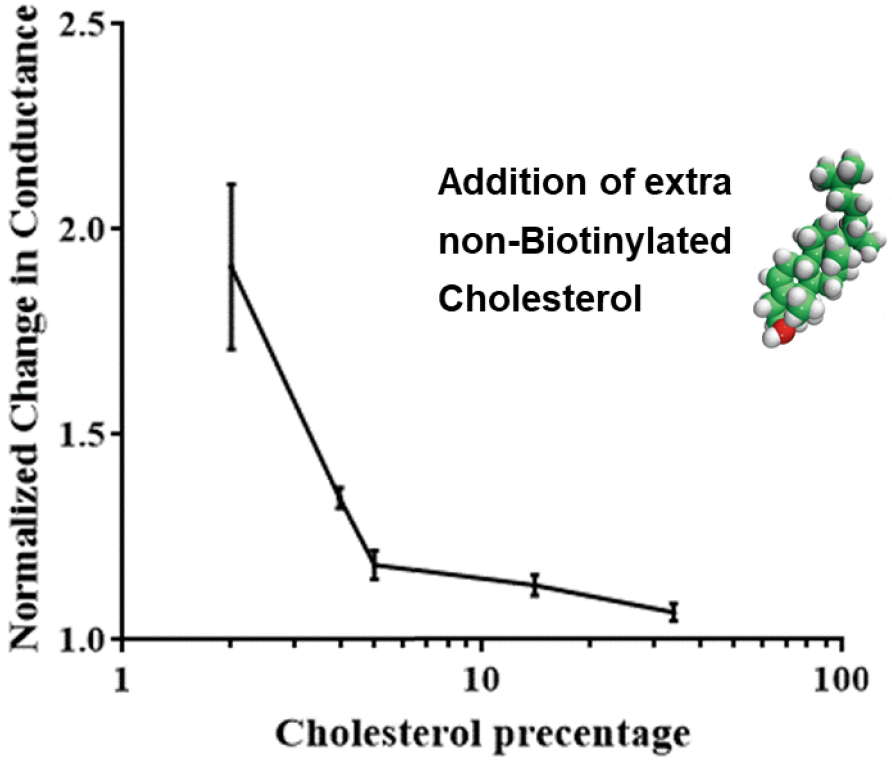

Figure 4.10: Normalized membrane conduction response for various cholesterol percentage. tBLMs had variable cholesterol concentrations of 32%, 12%, 3%, 2.5 %, and 2%. The error bars indicate the standard error of three independent impedance spectroscopy conductance measurements.

4.5.5 Studying interactions of irradiated GNUs-tBLMs interface and laser light specificity

The plasmon resonance wavelength is directly influenced by the absorption and scattering characteristics of GNPs. Thus, in this experiment, the streptavidin-conjugated 30 nm GNPs was substituted with streptavidin-conjugated 100nm GNUs, in order to compare the membrane electrical properties using different gold nanomaterials geometries (Figure 4.11 A).

Membrane amplitude conductance variation examined the extent to which membrane conductance could be affected by laser irradiation using a laser beam of wavelength (λ) = 650 nm. The application of laser irradiation alone does not show variation in membrane conductance. In contrast, membranes that had GNUs streptavidin conjugates specifically bound to the biotinylated membranes were found to be strongly affected by laser irradiation. As demonstrated in Figure 4.11 (C), an incredible variance between the laser On and OFF phases, with distinct increases in conductance amplitude during the laser ON phase was revealed.

In contrast, a control sample of a 30 nm GNPs streptavidin conjugate was employed over a biotinylated tBLM membrane that had been irradiated by laser beam light λ = 650 nm. As Figure 4.11 (D) indicates, no significant changes occur in irradiated streptavidin-conjugated 30nm GNPs with infrared laser irradiation wavelength λ = 650nm. The membrane amplitude conductance variations were comparable to the biotinylated membranes that had not been irradiated at all (OFF phase). These results are consistent with the known properties of different sized gold nanoparticles tuned to different light

wavelengths [475], thus demonstrating the plasmon resonance wavelength specificity based on gold nanomaterial dimensions.

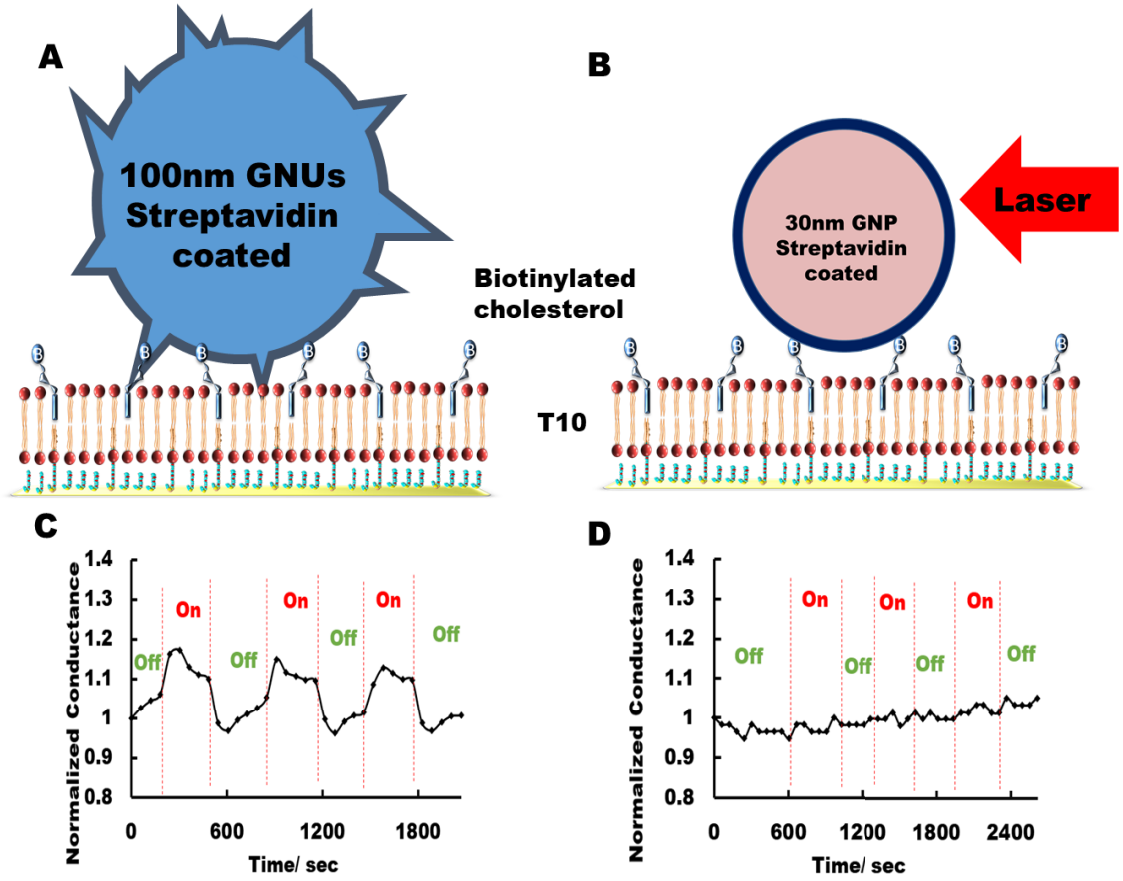

Figure 4.11: (A, B) Illustration of the assay set-up for real-time observation of tBLM conduction measurements whereupon irradiation of introduced nanoparticles. Samples were added above the tBLMs: (A) Streptavidin-coated 100nm GNUs added and irradiated with a laser beam light (λ = 650 nm); (B) Streptavidin functionalized 30nm GNPs introduced and irradiated with a laser (λ = 650 nm); Panels (C, D) Normalised conductance recordings over time. The period when the laser was turned ON is indicated in red: (C) Streptavidin-functionalized 100nm GNUs; (D) Streptavidin conjugated 30nm spherical GNPs. Results are demonstrative of at least three independent experiments.

4.5.6 Observation of tBLMs different design model effect on the thermal impact of irradiated GNPs

Another confirmation that the variation in membrane amplitude conductance was related to the attachment of streptavidin-coated gold nanomaterials to membranes that mimic natural lipid membranes were obtained by using a range of tBLM models that represent different types of membranes. In the previous experiments mentioned in this study, we have employed the tBLM model with 10% of tethering chemistry that provides the close mimic to natural lipid membranes of having water surrounding the two sides of membrane as well as providing phospholipid mobility [134, 379, 410].

Here we employed two different tBLM models in order to study the thermal activity of irradiated GNPs. Figure 4.12 (A) shows fully tethered lipid membrane model with gramicidin monomers that initiate ion channel. This model design was illustrated in details in Section 3.4. In contrast, another tBLM model of the fully tethered percentage constituted biotinylated gramicidin monomer in the upper membrane leaflet only, is illustrated in schematic Figure 4.12 (B).

Following the coupling of 30nm GNPs streptavidin conjugates with biotinylated gramicidin monomers within the upper leaflet of the bilayer lipid membrane. The laser irradiation of these GNPs showed an increase of ion membrane conduction during the laser ON phase in the gramicidin ion channel biosensor tBLM model, as indicated in Figure 4.12 (C). However, in the case of the other tBLM model of the fully tethered percentage constituted biotinylated gramicidin monomer only in the upper membrane leaflet, there was little to no noticeable change in membrane conduction measurements

as a result of laser irradiation between the laser ON and laser OFF phases, as seen in Figure 4.12 (D).

These results implied that the increase of membrane amplitude conductance was most likely due to the formation of gA ion channel that enable ions passages, while in the tBLM model that has no fully gA ion channel (absence of tethered gA monomer within the lower leaflet of the membrane) there were steady membrane amplitude conductance measurements.

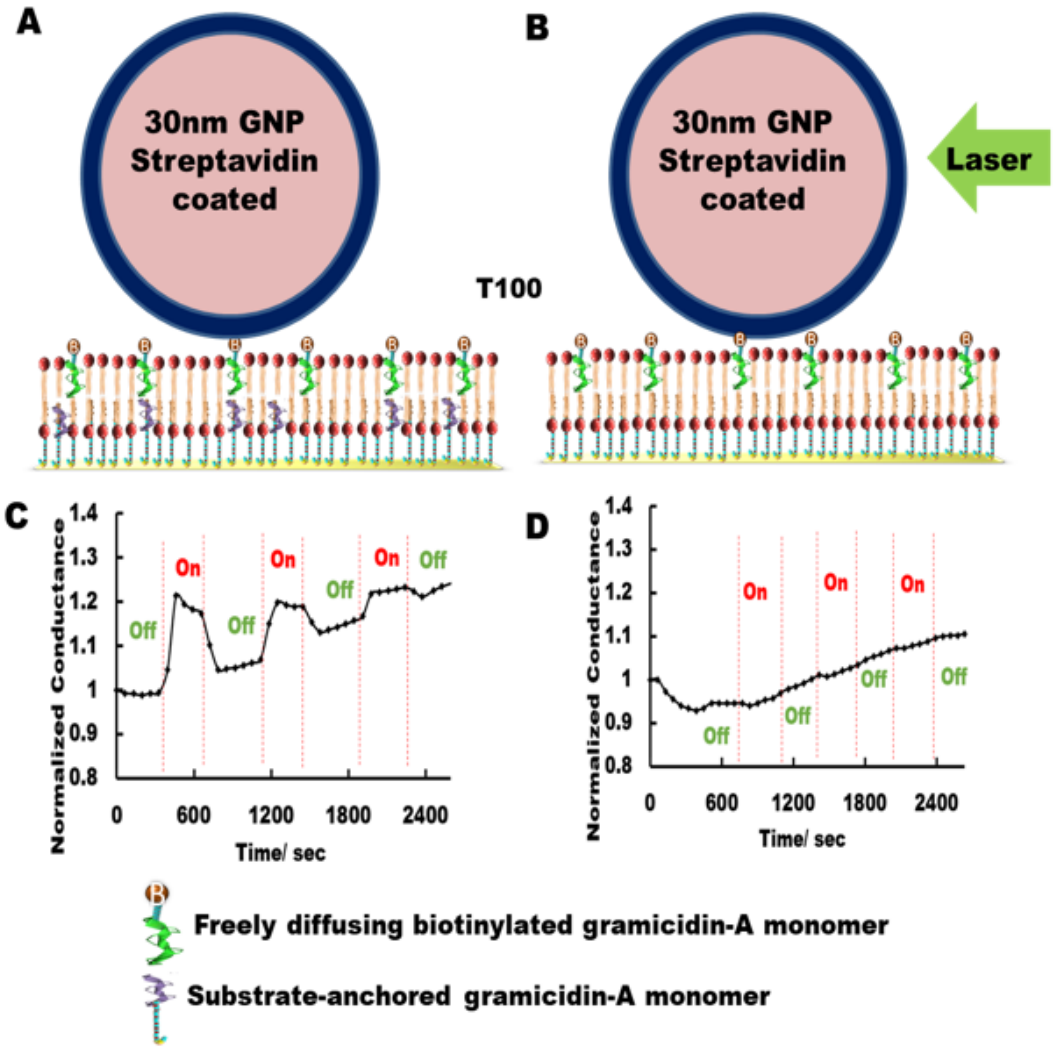

Figure 4.12: (A, B) Schematic representation of a fully tethered tBLMs model, with and without tethered gramicidin monomers. Samples were added above the tBLMs: (A) Gramicidin nano-switch biosensor; (B) Fully tethered tBLMs with the absence of tethered gramicidin-A monomers; Panels (C, D) Normalised conductance recordings over

time. The period when the laser was turned ON is indicated in red. Streptavidin conjugated 30nm spherical GNPs introduced. Results are demonstrative of at least three independent experiments.

4.6 Discussion

4.6.1 Development of nanomaterial-electrode interface

Thermal transfer plays an essential role in many biological processes. With a particular emphasis on bio-heat transfer, the use of gold nanomaterials heated by a laser has been considered as a powerful biomedical tool in selectively heating and destroying diseased cells [498]. It has been demonstrated that thermal cell destruction can be achieved by targeting (via active or passive methods) GNPs with antibodies directed against diseased cells, increasing laser light absorption and heat generation within the targeted cell [460].

Accordingly, investigating laser-induced heating phenomena of embedded nanoparticles in biological tissues could significantly enhance the understanding of heating effects of irradiated nanoparticles on the destruction of biological tissues. In this instance, we have demonstrated the role of heat transfer between GNPs and tBLMs. Our approach has the distinct advantage of the real-time recording of ion current changes across the membrane that corresponds to the heat generated by the coupled laser and gold nanoparticle interaction.

The choice to use the tBLM model to represent artificial lipid membrane is related to the distinct electrical sealing possessions of tBLM that mimic the natural lipid membranes characteristics [79]. tBLMs also can provide an aqueous ionic reservoir region amid the gold substrate and the subsequently formed membrane that offers sufficient space to incorporate membrane proteins, ion channel or other specific functionalization molecules [74, 134].

The surface irradiated gold nanomaterial and tBLM interface was examined for second pulses, across a range of parameters such as different lipid composition, wavelength, size and shape, various GNPs concentration and cholesterol percentage. In this context, membrane conduction is examined in terms of each of these parameters.

Our earlier experiments were performed using the upright laser alignment method in order to irradiate embedded GNPs across tBLM, as illustrated in Figure 4.4 (A). The elevation of membrane conduction peaks at the laser ON phase revealed insignificant variation in irradiation periods prior to and after GNPs addition (Figure 4.5). This is proposed to be as a result of bulk gold surface nanostructures that interact with the laser, thus masking heat production phenomena following the addition of the GNPs, thus indicating a combination of interactions at tBLM electrode surfaces [499].

Therefore, we have developed a novel approach that allows real-time recording of tBLM membrane conduction while at same time irradiated adjoining GNPs without illuminating the bulk gold surface by using horizontal laser beam alignment across the lipid-buffer interface, illustrated in Figure 4.3 (B).

4.6.2 Ion membrane conduction measurements of gold nanoparticles heated by laser irradiation

This study was conducted using two GNP functionalizations: 30nm bare GNPs and streptavidin-coated 30nm GNPs. Based on our obtained results it becomes clear that the streptavidin-coated GNPs that attached to adjoining biotinylated membrane demonstrate a discernible variation in membrane conduction (Figure 4.6 F), in comparison with their non-coated GNPs (Figure 4.6 E). This effect was due to the ability of the streptavidin-

coated particles to bind tightly to the available biotin moieties exposed on the surface of the tBLMs. This, therefore, suggests that intimate contact between the irradiated GNPs and the bilayer lipid membrane is critical in order to achieve a noticeable increase in the ion membrane permeability. Furthermore, this provides evidence that at this concentration of GNPs and ratio of biotin moieties, the distance between the irradiated GNPs and the adjacent membrane must be less than a certain distance in order to enable sufficient payload of heat from the particle to the membrane resulting in thermal disruption to the membrane architecture. This disturbance was transient and not usually potent enough to cause permanent membrane damage given that there was a trend of the conduction level returning to baseline in the ensuing laser OFF phase, which was also repeated in the subsequent rounds of laser ON / OFF.

Accordingly, as seen in Figure 4.5 (D), when a drop of the plain buffer of volume equivalent to introduced drop include GNPs, the results demonstrated no influence of volume variation or bulk gold interaction. Thus, from this, we can suggest that the only possible reason for this increase in membrane conduction is attributable to streptavidin-coated GNPs irradiation.

Capacitance parameter of EIS measurements is one of the valuable consideration in investigating the membrane lipid distribution and the consequence of biological events that are carried out across tBLMs. The capacitance of the membrane provides significant data of membrane thickness; for instance, protein insertion into the tBLM lead to membrane thinning that can be identified from an increase in membrane capacitance values [347]. Therefore, for each experiment, membrane capacitance was examined in order to confirm the thickness of the membrane bilayer within the reasonable ranges of intact membranes, which is 10.5 ± 0.7 nF, as shown in Figure 4.7 and see Appendix Figure

S1, Figure S2, Figure S3 and Figure S4 [496]. These capacitance ranges confirm the intact and well-formed tBLMs, also, indicate the formed tBLMs provide a stable and well-characterized system for subsequent examination. In addition, it has been shown that slight alterations in membrane capacitance were observed when the various type of GNPs were introduced. A possible explanation for the variation in membrane conduction, with slight change in membrane capacitance, would be the formation of pores or ion channels within the membrane, which would disrupt the packing of adjacent lipids, with minimum influence on packing structure of the membrane [134].

4.6.3 Studying the effect of gold nanoparticle concentration on thermal disruption over lipid membrane

Several studies have been carried out to examine the behavior of irradiated gold nanomaterials across bilayer lipid membrane using different approaches [490, 491]. For instance, the study of lipid membrane ion permeability by inducing local heating across the membrane using diverse laser intensities has indicated the ability to control lipid membrane ion permeability without the existence of ion channel. However, the too high laser power intensities damaged membrane by generating ruptures across the lipid membrane [490].

In this regards, the ion permeability across tBLM membrane mode was determined at different concentrations of 30nm streptavidin-coated GNPs, as seen in Figure 4.8. Based on our membrane conduction study, by comparing these irradiated GNPs-tBLM interfaces, it becomes evident that the increase of GNPs density demonstrated a growth in normalized membrane conduction values, which reflected the proliferation of membrane ion permeability that interpreted as heat consequence. This means that the

amount of generated heat proliferation was dependent on the concentration of introduced nanoparticles into the interface. This dependence demonstrated that temperature intensity would be higher in the presence of more plasmonic conjugated GNPs into the tBLMs. Moreover, a linear relationship between the number of GNPs and heat production could be identified.

4.6.4 Studying interactions of irradiated GNPs with a variable membrane-binding motif

Biological cell membranes are constituted of a variety of phospholipids, sterols, transmembrane proteins and membrane binding motifs [500]. Different compositions and concentration of these mentioned constituents can interact differently with introduced analytes. Using artificial lipid membrane model represented by tBLM, provide close mimic to the natural lipid membrane and at same time reduce their complexity by controlling the number of parameter across designed artificial lipid membrane model.

Therefore, in this chapter, it was of interest to determine if the different tethering chemistries would affect hyperthermia phenomena of irradiated GNPs. Thus, the tBLM model designed by incorporation of purely mobile lipids without any membrane binding motifs (Figure 4.9 A). Besides, tBLM form by a combination of mobile lipids and biotinylated cholesterol membrane-binding motif, as well as a mixture of biotinylated gramicidin monomers membrane-binding motif and the mobile lipids, as described in Figure 4.9 (B, C).

As it was realized from the results (Figure 4.9 D-F), tBLM model without biotinylated membrane binding motifs, demonstrated a nonsignificant variance in membrane

conductance amplitude during the laser ON phase. On the other hand, both tBLM-biotinylated membrane binding motifs models with and without cholesterol components demonstrated a distinct increase in membrane conductance amplitude during the laser ON phase in the presence of laser-tuned, membrane-bound GNPs.

Therefore, these findings displayed here further strengthen the proposal that direct attachment of GNPs to adjacent membranes is very efficient in heat transfer phenomena. Furthermore, these findings demonstrated that GNPs induced hyperthermia is not dependant on a specific membrane-binding motif.

4.6.5 Cholesterol different concentration affect membrane conduction of tBLM

In biological systems, membrane sterols are an essential parameter that affects membrane function and micro-fluidity [501]. Cholesterol existence across lipid membranes are also well known to provide improved membrane stabilization and variable transition phases [497].

In view of that, the effect of different concentration of cholesterol on membrane ion permeability using irradiated 30 nm streptavidin-coated GNPs was examined. Overall, our real-time EIS measurements of tBLMs made from zwitterionic lipids either with or without cholesterol showed a distinct increase of membrane conductance. There were some slight variations identified between different concentrations that indicated membranes containing less amount of cholesterol increase the ion permeability across the lipid membrane.

In that regards, for instance, several studies have investigated the impact of cholesterol moieties on membrane stability, revealed that the stability of the bilayer lipid membrane would be improved when the concentration of the cholesterol component across lipid membranes is increased, besides it would minimize the membrane permeability towards ions [502, 503]. Likewise, these studies revealed the impact of increasing cholesterol amounts to provide high packing of a phospholipid bilayer, in turn, would reducing ion passage through a membrane.

Accordingly, based on the obtained results, as shown in Figure 4.10, when the concentration of cholesterol was decreased in the membrane composition, the rate of membrane conduction was increased. This reflects the less amount of cholesterol was offered an increase of lipid membrane permeability due to local heating of irradiated adjoined GNPs. Our results are thus consistent with the aforementioned studies indicating that an increase in the cholesterol concentration within the lipid membrane pack phospholipids more tightly, thereby making the membrane less permeable to ions.

4.6.6 Studying heat transfer characteristics of functionalized tBLM with variable streptavidin-coated nanomaterials dimensions using laser beam λ =650nm

There are a variety of size and shapes of gold nanomaterials that can be excited at specific plasmon resonance wavelength. Numerous studies have shown that the plasmon resonance of nanomaterials is strongly dependent on the size and shape of the nanoparticle [473, 474, 504, 505].

In view of that, the absorption and scattering characteristics of gold nanomaterials were examined using various geometries. Thus, we examined streptavidin-coated 100nm GNUs, as described in Figure 4.11 (A). These type of gold nanomaterials were excited by laser and induced at laser beam light λ=650nm. From results as shown in Figure 4.11 (C) there was highly significant variation between the laser ON and OFF phases, with distinct increases in membrane conductance amplitude during the laser ON phase, when streptavidin conjugated 100 nm GNUs were introduced. Consequently, these finding proposes that direct contact between the irradiated GNUs and the bilayer lipid membrane is critical in order to achieve an evident increase in the ion membrane permeability.

Moreover, it has been shown that an irradiating 30 nm streptavidin-coated GNPs with laser beam light λ=650nm has not the ability to undergo the excitation of nanomaterials to induce hyperthermia (Figure 4.11 D). In contrast, irradiated 100nm GNUs at the same wavelength, which can absorb light significantly at the 650nm wavelength Figure 4.11 (C) showed a definite variance.

Accordingly, this study of heat production detection has confirmed the dependency of plasmon resonance wavelength on both the shape and the size of the gold nanomaterials. Indeed, this was further suggested that the increase in membrane conduction measurements was only resulted from irradiating specific gold nanomaterials with the equivalent plasmon resonance wavelength. These results are in correlation with other studies that proved the dependent relation between scattering properties of GNPs and their various size, shape and composition [506, 507].

4.6.7 Studying heat transfer characteristics of diverse tBLM model design

As part of the initial development to establish the use of the tBLM and impedance spectroscopy system for studying heat production of irradiated gold nanomaterials, we used the tBLM model with 10% tethering chemistry. This membrane model is well known for mimicking natural biological cell membranes due to the water content occurrence at both sides of the membrane bilayer. Further, this enables phospholipids to be mobile freely [76].

On the other hand, the fully tethered membranes (100%) model characterize with outstanding stability, as illustrated in Figure 4.12 (B). Though the integral component of this system prevents lateral membrane mobility. Consequently, phospholipids are usually not sufficiently mobile that interfere with ion permeability [64, 65].

However, insertion of ion channel across bilayer lipid membrane with 100% tethering chemistry such as gramicidin A, allows the ion passage through the embedded channel. A unique design of the gramicidin ion channel tBLMs sensor presented in Figure 4.12 (A) [79]. Briefly, the gramicidin A monomers in the lower leaflet of the bilayer membrane are tethered to the gold electrode while the biotinylated gramicidin A monomer in the upper layer is freely mobile. The gramicidin-A ion channel form when the mobile and fixed monomer is coupled; this is illustrated in details in Section 3.4.

Our results using these two diverse model demonstrated an increase of ion membrane conduction during the laser ON phase when streptavidin-coated 30nm GNPs were introduced to the nano-biosensor, as shown in Figure 4.12 (C). Whereas, unlike the gA

biosensor the membrane conduction recordings of the irradiated 30nm streptavidin-coated GNPs revealed slight discernible variance between the laser ON and laser OFF phases when the streptavidin-coated 30nm GNPs were added, as seen in Figure 4.12 (D).

Thus, the obtained result from gA biosensor is in correlation with the increase of membrane conduction due to the formation of ion channel across the bilayer lipid membrane, which was proposed that allows ion passages. However, the obtained result from fully tBLM, with the absence of fixed gramicidin monomer in the lower leaflet of lipid membrane bilayer and presence of biotinylated gramicidin monomer in the upper leaflet, as seen in Figure 4.12 (D). These real-time membrane conduction recordings were in correlation with the non-change in membrane conduction as a response to the lack of ability to initiate ion channel across the bilayer lipid membrane, which was proposed that prevented ion passages.

As a consequence, the evidence from this work suggests that the GNPs induced hyperthermia in membranes that have rigid non-diffusing lipids require the presence of ion channel to detect any change in membrane conductance. Incidence of gA dimer (ion channel) across the bilayer lipid membrane is critical in order to achieve an observable increase in the ion membrane permeability within the fully tBLM model. Additionally, this provides evidence that at this high percentage of tethering chemistry, which in turn, lead to immobilization of the membrane phospholipids, could diminish the ion permeability of the lipid membranes and result in eliminating thermal disruption to the membrane architecture.

4.7 Thermal predictive mathematical models

Whilst the effects of radiative heating on tethered membranes in real-time were investigated experimentally, thermal predictive mathematical models could provide crucial theoretical explanations of the experimental findings of the heat transfer phenomena. This combination of experimental and numerical studies allow the quantification of measures of membrane damage via determination of critical thresholds of heating required to disrupt cell membranes and kill targeted tissue [508, 509]. This can further provide useful data that can be directly utilised in designing strategies for thermal therapies permitting optimisation of the laser parameters and of the particle size and composition.

The use of numerical discretisation and marching techniques allows the extension of the numerical model to accommodate multi-dimensional analysis of the heat transfer characteristics of complex biological systems as well as to allow the prediction of heat transfer characteristics in biological materials. For example, a modified hyperbolic Fourier equation along with the consideration of the absorption and scattering properties of GNPs via a radiation sub-model has been used for this purpose [510, 511].

4.8 Conclusion

We have developed an *in situ* irradiated GNPs hyperthermia detection biosensor which can be utilized to study interactions of irradiated GNPs with lipid membrane entities of interest. This will provide a significant tool for the prediction of the level of cell membrane destruction that can be experienced by these heated nanoparticles.

Using real-time conductance amplitude recordings, including various controls, we were able to determine that the direct attachment of GNPs to adjacent tissue is very efficient in heat transfer phenomena. In addition, our results showed that the distance of GNPs to the cell membrane is a significant factor-governing uptake of heat by the membrane. Furthermore, this proves there is an insignificant influence on the irradiated GNPs that float freely in the solution above the living membranes. This definite the high specificity of irradiated GNPs a towards the binding sites on the membrane that related to variable GNPs functionalization.

Likewise, the method presented here provides a novel approach for a better understanding of laser-induced heating phenomena on ionic transport through biological membranes. Further, this application demonstrates a direct measurement of the effects of radiatively heated gold nanoparticles on adjacent lipid membranes. In particular, the impact of radiative heating on tethered membranes in real-time are investigated.

Generally, the combination of short-time pulsed laser irradiated GNPs and tBLMs provide useful data that can be directly utilized in designing strategies for thermal therapies permitting optimization of the laser parameters and the particle size and composition. They can also improve the thermophysical properties of semi-transparent materials, including the development of advanced thermo-polymers and thermally-setting ceramics. The techniques presented here provide a novel approach for future refining of GNP-laser-induced hyperthermia for clinical treatments as well as for optimization of the laser parameters and the particle size and composition.

Chapter 5

Conclusion and future directions

Chapter 5

Conclusions and future directions

5.1 Introduction

Artificial bilayer lipid membranes are of substantial interest on account of their potential applications in chemical, biological or medical detection of relevant analytes and for their promising applications in various types of implantable electrodes. These artificial lipid membranes can be engineered to mimic natural lipid membranes and they can also be functionalized with a variety of target receptors. The sparsely tBLMs are mechanically stabilised bilayer lipid membranes, fabricated on a solid supporting surface from which they are separated by only a few nanometres of a hydrated gel. These constructs provide the closest equivalents yet devised of natural biological membranes that enable a wide range of functional and structural membrane investigations [79, 134, 512].

The primary aim of engineered lipid membrane models has been to mimic the natural function of biological lipid membranes *in vitro* in order to improve our understanding of molecular interactions among the lipid membrane components through exploring the electrical properties of these membranes. Numerous research studies have been based on this technology such as pharmaceutical screening [90, 106, 108], antimicrobial peptide-membrane interfacing [109, 347, 513], membrane modeling [439, 514, 515], protein-membrane interactions [99, 516-518] and for biosensor development [79, 519-521].

Current electrode designs fall well short of their potential for an *in vivo* medical device. The core issues relate to their failure to meet the critical requirement of nanometre-scale intimacy between the electrode and its target cell. This nanoscale close contact is essential to achieve maximum efficiency of reading and stimulating active cells with minimal ion fluxes. Large distances beyond the nanoscale result in a dissipation of the ionic cloud targeting a cell or being produced by a cell firing and a loss of sensitivity. A further virtue of close contact is the maintenance of signal resolution. At present, the inefficient poorly resolved tissue stimulation caused by inadequate electrode design is compensated by increasing the stimulation signal magnitude, and by using electrode redundancies in order that at least a small number of electrodes can appropriately read or stimulate a target cell. Increasing the excitation level until a stimulus is achieved, has the undesirable effect of loss of resolution as well as potentially causing cell damage.

The core focus of this dissertation was to investigate ion fluxes arising from ionic to the electronic interface at the nanometer scale by using the detectable electrical signals. Membrane modification and feasibility for each study were examined *in vitro* using electrical impedance spectroscopy and fluorescence microscopy.

Summary

The main accomplishments of this research are:

1. The literature review in Chapter 1, which delivered a comprehensive understanding of different artificial lipid membrane models and the impedance spectroscopy, along with the main current applications of lipid membrane models used in research.

2. The design and creation of a functionalized RGD-tBLM used to form a new coating for bio-implantable electrodes in order to improve electrical signal transmission. The small distance attachment between the RGD functionalizing group and gold surfaces demonstrate the potential application in enhancing both cell adhesion and cellular growth in comparison to other employed surface modifications. The small radius-working electrode was more sensitive and had a higher magnitude of impedance values in order to better monitor cell adhesion and growth. Non-functionalized lipid membranes coated on gold surface electrodes, had cell-repellent characteristics. RGD functionalized tBLMs enhanced cell attachment at the electrode interface as indicated by improved impedance values. However, it was realised that there remained the challenge of too many leaks between cells, even using tBLM technology to enable the formation of a highly sealed, capacitively coupled, electrode implant.

3. An understanding of the challenges of developing gramicidin-A switch nano-biosensors for direct cell detection, as described in Chapter 3. Cell detection using both direct and competitive assay nano-biosensor designs were attempted, which also incorporated non-immunoglobulin binding motifs. A further study of streptavidin-biotinylated gA monomer interfaces demonstrated that 1nM streptavidin concentration displayed the highest gA ion channel gating using EIS measurements. While using neutron reflectometry demonstrated a non-significant change in membrane roughness before and after the introduction of streptavidin.

4. In Chapter 4, the merging of laser irradiation techniques with real-time electrical impedance spectroscopy measurements for gold nanoparticle irradiation hyperthermia monitoring was demonstrated. The use of horizontal laser alignment enabled the heat produced from irradiated GNPs to be detected by their subsequent

influence on the conduction of ions across adjacent tBLMs. This project broadens the application of tBLM architectures to GNPs hyperthermia assay evaluation. It demonstrated that the size of the GNPs, the wavelength of the irradiated light and the distance of GNPs to the cell membrane is are all significant factors governing the production of highly-localised thermal fluctuations, as expected, but more significantly, there is now a mechanism for by which these fluctuations can be measured and assessed *in vitro*

5.2 Perspectives and future direction

5.2.1 Experimental testing

5.2.1.1 Improving implantable medical devices

In Chapter 2, the use of the tBLM model, with some membrane modifications, attempted to create a highly sealed electrode coating for highly specific cell-electrode contact. Two factors impeded progress with this endeavor. The first was that cells are not naturally attracted to growing on a tBLM surface. In this study we investigated a variety of membrane functionalizations, such as RGD ligands, fibronectin, laminin, different phospholipids types such as negative charged phospholipids (PS) and positively charged phospholipids (DOTAP), as well as different rigidities of the bilayer lipid membrane by using 10% of tethering molecules and fully tethering chemistries (100%), in order to improve the cell attachment and growth over tBLM coating. Our trials using the RGD functionalized fluid tBLM (T10) showed some limited success in attaching and growing cells. On the other hand, our trials to grow and attach cells over the rigid membrane

(T100) were unsuccessful, even though a highly adherent cell line such as CHO-K1 cells were used.

The other factor impeding progress was the number of leakage pathways between the tBLM and the cells were too large or too numerous to be able to effectively restrict the flow of ions and significantly alter the overall resistance of the membrane. The aim of this study was to develop a highly sealed coting using the lipid membrane coated electrode that is able to promote cell adhesion and growth in order to minimize leakage pathways between the implanted electrode and adjoining cells, as well as to control the passage of ions by inserting specific ion channel across the bilayer lipid membrane coating [159].

The results achieved in this study are still promising and can be further improved by more research. For instance, a more detailed investigation on the membrane fluidity could offer new insights on the bilayer membrane behavior, that can then be used to optimize the cell adhesion and growth to achieve improved sealing layer and coating performances. Other studies revealed that membrane fluidity and architecture has a significant role in cell adhesion [40, 64, 65]. For instance, membrane fluidity has a crucial role in cells differentiation and maintenance, such as the formation of adhesion complexes is dependent on their lateral membrane diffusion [522, 523]. For example, extremely fluid lipid bilayers mostly block cell adhesion [40].

Moreover, a detailed study of spacing between binding motifs could serve to improve and promote cell adhesion and growth. It has been revealed that spacing of binding motifs over a surface, influence cell coverage and sealing, providing close mimic to natural

binding site distribution within integrins, which would enhance cell adhesion efficiently [329, 524-526].

5.2.1.2 Developing ion-channel switch biosensors for direct cell detection

A further study to extend the uses of the tBLM platform for diagnostic applications such as a direct cell detector with the aim of detecting a specific type of cell within the heterogeneous population was described in Chapter 3.

The resulting variation in membrane conduction was insignificant, probably due to the low binding affinity between the examined binding motifs and cells or artificial receptors. The reason for the weak changes in membrane conduction upon cell binding is likely due to the introduction of streptavidin that immobilises most of the mobile biotinylated gA monomers in the outer leaflet of the tBLM (preventing the formation of gA ion channel) and leaving only a small number of free mobile gA monomers. Attempts to investigate cells that previously functionalized with biotinylated binding motif then streptavidin could not rule out effects induced by leftover streptavidin in residual supernatant surrounding the cells. Thus, in future, the attempt to develop the ICS biosensor might exclude streptavidin as a linker and use different conjugation methods such as click-chemistry or a direct linker approach.

As a result of this study, it was concluded that the gA ICS biosensor architecture is probably not suited for detecting the presence of large objects like cells.

5.2.1.3 Heat transfer characteristics of nanoparticles measured with tethered bilayer lipid membranes

Achieving a deeper understanding of the mechanisms behind the gold nanoparticle-induced hyperthermia phenomena will aid in developing more effective therapies. Most of the current laser irradiation therapies target a specific type of cell to trigger cell death responses. It was found in this research study that the direct attachment of GNPs to adjacent tissue is critical in heat transfer phenomena. In addition, we have confirmed that the distance of GNPs to the cell membrane is a significant factor-governing uptake of heat (Chapter 4).

It was shown in this project and the literature [457, 458] that laser irradiation of gold nanomaterials induces hyperthermia in surrounding tissues. The developed setup using tBLM and electrical impedance spectroscopy can be used to answer questions on the heat transfer phenomena. Achieving a deeper understanding of the pathways behind the heat transfer phenomena would assist in developing more efficient therapies.

In future experiments, different lipid membrane compositions can be used to mimic various natural cells types. For instance, harvesting natural cell membranes can be included to form tBLM before the addition of GNPs to determine the impact of localised GNP induced radiation on specific cell types. This could also have significance in the use of hypothermia in targeting bacterial biofilm formation in infected patients [527].

Subsequently, other types of modified gold nanomaterials such as specific antibody modified gold nanomaterials that bind precisely to particular kinds of cell membranes can be used to examine the role of laser irradiation in response to heat production [528, 529].

This amalgamation of high-frequency pulsed laser irradiated gold nanomaterials and tBLMs and other potential candidates can be used to attain a better understanding of the mechanism of behind the effects of hyperthermia phenomena on cells. This approach provides useful data that can be directly utilized in designing strategies for thermal therapies, permitting optimization of the laser parameters and the particle size and composition.

5.2.2 Future outlooks employing tBLMs membrane model

There are still various unanswered questions regarding lipid membrane-targeting compounds, cell-cell interactions, pharmaceutical, toxicity testing and other functional biochemical components, where solutions for each could be reached by applying the tBLM membrane model.

The tBLM nano-biosensor has the potential for the reduction of animal involvement in experimental studies, such as examining the effects of newly-developed compounds and various stimuli cell membrane model *in vitro* [307, 530-532]. Cells naturally have an extremely complicated sensing system where their receptors and ion channel detect a broad range of drugs, toxins, or other test compounds. A functionalized-membrane electrode designed to mimic the natural environment of living cells that can detect even the slightest signal responses from introduced analytes is highly desirable. In addition, the tBLM model offers the ability to construct powerful synthetic machinery, for instance, specific ligand-tBLMs could be included as a coating for nanodevices such as artificial cells or nanoscale factory development [533-535].

Surfaces coated with lipid membranes could be micropatterned to control and direct cell adhesion and growth. Micropatterned membrane coatings could be made by the incorporation of a combination of zwitterionic non-toxic phospholipids that have cell-repellent characteristics amongst phospholipid moieties as well as having bespoke phospholipids that bear adhesion binding motifs such as RGD and IKVAV peptides [37, 536, 537].

Further development of specific binding motifs functionalized on the surface of tBLMs has the potential to be used as smart nano-electrodes. For instance, the development of gold nanomaterials functionalized with tBLMs could be used in targeting specific malignant cells as well as developing a new tBLM architecture that can resist air-drying, such as polymer-coated membrane-like structures [538, 539] and cholesteryl-tethered bilayers structures [540].

The ultimate aim of this dissertation was to explore the designs and applications of the tBLM platform. This thesis demonstrated the limits of using the tBLM architectures for implanted electrode-coatings or as a cell detection biosensor. However, the tBLMs platform was successfully employed to investigate highly localised gold-nanoparticle induced hyperthermia. In the future, the tBLM membrane model will continue to perform a crucial role in the improvement of our understanding in many biological and pharmaceuticals fields as well as in the development of biosensors.

To conclude, these ideas pose a series of challenging goals which, although technically very difficult, appear almost inevitable given the progress now made on tBLMs. At its most ambitious, it takes the open-loop diagnostic treatment of contemporary medicine and recreates an autonomous health process that closely parallels that which very likely

evolved in nature. Accessing and participating in the intercellular conversations between active cells is likely to permit access to patterns that match the successful function of complex multicellular organisms that evolved by genetic reinforcement. A further possible outcome is that insights will be gained on ways of tailoring the activities of multicellular organisms to perform tasks more suited to our needs that their original evolved functions.

References

1. Simons, Kai and Elina Ikonen, *Functional rafts in cell membranes.* Nature, 1997. 387(6633): p. 569.
2. Nicolson, Garth L, *The fluid—mosaic model of membrane structure: Still relevant to understanding the structure, function and dynamics of biological membranes after more than 40 years.* Biochimica et Biophysica Acta (BBA)-Biomembranes, 2014. 1838(6): p. 1451-1466.
3. Simons, Kai, *Cell membranes: A subjective perspective.* Biochimica et Biophysica Acta (BBA)-Biomembranes, 2016. 1858(10): p. 2569-2572.
4. Blom, Tomas, Pentti Somerharju, and Elina Ikonen, *Synthesis and biosynthetic trafficking of membrane lipids.* Cold Spring Harbor perspectives in biology, 2011. 3(8): p. a004713.
5. Santos, Ana L and Giulio Preta, *Lipids in the cell: Organisation regulates function.* Cellular and Molecular Life Sciences, 2018: p. 1-19.
6. Van Meer, Gerrit, Dennis R Voelker, and Gerald W Feigenson, *Membrane lipids: Where they are and how they behave.* Nature reviews Molecular cell biology, 2008. 9(2): p. 112.
7. Nikolelis, Dimitrios P and Ulrich J Krull, *Bilayer lipid membranes for electrochemical sensing.* Electroanalysis, 1993. 5(7): p. 539-545.
8. Mueller, Paul, Donald O Rudin, H Ti Tien, and William C Wescott, *Reconstitution of cell membrane structure in vitro and its transformation into an excitable system.* Nature, 1962. 194(4832): p. 979.
9. Gómez-Lagunas, F., A. Peña, A. Liévano, and A. Darszon *Incorporation of ionic channels from yeast plasma membranes into black lipid membranes*. Biophysical journal, 1989. 56, 115-119.
10. P, Van Gelder, Dumas, and Winterhalter *Understanding the function of bacterial outer membrane channels by reconstitution into black lipid membranes*. Biophysical chemistry, 2000. 85, 153-167.
11. Gu, Li-Qun, Orit Braha, Sean Conlan, Stephen Cheley, and Hagan Bayley, *Stochastic sensing of organic analytes by a pore-forming protein containing a molecular adapter.* Nature, 1999. 398(6729): p. 686.
12. Winterhalter, Mathias, *Black lipid membranes.* Current Opinion in Colloid & Interface Science, 2000. 5(3-4): p. 250-255.
13. Braha, Orit, Li-Qun Gu, Li Zhou, Xiaofeng Lu, Stephen Cheley, and Hagan Bayley *Simultaneous stochastic sensing of divalent metal ions*. 2000. 18, 1005-1007.
14. *Designed protein pores as components for biosensors: Braha, o; walker, b; cheley, s.;kasianowicz, jj; song, lz; gouaux, je & bayley, h. Chemistry & biology (1977) 4 (7 :-497–505*. Biosensors and bioelectronics. Vol. 12. 1997. iii-iv.
15. Tien, H.T. *Black lipid membranes: Thickness determination and molecular organization by optical methods*. Journal of Theoretical Biology, 1967. 16, 97-110.
16. Ries, R.S., H. Choi, R. Blunck, F. Bezanilla, and J.R. Heath *Black lipid membranes: Visualizing the structure, dynamics, and substrate dependence of membranes*. Journal of Physical Chemistry B, 2004. 108, 16040-16049.
17. Cheley, Stephen, Li-Qun Gu, and Hagan Bayley, *Stochastic sensing of nanomolar inositol 1, 4, 5-trisphosphate with an engineered pore.* Chemistry & biology, 2002. 9(7): p. 829-838.
18. Florin, E-L and HE Gaub, *Painted supported lipid membranes.* Biophysical journal, 1993. 64(2): p. 375-383.

19. Nikolelis, Dimitrios P and Ulrich J Krull, *Establishment and control of artificial ion-conductive zones for lipid membrane biosensor development.* Analytica chimica acta, 1992. 257(2): p. 239-245.
20. Tamm, Lukas K and Harden M McConnell, *Supported phospholipid bilayers.* Biophysical journal, 1985. 47(1): p. 105-113.
21. Sterling, Sarah m., Ryan Dawes, Edward s. Allgeyer, Sharon l. Ashworth, and David j. Neivandt *Comparison of actin- and glass-supported phospholipid bilayer diffusion coefficients*. Biophysical journal, 2015. 108, 1946-1953.
22. Seeger, Heiko M, Alessandro Di Cerbo, Andrea Alessandrini, and Paolo Facci *Supported lipid bilayers on mica and silicon oxide: Comparison of the main phase transition behavior*. The journal of physical chemistry. B, 2010. 114, 8926-8933.
23. Tien, H Ti and AL Ottova, *Supported planar lipid bilayers (s-blms) as electrochemical biosensors.* Electrochimica Acta, 1998. 43(23): p. 3587-3610.
24. Nayar, Rajiv, Michael J. Hope, and Pieter R. Cullis *Generation of large unilamellar vesicles from long-chain saturated phosphatidylcholines by extrusion technique*. BBA - Biomembranes, 1989. 986, 200-206.
25. Kalb, Edwin, Sammy Frey, and Lukas K Tamm, *Formation of supported planar bilayers by fusion of vesicles to supported phospholipid monolayers.* Biochimica et Biophysica Acta (BBA)-Biomembranes, 1992. 1103(2): p. 307-316.
26. Frisken, BJ, C Asman, and PJ Patty, *Studies of vesicle extrusion.* Langmuir, 2000. 16(3): p. 928-933.
27. Barenholz, Y, DLBJGJTTERD Gibbes, BJ Litman, J Goll, TE Thompson, and FD Carlson, *A simple method for the preparation of homogeneous phospholipid vesicles.* Biochemistry, 1977. 16(12): p. 2806-2810.
28. Roessner, Charles A, Douglas K Struck, and Garret M Ihler, *Injection of DNA into liposomes by bacteriophage lambda.* Journal of Biological Chemistry, 1983. 258(1): p. 643-648.
29. Mimms, Larry T, Guido Zampighi, Yasuhiko Nozaki, Charles Tanford, and Jacqueline A Reynolds, *Phospholipid vesicle formation and transmembrane protein incorporation using octyl glucoside.* Biochemistry, 1981. 20(4): p. 833-840.
30. Johnson, Joseph M, Taekjip Ha, Steve Chu, and Steven G Boxer, *Early steps of supported bilayer formation probed by single vesicle fluorescence assays.* Biophysical journal, 2002. 83(6): p. 3371-3379.
31. Castellana, Edward T and Paul S Cremer, *Solid supported lipid bilayers: From biophysical studies to sensor design.* Surface Science Reports, 2006. 61(10): p. 429-444.
32. Khan, Muhammad, Noura Dosoky, and John Williams, *Engineering lipid bilayer membranes for protein studies.* International journal of molecular sciences, 2013. 14(11): p. 21561-21597.
33. Reimhult, Erik, Bengt Kasemo, and Fredrik Höök, *Rupture pathway of phosphatidylcholine liposomes on silicon dioxide.* International journal of molecular sciences, 2009. 10(4): p. 1683-1696.
34. Stelzle, M., G. Weissmüller, and E. Sackmann *On the application of supported bilayers as receptive layers for biosensors with electrical detection*. Journal of Physical Chemistry, 1993. 97, 2974-2981.
35. Larsson, Charlotte, Michael Rodahl, and Fredrik Höök *Characterization of DNA immobilization and subsequent hybridization on a 2d arrangement of streptavidin on a biotin-modified lipid bilayer supported on sio2*. Analytical chemistry, 2003. 75, 5080-5087.

36. Yu, Cheng-han and Jay T Groves, *Engineering supported membranes for cell biology.* Medical & biological engineering & computing, 2010. 48(10): p. 955-963.
37. Groves, Jay T, Lara K Mahal, and Carolyn R Bertozzi, *Control of cell adhesion and growth with micropatterned supported lipid membranes.* Langmuir, 2001. 17(17): p. 5129-5133.
38. Afanasenkau, Dzmitry and Andreas Offenhäusser, *Positively charged supported lipid bilayers as a biomimetic platform for neuronal cell culture.* Langmuir, 2012. 28(37): p. 13387-13394.
39. Choi, Sung-Eun, Kyrylo Greben, Roger Wördenweber, and Andreas Offenhäusser, *Positively charged supported lipid bilayer formation on gold surfaces for neuronal cell culture.* Biointerphases, 2016. 11(2): p. 021003.
40. Oliver, Ann E, Viviane Ngassam, Phuong Dang, Babak Sanii, Huawen Wu, Chanel K Yee, Yin Yeh, and Atul N Parikh, *Cell attachment behavior on solid and fluid substrates exhibiting spatial patterns of physical properties.* Langmuir, 2009. 25(12): p. 6992-6996.
41. Svedhem, S, D Dahlborg, Johan Ekeroth, J Kelly, F Höök, and J Gold, *In situ peptide-modified supported lipid bilayers for controlled cell attachment.* Langmuir, 2003. 19(17): p. 6730-6736.
42. Thid, Dorota, K Holm, Peter S Eriksson, Johan Ekeroth, Bengt Kasemo, and Julie Gold, *Supported phospholipid bilayers as a platform for neural progenitor cell culture.* Journal of Biomedical Materials Research Part A, 2008. 84(4): p. 940-953.
43. Bérat, Rémi, Murielle Rémy-Zolghadry, Céline Gounou, Claude Manigand, Sisareuth Tan, Carmen Saltó, Ernest Arenas, Laurence Bordenave, and Alain R Brisson, *Peptide-presenting two-dimensional protein matrix on supported lipid bilayers: An efficient platform for cell adhesion.* Biointerphases, 2007. 2(4): p. 165-172.
44. Sandrin, Ludivine, Liliane Coche-Guérente, Amandine Bernstein, Hajra Basit, Pierre Labbé, Pascal Dumy, and Didier Boturyn, *Cell adhesion through clustered ligand on fluid supported lipid bilayers.* Organic & biomolecular chemistry, 2010. 8(7): p. 1531-1534.
45. Huang, Chun-Jen, Nam-Joon Cho, Chih-Jung Hsu, Po-Yuan Tseng, Curtis W Frank, and Ying-Chih Chang, *Type i collagen-functionalized supported lipid bilayer as a cell culture platform.* Biomacromolecules, 2010. 11(5): p. 1231-1240.
46. Berndt, Peter, Gregg B Fields, and Matthew Tirrell, *Synthetic lipidation of peptides and amino acids: Monolayer structure and properties.* Journal of the American Chemical Society, 1995. 117(37): p. 9515-9522.
47. Zhu, Xiaohua, Zhao Wang, Ansha Zhao, Nan Huang, Huadong Chen, Shuo Zhou, and Xiao Xie, *Cell adhesion on supported lipid bilayers functionalized with rgd peptides monitored by using a quartz crystal microbalance with dissipation.* Colloids and Surfaces B: Biointerfaces, 2014. 116: p. 459-464.
48. Hu, Bin, Dirk Finsinger, Kai Peter, Zeno Guttenberg, Michael Bärmann, Horst Kessler, Achim Escherich, Luis Moroder, Jochen Böhm, and Wolfgang Baumeister, *Intervesicle cross-linking with integrin αiibβ3 and cyclic-rgd-lipopeptide. A model of cell-adhesion processes.* Biochemistry, 2000. 39(40): p. 12284-12294.
49. Pautot, Sophie, Hanson Lee, Ehud Y Isacoff, and Jay T Groves, *Neuronal synapse interaction reconstituted between live cells and supported lipid bilayers.* Nature chemical biology, 2005. 1(5): p. 283-289.

50. Baksh, Michael M, Camin Dean, Sophie Pautot, Shannon DeMaria, Ehud Isacoff, and Jay T Groves, *Neuronal activation by gpi-linked neuroligin-1 displayed in synthetic lipid bilayer membranes.* Langmuir, 2005. 21(23): p. 10693-10698.
51. Ghosh Moulick, R, Dzmitry Afanasenkau, S-E Choi, Jonas Albers, Wienke Lange, Vanessa Maybeck, Tillmann Utesch, and A Offenhäusser, *Reconstitution of fusion proteins in supported lipid bilayers for the study of cell surface receptor–ligand interactions in cell–cell contact.* Langmuir, 2016. 32(14): p. 3462-3469.
52. Groves, Jay T and Michael L Dustin, *Supported planar bilayers in studies on immune cell adhesion and communication.* Journal of immunological methods, 2003. 278(1): p. 19-32.
53. Groves, Jay T, Steven G Boxer, and Harden M McConnell, *Electric field-induced reorganization of two-component supported bilayer membranes.* Proceedings of the National Academy of Sciences, 1997. 94(25): p. 13390-13395.
54. Groves, Jay T, Nick Ulman, and Steven G Boxer, *Micropatterning fluid lipid bilayers on solid supports.* Science, 1997. 275(5300): p. 651-653.
55. Glazier, SA, David J Vanderah, Anne L Plant, H Bayley, Gintaras Valincius, and John J Kasianowicz, *Reconstitution of the pore-forming toxin α-hemolysin in phospholipid/18-octadecyl-1-thiahexa (ethylene oxide) and phospholipid/n-octadecanethiol supported bilayer membranes.* Langmuir, 2000. 16(26): p. 10428-10435.
56. Plant, Anne L, *Supported hybrid bilayer membranes as rugged cell membrane mimics.* Langmuir, 1999. 15(15): p. 5128-5135.
57. Plant, A.L. *Self-assembled phospholipid/alkanethiol biomimetic bilayers on gold*. Langmuir, 1993. 9, 2764-2767.
58. Nuzzo, R.G. and D.L. Allara *Adsorption of bifunctional organic disulfides on gold surfaces*. Journal of the American Chemical Society, 1983. 105, 4481-4483.
59. Hąc-Wydro, K and P Dynarowicz-Łątka, *Biomedical applications of the langmuir monolayer technique.* Annales UMCS, Chemistry, 2008. 63: p. 47-60.
60. Kastl, K., M. Ross, V. Gerke, and C. Steinem *Kinetics and thermodynamics of annexin a1 binding to solid-supported membranes: A qcm study*. Biochemistry, 2002. 41, 10087-10094.
61. Glazier, S.A., D.J. Vanderah, A.L. Plant, H. Bayley, G. Valincius, and J.J. Kasianowicz *Reconstitution of the pore-forming toxin α-hemolysin in phospholipid/18-octadecyl-1-thiahexa(ethylene oxide) and phospholipid/n-octadecanethiol supported bilayer membranes*. Langmuir, 2000. 16, 10428-10435.
62. Krueger, S., C.W. Meuse, C.F. Majkrzak, J.A. Dura, N.F. Berk, M. Tarek, and A.L. Plant *Investigation of hybrid bilayer membranes with neutron reflectometry: Probing the interactions of melittin*. Langmuir, 2001. 17, 511-521.
63. Yuan, Qing, Zhongkang Wang, Siji Nian, Youping Yin, Gang Chen, and Yuxian Xia *Screening of high-affinity scfvs from a ribosome displayed library using biacore biosensor*. Part A: Enzyme Engineering and Biotechnology, 2009. 152, 224-234.
64. Cooper, Matthew A, *Advances in membrane receptor screening and analysis.* Journal of Molecular Recognition, 2004. 17(4): p. 286-315.
65. Nishimura, Toshiki, Fuyuko Tamura, Sawako Kobayashi, Yasushi Tanimoto, Fumio Hayashi, Yuki Sudo, Yasuhiko Iwasaki, and Kenichi Morigaki, *Hybrid model membrane combining micropatterned lipid bilayer and hydrophilic polymer brush.* Langmuir, 2017. 33(23): p. 5752-5759.

66. Sackmann, Erich, *Supported membranes: Scientific and practical applications.* Science, 1996. 271(5245): p. 43-48.
67. Wagner, Michael L and Lukas K Tamm, *Tethered polymer-supported planar lipid bilayers for reconstitution of integral membrane proteins: Silane-polyethyleneglycol-lipid as a cushion and covalent linker.* Biophysical journal, 2000. 79(3): p. 1400-1414.
68. Ke, P.C. and C.A. Naumann *Hindered diffusion in polymer-tethered phospholipid monolayers at the air-water interface: A single molecule fluorescence imaging study*. Langmuir, 2001. 17, 5076-5081.
69. Wagner, Michael L. and Lukas K. Tamm *Tethered polymer-supported planar lipid bilayers for reconstitution of integral membrane proteins: Silane-polyethyleneglycol-lipid as a cushion and covalent linker*. Biophysical journal, 2000. 79, 1400-1414.
70. Wong, Joyce Y, Jaroslaw Majewski, Markus Seitz, Chad K Park, Jacob N Israelachvili, and Gregory S Smith, *Polymer-cushioned bilayers. I. A structural study of various preparation methods using neutron reflectometry.* Biophysical journal, 1999. 77(3): p. 1445-1457.
71. Ataka, K., F. Giess, W. Knoll, R. Naumann, S. Haber-Pohlmeier, B. Richter, and J. Heberle *Oriented attachment and membrane reconstitution of his-tagged cytochrome c oxidase to a gold electrode: In situ monitoring by surface-enhanced infrared absorption spectroscopy*. Journal of the American Chemical Society, 2004. 126, 16199-16206.
72. Ge, Y, YH Lin, LA Lautscham, WH Goldmann, B Fabry, and CA Naumann, *N-cadherin-functionalized polymer-tethered multi-bilayer: A cell surface-mimicking substrate to probe cellular mechanosensitivity.* Soft Matter, 2016. 12(40): p. 8274-8284.
73. Kametani, Yoshiko and Masatoshi Takeichi, *Basal-to-apical cadherin flow at cell junctions.* Nature cell biology, 2007. 9(1): p. 92-98.
74. Cranfield, Charles G, Bruce A Cornell, Stephan L Grage, Paul Duckworth, Sonia Carne, Anne S Ulrich, and Boris Martinac, *Transient potential gradients and impedance measures of tethered bilayer lipid membranes: Pore-forming peptide insertion and the effect of electroporation.* Biophysical journal, 2014. 106(1): p. 182-189.
75. Heinrich, Frank, Tiffany Ng, David J Vanderah, Prabhanshu Shekhar, Mihaela Mihailescu, Hirsh Nanda, and Mathias Losche, *A new lipid anchor for sparsely tethered bilayer lipid membranes.* Langmuir, 2009. 25(7): p. 4219-4229.
76. Cornell, Bruce A, Gowri Krishna, Peter D Osman, RD Pace, and Lech Wieczorek, *Tethered-bilayer lipid membranes as a support for membrane-active peptides*. 2001, Portland Press Limited.
77. Naumann, Renate, EK Schmidt, A Jonczyk, K Fendler, B Kadenbach, T Liebermann, Andreas Offenhäusser, and Wolfgang Knoll, *The peptide-tethered lipid membrane as a biomimetic system to incorporate cytochrome c oxidase in a functionally active form.* Biosensors and Bioelectronics, 1999. 14(7): p. 651-662.
78. Salamon, Z, JT Hazzard, and G Tollin, *Direct measurement of cyclic current-voltage responses of integral membrane proteins at a self-assembled lipid-bilayer-modified electrode: Cytochrome f and cytochrome c oxidase.* Proceedings of the National Academy of Sciences, 1993. 90(14): p. 6420-6423.
79. Cornell, B Al, VLB Braach-Maksvytis, LG King, and PDJ Osman, *A biosensor that uses ion-channel switches.* Nature, 1997. 387(6633): p. 580.

80. Markx, Gerard H and Christopher L Davey, *The dielectric properties of biological cells at radiofrequencies: Applications in biotechnology.* Enzyme and Microbial Technology, 1999. 25(3-5): p. 161-171.
81. https://www.sdxtetheredmembranes.com/technical-background, SDx Tethered Membranes Pty Ltd.
82. Rebaud, Samuel, Ofelia Maniti, and Agnes P Girard-Egrot, *Tethered bilayer lipid membranes (tblms): Interest and applications for biological membrane investigations.* Biochimie, 2014. 107: p. 135-142.
83. Stora, Thierry, Jeremy H. Lakey, and Horst Vogel *Ion-channel gating in transmembrane receptor proteins: Functional activity in tethered lipid membranes*. Angewandte Chemie International Edition, 1999. 38, 389-392.
84. Andersson, Martin, Henk M Keizer, Chenyu Zhu, Daniel Fine, Ananth Dodabalapur, and Randolph S Duran *Detection of single ion channel activity on a chip using tethered bilayer membranes*. Langmuir : the ACS journal of surfaces and colloids, 2007. 23, 2924-2927.
85. Andersson, Martin, George Okeyo, Danyell Wilson, Henk Keizer, Paul Moe, Paul Blount, Daniel Fine, Ananth Dodabalapur, and Randolph S. Duran *Voltage-induced gating of the mechanosensitive mscl ion channel reconstituted in a tethered lipid bilayer membrane*. Biosensors and Bioelectronics, 2008. 23, 919-923.
86. Vockenroth, Inga K., Petia P. Atanasova, Joanna R. Long, A. Toby A. Jenkins, Wolfgang Knoll, and Ingo Köper *Functional incorporation of the pore forming segment of achr m2 into tethered bilayer lipid membranes*. BBA - Biomembranes, 2007. 1768, 1114-1120.
87. Terrettaz, S., M. Mayer, and H. Vogel *Highly electrically insulating tethered lipid bilayers for probing the function of ion channel proteins*. Langmuir, 2003. 19, 5567-5569.
88. Terrettaz, Samuel, Wolf-Peter Ulrich, Remo Guerrini, Antonio Verdini, and Horst Vogel *Immunosensing by a synthetic ligand-gated ion channel*. Angew. Chem. Int. Ed., 2001. 40, 1740-1743.
89. Naumann, Renate, D Walz, SM Schiller, and Wolfgang Knoll, *Kinetics of valinomycin-mediated k+ ion transport through tethered bilayer lipid membranes.* Journal of Electroanalytical Chemistry, 2003. 550: p. 241-252.
90. Schiller, Stefan M, Renate Naumann, Katherine Lovejoy, Horst Kunz, and Wolfgang Knoll, *Archaea analogue thiolipids for tethered bilayer lipid membranes on ultrasmooth gold surfaces.* Angewandte Chemie International Edition, 2003. 42(2): p. 208-211.
91. Peggion, Cristina, Fernando Formaggio, Claudio Toniolo, Lucia Becucci, Maria Rosa Moncelli, and Rolando Guidelli, *A peptide-tethered lipid bilayer on mercury as a biomimetic system.* Langmuir, 2001. 17(21): p. 6585-6592.
92. Raguse, Burkhard, Vijoleta Braach-Maksvytis, Bruce A Cornell, Lionel G King, Peter DJ Osman, Ron J Pace, and Lech Wieczorek, *Tethered lipid bilayer membranes: Formation and ionic reservoir characterization.* Langmuir, 1998. 14(3): p. 648-659.
93. Krishna, Gowri, Jurgen Schulte, Bruce A Cornell, Ron Pace, Lech Wieczorek, and Peter D Osman, *Tethered bilayer membranes containing ionic reservoirs: The interfacial capacitance.* Langmuir, 2001. 17(16): p. 4858-4866.
94. Cranfield, C. G., T. Bettler, and B. Cornell, *Nanoscale ion sequestration to determine the polarity selectivity of ion conductance in carriers and channels.* Langmuir, 2015. 31(1): p. 292-298.

95. Lee, Sang-Kyu, Luis G Cascão-Pereira, Rafael F Sala, Susan P Holmes, Kevin J Ryan, and Todd Becker, *Ion channel switch array: A biosensor for detecting multiple pathogens.* Industrial Biotechnology, 2005. 1(1): p. 26-31.
96. Oh, SY, B Cornell, D Smith, G Higgins, CJ Burrell, and TW Kok, *Rapid detection of influenza a virus in clinical samples using an ion channel switch biosensor.* Biosensors and Bioelectronics, 2008. 23(7): p. 1161-1165.
97. Keizer, Henk M., Brian R. Dorvel, Martin Andersson, Daniel Fine, Rebecca B. Price, Joanna R. Long, Ananth Dodabalapur, Ingo Köper, Wolfgang Knoll, Peter A. V. Anderson, and Randolph S. Duran *Functional ion channels in tethered bilayer membranes—implications for biosensors*. ChemBioChem, 2007. 8, 1246-1250.
98. Valenzuela, Stella M, Heba Alkhamici, Louise J Brown, Oscar C Almond, Sophia C Goodchild, Sonia Carne, Paul M G Curmi, Stephen A Holt, and Bruce A Cornell *Regulation of the membrane insertion and conductance activity of the metamorphic chloride intracellular channel protein clic1 by cholesterol*. PloS one. 8, e56948.
99. Al Khamici, Heba, Khondker Hossain, Bruce Cornell, and Stella Valenzuela, *Investigating sterol and redox regulation of the ion channel activity of clic1 using tethered bilayer membranes.* Membranes, 2016. 6(4): p. 51.
100. Stora, Thierry, Jeremy H Lakey, and Horst Vogel, *Ion-channel gating in transmembrane receptor proteins: Functional activity in tethered lipid membranes.* Angewandte Chemie International Edition, 1999. 38(3): p. 389-392.
101. Terrettaz, Samuel, Wolf-Peter Ulrich, Horst Vogel, Qi Hong, Lynn G Dover, and Jeremy H Lakey, *Stable self-assembly of a protein engineering scaffold on gold surfaces.* Protein Science, 2002. 11(8): p. 1917-1925.
102. Yin, Ping, Christopher J Burns, Peter DJ Osman, and Bruce A Cornell, *A tethered bilayer sensor containing alamethicin channels and its detection of amiloride based inhibitors.* Biosensors and Bioelectronics, 2003. 18(4): p. 389-397.
103. McGillivray, Duncan J, Gintaras Valincius, Frank Heinrich, Joseph WF Robertson, David J Vanderah, Wilma Febo-Ayala, Ilja Ignatjev, Mathias Lösche, and John J Kasianowicz, *Structure of functional staphylococcus aureus α-hemolysin channels in tethered bilayer lipid membranes.* Biophysical journal, 2009. 96(4): p. 1547-1553.
104. McGillivray, Duncan J, Gintaras Valincius, David J Vanderah, Wilma Febo-Ayala, John T Woodward, Frank Heinrich, John J Kasianowicz, and Mathias Lösche, *Molecular-scale structural and functional characterization of sparsely tethered bilayer lipid membranes.* Biointerphases, 2007. 2(1): p. 21-33.
105. Valincius, Gintaras, Frank Heinrich, Rima Budvytyte, David J Vanderah, Duncan J McGillivray, Yuri Sokolov, James E Hall, and Mathias Lösche, *Soluble amyloid β-oligomers affect dielectric membrane properties by bilayer insertion and domain formation: Implications for cell toxicity.* Biophysical journal, 2008. 95(10): p. 4845-4861.
106. Becucci, Lucia and Rolando Guidelli, *Kinetics of channel formation in bilayer lipid membranes (blms) and tethered blms: Monazomycin and melittin.* Langmuir, 2007. 23(10): p. 5601-5608.
107. Tun, Thet Naing and A Toby A Jenkins, *An electrochemical impedance study of the effect of pathogenic bacterial toxins on tethered bilayer lipid membrane.* Electrochemistry communications, 2010. 12(10): p. 1411-1415.
108. Spencelayh, Michael J, Yaling Cheng, Richard J Bushby, Timothy DH Bugg, Jian-jun Li, Peter JF Henderson, John O'Reilly, and Stephen D Evans, *Antibiotic action*

and peptidoglycan formation on tethered lipid bilayer membranes. Angewandte Chemie, 2006. 118(13): p. 2165-2170.
109. Becucci, Lucia, Flavio Maran, and Rolando Guidelli, *Probing membrane permeabilization by the antibiotic lipopeptaibol trichogin ga iv in a tethered bilayer lipid membrane.* Biochimica et Biophysica Acta (BBA)-Biomembranes, 2012. 1818(7): p. 1656-1662.
110. Kuppusamy, Rajesh, Muhammad Yasir, Thomas Berry, Charles G Cranfield, Shashidhar Nizalapur, Eugene Yee, Onder Kimyon, Aditi Taunk, Kitty KK Ho, and Bruce Cornell, *Design and synthesis of short amphiphilic cationic peptidomimetics based on biphenyl backbone as antibacterial agents.* European journal of medicinal chemistry, 2018. 143: p. 1702-1722.
111. Nizalapur, Shashidhar, Kitty KK Ho, Önder Kimyon, Eugene Yee, Thomas Berry, Mike Manefield, Charles G Cranfield, Mark Willcox, David StC Black, and Naresh Kumar, *Synthesis and biological evaluation of n-naphthoyl-phenylglyoxamide-based small molecular antimicrobial peptide mimics as novel antimicrobial agents and biofilm inhibitors.* Organic & biomolecular chemistry, 2016. 14(14): p. 3623-3637.
112. Yu, Tsz Tin, Shashidhar Nizalapur, Kitty KK Ho, Eugene Yee, Thomas Berry, Charles G Cranfield, Mark Willcox, David StC Black, and Naresh Kumar, *Design, synthesis and biological evaluation of n-sulfonylphenyl glyoxamide-based antimicrobial peptide mimics as novel antimicrobial agents.* ChemistrySelect, 2017. 2(12): p. 3452-3461.
113. Andersson, Jakob, Melanie A Fuller, Kathleen Wood, Stephen A Holt, and Ingo Köper, *A tethered bilayer lipid membrane that mimics microbial membranes.* Physical Chemistry Chemical Physics, 2018. 20(18): p. 12958-12969.
114. Niu, Lifang, Thorsten Wohland, Wolfgang Knoll, and Ingo Köper, *Interaction of a synthetic antimicrobial peptide with a model bilayer platform mimicking bacterial membranes.* Biointerphases, 2017. 12(4): p. 04E404.
115. Valincius, Gintaras, Duncan J McGillivray, Wilma Febo-Ayala, David J Vanderah, John J Kasianowicz, and Mathias Lösche, *Enzyme activity to augment the characterization of tethered bilayer membranes.* The Journal of Physical Chemistry B, 2006. 110(21): p. 10213-10216.
116. Budvytyte, Rima, Milda Pleckaityte, Aurelija Zvirbliene, David J Vanderah, and Gintaras Valincius, *Reconstitution of cholesterol-dependent vaginolysin into tethered phospholipid bilayers: Implications for bioanalysis.* PloS one, 2013. 8(12): p. e82536.
117. Rossi, Claire, Samah Doumiati, Clarine Lazzarelli, Marilyne Davi, Fetta Meddar, Daniel Ladant, and Joël Chopineau, *A tethered bilayer assembled on top of immobilized calmodulin to mimic cellular compartmentalization.* PloS one, 2011. 6(4): p. e19101.
118. Veneziano, Rémi, Claire Rossi, Alexandre Chenal, Catherine Brenner, Daniel Ladant, and Joël Chopineau, *Synthesis and characterization of tethered lipid assemblies for membrane protein reconstitution.* Biointerphases, 2017. 12(4): p. 04E301.
119. Deniaud, Aurélien, Claire Rossi, Alexandre Berquand, Johanne Homand, Sylvie Campagna, Wolfgang Knoll, Catherine Brenner, and Joël Chopineau, *Voltage-dependent anion channel transports calcium ions through biomimetic membranes.* Langmuir, 2007. 23(7): p. 3898-3905.

120. Veneziano, Rémi, Claire Rossi, Alexandre Chenal, Jean-Marie Devoisselle, Daniel Ladant, and Joel Chopineau, *Bordetella pertussis adenylate cyclase toxin translocation across a tethered lipid bilayer.* Proceedings of the National Academy of Sciences, 2013. 110(51): p. 20473-20478.
121. Raliya, Ramesh, Tandeep Singh Chadha, Kelsey Haddad, and Pratim Biswas, *Perspective on nanoparticle technology for biomedical use.* Current pharmaceutical design, 2016. 22(17): p. 2481-2490.
122. *Nanotechnology - nanoparticles; new findings on nanoparticles from autonomous university summarized (bacterial exopolysaccharides as reducing and/or stabilizing agents during synthesis of metal nanoparticles with biomedical applications)*, in *Drug Week*. 2018.
123. Goreham, Renee V, Vanessa C Thompson, Yuya Samura, Christopher T Gibson, Joseph G Shapter, and Ingo Köper, *Interaction of silver nanoparticles with tethered bilayer lipid membranes.* Langmuir, 2015. 31(21): p. 5868-5874.
124. Li, Xiaoqin, Jinru Li, and Long Jiang, *A silica-gold core-shell structure to mimic the large size of gold particles for promoting cell growth: A comparative study of the silica core size and the nanogold amount in the shell.* Colloids and Surfaces A: Physicochemical and Engineering Aspects, 2014. 459: p. 211-216.
125. Liu, Ying and R Mark Worden, *Size dependent disruption of tethered lipid bilayers by functionalized polystyrene nanoparticles.* Biochimica et Biophysica Acta (BBA)-Biomembranes, 2015. 1848(1): p. 67-75.
126. Salomoni, Roseli, P Léo, AF Montemor, BG Rinaldi, and MFA Rodrigues, *Antibacterial effect of silver nanoparticles in pseudomonas aeruginosa.* Nanotechnology, science and applications, 2017. 10: p. 115.
127. Kaur, Manpreet, Neha Gupta, Jaspreet Kaur, and Anshu Sibbal Chatli, *Biosynthesis and characterization of agnps and their antibacterial effects.* Int. J. Adv. Res. Biol. Sci, 2019. 6(3): p. 226-231.
128. da Conceição, Rodrigo Rodrigues, Janaina Sena de Souza, Kelen Carneiro de Oliveira, Renata Marino Romano, Rui Monteiro de Barros Maciel, Magnus Régios Dias-da-Silva, Marco Aurélio Romano, Maria Izabel Chiamolera, and Gisele Giannocco, *Evaluation of neuroglobin and cytoglobin expression in adult rats exposed to silver nanoparticles during prepubescence.* Metabolic brain disease, 2019: p. 1-9.
129. Li, Zongxi, Jonathan C Barnes, Aleksandr Bosoy, J Fraser Stoddart, and Jeffrey I Zink, *Mesoporous silica nanoparticles in biomedical applications.* Chemical Society Reviews, 2012. 41(7): p. 2590-2605.
130. Barandeh, Farda, Phuong-Lan Nguyen, Rajiv Kumar, Gary J Iacobucci, Michelle L Kuznicki, Andrew Kosterman, Earl J Bergey, Paras N Prasad, and Shermali Gunawardena, *Organically modified silica nanoparticles are biocompatible and can be targeted to neurons in vivo.* PloS one, 2012. 7(1): p. e29424.
131. Liu, Ying, Zhen Zhang, Quanxuan Zhang, Gregory L Baker, and R Mark Worden, *Biomembrane disruption by silica-core nanoparticles: Effect of surface functional group measured using a tethered bilayer lipid membrane.* Biochimica et Biophysica Acta (BBA)-Biomembranes, 2014. 1838(1): p. 429-437.
132. Kennelly, AE, *Impedance.* Proceedings of the IEEE, 1984. 72(4): p. 463-492.
133. Mu, Xiaoyi, Daniel Rairigh, Xiaowen Liu, and Andrew J Mason. *Rapid impedance measurement of tethered bilayer lipid membrane biosensors*. in *2011 Annual International Conference of the IEEE Engineering in Medicine and Biology Society*. 2011. IEEE.

134. Alghalayini, Amani, Alvaro Garcia, Thomas Berry, and Charles G Cranfield, *The use of tethered bilayer lipid membranes to identify the mechanisms of antimicrobial peptide interactions with lipid bilayers.* Antibiotics, 2019. 8(1): p. 12.
135. Valincius, Gintaras, Tadas Meškauskas, and Feliksas Ivanauskas, *Electrochemical impedance spectroscopy of tethered bilayer membranes.* Langmuir, 2011. 28(1): p. 977-990.
136. Xu, Youchun, Xinwu Xie, Yong Duan, Lei Wang, Zhen Cheng, and Jing Cheng, *A review of impedance measurements of whole cells.* Biosensors and Bioelectronics, 2016. 77: p. 824-836.
137. Tiruppathi, Chinnaswamy, Asrar B Malik, Peter J Del Vecchio, Charles R Keese, and Ivar Giaever, *Electrical method for detection of endothelial cell shape change in real time: Assessment of endothelial barrier function.* Proceedings of the National Academy of Sciences, 1992. 89(17): p. 7919-7923.
138. Giaever, Ivar and Charles R Keese, *A morphological biosensor for mammalian cells.* Nature, 1993. 366(6455): p. 591.
139. Giaever, Ivar and Charles R Keese, *Micromotion of mammalian cells measured electrically.* Proceedings of the National Academy of Sciences, 1991. 88(17): p. 7896-7900.
140. Ramasamy, Sakthivel, Devasier Bennet, and Sanghyo Kim, *Drug and bioactive molecule screening based on a bioelectrical impedance cell culture platform.* International journal of nanomedicine, 2014. 9: p. 5789.
141. Hayes, Thomas C and Paul Horowitz, *Student manual for the art of electronics*. 1989: Cambridge university press Cambridge.
142. Macdonald, J. *Impedance spectroscopy*. Ann Biomed Eng, 1992. 20, 289-305.
143. Asphahani, Fareid and Miqin Zhang, *Cellular impedance biosensors for drug screening and toxin detection.* Analyst, 2007. 132(9): p. 835-841.
144. Pancrazio, JJ, JP Whelan, DA Borkholder, W Ma, and DA Stenger, *Development and application of cell-based biosensors.* Annals of biomedical engineering, 1999. 27(6): p. 697-711.
145. Lo, Chun-Min, Charles R Keese, and Ivar Giaever, *Impedance analysis of mdck cells measured by electric cell-substrate impedance sensing.* Biophysical journal, 1995. 69(6): p. 2800.
146. Chang, Bin-Wha, Che-Hsiung Chen, Shin-Jyh Ding, David Chan-Hen Chen, and Hsien-Chang Chang, *Impedimetric monitoring of cell attachment on interdigitated microelectrodes.* Sensors and Actuators B: Chemical, 2005. 105(2): p. 159-163.
147. Polonschii, Cristina, Sorin David, Szilveszter Gáspár, Mihaela Gheorghiu, Mihnea Rosu-Hamzescu, and Eugen Gheorghiu, *Complementarity of eis and spr to reveal specific and nonspecific binding when interrogating a model bioaffinity sensor; perspective offered by plasmonic based eis.* Analytical chemistry, 2014. 86(17): p. 8553-8562.
148. Szulcek, Robert, Harm Jan Bogaard, and Geerten P van Nieuw Amerongen, *Electric cell-substrate impedance sensing for the quantification of endothelial proliferation, barrier function, and motility.* JoVE (Journal of Visualized Experiments), 2014(85): p. e51300-e51300.
149. Stolwijk, Judith A, Christoph Hartmann, Poonam Balani, Silke Albermann, Charles R Keese, Ivar Giaever, and Joachim Wegener, *Impedance analysis of adherent cells after in situ electroporation: Non-invasive monitoring during intracellular manipulations.* Biosensors and Bioelectronics, 2011. 26(12): p. 4720-4727.

150. Benson, Kathrin, Sandra Cramer, and Hans-Joachim Galla, *Impedance-based cell monitoring: Barrier properties and beyond.* Fluids and Barriers of the CNS, 2013. 10(1): p. 1.
151. Wegener, Joachim, Charles R Keese, and Ivar Giaever, *Electric cell–substrate impedance sensing (ecis) as a noninvasive means to monitor the kinetics of cell spreading to artificial surfaces.* Experimental cell research, 2000. 259(1): p. 158-166.
152. http://www.biophysics.com/ecis-theory.php., Applied Bio Physics.
153. Parviz, Maryam, Katharina Gaus, and John Justin Gooding, *Simultaneous impedance spectroscopy and fluorescence microscopy for the real-time monitoring of the response of cells to drugs.* Chemical science, 2017.
154. Goding, Josef, Aaron Gilmour, Ulises Aregueta Robles, Laura Poole-Warren, Nigel Lovell, Penny Martens, and Rylie Green, *A living electrode construct for incorporation of cells into bionic devices.* MRS Communications, 2017. 7(3): p. 487-495.
155. Gilmour, Aaron, Josef Goding, Ulises Aregueta Robles, Naomi Staples, Philip Byrnes-Preston, John Morley, Nigel H Lovell, Daniel J Chew, and Rylie Green. *Stimulation of peripheral nerves using conductive hydrogel electrodes*. in *2018 40th Annual International Conference of the IEEE Engineering in Medicine and Biology Society (EMBC)*. 2018. IEEE.
156. Arsiwala, Ammar, Preshita Desai, and Vandana Patravale, *Recent advances in micro/nanoscale biomedical implants.* Journal of Controlled Release, 2014. 189: p. 25-45.
157. Fabbro, A., D. Scaini, V. Leon, E. Vazquez, G. Cellot, G. Privitera, L. Lombardi, F. Torrisi, F. Tomarchio, F. Bonaccorso, S. Bosi, A. C. Ferrari, L. Ballerini, and M. Prato, *Graphene-based interfaces do not alter target nerve cells.* ACS nano, 2016. 10(1): p. 615-623.
158. Jansen, Lauren E, Luke D Amer, Esther Y-T Chen, Thuy V Nguyen, Leila S Saleh, Todd Emrick, Wendy F Liu, Stephanie J Bryant, and Shelly R Peyton, *Zwitterionic peg-pc hydrogels modulate the foreign body response in a modulus-dependent manner.* Biomacromolecules, 2018. 19(7): p. 2880-2888.
159. Wilke, R. G., G. K. Moghadam, N. H. Lovell, G. J. Suaning, and S. Dokos, *Electric crosstalk impairs spatial resolution of multi-electrode arrays in retinal implants.* J Neural Eng, 2011. 8(4): p. 046016.
160. Lin, Tai-Chi, Hua-Ming Chang, Chih-Chien Hsu, Kuo-Hsuan Hung, Yan-Ting Chen, Szu-Yu Chen, and Shih-Jen Chen, *Retinal prostheses in degenerative retinal diseases.* Journal of the Chinese Medical Association, 2015. 78(9): p. 501-505.
161. Shire, Douglas B, Shawn K Kelly, Jinghua Chen, Patrick Doyle, Marcus D Gingerich, Stuart F Cogan, William A Drohan, Oscar Mendoza, Luke Theogarajan, and John L Wyatt, *Development and implantation of a minimally invasive wireless subretinal neurostimulator.* IEEE Transactions on Biomedical Engineering, 2009. 56(10): p. 2502-2511.
162. Zrenner, Eberhart, *Will retinal implants restore vision?* Science, 2002. 295(5557): p. 1022-1025.
163. Weiland, James D. *Bioelectronic retinal prosthesis*. in *SPIE Defense+ Security*. 2016. International Society for Optics and Photonics.
164. Dagnelie, Gislin, Punita Christopher, Aries Arditi, Lyndon Cruz, Jacque L Duncan, Allen C Ho, Lisa C Olmos de Koo, José-Alain Sahel, Paulo E Stanga, and Gabriele Thumann, *Performance of real-world functional vision tasks by blind subjects*

improves after implantation with the argus® ii retinal prosthesis system. Clinical & experimental ophthalmology, 2016.
165. Margalit, Eyal, Mauricio Maia, James D Weiland, Robert J Greenberg, Gildo Y Fujii, Gustavo Torres, Duke V Piyathaisere, Thomas M O'Hearn, Wentai Liu, and Gianluca Lazzi, *Retinal prosthesis for the blind.* Survey of ophthalmology, 2002. 47(4): p. 335-356.
166. Hadjinicolaou, Alex E., Ronald T. Leung, David J. Garrett, Kumaravelu Ganesan, Kate Fox, David A.X. Nayagam, Mohit N. Shivdasani, Hamish Meffin, Michael R. Ibbotson, Steven Prawer, and Brendan J. O'brien *Electrical stimulation of retinal ganglion cells with diamond and the development of an all diamond retinal prosthesis*. Biomaterials, 2012. 33, 5812-5820.
167. Tassicker, GE, *Preliminary report on a retinal stimulator.* The British journal of physiological optics, 1956. 13(2): p. 102-105.
168. Brindley, Giles S and WS Lewin, *The sensations produced by electrical stimulation of the visual cortex.* The Journal of physiology, 1968. 196(2): p. 479.
169. Humayun, Mark S, Eugene de Juan Jr, James D Weiland, Gislin Dagnelie, Steve Katona, Robert Greenberg, and Satoshi Suzuki, *Pattern electrical stimulation of the human retina.* Vision research, 1999. 39(15): p. 2569-2576.
170. Rizzo, Joseph F, John Wyatt, John Loewenstein, Shawn Kelly, and Doug Shire, *Perceptual efficacy of electrical stimulation of human retina with a microelectrode array during short-term surgical trials.* Investigative ophthalmology & visual science, 2003. 44(12): p. 5362-5369.
171. Humayun, Mark S, Eugene de Juan, Gislin Dagnelie, Robert J Greenberg, Roy H Propst, and D Howard Phillips, *Visual perception elicited by electrical stimulation of retina in blind humans.* Archives of ophthalmology, 1996. 114(1): p. 40-46.
172. Humayun, Mark S, James D Weiland, Gildo Y Fujii, Robert Greenberg, Richard Williamson, Jim Little, Brian Mech, Valerie Cimmarusti, Gretchen Van Boemel, and Gislin Dagnelie, *Visual perception in a blind subject with a chronic microelectronic retinal prosthesis.* Vision research, 2003. 43(24): p. 2573-2581.
173. Zrenner, Eberhart, *Fighting blindness with microelectronics.* Science translational medicine, 2013. 5(210): p. 210ps216-210ps216.
174. Weiland, James D and Mark S Humayun, *Retinal prosthesis.* IEEE Transactions on Biomedical Engineering, 2014. 61(5): p. 1412-1424.
175. Hadjinicolaou, Alex E, Hamish Meffin, Matias I Maturana, Shaun L Cloherty, and Michael R Ibbotson, *Prosthetic vision: Devices, patient outcomes and retinal research.* Clinical and Experimental Optometry, 2015. 98(5): p. 395-410.
176. Luo, Yvonne Hsu-Lin and Lyndon da Cruz, *The argus® ii retinal prosthesis system.* Progress in Retinal and Eye Research, 2016. 50: p. 89-107.
177. Dagnelie, Gislin, *Retinal implants: Emergence of a multidisciplinary field.* Current opinion in neurology, 2012. 25(1): p. 67-75.
178. Lewis, Philip M, Lauren N Ayton, Robyn H Guymer, Arthur J Lowery, Peter J Blamey, Penelope J Allen, Chi D Luu, and Jeffrey V Rosenfeld, *Advances in implantable bionic devices for blindness: A review.* ANZ Journal of Surgery, 2016. 86(9): p. 654-659.
179. Stingl, Katarina, Karl Ulrich Bartz-Schmidt, Dorothea Besch, Angelika Braun, Anna Bruckmann, Florian Gekeler, Udo Greppmaier, Stephanie Hipp, Gernot Hörtdörfer, and Christoph Kernstock. *Artificial vision with wirelessly powered subretinal electronic implant alpha-ims*. in *Proc. R. Soc. B*. 2013. The Royal Society.

180. Benav, Heval, Karl U Bartz-Schmidt, Dorothea Besch, Anna Bruckmann, Florian Gekeler, Udo Greppmaier, Alex Harscher, Steffen Kibbel, Akos Kusnyerik, and Tobias Peters. *Restoration of useful vision up to letter recognition capabilities using subretinal microphotodiodes*. in *Engineering in Medicine and Biology Society (EMBC), 2010 Annual International Conference of the IEEE*. 2010. IEEE.
181. Zrenner, Eberhart, Karl Ulrich Bartz-Schmidt, Heval Benav, Dorothea Besch, Anna Bruckmann, Veit-Peter Gabel, Florian Gekeler, Udo Greppmaier, Alex Harscher, and Steffen Kibbel, *Subretinal electronic chips allow blind patients to read letters and combine them to words.* Proceedings of the Royal Society of London B: Biological Sciences, 2011. 278(1711): p. 1489-1497.
182. Bergonzo, P, A Bongrain, E Scorsone, A Bendali, L Rousseau, G Lissorgues, P Mailley, Y Li, T Kauffmann, and F Goy, *3d shaped mechanically flexible diamond microelectrode arrays for eye implant applications: The medinas project.* Irbm, 2011. 32(2): p. 91-94.
183. Merrill, Daniel R, Marom Bikson, and John GR Jefferys, *Electrical stimulation of excitable tissue: Design of efficacious and safe protocols.* Journal of neuroscience methods, 2005. 141(2): p. 171-198.
184. Cogan, Stuart F, *Neural stimulation and recording electrodes.* Annu. Rev. Biomed. Eng., 2008. 10: p. 275-309.
185. Fornos, Angélica Pérez, Jörg Sommerhalder, Lyndon da Cruz, Jose Alain Sahel, Saddek Mohand-Said, Farhad Hafezi, and Marco Pelizzone, *Temporal properties of visual perception on electrical stimulation of the retinaperception upon electrical stimulation of the retina.* Investigative ophthalmology & visual science, 2012. 53(6): p. 2720-2731.
186. Wilke, RGH, G Khalili Moghadam, NH Lovell, GJ Suaning, and S Dokos, *Electric crosstalk impairs spatial resolution of multi-electrode arrays in retinal implants.* Journal of neural engineering, 2011. 8(4): p. 046016.
187. Yue, Lan, James D. Weiland, Botond Roska, and Mark S. Humayun *Retinal stimulation strategies to restore vision: Fundamentals and systems*. Progress in Retinal and Eye Research, 2016. 53, 21-47.
188. Eiber, Calvin D, Nigel H Lovell, and Gregg J Suaning, *Attaining higher resolution visual prosthetics: A review of the factors and limitations.* Journal of neural engineering, 2013. 10(1): p. 011002.
189. Zeng, Fan-Gang, Stephen J Rebscher, Qian-Jie Fu, Hongbin Chen, Xiaoan Sun, Li Yin, Lichuan Ping, Haihong Feng, Shiming Yang, and Shusheng Gong, *Development and evaluation of the nurotron 26-electrode cochlear implant system.* Hearing research, 2015. 322: p. 188-199.
190. Gantz, Bruce J, Brian F Mccabe, and Richard S Tyler, *Use of multichannel cochlear implants in obstructed and obliterated cochleas.* Otolaryngology--Head and Neck Surgery, 1988. 98(1): p. 72-81.
191. Roche, Joseph P and Marlan R Hansen, *On the horizon: Cochlear implant technology.* Otolaryngologic Clinics of North America, 2015. 48(6): p. 1097-1116.
192. Volta, A, *Historical records documenting the first galvanic battery,''the volta column.''circa 1800. Asimov's biographical encyclopedia of science and technology*. 1982, Garden City, New York: Doubleday & Company.
193. Davis, Hallowell. *A model for transducer action in the cochlea*. in *Cold Spring Harbor Symposia on Quantitative Biology*. 1965. Cold Spring Harbor Laboratory Press.

194. Dallos, PETER and DAVID Harris, *Properties of auditory nerve responses in absence of outer hair cells.* Journal of Neurophysiology, 1978. 41(2): p. 365-383.
195. Dallos, Peter, *The active cochlea.* Journal of Neuroscience, 1992. 12: p. 4575-4575.
196. Wilson, Blake S. and Michael F. Dorman *Cochlear implants: A remarkable past and a brilliant future*. Hearing Research, 2008. 242, 3-21.
197. Chouard, CH, *The early days of the multi channel cochlear implant: Efforts and achievement in france.* Hearing research, 2015. 322: p. 47-51.
198. Guevara, Nicolas, Michel Hoen, Eric Truy, and Stéphane Gallego *A cochlear implant performance prognostic test based on electrical field interactions evaluated by eabr (electrical auditory brainstem responses)*. PloS one, 2016. 11, n/a.
199. Clark, Graeme M, Yit Chow Tong, and Lois FA Martin, *A multiple-channel cochlear implant: An evaluation using open-set cid sentences.* The Laryngoscope, 1981. 91(4): p. 628-634.
200. Eshraghi, Adrien A, Ronen Nazarian, Fred F Telischi, Suhrud M Rajguru, Eric Truy, and Chhavi Gupta, *The cochlear implant: Historical aspects and future prospects.* The Anatomical Record, 2012. 295(11): p. 1967-1980.
201. Carlson, Matthew L, Colin LW Driscoll, René H Gifford, and Sean O McMenomey, *Cochlear implantation: Current and future device options.* Otolaryngologic Clinics of North America, 2012. 45(1): p. 221-248.
202. Patrick, James F, Peter A Busby, and Peter J Gibson, *The development of the nucleus® freedom™ cochlear implant system.* Trends in amplification, 2006. 10(4): p. 175-200.
203. Arora, Komal, Richard Dowell, Pam Dawson, and S Ramakrishnan, *Cochlear implant stimulation rates and speech perception*. 2012: INTECH Open Access Publisher.
204. Sato, Mika, Peter Baumhoff, and Andrej Kral, *Cochlear implant stimulation of a hearing ear generates separate electrophonic and electroneural responses.* The Journal of Neuroscience, 2016. 36(1): p. 54-64.
205. Donaldson, Gail S, Heather A Kreft, and Leonid Litvak, *Place-pitch discrimination of single-versus dual-electrode stimuli by cochlear implant users a.* The Journal of the Acoustical Society of America, 2005. 118(2): p. 623-626.
206. Langner, Florian, Aniket A Saoji, Andreas Büchner, and Waldo Nogueira, *Adding simultaneous stimulating channels to reduce power consumption in cochlear implants.* Hearing research, 2017. 345: p. 96-107.
207. Pinyon, Jeremy L, Sherif F Tadros, Kristina E Froud, Ann CY Wong, Isabella T Tompson, Edward N Crawford, Myungseo Ko, Renée Morris, Matthias Klugmann, and Gary D Housley, *Close-field electroporation gene delivery using the cochlear implant electrode array enhances the bionic ear.* Science translational medicine, 2014. 6(233): p. 233ra254-233ra254.
208. Loo, Ching-Yee, Paul M. Young, Wing-Hin Lee, Rosalia Cavaliere, Cynthia B. Whitchurch, and Ramin Rohanizadeh *Superhydrophobic, nanotextured polyvinyl chloride films for delaying pseudomonas aeruginosa attachment to intubation tubes and medical plastics*. Acta biomaterialia, 2012. 8, 1881-1890.
209. Tang, Haiying, Ting Cao, Xuemei Liang, Anfeng Wang, Steven O Salley, James McAllister, and KY Ng, *Influence of silicone surface roughness and hydrophobicity on adhesion and colonization of staphylococcus epidermidis.* Journal of Biomedical Materials Research Part A, 2009. 88(2): p. 454-463.

210. Tan, Fei, Peter Walshe, Laura Viani, and Mohamed Al-Rubeai, *Surface biotechnology for refining cochlear implants.* TRENDS in Biotechnology, 2013. 31(12): p. 678-687.
211. Richardson, Rachael T, Brianna Thompson, Simon Moulton, Carrie Newbold, May Ghee Lum, Adrian Cameron, Gordon Wallace, Robert Kapsa, Graeme Clark, and Stephen O'Leary, *The effect of polypyrrole with incorporated neurotrophin-3 on the promotion of neurite outgrowth from auditory neurons.* Biomaterials, 2007. 28(3): p. 513-523.
212. Richardson, Rachael T, Andrew K Wise, Jacqueline K Andrew, and Stephen J O'Leary, *Novel drug delivery systems for inner ear protection and regeneration after hearing loss.* Expert Opinion on drug delivery, 2008. 5(10): p. 1059-1076.
213. Bohl, A, T Eickner, S Petersen, KP Schmitz, and K Sternberg, *Specific surface modification of cochlear implant electrode carriers for enhancement of spiral ganglion cell growth.* Biomedical Engineering/Biomedizinische Technik, 2013.
214. Izzo, Agnella D, Joseph T Walsh, Heather Ralph, Jim Webb, Mark Bendett, Jonathon Wells, and Claus-Peter Richter, *Laser stimulation of auditory neurons: Effect of shorter pulse duration and penetration depth.* Biophysical journal, 2008. 94(8): p. 3159-3166.
215. Moser, Tobias, *Optogenetic stimulation of the auditory pathway for research and future prosthetics.* Current opinion in neurobiology, 2015. 34: p. 29-36.
216. Jeschke, Marcus and Tobias Moser, *Considering optogenetic stimulation for cochlear implants.* Hearing research, 2015. 322: p. 224-234.
217. Bean, Bruce P, *The action potential in mammalian central neurons.* Nature Reviews Neuroscience, 2007. 8(6): p. 451-465.
218. Pereda, Alberto E, *Electrical synapses and their functional interactions with chemical synapses.* Nature reviews. Neuroscience, 2014. 15(4): p. 250.
219. Bennett, Michael VL and R Suzanne Zukin, *Electrical coupling and neuronal synchronization in the mammalian brain.* Neuron, 2004. 41(4): p. 495-511.
220. Connors, Barry W and Michael A Long, *Electrical synapses in the mammalian brain.* Annu. Rev. Neurosci., 2004. 27: p. 393-418.
221. Fuxe, Kjell and Dasiel O Borroto-Escuela, *Volume transmission and receptor-receptor interactions in heteroreceptor complexes: Understanding the role of new concepts for brain communication.* Neural Regeneration Research, 2016. 11(8): p. 1220.
222. Faber, DONALD S and HENRI Korn, *Electrical field effects: Their relevance in central neural networks.* Physiological reviews, 1989. 69(3): p. 821-863.
223. Zoli, Michele, Carla Torri, Rosaria Ferrari, Anders Jansson, Isabella Zini, Kjell Fuxe, and Luigi F Agnati, *The emergence of the volume transmission concept.* Brain Research Reviews, 1998. 26(2): p. 136-147.
224. Agnati, LF, K Fuxe, M Zoli, I Ozini, G Toffano, and F Ferraguti, *A correlation analysis of the regional distribution of central enkephalin and β-endorphin immunoreactive terminals and of opiate receptors in adult and old male rats. Evidence for the existence of two main types of communication in the central nervous system: The volume transmission and the wiring transmission.* Acta Physiologica, 1986. 128(2): p. 201-207.
225. Agnati, Luigi F, Diego Guidolin, Michele Guescini, Susanna Genedani, and Kjell Fuxe, *Understanding wiring and volume transmission.* Brain research reviews, 2010. 64(1): p. 137-159.

226. Rustom, Amin, Rainer Saffrich, Ivanka Markovic, Paul Walther, and Hans-Hermann Gerdes, *Nanotubular highways for intercellular organelle transport.* Science, 2004. 303(5660): p. 1007-1010.
227. Ananthanarayanan, Badriprasad, Lauren Little, David V Schaffer, Kevin E Healy, and Matthew Tirrell, *Neural stem cell adhesion and proliferation on phospholipid bilayers functionalized with rgd peptides.* Biomaterials, 2010. 31(33): p. 8706-8715.
228. Gerdes, Hans-Hermann and Raquel Negrão Carvalho, *Intercellular transfer mediated by tunneling nanotubes.* Current opinion in cell biology, 2008. 20(4): p. 470-475.
229. Park, Joong Yull, Shuichi Takayama, and Sang-Hoon Lee, *Regulating microenvironmental stimuli for stem cells and cancer cells using microsystems.* Integrative biology, 2010. 2(5-6): p. 229-240.
230. Stukel, Jessica M and Rebecca Kuntz Willits, *Mechanotransduction of neural cells through cell–substrate interactions.* Tissue Engineering Part B: Reviews, 2016. 22(3): p. 173-182.
231. Kempermann, Gerd and Fred H Gage, *New nerve cells for the adult brain.* SCIENTIFIC AMERICAN-AMERICAN EDITION-, 1999. 280: p. 48-67.
232. Reynolds, Brent A and Samuel Weiss, *Generation of neurons and astrocytes from isolated cells of the adult mammalian central nervous system.* Science, 1992. 255(5052): p. 1707.
233. Yu, Juan, Shuyun Lin, Mei Wang, Lijun Liang, Zijiao Zou, Xinfeng Zhou, Meichi Wang, Ping Chen, and Ying Wang, *Metastasis suppressor 1 regulates neurite outgrowth in primary neuron cultures.* Neuroscience, 2016. 333: p. 123-131.
234. Friedl, Peter and Darren Gilmour, *Collective cell migration in morphogenesis, regeneration and cancer.* Nature reviews Molecular cell biology, 2009. 10(7): p. 445-457.
235. Roca-Cusachs, Pere, Raimon Sunyer, and Xavier Trepat, *Mechanical guidance of cell migration: Lessons from chemotaxis.* Current opinion in cell biology, 2013. 25(5): p. 543-549.
236. Brown, Martin J and Leslie M Loew, *Electric field-directed fibroblast locomotion involves cell surface molecular reorganization and is calcium independent.* The Journal of cell biology, 1994. 127(1): p. 117-128.
237. Saranak, Jureepan and Kenneth W Foster, *Rhodopsin guides fungal phototaxis.* Nature, 1997. 387(6632): p. 465.
238. Shellard, Adam and Roberto Mayor. *Chemotaxis during neural crest migration*. in *Seminars in cell & developmental biology*. 2016. Elsevier.
239. Colamarino, Sophia A and Marc Tessier-Lavigne, *The axonal chemoattractant netrin-1 is also a chemorepellent for trochlear motor axons.* cell, 1995. 81(4): p. 621-629.
240. McLennan, Rebecca, Jessica M Teddy, Jennifer C Kasemeier-Kulesa, Morgan H Romine, and Paul M Kulesa, *Vascular endothelial growth factor (vegf) regulates cranial neural crest migration in vivo.* Developmental biology, 2010. 339(1): p. 114-125.
241. Shellard, Adam and Roberto Mayor. *Chemotaxis during neural crest migration*. in *Seminars in cell & developmental biology*. 2016. Elsevier.
242. Lo, Chun-Min, Hong-Bei Wang, Micah Dembo, and Yu-li Wang, *Cell movement is guided by the rigidity of the substrate.* Biophysical journal, 2000. 79(1): p. 144-152.

243. Kuo, Cheng-Hwa R, Jian Xian, James D Brenton, Kristian Franze, and Easan Sivaniah, *Complex stiffness gradient substrates for studying mechanotactic cell migration.* Advanced materials, 2012. 24(45): p. 6059-6064.
244. Engler, Adam J, Shamik Sen, H Lee Sweeney, and Dennis E Discher, *Matrix elasticity directs stem cell lineage specification.* cell, 2006. 126(4): p. 677-689.
245. Lee, Man Ryul, Keon Woo Kwon, Hosup Jung, Hong Nam Kim, Kahp Y Suh, Keesung Kim, and Kye-Seong Kim, *Direct differentiation of human embryonic stem cells into selective neurons on nanoscale ridge/groove pattern arrays.* Biomaterials, 2010. 31(15): p. 4360-4366.
246. Nakamoto, Tetsuya, Kristin H Kain, and Mark H Ginsberg, *Neurobiology: New connections between integrins and axon guidance.* Current Biology, 2004. 14(3): p. R121-R123.
247. Barros, Claudia S, Santos J Franco, and Ulrich Müller, *Extracellular matrix: Functions in the nervous system.* Cold Spring Harbor perspectives in biology, 2011. 3(1): p. a005108.
248. Leshchyns' ka, Iryna and Vladimir Sytnyk, *Reciprocal interactions between cell adhesion molecules of the immunoglobulin superfamily and the cytoskeleton in neurons.* Frontiers in cell and developmental biology, 2016. 4.
249. Samatov, Timur R, Daniel Wicklein, and Alexander G Tonevitsky, *L1cam: Cell adhesion and more.* Progress in histochemistry and cytochemistry, 2016.
250. Matsumoto, Kotaro, Chie Sato, Yukie Naka, Ayako Kitazawa, Raymond LD Whitby, and Norio Shimizu, *Neurite outgrowths of neurons with neurotrophin-coated carbon nanotubes.* Journal of bioscience and bioengineering, 2007. 103(3): p. 216-220.
251. Paviolo, Chiara, John W Haycock, Jiawey Yong, Aimin Yu, Paul R Stoddart, and Sally L McArthur, *Laser exposure of gold nanorods can increase neuronal cell outgrowth.* Biotechnology and bioengineering, 2013. 110(8): p. 2277-2291.
252. Nakano, Norihiko, Kenji Kanekiyo, Takatoshi Nakagawa, Michio Asahi, and Chizuka Ide, *Ntak/neuregulin-2 secreted by astrocytes promotes survival and neurite outgrowth of neurons via erbb3.* Neuroscience letters, 2016. 622: p. 88-94.
253. Lander, Arthur D, Dennis K Fujii, and Louis F Reichardt, *Purification of a factor that promotes neurite outgrowth: Isolation of laminin and associated molecules.* The Journal of cell biology, 1985. 101(3): p. 898-913.
254. Menager, Celine, Nariko Arimura, Yuko Fukata, and Kozo Kaibuchi, *Pip3 is involved in neuronal polarization and axon formation.* Journal of neurochemistry, 2004. 89(1): p. 109-118.
255. García-Alonso, Luis, Richard D Fetter, and Corey S Goodman, *Genetic analysis of laminin a in drosophila: Extracellular matrix containing laminin a is required for ocellar axon pathfinding.* Development, 1996. 122(9): p. 2611-2621.
256. Zhou, Xingxing, Anneng Yang, Zhongbing Huang, Guangfu Yin, Ximing Pu, and Juan Jin, *Enhancement of neurite adhesion, alignment and elongation on conductive polypyrrole-poly (lactide acid) fibers with cell-derived extracellular matrix.* Colloids and Surfaces B: Biointerfaces, 2017. 149: p. 217-225.
257. Cai, Yixiao, Fredrik Edin, Zhe Jin, Andrei Alexsson, Olafur Gudjonsson, Wei Liu, Helge Rask-Andersen, Mikael Karlsson, and Hao Li, *Strategy towards independent electrical stimulation from cochlear implants: Guided auditory neuron growth on topographically modified nanocrystalline diamond.* Acta biomaterialia, 2016. 31: p. 211-220.

258. Arslan-Yildiz, Ahu, Rami El Assal, Pu Chen, Sinan Guven, Fatih Inci, and Utkan Demirci, *Towards artificial tissue models: Past, present, and future of 3d bioprinting.* Biofabrication, 2016. 8(1): p. 014103.
259. Huang, Sui and Donald E Ingber, *The structural and mechanical complexity of cell-growth control.* Nature cell biology, 1999. 1(5): p. E131-E138.
260. Khalili, Amelia Ahmad and Mohd Ridzuan Ahmad, *A review of cell adhesion studies for biomedical and biological applications.* International journal of molecular sciences, 2015. 16(8): p. 18149-18184.
261. Lock, John G, Bernhard Wehrle-Haller, and Staffan Strömblad. *Cell–matrix adhesion complexes: Master control machinery of cell migration*. in *Seminars in cancer biology*. 2008. Elsevier.
262. Petrova, Yuliya I, Leslayann Schecterson, and Barry M Gumbiner, *Roles for e-cadherin cell surface regulation in cancer.* Molecular Biology of the Cell, 2016. 27(21): p. 3233-3244.
263. Hirohashi, Setsuo and Yae Kanai, *Cell adhesion system and human cancer morphogenesis.* Cancer science, 2003. 94(7): p. 575-581.
264. Wilke, RGH, G Khalili Moghadam, NH Lovell, GJ Suaning, and S Dokos, *Electric crosstalk impairs spatial resolution of multi-electrode arrays in retinal implantsthis paper was originally submitted for the special issue containing contributions from the sixth biennial research congress of the eye and the chip.* Journal of neural engineering, 2011. 8(4): p. 046016.
265. Critchley, DR, *Cytoskeletal proteins talin and vinculin in integrin-mediated adhesion.* Biochemical Society Transactions, 2004. 32(5): p. 831-836.
266. Koshland, Daniel E, *The key–lock theory and the induced fit theory.* Angewandte Chemie International Edition in English, 1995. 33(23-24): p. 2375-2378.
267. Liddington, RC and Mark H Ginsberg, *Integrin activation takes shape.* The Journal of cell biology, 2002. 158(5): p. 833-839.
268. Parsons, J Thomas, Alan Rick Horwitz, and Martin A Schwartz, *Cell adhesion: Integrating cytoskeletal dynamics and cellular tension.* Nature reviews Molecular cell biology, 2010. 11(9): p. 633-643.
269. Mui, Keeley L, Christopher S Chen, and Richard K Assoian, *The mechanical regulation of integrin–cadherin crosstalk organizes cells, signaling and forces.* J Cell Sci, 2016. 129(6): p. 1093-1100.
270. Geiger, Benjamin, Joachim P Spatz, and Alexander D Bershadsky, *Environmental sensing through focal adhesions.* Nature reviews Molecular cell biology, 2009. 10(1): p. 21-33.
271. Smith, Ana-Sunčana, Kheya Sengupta, Stefanie Goennenwein, Udo Seifert, and Erich Sackmann, *Force-induced growth of adhesion domains is controlled by receptor mobility.* Proceedings of the National Academy of Sciences, 2008. 105(19): p. 6906-6911.
272. Hynes, Richard O, *Integrins: Bidirectional, allosteric signaling machines.* cell, 2002. 110(6): p. 673-687.
273. Bockaert, Joël and Jean Philippe Pin, *Molecular tinkering of g protein-coupled receptors: An evolutionary success.* The EMBO journal, 1999. 18(7): p. 1723-1729.
274. DeSIMONE, DOUGLAS W, MARY ANN STEPP, RAMILA S PATEL, and RICHARD O HYNES, *The integrin family of cell surface receptors.* Biochemical Society Transactions, 1987. 15(5): p. 789-791.
275. García, Andrés J, *Interfaces to control cell-biomaterial adhesive interactions*, in *Polymers for regenerative medicine*. 2006, Springer. p. 171-190.

276. Rønn, Lars Christian Biilman, BP Hartz, and Elisabeth Bock, *The neural cell adhesion molecule (ncam) in development and plasticity of the nervous system.* Experimental gerontology, 1998. 33(7): p. 853-864.
277. Slapšak, Urška, Giulia Salzano, Ladan Amin, Romany NN Abskharon, Gregor Ilc, Blaž Zupančič, Ivana Biljan, Janez Plavec, Gabriele Giachin, and Giuseppe Legname, *The n terminus of the prion protein mediates functional interactions with the neuronal cell adhesion molecule (ncam) fibronectin domain.* Journal of Biological Chemistry, 2016. 291(42): p. 21857-21868.
278. Geiger, Benjamin, Alexander Bershadsky, Roumen Pankov, and Kenneth M Yamada, *Transmembrane crosstalk between the extracellular matrix and the cytoskeleton.* Nature reviews Molecular cell biology, 2001. 2(11): p. 793-805.
279. Santiago, Lizzie Y, Julio Clavijo-Alvarez, Candace Brayfield, J Peter Rubin, and Kacey G Marra, *Delivery of adipose-derived precursor cells for peripheral nerve repair.* Cell transplantation, 2009. 18(2): p. 145-158.
280. Neal, Rebekah A, Sunil S Tholpady, Patricia L Foley, Nathan Swami, Roy C Ogle, and Edward A Botchwey, *Alignment and composition of laminin–polycaprolactone nanofiber blends enhance peripheral nerve regeneration.* Journal of Biomedical Materials Research Part A, 2012. 100(2): p. 406-423.
281. Liu, F, AN Nordin, F Li, and I Voiculescu, *A lab-on-chip cell-based biosensor for label-free sensing of water toxicants.* Lab on a Chip, 2014. 14(7): p. 1270-1280.
282. Xiao, Caide, Bernard Lachance, Geoffrey Sunahara, and John HT Luong, *An in-depth analysis of electric cell-substrate impedance sensing to study the attachment and spreading of mammalian cells.* Analytical chemistry, 2002. 74(6): p. 1333-1339.
283. Liu, Qingjun, Jinjiang Yu, Lidan Xiao, Johnny Cheuk On Tang, Yu Zhang, Ping Wang, and Mo Yang, *Impedance studies of bio-behavior and chemosensitivity of cancer cells by micro-electrode arrays.* Biosensors and Bioelectronics, 2009. 24(5): p. 1305-1310.
284. Hartmann, Christoph, Alla Zozulya, Joachim Wegener, and Hans-Joachim Galla, *The impact of glia-derived extracellular matrices on the barrier function of cerebral endothelial cells: An in vitro study.* Experimental cell research, 2007. 313(7): p. 1318-1325.
285. Jun, Sang Beom, Matthew R Hynd, Natalie Dowell-Mesfin, Karen L Smith, James N Turner, William Shain, and Sung June Kim, *Low-density neuronal networks cultured using patterned poly-l-lysine on microelectrode arrays.* Journal of neuroscience methods, 2007. 160(2): p. 317-326.
286. Koh, HS, T Yong, WE Teo, CK Chan, ME Puhaindran, TC Tan, A Lim, BH Lim, and S Ramakrishna, *In vivo study of novel nanofibrous intra-luminal guidance channels to promote nerve regeneration.* Journal of neural engineering, 2010. 7(4): p. 046003.
287. Yu, Xiaojun and Ravi V Bellamkonda, *Tissue-engineered scaffolds are effective alternatives to autografts for bridging peripheral nerve gaps.* Tissue engineering, 2003. 9(3): p. 421-430.
288. Armstrong, Stephanie J, Mikael Wiberg, Giorgio Terenghi, and Paul J Kingham, *Ecm molecules mediate both schwann cell proliferation and activation to enhance neurite outgrowth.* Tissue engineering, 2007. 13(12): p. 2863-2870.
289. Mukhatyar, Vivek J, Manuel Salmerón-Sánchez, Soumon Rudra, Shoumit Mukhopadaya, Thomas H Barker, Andrés J García, and Ravi V Bellamkonda, *Role*

of fibronectin in topographical guidance of neurite extension on electrospun fibers. Biomaterials, 2011. 32(16): p. 3958-3968.
290. Lam, Mai T and Michael T Longaker, *Comparison of several attachment methods for human ips, embryonic and adipose-derived stem cells for tissue engineering.* Journal of tissue engineering and regenerative medicine, 2012. 6(S3): p. s80-s86.
291. Kristiansen, Kurt, *Molecular mechanisms of ligand binding, signaling, and regulation within the superfamily of g-protein-coupled receptors: Molecular modeling and mutagenesis approaches to receptor structure and function.* Pharmacology & therapeutics, 2004. 103(1): p. 21-80.
292. LeBaron, Richard G and Kyriacos A Athanasiou, *Extracellular matrix cell adhesion peptides: Functional applications in orthopedic materials.* Tissue engineering, 2000. 6(2): p. 85-103.
293. Ruoslahti, Erkki, *Rgd and other recognition sequences for integrins.* Annual review of cell and developmental biology, 1996. 12(1): p. 697-715.
294. Yoon, Sang-Hee and Mohammad RK Mofrad, *Cell adhesion and detachment on gold surfaces modified with a thiol-functionalized rgd peptide.* Biomaterials, 2011. 32(30): p. 7286-7296.
295. Pierschbacher, Michael D and Erkki Ruoslahti, *Cell attachment activity of fibronectin can be duplicated by small synthetic fragments of the molecule.* Nature, 1984. 309(5963): p. 30.
296. Soylemez, Saniye, Bilal Demir, Gizem Oyman Eyrilmez, Seçkin Kesici, Aytül Saylam, Dilek Odaci Demirkol, Salih Özçubukçu, Suna Timur, and Levent Toppare, *Comparative cell adhesion properties of cysteine extended peptide architectures.* RSC Advances, 2016. 6(4): p. 2695-2702.
297. Bhagwat, Nandita, Roy E Murray, S Ismat Shah, Kristi L Kiick, and David C Martin, *Biofunctionalization of pedot films with laminin-derived peptides.* Acta biomaterialia, 2016.
298. Huang, Tiffany H, Yi Pei, Douglas Zhang, Yanfen Li, and Kristopher A Kilian, *Patterned porous silicon photonic crystals with modular surface chemistry for spatial control of neural stem cell differentiation.* Nanoscale, 2016. 8(21): p. 10891-10895.
299. Aota, Shin-ichi, Motoyoshi Nomizu, and Kenneth M Yamada, *The short amino acid sequence pro-his-ser-arg-asn in human fibronectin enhances cell-adhesive function.* Journal of Biological Chemistry, 1994. 269(40): p. 24756-24761.
300. Castellanos, Maria Isabel, Carlos Mas-Moruno, Anna Grau, Xavier Serra-Picamal, Xavier Trepat, Fernando Albericio, Michael Joner, Francisco Javier Gil, Maria Pau Ginebra, and Jose María Manero, *Functionalization of cocr surfaces with cell adhesive peptides to promote huvecs adhesion and proliferation.* Applied Surface Science, 2017. 393: p. 82-92.
301. Castellanos, Maria Isabel, Jordi Guillem-Marti, Carlos Mas-Moruno, Maribel Díaz-Ricart, Ginés Escolar, Maria Pau Ginebra, Francisco Javier Gil, Marta Pegueroles, and Jose María Manero, *Cell adhesive peptides functionalized on cocr alloy stimulate endothelialization and prevent thrombogenesis and restenosis.* Journal of Biomedical Materials Research Part A, 2016.
302. Kato, Mihoko and Milan Mrksich, *Using model substrates to study the dependence of focal adhesion formation on the affinity of integrin-ligand complexes.* Biochemistry, 2004. 43(10): p. 2699-2707.
303. Choi, Chang K, Anthony E English, Seung-Ik Jun, Kenneth D Kihm, and Philip D Rack, *An endothelial cell compatible biosensor fabricated using optically thin*

indium tin oxide silicon nitride electrodes. Biosensors and Bioelectronics, 2007. 22(11): p. 2585-2590.
304. Gao, Hui, Reto Luginbühl, and Hans Sigrist, *Bioengineering of silicon nitride.* Sensors and Actuators B: Chemical, 1997. 38(1): p. 38-41.
305. Agrawal, C and Robert B Ray, *Biodegradable polymeric scaffolds for musculoskeletal tissue engineering.* Journal of biomedical materials research, 2001. 55(2): p. 141-150.
306. Dahl, Roger W, David K Swanson, Stephen J Hahn, Douglas J Lang, and John E Heil, *Process for implanting subcutaneous defibrillation electrodes*. 1993, Google Patents.
307. Liu, Qingjun, Chunsheng Wu, Hua Cai, Ning Hu, Jun Zhou, and Ping Wang, *Cell-based biosensors and their application in biomedicine.* Chemical reviews, 2014. 114(12): p. 6423-6461.
308. Ventre, Maurizio and Paolo A Netti, *Controlling cell functions and fate with surfaces and hydrogels: The role of material features in cell adhesion and signal transduction.* Gels, 2016. 2(1): p. 12.
309. Attwood, Simon J, Ernesto Cortes, Alexander William M Haining, Benjamin Robinson, Danyang Li, Julien Gautrot, and Armando del Río Hernández, *Adhesive ligand tether length affects the size and length of focal adhesions and influences cell spreading and attachment.* Scientific reports, 2016. 6.
310. Chen, Weiqiang, Luis G Villa-Diaz, Yubing Sun, Shinuo Weng, Jin Koo Kim, Raymond HW Lam, Lin Han, Rong Fan, Paul H Krebsbach, and Jianping Fu, *Nanotopography influences adhesion, spreading, and self-renewal of human embryonic stem cells.* ACS nano, 2012. 6(5): p. 4094-4103.
311. Murphy, William L, Todd C McDevitt, and Adam J Engler, *Materials as stem cell regulators.* Nature materials, 2014. 13(6): p. 547-557.
312. Lim, Jung Yul and Henry J Donahue, *Cell sensing and response to micro-and nanostructured surfaces produced by chemical and topographic patterning.* Tissue engineering, 2007. 13(8): p. 1879-1891.
313. Calvert, Jeffrey M, *Lithographic patterning of self-assembled films.* Journal of Vacuum Science & Technology B: Microelectronics and Nanometer Structures Processing, Measurement, and Phenomena, 1993. 11(6): p. 2155-2163.
314. Ruiz, Sami Alom and Christopher S Chen, *Microcontact printing: A tool to pattern.* Soft Matter, 2007. 3(2): p. 168-177.
315. Perl, András, David N Reinhoudt, and Jurriaan Huskens, *Microcontact printing: Limitations and achievements.* Advanced Materials, 2009. 21(22): p. 2257-2268.
316. Ratner, Buddy D, Allan S Hoffman, Frederick J Schoen, and Jack E Lemons, *Biomaterials science: An introduction to materials in medicine*. 2004: Academic press.
317. Murphy, William L, Kwesi O Mercurius, Shohei Koide, and Milan Mrksich, *Substrates for cell adhesion prepared via active site-directed immobilization of a protein domain.* Langmuir, 2004. 20(4): p. 1026-1030.
318. Hudalla, Gregory A and William L Murphy, *Chemically well-defined self-assembled monolayers for cell culture: Toward mimicking the natural ecm.* Soft Matter, 2011. 7(20): p. 9561-9571.
319. Wang, Hua, Shengfu Chen, Lingyan Li, and Shaoyi Jiang, *Improved method for the preparation of carboxylic acid and amine terminated self-assembled monolayers of alkanethiolates.* Langmuir, 2005. 21(7): p. 2633-2636.

320. Roach, Paul, David Eglin, Kirsty Rohde, and Carole C Perry, *Modern biomaterials: A review—bulk properties and implications of surface modifications.* Journal of Materials Science: Materials in Medicine, 2007. 18(7): p. 1263-1277.
321. Ifkovits, Jamie L, Jeffrey J Devlin, George Eng, Timothy P Martens, Gordana Vunjak-Novakovic, and Jason A Burdick, *Biodegradable fibrous scaffolds with tunable properties formed from photo-cross-linkable poly (glycerol sebacate).* ACS applied materials & interfaces, 2009. 1(9): p. 1878-1886.
322. Buck, Maren E, Anthony S Breitbach, Sonja K Belgrade, Helen E Blackwell, and David M Lynn, *Chemical modification of reactive multilayered films fabricated from poly (2-alkenyl azlactone) s: Design of surfaces that prevent or promote mammalian cell adhesion and bacterial biofilm growth.* Biomacromolecules, 2009. 10(6): p. 1564-1574.
323. Pan, Jian-feng, Ning-hua Liu, Lin-yuan Shu, and Hui Sun, *Application of avidin-biotin technology to improve cell adhesion on nanofibrous matrices.* Journal of nanobiotechnology, 2015. 13(1): p. 1.
324. Shim, Moonsub, Nadine Wong Shi Kam, Robert J Chen, Yiming Li, and Hongjie Dai, *Functionalization of carbon nanotubes for biocompatibility and biomolecular recognition.* Nano letters, 2002. 2(4): p. 285-288.
325. Discher, Dennis E, Paul Janmey, and Yu-li Wang, *Tissue cells feel and respond to the stiffness of their substrate.* Science, 2005. 310(5751): p. 1139-1143.
326. Saranya, N, S Saravanan, A Moorthi, B Ramyakrishna, and N Selvamurugan, *Enhanced osteoblast adhesion on polymeric nano-scaffolds for bone tissue engineering.* Journal of biomedical nanotechnology, 2011. 7(2): p. 238-244.
327. Yeung, Tony, Penelope C Georges, Lisa A Flanagan, Beatrice Marg, Miguelina Ortiz, Makoto Funaki, Nastaran Zahir, Wenyu Ming, Valerie Weaver, and Paul A Janmey, *Effects of substrate stiffness on cell morphology, cytoskeletal structure, and adhesion.* Cell motility and the cytoskeleton, 2005. 60(1): p. 24-34.
328. Schwartz, Martin A, Michael D Schaller, and Mark H Ginsberg, *Integrins: Emerging paradigms of signal transduction.* Annual review of cell and developmental biology, 1995. 11(1): p. 549-599.
329. Cavalcanti-Adam, Elisabetta Ada, Tova Volberg, Alexandre Micoulet, Horst Kessler, Benjamin Geiger, and Joachim Pius Spatz, *Cell spreading and focal adhesion dynamics are regulated by spacing of integrin ligands.* Biophysical journal, 2007. 92(8): p. 2964-2974.
330. Teixeira, Ana I, George A Abrams, Paul J Bertics, Christopher J Murphy, and Paul F Nealey, *Epithelial contact guidance on well-defined micro-and nanostructured substrates.* Journal of cell science, 2003. 116(10): p. 1881-1892.
331. Schvartzman, Mark, Matteo Palma, Julia Sable, Justin Abramson, Xian Hu, Michael P Sheetz, and Shalom J Wind, *Nanolithographic control of the spatial organization of cellular adhesion receptors at the single-molecule level.* Nano letters, 2011. 11(3): p. 1306-1312.
332. Houseman, BT and M Mrksich, *The microenvironment of immobilized arg-gly-asp peptides is an important determinant of cell adhesion.* Biomaterials, 2001. 22(9): p. 943-955.
333. Prime, Kevin L and George M Whitesides, *Adsorption of proteins onto surfaces containing end-attached oligo (ethylene oxide): A model system using self-assembled monolayers.* Journal of the American Chemical Society, 1993. 115(23): p. 10714-10721.

334. Yim, Evelyn KF, Eric M Darling, Karina Kulangara, Farshid Guilak, and Kam W Leong, *Nanotopography-induced changes in focal adhesions, cytoskeletal organization, and mechanical properties of human mesenchymal stem cells.* Biomaterials, 2010. 31(6): p. 1299-1306.
335. Yim, Evelyn KF, Stella W Pang, and Kam W Leong, *Synthetic nanostructures inducing differentiation of human mesenchymal stem cells into neuronal lineage.* Experimental cell research, 2007. 313(9): p. 1820-1829.
336. Shoval, A., C. Adams, M. David-Pur, M. Shein, Y. Hanein, and E. Sernagor, *Carbon nanotube electrodes for effective interfacing with retinal tissue.* Front Neuroeng, 2009. 2: p. 4.
337. Li, Wei, Qing Yuan Tang, Amol D Jadhav, Ankit Narang, Wei Xian Qian, Peng Shi, and Stella W Pang, *Large-scale topographical screen for investigation of physical neural-guidance cues.* Scientific reports, 2015. 5.
338. Hoffman-Kim, Diane, Jennifer A Mitchel, and Ravi V Bellamkonda, *Topography, cell response, and nerve regeneration.* Annual review of biomedical engineering, 2010. 12: p. 203.
339. Kriparamanan, Rammohan, Pranesh Aswath, Anhong Zhou, Liping Tang, and Kytai T Nguyen, *Nanotopography: Cellular responses to nanostructured materials.* Journal of nanoscience and nanotechnology, 2006. 6(7): p. 1905-1919.
340. Wieringa, Paul, Ilaria Tonazzini, Silvestro Micera, and Marco Cecchini, *Nanotopography induced contact guidance of the f11 cell line during neuronal differentiation: A neuronal model cell line for tissue scaffold development.* Nanotechnology, 2012. 23(27): p. 275102.
341. Fan, YW, FZ Cui, SP Hou, QY Xu, LN Chen, and I-S Lee, *Culture of neural cells on silicon wafers with nano-scale surface topograph.* Journal of neuroscience methods, 2002. 120(1): p. 17-23.
342. Fan, YW, FZ Cui, LN Chen, Y Zhai, and QY Xu, *Improvement of neural cell adherence to silicon surface by hydroxyl ion implantation.* Surface and Coatings Technology, 2000. 131(1): p. 355-359.
343. Kanda, Teru, Kevin F Sullivan, and Geoffrey M Wahl, *Histone–gfp fusion protein enables sensitive analysis of chromosome dynamics in living mammalian cells.* Current Biology, 1998. 8(7): p. 377-385.
344. Hawley-Nelson, Pamela, Valentina Ciccarone, and Meredith L Moore, *Transfection of cultured eukaryotic cells using cationic lipid reagents.* Current protocols in molecular biology, 2008. 81(1): p. 9.4. 1-9.4. 17.
345. Cranfield, Charles, Sonia Carne, Boris Martinac, and Bruce Cornell, *The assembly and use of tethered bilayer lipid membranes (tblms).* Methods in Membrane Lipids, 2015: p. 45-53.
346. Cranfield, Charles G, Taren Bettler, and Bruce Cornell, *Nanoscale ion sequestration to determine the polarity selectivity of ion conductance in carriers and channels.* Langmuir, 2014. 31(1): p. 292-298.
347. Cranfield, Charles G, Sónia Troeira Henriques, Boris Martinac, Paul Duckworth, David J Craik, and Bruce Cornell, *Kalata b1 and kalata b2 have a surfactant-like activity in phosphatidylethanolomine-containing lipid membranes.* Langmuir, 2017. 33(26): p. 6630-6637.
348. Abramczuk, J, D Solter, and H Koprowski, *The beneficial effect of edta on development of mouse one-cell embryos in chemically defined medium.* Developmental biology, 1977. 61(2): p. 378-383.

349. De Kerchove, Alexis J and Menachem Elimelech, *Calcium and magnesium cations enhance the adhesion of motile and nonmotile pseudomonas aeruginosa on alginate films.* Langmuir, 2008. 24(7): p. 3392-3399.
350. Zhang, Jing, Xiaoyu Ma, Dan Lin, Hengsong Shi, Yuan Yuan, Wei Tang, Huanjun Zhou, Han Guo, Jiangchao Qian, and Changsheng Liu, *Magnesium modification of a calcium phosphate cement alters bone marrow stromal cell behavior via an integrin-mediated mechanism.* Biomaterials, 2015. 53: p. 251-264.
351. Armstrong, Peter B, *On the role of metal cations in cellular adhesion: Effect on cell surface charge.* Journal of Experimental Zoology, 1966. 163(1): p. 99-109.
352. Thein, Myo, Fareid Asphahani, An Cheng, Ryan Buckmaster, Miqin Zhang, and Jian Xu, *Response characteristics of single-cell impedance sensors employed with surface-modified microelectrodes.* Biosensors and Bioelectronics, 2010. 25(8): p. 1963-1969.
353. Le Saux, Guillaume, Astrid Magenau, Till Böcking, Katharina Gaus, and J Justin Gooding, *The relative importance of topography and rgd ligand density for endothelial cell adhesion.* PloS one, 2011. 6(7): p. e21869.
354. Parviz, Maryam, Katharina Gaus, and J Justin Gooding, *Simultaneous impedance spectroscopy and fluorescence microscopy for the real-time monitoring of the response of cells to drugs.* Chemical science, 2017. 8(3): p. 1831-1840.
355. Huang, Jinghuan, Stefan V Grater, Francesca Corbellini, Sabine Rinck, Eva Bock, Ralf Kemkemer, Horst Kessler, Jiandong Ding, and Joachim P Spatz, *Impact of order and disorder in rgd nanopatterns on cell adhesion.* Nano letters, 2009. 9(3): p. 1111-1116.
356. Gailit, James and Richard AF Clark, *Studies in vitro on the role of αv and β1 integrins in the adhesion of human dermal fibroblasts to provisional matrix proteins fibronectin, vitronectin, and fibrinogen.* Journal of Investigative Dermatology, 1996. 106(1): p. 102-108.
357. Lo, Chun-Min, Charles R Keese, and Ivar Giaever, *Monitoring motion of confluent cells in tissue culture.* Experimental cell research, 1993. 204(1): p. 102-109.
358. Attwood, Simon J, Ernesto Cortes, Alexander William M Haining, Benjamin Robinson, Danyang Li, Julien Gautrot, and Armando del Río Hernández, *Adhesive ligand tether length affects the size and length of focal adhesions and influences cell spreading and attachment.* Scientific reports, 2016. 6: p. 34334.
359. Massia, Stephen P, Matthew M Holecko, and Gholam R Ehteshami, *In vitro assessment of bioactive coatings for neural implant applications.* Journal of Biomedical Materials Research Part A, 2004. 68(1): p. 177-186.
360. Kilian, Kristopher A and Milan Mrksich, *Directing stem cell fate by controlling the affinity and density of ligand–receptor interactions at the biomaterials interface.* Angewandte Chemie International Edition, 2012. 51(20): p. 4891-4895.
361. Liu, BF, J Ma, QY Xu, and FZ Cui, *Regulation of charged groups and laminin patterns for selective neuronal adhesion.* Colloids and Surfaces B: Biointerfaces, 2006. 53(2): p. 175-178.
362. Ingber, Donald E, *The riddle of morphogenesis: A question of solution chemistry or molecular cell engineering?* cell, 1993. 75(7): p. 1249-1252.
363. Farrukh, Aleeza, Julieta I Paez, Marcelo Salierno, Wenqiang Fan, Benedikt Berninger, and Aránzazu del Campo, *Bifunctional poly (acrylamide) hydrogels through orthogonal coupling chemistries.* Biomacromolecules, 2017. 18(3): p. 906-913.

364. Jucker, M, HK Kleinman, and DK Ingram, *Fetal rat septal cells adhere to and extend processes on basement membrane, laminin, and a synthetic peptide from the laminin a chain sequence.* Journal of neuroscience research, 1991. 28(4): p. 507-517.
365. Kibbey, Maura C, Mathias Jucker, Benjamin S Weeks, Rachael L Neve, Wiliam E Van Nostrand, and Hynda K Kleinman, *Beta-amyloid precursor protein binds to the neurite-promoting ikvav site of laminin.* Proceedings of the National Academy of Sciences, 1993. 90(21): p. 10150-10153.
366. Liesi, Paivi, *Do neurons in the vertebrate cns migrate on laminin?* The EMBO journal, 1985. 4(5): p. 1163-1170.
367. Nirwane, Abhijit and Yao Yao, *Laminins and their receptors in the cns.* Biological Reviews, 2019. 94(1): p. 283-306.
368. Temming, Kai, Raymond M Schiffelers, Grietje Molema, and Robbert J Kok, *Rgd-based strategies for selective delivery of therapeutics and imaging agents to the tumour vasculature.* Drug resistance updates, 2005. 8(6): p. 381-402.
369. Andersson, Ann-Sofie, Karin Glasmästar, Duncan Sutherland, Ulf Lidberg, and Bengt Kasemo, *Cell adhesion on supported lipid bilayers.* Journal of Biomedical Materials Research Part A, 2003. 64(4): p. 622-629.
370. Kam, Lance and Steven G Boxer, *Cell adhesion to protein-micropatterned-supported lipid bilayer membranes.* Journal of biomedical materials research, 2001. 55(4): p. 487-495.
371. Ostuni, Emanuele, Robert G Chapman, Michael N Liang, Gloria Meluleni, Gerald Pier, Donald E Ingber, and George M Whitesides, *Self-assembled monolayers that resist the adsorption of proteins and the adhesion of bacterial and mammalian cells.* Langmuir, 2001. 17(20): p. 6336-6343.
372. Stroumpoulis, Dimitrios, Haining Zhang, Leticia Rubalcava, Jill Gliem, and Matthew Tirrell, *Cell adhesion and growth to peptide-patterned supported lipid membranes.* Langmuir, 2007. 23(7): p. 3849-3856.
373. Li, Jianjun, Dong Han, and Ya-Pu Zhao, *Kinetic behaviour of the cells touching substrate: The interfacial stiffness guides cell spreading.* Scientific reports, 2014. 4: p. 3910.
374. Trappmann, Britta, Julien E Gautrot, John T Connelly, Daniel GT Strange, Yuan Li, Michelle L Oyen, Martien A Cohen Stuart, Heike Boehm, Bojun Li, and Viola Vogel, *Extracellular-matrix tethering regulates stem-cell fate.* Nature materials, 2012. 11(7): p. 642.
375. Fu, Jianping, Yang-Kao Wang, Michael T Yang, Ravi A Desai, Xiang Yu, Zhijun Liu, and Christopher S Chen, *Mechanical regulation of cell function with geometrically modulated elastomeric substrates.* Nature methods, 2010. 7(9): p. 733.
376. Maheshwari, Gargi, Gillian Brown, Douglas A Lauffenburger, Alan Wells, and Linda G Griffith, *Cell adhesion and motility depend on nanoscale rgd clustering.* J Cell Sci, 2000. 113(10): p. 1677-1686.
377. Asati, Saket, Vikas Pandey, and Vandana Soni, *Rgd peptide as a targeting moiety for theranostic purpose: An update study.* International Journal of Peptide Research and Therapeutics, 2019. 25(1): p. 49-65.
378. Saxena, Tarun, Lohitash Karumbaiah, Eric A Gaupp, Radhika Patkar, Ketki Patil, Martha Betancur, Garrett B Stanley, and Ravi V Bellamkonda, *The impact of chronic blood–brain barrier breach on intracortical electrode function.* Biomaterials, 2013. 34(20): p. 4703-4713.

379. Cranfield, Charles G, Thomas Berry, Stephen A Holt, Khondker R Hossain, Anton P Le Brun, Sonia Carne, Heba Al Khamici, Hans Coster, Stella M Valenzuela, and Bruce Cornell, *Evidence of the key role of h3o+ in phospholipid membrane morphology.* Langmuir, 2016. 32(41): p. 10725-10734.
380. Zhang, Xudong, William Wang, Anis Nurashikin Nordin, Fang Li, Sunghoon Jang, and Ioana Voiculescu, *The influence of the electrode dimension on the detection sensitivity of electric cell–substrate impedance sensing (ecis) and its mathematical modeling.* Sensors and Actuators B: Chemical, 2017. 247: p. 780-790.
381. Geddes, Leslie A and R Roeder, *Criteria for the selection of materials for implanted electrodes.* Annals of biomedical engineering, 2003. 31(7): p. 879-890.
382. Campbell, Patrick K, Kelly E Jones, Robert J Huber, Kenneth W Horch, and Richard A Normann, *A silicon-based, three-dimensional neural interface: Manufacturing processes for an intracortical electrode array.* IEEE Transactions on Biomedical Engineering, 1991. 38(8): p. 758-768.
383. Lawand, NS, PJ French, JJ Briaire, and JHM Frijns. *Long term cochlear implant electrode improvement for stimulation and sensing neuronal activity*. in *2012 Sixth International Conference on Sensing Technology (ICST)*. 2012. IEEE.
384. Neuburger, J, T Lenarz, A Lesinski-Schiedat, and A Büchner, *Spontaneous increases in impedance following cochlear implantation: Suspected causes and management.* International journal of audiology, 2009. 48(5): p. 233-239.
385. Wingren, Christer and Carl AK Borrebaeck, *Antibody microarrays: Current status and key technological advances.* Omics: a journal of integrative biology, 2006. 10(3): p. 411-427.
386. Koeppe, RE and OS Anderson, *Engineering the gramicidin channel.* Annual review of biophysics and biomolecular structure, 1996. 25(1): p. 231-258.
387. Sarges, Reinhard and Bernhard Witkop, *Gramicidin. Viii. The structure of valine- and isoleucine-gramicidin c.* Biochemistry, 1965. 4(11): p. 2491-2494.
388. Sarges, Reinhard and Bernhard Witkop, *Gramicidin av the structure of valine-and isoleucine-gramicidin a.* Journal of the American Chemical Society, 1965. 87(9): p. 2011-2020.
389. Mukherjee, Sushmita and Amitabha Chattopadhyay, *Motionally restricted tryptophan environments at the peptide-lipid interface of gramicidin channels.* Biochemistry, 1994. 33(17): p. 5089-5097.
390. Kelkar, Devaki A and Amitabha Chattopadhyay, *The gramicidin ion channel: A model membrane protein.* Biochimica et Biophysica Acta (BBA)-Biomembranes, 2007. 1768(9): p. 2011-2025.
391. Bamberg, E, K Noda, and P Läuger, *Single-channel parameters of gramicidin a, b, and c.* Biochimica et Biophysica Acta (BBA)-Biomembranes, 1976. 419(2): p. 223-228.
392. Becker, Murray D, RE Koeppe, and OS Andersen, *Amino acid substitutions and ion channel function. Model-dependent conclusions.* Biophysical journal, 1992. 62(1): p. 25-27.
393. Chattopadhyay, Amitabha, Satinder S Rawat, Denise V Greathouse, Devaki A Kelkar, and Roger E Koeppe II, *Role of tryptophan residues in gramicidin channel organization and function.* Biophysical journal, 2008. 95(1): p. 166-175.
394. Clayton, Andrew HA and William H Sawyer, *Tryptophan rotamer distributions in amphipathic peptides at a lipid surface.* Biophysical journal, 1999. 76(6): p. 3235-3242.

395. White, Stephen H and William C Wimley, *Hydrophobic interactions of peptides with membrane interfaces.* Biochimica et Biophysica Acta (BBA)-Reviews on Biomembranes, 1998. 1376(3): p. 339-352.
396. Yau, Wai-Ming, William C Wimley, Klaus Gawrisch, and Stephen H White, *The preference of tryptophan for membrane interfaces.* Biochemistry, 1998. 37(42): p. 14713-14718.
397. Rokitskaya, TI, Yuri N Antonenko, and Elena A Kotova, *Effect of the dipole potential of a bilayer lipid membrane on gramicidin channel dissociation kinetics.* Biophysical journal, 1997. 73(2): p. 850-854.
398. Bamberg, E, HJ Apell, and H Alpes, *Structure of the gramicidin a channel: Discrimination between the πl, d and the β helix by electrical measurements with lipid bilayer membranes.* Proceedings of the National Academy of Sciences, 1977. 74(6): p. 2402-2406.
399. Fonseca, V, P Daumas, L Ranjalahy-Rasoloarijao, F Heitz, R Lazaro, Y Trudelle, and OS Andersen, *Gramicidin channels that have no tryptophan residues.* Biochemistry, 1992. 31(23): p. 5340-5350.
400. Wallace, BA, *Structure of gramicidin a.* Biophysical journal, 1986. 49(1): p. 295-306.
401. Lomize, A. L., VIu Orekhov, and A. S. Arsen'ev, *[refinement of the spatial structure of the gramicidin a ion channel]*. Bioorg Khim, 1992. 18(2): p. 182-200.
402. Andersen, Olaf S, C Nielsen, Andreia M Maer, Jens A Lundbæk, Mark Goulian, and Roger E Koeppe II, *[10] ion channels as tools to monitor lipid bilayer-membrane protein interactions: Gramicidin channels as molecular force transducers*, in *Methods in enzymology*. 1999, Elsevier. p. 208-224.
403. Urban, BW, SB Hladky, and DA Haydon, *Ion movements in gramicidin pores. An example of single-file transport.* Biochimica et Biophysica Acta (BBA)-Biomembranes, 1980. 602(2): p. 331-354.
404. Hladky, SB and DA Haydon, *Discreteness of conductance change in bimolecular lipid membranes in the presence of certain antibiotics.* Nature, 1970. 225(5231): p. 451.
405. Sandblom, John, Juris Galvanovskis, and Barbro Jilderos, *Voltage-dependent formation of gramicidin channels in lipid bilayers.* Biophysical journal, 2001. 81(2): p. 827-837.
406. Ring, Avi, *Influence of ion occupancy and membrane deformation on gramicidin a channel stability in lipid membranes.* Biophysical journal, 1992. 61(5): p. 1306-1315.
407. Haydon, DA and JR Elliott, *Surface potential changes in lipid monolayers and the 'cut-off'in anaesthetic effects of n-alkanols.* Biochimica et Biophysica Acta (BBA)-Biomembranes, 1986. 863(2): p. 337-340.
408. Wanasundara, Surajith N, Vikram Krishnamurthy, and Shin-Ho Chung, *Free energy calculations of gramicidin dimer dissociation.* The Journal of Physical Chemistry B, 2011. 115(46): p. 13765-13770.
409. Rudnev, VS, LN Ermishkin, LA Fonina, and Yu G Rovin, *The dependence of the conductance and lifetime of gramicidin channels on the thickness and tension of lipid bilayers.* Biochimica et Biophysica Acta (BBA)-Biomembranes, 1981. 642(1): p. 196-202.
410. Moradi-Monfared, Sahar, Vikram Krishnamurthy, and Bruce Cornell, *A molecular machine biosensor: Construction, predictive models and experimental studies.* Biosensors and Bioelectronics, 2012. 34(1): p. 261-266.

411. Green, NM, *Avidin. 3. The nature of the biotin-binding site.* Biochemical Journal, 1963. 89(3): p. 599.
412. Le Trong, Isolde, Nicolas Humbert, Thomas R Ward, and Ronald E Stenkamp, *Crystallographic analysis of a full-length streptavidin with its c-terminal polypeptide bound in the biotin binding site.* Journal of molecular biology, 2006. 356(3): p. 738-745.
413. Sano, T, MW Pandori, X Chen, CL Smith, and CR Cantor, *Advances in biomagnetic separation, eds.* Uhlén, M., Hornes, E. & Olsvik, O.(Eaton, Natick, MA), 1994: p. 21-29.
414. Peters, Verena and Bernd HA Rehm, *Protein engineering of streptavidin for in vivo assembly of streptavidin beads.* Journal of biotechnology, 2008. 134(3-4): p. 266-274.
415. Albelda, STEVEN M and Clayton A Buck, *Integrins and other cell adhesion molecules.* The FASEB Journal, 1990. 4(11): p. 2868-2880.
416. Wattam, B, D Shang, S Rahman, S Egglezou, M Scully, V Kakkar, and X Lu *Arg-tyr-asp (ryd) and arg-cys-asp (rcd) motifs in dendroaspin promote selective inhibition of beta1 and beta3 integrins*. The Biochemical journal, 2001. 356, 11-17.
417. Guo, C.X., S.R. Ng, S.Y. Khoo, X. Zheng, P. Chen, and C.M. Li *Rgd-peptide functionalized graphene biomimetic live-cell sensor for real-time detection of nitric oxide molecules*. ACS nano, 2012. 6, 6944-6951.
418. Xiao, Lifu, Hao Wang, and Zachary D Schultz, *Selective detection of rgd-integrin binding in cancer cells using tip enhanced raman scattering microscopy.* Analytical chemistry, 2016. 88(12): p. 6547-6553.
419. Clark, Edwin A and Joan S Brugge, *Integrins and signal transduction pathways: The road taken.* Science, 1995. 268(5208): p. 233-239.
420. Hynes, Richard O, *Integrins: Versatility, modulation, and signaling in cell adhesion.* cell, 1992. 69(1): p. 11-25.
421. Xiao, Yao and George A Truskey, *Effect of receptor-ligand affinity on the strength of endothelial cell adhesion.* Biophysical journal, 1996. 71(5): p. 2869-2884.
422. Ilic, B, D Czaplewski, M Zalalutdinov, HG Craighead, P Neuzil, C Campagnolo, and C Batt, *Single cell detection with micromechanical oscillators.* Journal of Vacuum Science & Technology B: Microelectronics and Nanometer Structures Processing, Measurement, and Phenomena, 2001. 19(6): p. 2825-2828.
423. Alon, Ronen, Edward A Bayer, and Meir Wilchek, *Streptavidin contains an ryd sequence which mimics the rgd receptor domain of fibronectin.* Biochemical and biophysical research communications, 1990. 170(3): p. 1236-1241.
424. Kunicki, Thomas J, Kathryn R Ely, Thomas C Kunicki, Yoshiaki Tomiyama, and Douglas S Annis, *The exchange of arg-gly-asp (rgd) and arg-tyr-asp (ryd) binding sequences in a recombinant murine fab fragment specific for the integrin αiibβ3 does not alter integrin recognition.* Journal of Biological Chemistry, 1995. 270(28): p. 16660-16665.
425. Seed, Brian and Gerd Walz, *Inhibition of cell adhesion protein-carbohydrate interactions*. 1999, Google Patents.
426. Disney, Matthew D and Peter H Seeberger, *The use of carbohydrate microarrays to study carbohydrate-cell interactions and to detect pathogens.* Chemistry & biology, 2004. 11(12): p. 1701-1707.
427. Gunther, Gary R, John L Wang, Ichiro Yahara, Bruce A Cunningham, and Gerald M Edelman, *Concanavalin a derivatives with altered biological activities.* Proceedings of the National Academy of Sciences, 1973. 70(4): p. 1012-1016.

428. Naismith, James H and Robert A Field, *Structural basis of trimannoside recognition by concanavalin a.* Journal of Biological Chemistry, 1996. 271(2): p. 972-976.
429. Matta, Leann Lerie, Johnathan Harrison, Gurveer Singh Deol, and Evangelyn C Alocilja, *Carbohydrate-functionalized nanobiosensor for rapid extraction of pathogenic bacteria directly from complex liquids with quick detection using cyclic voltammetry.* IEEE transactions on nanotechnology, 2018. 17(5): p. 1006-1013.
430. Disney, Matthew D. and Peter H. Seeberger *The use of carbohydrate microarrays to study carbohydrate-cell interactions and to detect pathogens*. Chemistry & biology, 2004. 11, 1701-1707.
431. Yang, Haiying, Yaqin Wang, Honglan Qi, Qiang Gao, and Chengxiao Zhang *Electrogenerated chemiluminescence biosensor incorporating ruthenium complex-labelled concanavalin a as a probe for the detection of escherichia coli*. Biosensors and Bioelectronics, 2012. 35, 376-381.
432. Trowbridge, Ian S, Jayne Lesley, Roberta Schulte, Robert Hyman, and Joseph Trotter, *Biochemical characterization and cellular distribution of a polymorphic, murine cell-surface glycoprotein expressed on lymphoid tissues.* Immunogenetics, 1982. 15(3): p. 299-312.
433. Shylaja, M and HS Seshadri, *Glycoproteins: An overview.* Biochemical Education, 1989. 17(4): p. 170-178.
434. Pasqualini, Renata, Erkki Koivunen, and Erkki Ruoslahti, *A peptide isolated from phage display libraries is a structural and functional mimic of an rgd-binding site on integrins.* The Journal of cell biology, 1995. 130(5): p. 1189-1196.
435. Arza, Begoña and Jordi Félez, *The emerging impact of phage display technology in thrombosis and haemostasis.* Thrombosis and haemostasis, 1998. 80(09): p. 354-362.
436. Abelès, Florin, *La théorie générale des couches minces.* Journal de Physique et le Radium, 1950. 11(7): p. 307-309.
437. Rasband, WS, *Imagej (software). Us national institutes of health, bethesda, maryland, USA*. 1997.
438. Katoh, Kazunobu, Hiroshi Mohri, Kouji Ogawa, and Takao Okubo, *Human plasma fibronectin mediates adhesion of u937 cells by rgd and cs1.* Journal of thrombosis and thrombolysis, 1998. 5(2): p. 129-134.
439. Monfared, Sahar M, Vikram Krishnamurthy, and Bruce Cornell. *Mathematical modeling of a tethered bilayer sensor containing gramicidin a ion channels*. in *2009 Annual International Conference of the IEEE Engineering in Medicine and Biology Society*. 2009. IEEE.
440. Imada, Sumi and Masaru Imada, *Increase of a surface glycoprotein by cyclic amp in chinese hamster ovary cells. Dependence on cell-cell interaction.* Journal of Biological Chemistry, 1982. 257(15): p. 9108-9113.
441. Weinacker, Ann, AILEEN Chen, M Agrez, RI Cone, S Nishimura, E Wayner, R Pytela, and D Sheppard, *Role of the integrin alpha v beta 6 in cell attachment to fibronectin. Heterologous expression of intact and secreted forms of the receptor.* Journal of Biological Chemistry, 1994. 269(9): p. 6940-6948.
442. Lawrence, Paul, Michael LaRocco, Barry Baxt, and Elizabeth Rieder, *Examination of soluble integrin resistant mutants of foot-and-mouth disease virus.* Virology journal, 2013. 10(1): p. 2.

443. Lawler, Jack, Robert Weinstein, and Richard O Hynes, *Cell attachment to thrombospondin: The role of arg-gly-asp, calcium, and integrin receptors.* The Journal of cell biology, 1988. 107(6): p. 2351-2361.
444. Pucillo, CE, A Colombatti, M Vitale, S Salzano, G Rossi, and S Formisano, *Interactions of promonocytic u937 cells with proteins of the extracellular matrix.* Immunology, 1993. 80(2): p. 248.
445. Lichtenthaler, Stefan F, Diana-ines Dominguez, Gil G Westmeyer, Karina Reiss, Christian Haass, Paul Saftig, Bart De Strooper, and Brian Seed, *The cell adhesion protein p-selectin glycoprotein ligand-1 is a substrate for the aspartyl protease bace1.* Journal of Biological Chemistry, 2003. 278(49): p. 48713-48719.
446. Tandon, Narendra N, Robert H Lipsky, Wilson H Burgess, and GA Jamieson, *Isolation and characterization of platelet glycoprotein iv (cd36).* Journal of Biological Chemistry, 1989. 264(13): p. 7570-7575.
447. Ryu, Hyunil, Hwankyu Lee, Seigo Iwata, Sangbaek Choi, Moon Ki Kim, Young-Rok Kim, Shinsaku Maruta, Sun Min Kim, and Tae-Joon Jeon, *Investigation of ion channel activities of gramicidin a in the presence of ionic liquids using model cell membranes.* Scientific reports, 2015. 5: p. 11935.
448. Petersen, Svea, José María Alonso, Alexandre Specht, Portia Duodu, Maurice Goeldner, and Aranzazu del Campo, *Phototriggering of cell adhesion by caged cyclic rgd peptides.* Angewandte Chemie, 2008. 120(17): p. 3236-3239.
449. Gersthagen, Thomas, Carsten Schmuck, and Thomas Schrader, *Artificial rgd receptor molecules.* Supramolecular Chemistry, 2010. 22(11-12): p. 853-861.
450. Sun, Tiantong, Zhentao Man, Changliang Peng, Guozong Wang, and Shui Sun, *A specific affinity cyclic peptide enhances the adhesion, expansion and proliferation of rat bone mesenchymal stem cells on β-tricalcium phosphate scaffolds.* Molecular medicine reports, 2019.
451. Cortese, Riccardo, Paolo Monaci, Alessandra Luzzago, Claudia Santini, Fabrizia Bartoli, Irene Cortese, Paola Fortugno, Giovanni Galfrè, Alfredo Nicosia, and Franco Felici, *Selection of biologically active peptides by phage display of random peptide libraries.* Current opinion in biotechnology, 1996. 7(6): p. 616-621.
452. Hong, Saw See and Pierre Boulanger, *Protein ligands of the human adenovirus type 2 outer capsid identified by biopanning of a phage-displayed peptide library on separate domains of wild-type and mutant penton capsomers.* The EMBO journal, 1995. 14(19): p. 4714-4727.
453. Dundas, Christopher M, Daniel Demonte, and Sheldon Park, *Streptavidin–biotin technology: Improvements and innovations in chemical and biological applications.* Applied microbiology and biotechnology, 2013. 97(21): p. 9343-9353.
454. Lee, Jie-Oh, Philippe Rieu, M Amin Arnaout, and Robert Liddington, *Crystal structure of the a domain from the a subunit of integrin cr3 (cd11 b/cd18).* cell, 1995. 80(4): p. 631-638.
455. Cierniewski, Czeslaw S, Tatiana Byzova, Malgorzata Papierak, Thomas A Haas, Jolanta Niewiarowska, Li Zhang, Marcin Cieslak, and Edward F Plow, *Peptide ligands can bind to distinct sites in integrin αiibβ3 and elicit different functional responses.* Journal of Biological Chemistry, 1999. 274(24): p. 16923-16932.
456. Rensing, Stephan, Markus Arendt, Andreas Springer, Thomas Grawe, and Thomas Schrader, *Optimization of a synthetic arginine receptor. Systematic tuning of noncovalent interactions.* The Journal of organic chemistry, 2001. 66(17): p. 5814-5821.

457. Gobin, André M, Min Ho Lee, Naomi J Halas, William D James, Rebekah A Drezek, and Jennifer L West, *Near-infrared resonant nanoshells for combined optical imaging and photothermal cancer therapy.* Nano letters, 2007. 7(7): p. 1929-1934.
458. Jackson, Joseph B and Naomi J Halas, *Surface-enhanced raman scattering on tunable plasmonic nanoparticle substrates.* Proceedings of the National Academy of Sciences, 2004. 101(52): p. 17930-17935.
459. Emelianov, Stanislav Y, Pai-Chi Li, and Matthew O'Donnell, *Photoacoustics for molecular imaging and therapy.* Physics today, 2009. 62(8): p. 34.
460. Pissuwan, Dakrong, Stella M Valenzuela, and Michael B Cortie, *Therapeutic possibilities of plasmonically heated gold nanoparticles.* TRENDS in Biotechnology, 2006. 24(2): p. 62-67.
461. Her, Sohyoung, David A Jaffray, and Christine Allen, *Gold nanoparticles for applications in cancer radiotherapy: Mechanisms and recent advancements.* Advanced drug delivery reviews, 2017. 109: p. 84-101.
462. Alkilany, Alaaldin M and Catherine J Murphy, *Toxicity and cellular uptake of gold nanoparticles: What we have learned so far?* Journal of Nanoparticle Research, 2010. 12(7): p. 2313-2333.
463. Schmidbaur, Hubert, *The fascinating implications of new results in gold chemistry.* Gold Bulletin, 1990. 23(1): p. 11-21.
464. Cortie, MB and E Van der Lingen. *Catalytic gold nano-particles*. in *Materials Forum*. 2002.
465. Myroshnychenko, Viktor, Jessica Rodríguez-Fernández, Isabel Pastoriza-Santos, Alison M Funston, Carolina Novo, Paul Mulvaney, Luis M Liz-Marzan, and F Javier García de Abajo, *Modelling the optical response of gold nanoparticles.* Chemical Society Reviews, 2008. 37(9): p. 1792-1805.
466. Jiang, Wen, Betty YS Kim, James T Rutka, and Warren CW Chan, *Nanoparticle-mediated cellular response is size-dependent.* Nature nanotechnology, 2008. 3(3): p. 145.
467. Gellner, M, M Schütz, M Salehi, J Packeisen, P Ströbel, A Marx, C Schmuck, and S Schlücker. *Sers microscopy: Plasmonic nanoparticle probes and biomedical applications*. in *Plasmonics: Metallic Nanostructures and Their Optical Properties VIII*. 2010. International Society for Optics and Photonics.
468. Huang, Xiaohua, Ivan H El-Sayed, Wei Qian, and Mostafa A El-Sayed, *Cancer cell imaging and photothermal therapy in the near-infrared region by using gold nanorods.* Journal of the American Chemical Society, 2006. 128(6): p. 2115-2120.
469. Richardson, Hugh H, Michael T Carlson, Peter J Tandler, Pedro Hernandez, and Alexander O Govorov, *Experimental and theoretical studies of light-to-heat conversion and collective heating effects in metal nanoparticle solutions.* Nano letters, 2009. 9(3): p. 1139-1146.
470. Huff, Terry B, Ling Tong, Yan Zhao, Matthew N Hansen, Ji-Xin Cheng, and Alexander Wei, *Hyperthermic effects of gold nanorods on tumor cells.* 2007.
471. Gannon, Christopher J, Chitta Ranjan Patra, Resham Bhattacharya, Priyabrata Mukherjee, and Steven A Curley, *Intracellular gold nanoparticles enhance non-invasive radiofrequency thermal destruction of human gastrointestinal cancer cells.* Journal of nanobiotechnology, 2008. 6(1): p. 2.
472. Johannsen, Manfred, U Gneveckow, L Eckelt, A Feussner, N Waldöfner, R Scholz, S Deger, P Wust, SA Loening, and A Jordan, *Clinical hyperthermia of prostate*

cancer using magnetic nanoparticles: Presentation of a new interstitial technique. International journal of hyperthermia, 2005. 21(7): p. 637-647.
473. Kelly, K Lance, Eduardo Coronado, Lin Lin Zhao, and George C Schatz, *The optical properties of metal nanoparticles: The influence of size, shape, and dielectric environment*. 2003, ACS Publications.
474. Jain, Prashant K, Kyeong Seok Lee, Ivan H El-Sayed, and Mostafa A El-Sayed, *Calculated absorption and scattering properties of gold nanoparticles of different size, shape, and composition: Applications in biological imaging and biomedicine.* The Journal of Physical Chemistry B, 2006. 110(14): p. 7238-7248.
475. Link, Stephan and Mostafa A El-Sayed, *Shape and size dependence of radiative, non-radiative and photothermal properties of gold nanocrystals.* International reviews in physical chemistry, 2000. 19(3): p. 409-453.
476. Link, Stephan and Mostafa A El-Sayed, *Spectral properties and relaxation dynamics of surface plasmon electronic oscillations in gold and silver nanodots and nanorods*. 1999, ACS Publications.
477. http://www.cytodiagnostics.com/store/pc/Gold-NanoUrchins-c214.htm, Cytodiagnostics Pty Ltd.
478. Zheng, Mingbin, Ze Chen, Zhenyu Luo, Pengfei Zhao, Ping Gong, and Lintao Cai *Cancer cell membrance-functionalized nanoparticles for homotypic-targeted cancer imaging and highly effective photothermal therapy*. Nanomedicine: Nanotechnology, Biology, and Medicine, 2016. 12, 488-488.
479. Kennedy, Laura C, Lissett R Bickford, Nastassja A Lewinski, Andrew J Coughlin, Ying Hu, Emily S Day, Jennifer L West, and Rebekah A Drezek, *A new era for cancer treatment: Gold-nanoparticle-mediated thermal therapies.* Small, 2011. 7(2): p. 169-183.
480. Jain, S, DG Hirst, and JM O'sullivan, *Gold nanoparticles as novel agents for cancer therapy.* The British journal of radiology, 2012. 85(1010): p. 101-113.
481. Hahn, Megan, Amit Singh, Parvesh Sharma, Scott Brown, and Brij Moudgil *Nanoparticles as contrast agents for in-vivo bioimaging: Current status and future perspectives*. Anal Bioanal Chem, 2011. 399, 3-27.
482. Pissuwan, Dakrong, Stella M Valenzuela, Murray C Killingsworth, Xiaoda Xu, and Michael B Cortie, *Targeted destruction of murine macrophage cells with bioconjugated gold nanorods.* Journal of Nanoparticle Research, 2007. 9(6): p. 1109-1124.
483. Pissuwan, Dakrong, Stella M Valenzuela, Catherine M Miller, and Michael B Cortie, *A golden bullet? Selective targeting of toxoplasma gondii tachyzoites using antibody-functionalized gold nanorods.* Nano letters, 2007. 7(12): p. 3808-3812.
484. Delp, Scott L, Michael E Llewellyn, Karl Deisseroth, and Christine A McLeavey Payne, *Materials and approaches for optical stimulation of the peripheral nervous system*. 2015, Google Patents.
485. Yong, Jiawey, Karina Needham, William GA Brown, Bryony A Nayagam, Sally L McArthur, Aimin Yu, and Paul R Stoddart, *Gold-nanorod-assisted near-infrared stimulation of primary auditory neurons.* Advanced healthcare materials, 2014. 3(11): p. 1862-1868.
486. Yoo, Sangjin, Soonwoo Hong, Yeonho Choi, Ji-Ho Park, and Yoonkey Nam, *Photothermal inhibition of neural activity with near-infrared-sensitive nanotransducers.* ACS nano, 2014. 8(8): p. 8040-8049.
487. Lukianova-Hleb, Ekaterina Y, Leslie E Huye, Malcolm K Brenner, and Dmitri O Lapotko. *Plasmonic nanobubbles for target cell-specific gene and drug delivery*

and multifunctional processing of heterogeneous cell systems. in *Frontiers in Ultrafast Optics: Biomedical, Scientific, and Industrial Applications XIV*. 2014. International Society for Optics and Photonics.
488. Han, Gang, Partha Ghosh, and Vincent M Rotello, *Functionalized gold nanoparticles for drug delivery.* 2007.
489. Zhang, Hua-Gang, Keyur Mehta, Patrice Cohen, and Chandan Guha, *Hyperthermia on immune regulation: A temperature's story.* Cancer letters, 2008. 271(2): p. 191-204.
490. Urban, Patrick, Silke R Kirchner, Christian Mühlbauer, Theobald Lohmüller, and Jochen Feldmann, *Reversible control of current across lipid membranes by local heating.* Scientific reports, 2016. 6: p. 22686.
491. Palankar, Raghavendra, Bat-El Pinchasik, Boris N Khlebtsov, Tatiana A Kolesnikova, Helmuth Möhwald, Mathias Winterhalter, and Andre G Skirtach, *Nanoplasmonically-induced defects in lipid membrane monitored by ion current: Transient nanopores versus membrane rupture.* Nano letters, 2014. 14(8): p. 4273-4279.
492. Bendix, Poul M, S Nader S Reihani, and Lene B Oddershede, *Direct measurements of heating by electromagnetically trapped gold nanoparticles on supported lipid bilayers.* ACS nano, 2010. 4(4): p. 2256-2262.
493. Plaksin, Michael, Einat Shapira, Eitan Kimmel, and Shy Shoham, *Thermal transients excite neurons through universal intramembrane mechanoelectrical effects.* Physical Review X, 2018. 8(1): p. 011043.
494. Urban, AS, M Fedoruk, MR Horton, JO Radler, FD Stefani, and J Feldmann, *Controlled nanometric phase transitions of phospholipid membranes by plasmonic heating of single gold nanoparticles.* Nano letters, 2009. 9(8): p. 2903-2908.
495. Lösche, M and Helmuth Möhwald, *Impurity controlled phase transitions of phospholipid monolayers.* European Biophysics Journal, 1984. 11(1): p. 35-42.
496. Hoiles, William, Vikram Krishnamurthy, Charles G Cranfield, and Bruce Cornell, *An engineered membrane to measure electroporation: Effect of tethers and bioelectronic interface.* Biophysical journal, 2014. 107(6): p. 1339-1351.
497. Dufourc, Erick *Sterols and membrane dynamics*. J Chem Biol, 2008. 1, 63-77.
498. Piñol, Rafael, Carlos DS Brites, Nuno J Silva, Luis D Carlos, and Angel Millán, *Nanoscale thermometry for hyperthermia applications*, in *Nanomaterials for magnetic and optical hyperthermia applications*. 2019, Elsevier. p. 139-172.
499. Wang, Fu Xiang, Francisco J Rodríguez, Willem M Albers, Risto Ahorinta, JE Sipe, and Martti Kauranen, *Surface and bulk contributions to the second-order nonlinear optical response of a gold film.* Physical Review B, 2009. 80(23): p. 233402.
500. Clair, Johnna Wellman St and Erwin London, *Effect of sterol structure on ordered membrane domain (raft) stability in symmetric and asymmetric vesicles.* Biochimica et Biophysica Acta (BBA)-Biomembranes, 2019.
501. Tillman, Tommy S and Michael Cascio, *Effects of membrane lipids on ion channel structure and function.* Cell biochemistry and biophysics, 2003. 38(2): p. 161-190.
502. Beugin-Deroo, Sophie, Michel Ollivon, and Sylviane Lesieur, *Bilayer stability and impermeability of nonionic surfactant vesicles sterically stabilized by peg–cholesterol conjugates.* Journal of colloid and interface science, 1998. 202(2): p. 324-333.
503. Kendall, James KR, Benjamin RG Johnson, Philip H Symonds, Guiseppi Imperato, Richard J Bushby, James D Gwyer, Cees van Berkel, Stephen D Evans, and Lars

JC Jeuken, *Effect of the structure of cholesterol-based tethered bilayer lipid membranes on ionophore activity.* ChemPhysChem, 2010. 11(10): p. 2191-2198.
504. Chen, Huanjun, Xiaoshan Kou, Zhi Yang, Weihai Ni, and Jianfang Wang, *Shape- and size-dependent refractive index sensitivity of gold nanoparticles.* Langmuir, 2008. 24(10): p. 5233-5237.
505. Oldenburg, SJ, RD Averitt, SL Westcott, and NJ Halas, *Nanoengineering of optical resonances.* Chemical Physics Letters, 1998. 288(2-4): p. 243-247.
506. Jans, Hilde, Xiong Liu, Lauren Austin, Guido Maes, and Qun Huo, *Dynamic light scattering as a powerful tool for gold nanoparticle bioconjugation and biomolecular binding studies.* Analytical chemistry, 2009. 81(22): p. 9425-9432.
507. Dykman, Lev and Nikolai Khlebtsov, *Gold nanoparticles in biomedical applications: Recent advances and perspectives.* Chemical Society Reviews, 2012. 41(6): p. 2256-2282.
508. Dombrovsky, Leonid A, Victoria Timchenko, Michael Jackson, and Guan H Yeoh, *A combined transient thermal model for laser hyperthermia of tumors with embedded gold nanoshells.* International Journal of Heat and Mass Transfer, 2011. 54(25-26): p. 5459-5469.
509. Dombrovsky, Leonid A, *Radiation heat transfer in disperse systems*. 1996, New York: Begell House.
510. Vernotte, Pierre, *Les paradoxes de la theorie continue de l'equation de la chaleur.* Compt. Rendu, 1958. 246: p. 3154-3155.
511. Cattaneo, Carlo, *A form of heat-conduction equations which eliminates the paradox of instantaneous propagation.* Comptes Rendus, 1958. 247: p. 431.
512. Penkauskas, Tadas and Giulio Preta, *Biological applications of tethered bilayer lipid membranes.* Biochimie, 2018.
513. Berry, Thomas, Debarun Dutta, Renxun Chen, Andrea Leong, Huixin Wang, William Alexander Donald, Maryam Parviz, Bruce Cornell, Mark Willcox, and Naresh Kumar, *The lipid membrane interactions of the cationic antimicrobial peptide chimeras melimine and cys-melimine.* Langmuir, 2018.
514. Robertson, Joseph WF, Marcel G Friedrich, Asmorom Kibrom, Wolfgang Knoll, Renate LC Naumann, and Dieter Walz, *Modeling ion transport in tethered bilayer lipid membranes. 1. Passive ion permeation.* The Journal of Physical Chemistry B, 2008. 112(34): p. 10475-10482.
515. Knoll, Wolfgang, Ingo Köper, Renate Naumann, and Eva-Kathrin Sinner, *Tethered bimolecular lipid membranes—a novel model membrane platform.* Electrochimica Acta, 2008. 53(23): p. 6680-6689.
516. Sévin-Landais, Anne, Per Rigler, Socrates Tzartos, Ferdinand Hucho, Ruud Hovius, and Horst Vogel, *Functional immobilisation of the nicotinic acetylcholine receptor in tethered lipid membranes.* Biophysical chemistry, 2000. 85(2-3): p. 141-152.
517. Rossi, Claire and Joël Chopineau, *Biomimetic tethered lipid membranes designed for membrane-protein interaction studies.* European Biophysics Journal, 2007. 36(8): p. 955-965.
518. Köper, Ingo, *Insulating tethered bilayer lipid membranes to study membrane proteins.* Molecular BioSystems, 2007. 3(10): p. 651-657.
519. Cornell, BA, VBL Braach-Maksvytis, LG King, PDJ Osman, B Raguse, L Wieczorek, and RJ Pace. *The gramicidin-based biosensor: A functioning nano-machine*. in *Novartis Foundation symposium*. 1999. Wiley Online Library.

520. Vockenroth, Inga K, Petia P Atanasova, Joanna R Long, A Toby A Jenkins, Wolfgang Knoll, and Ingo Köper, *Functional incorporation of the pore forming segment of achr m2 into tethered bilayer lipid membranes.* Biochimica et Biophysica Acta (BBA)-Biomembranes, 2007. 1768(5): p. 1114-1120.
521. Atanasov, Vladimir, Nikolaus Knorr, Randolph S Duran, Sven Ingebrandt, Andreas Offenhäusser, Wolfgang Knoll, and Ingo Köper, *Membrane on a chip: A functional tethered lipid bilayer membrane on silicon oxide surfaces.* Biophysical journal, 2005. 89(3): p. 1780-1788.
522. Gaus, Katharina, Soazig Le Lay, Nagaraj Balasubramanian, and Martin A Schwartz, *Integrin-mediated adhesion regulates membrane order.* The Journal of cell biology, 2006. 174(5): p. 725-734.
523. Eich, Christina, Carlo Manzo, Sandra De Keijzer, Gert-Jan Bakker, Inge Reinieren-Beeren, Maria F García-Parajo, and Alessandra Cambi, *Changes in membrane sphingolipid composition modulate dynamics and adhesion of integrin nanoclusters.* Scientific reports, 2016. 6: p. 20693.
524. Arnold, Marco, Elisabetta Ada Cavalcanti-Adam, Roman Glass, Jacques Blümmel, Wolfgang Eck, Martin Kantlehner, Horst Kessler, and Joachim P Spatz, *Activation of integrin function by nanopatterned adhesive interfaces.* ChemPhysChem, 2004. 5(3): p. 383-388.
525. Poole, Kate, Khaled Khairy, Jens Friedrichs, Clemens Franz, David A Cisneros, Jonathon Howard, and Daniel Mueller, *Molecular-scale topographic cues induce the orientation and directional movement of fibroblasts on two-dimensional collagen surfaces.* Journal of molecular biology, 2005. 349(2): p. 380-386.
526. Le Saux, Guillaume, Astrid Magenau, Krishanthi Gunaratnam, Kristopher A Kilian, Till Böcking, J Justin Gooding, and Katharina Gaus, *Spacing of integrin ligands influences signal transduction in endothelial cells.* Biophysical journal, 2011. 101(4): p. 764-773.
527. Hauser, Alan R, Joan Mecsas, and Donald T Moir, *Beyond antibiotics: New therapeutic approaches for bacterial infections.* Clinical Infectious Diseases, 2016. 63(1): p. 89-95.
528. Gizeli, Electra, Martha Liley, Christopher R Lowe, and Horst Vogel, *Antibody binding to a functionalized supported lipid layer: A direct acoustic immunosensor.* Analytical chemistry, 1997. 69(23): p. 4808-4813.
529. Botosoa, Eliot, Mike Maillasson, Marie Mougin-Degraef, Remaud-Le Saëc, Jean-François Gestin, Yannick Jacques, Jacques Barbet, and Alain Faivre-Chauvet, *Antibody-hapten recognition at the surface of functionalized liposomes studied by spr: Steric hindrance of pegylated phospholipids in stealth liposomes prepared for targeted radionuclide delivery.* Journal of drug delivery, 2011. 2011.
530. Benderitter, M, L Vincent-Genod, JP Pouget, and P Voisin, *The cell membrane as a biosensor of oxidative stress induced by radiation exposure: A multiparameter investigation.* Radiation research, 2003. 159(4): p. 471-483.
531. May, Kimberly ML, Yong Wang, Leonidas G Bachas, and Kimberly W Anderson, *Development of a whole-cell-based biosensor for detecting histamine as a model toxin.* Analytical chemistry, 2004. 76(14): p. 4156-4161.
532. Ahmad, Azrilawani and Eric J Moore, *Comparison of cell-based biosensors with traditional analytical techniques for cytotoxicity monitoring and screening of polycyclic aromatic hydrocarbons in the environment.* Analytical Letters, 2009. 42(1): p. 1-28.

533. Xu, Can, Shuo Hu, and Xiaoyuan Chen, *Artificial cells: From basic science to applications.* Materials Today, 2016. 19(9): p. 516-532.
534. Buddingh', Bastiaan C and Jan CM van Hest, *Artificial cells: Synthetic compartments with life-like functionality and adaptivity.* Accounts of chemical research, 2017. 50(4): p. 769-777.
535. Lentini, Roberta, Noël Yeh Martín, and Sheref S Mansy, *Communicating artificial cells.* Current opinion in chemical biology, 2016. 34: p. 53-61.
536. Fang, Ye, Anthony G Frutos, and Joydeep Lahiri, *Membrane protein microarrays.* Journal of the American Chemical Society, 2002. 124(11): p. 2394-2395.
537. Kam, Lance and Steven G Boxer, *Cell adhesion to protein-micropatterned-supported lipid bilayer membranes.* Journal of Biomedical Materials Research: An Official Journal of The Society for Biomaterials, The Japanese Society for Biomaterials, and The Australian Society for Biomaterials and the Korean Society for Biomaterials, 2001. 55(4): p. 487-495.
538. Zhang, Xiaoyan, Pascal Tanner, Alexandra Graff, Cornelia G Palivan, and Wolfgang Meier, *Mimicking the cell membrane with block copolymer membranes.* Journal of polymer science part A: polymer chemistry, 2012. 50(12): p. 2293-2318.
539. Amado, E and J Kressler, *Interactions of amphiphilic block copolymers with lipid model membranes.* Current Opinion in Colloid & Interface Science, 2011. 16(6): p. 491-498.
540. Deng, Yang, Yini Wang, Bryan Holtz, Jingyi Li, Nathan Traaseth, Gianluigi Veglia, Benjamin J Stottrup, Robert Elde, Duanqing Pei, and Athena Guo, *Fluidic and air-stable supported lipid bilayer and cell-mimicking microarrays.* Journal of the American Chemical Society, 2008. 130(19): p. 6267-6271.

Appendix

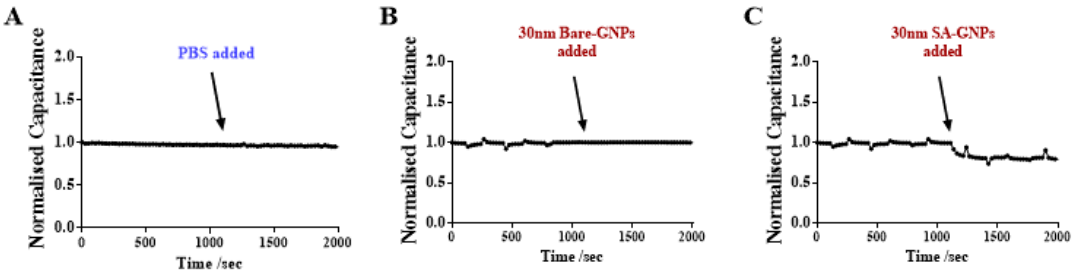

Figure S1: Figure 4.6 supplementary data: Capacitance changes across tBLMs arising from laser illumination (λ= 530 nm). (A) PBS buffer control; (B) Bare 30nm spherical GNPs; (C) Streptavidin-coated 30nmGNPs.

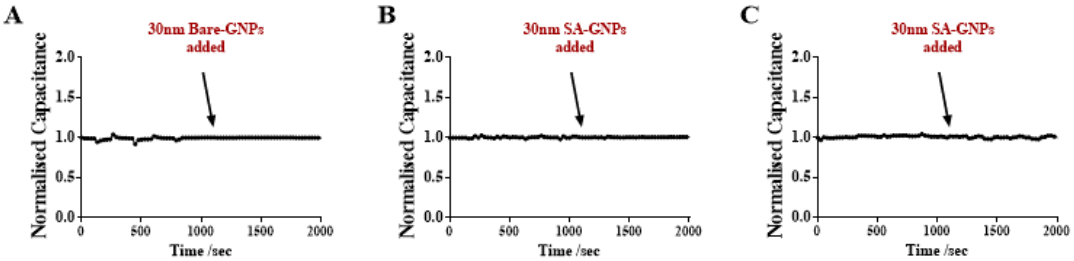

Figure S2: Figure 4.9 supplementary data: Capacitance changes across tBLMs arising from laser illumination (λ = 530 nm). (A) tBLMs constituted of mobile lipids without any functionalizations; (B) tBLMs functionalized with biotinylated polyethylene-glycol cholesterol; (C) tBLMs functionalized with biotinylated gramicidin monomers.

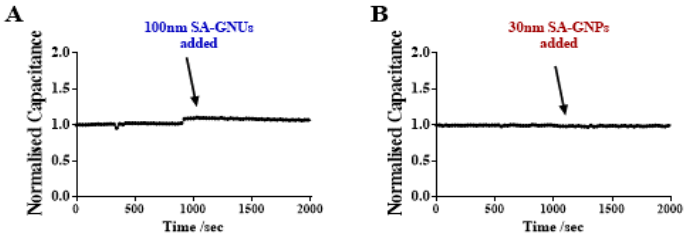

Figure S3: Figure 4.11 supplementary data: Capacitance changes across tBLMs arising from laser illumination (λ = 650 nm). (A) Gramicidin nano-switch biosensor; (B) Fully tethered tBLMs with the absence of tethered gramicidin-A monomers

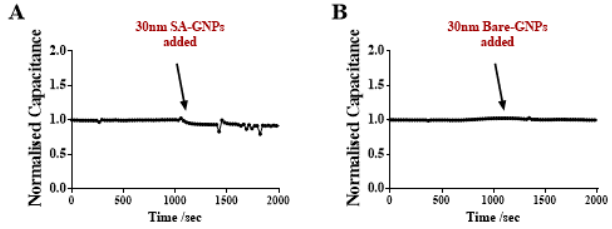

Figure S4: Figure 4.12 supplementary data: Capacitance changes across tBLMs arising from laser illumination (λ = 530 nm). (A) Gramicidin nano-switch biosensor; (B) Fully tethered tBLMs with the absence of tethered gramicidin-A monomers